UNIVERSITY OF OKLAHOMA

GRADUATE COLLEGE

HIGH AMBIENT PRESSURE TESTING APPARATUS AND DEMONSTRATION OF USE FOR MATERIAL TESTING

A THESIS

SUBMITTED TO THE GRADUATE FACULTY

in partial fulfillment of the requirements for the

Degree of

MASTER OF SCIENCE

By

PHILIP M. RESNICK

Norman, Oklahoma

2023

HIGH AMBIENT PRESSURE TESTING APPARATUS AND

DEMONSTRATION OF USE FOR MATERIAL TESTING

A THESIS APPROVED FOR THE

SCHOOL OF AEROSPACE AND MECHANICAL ENGINEERING

BY THE COMMITTEE CONSISTING OF

Dr. Zahed Siddique, Chair

Dr. J. David Baldwin

Dr. Andrew Hinkle

Dr. Yingtao Liu

Acknowledgments

I would like to start by thanking Dr. Farrokh Mistree for convincing the Aerospace and Mechanical Engineering college to take a risk on me when I started my graduate journey and believing me when I said I had learned how to be a good student and engineer since my poor GPA undergraduate days. To Dr. Subramanyam Gollahalli for providing me wonderful council and guidance for the last several decades as a mentor and friend. I would like to thank my committee members for signing on and reviewing my thesis to ensure I contributed to the field of engineering in even a small way. A special thanks to Dr. Zahed Siddique for putting so much trust in me with this research and allowing me to share my experience with some of his other graduate students. To Dr. Andrew Hinkle and David Hass for being such good colleagues and indulging my questions on any number of engineering topics and insight into what I should do with my future. A heartfelt appreciation to my parents, Alex and Jane Resnick, the wisest people I know, for their steadfastness and love during all the triumphs and tribulations of my life. And most of all to my loving wife, Amanda Resnick. For always providing me with support as I worked so hard on my studies, sometimes forgetting other things. And as always, to my spirit guides, Freckles, Aurora, Tovah, and Bowie for all the tail wags.

Table of Contents

List of Tables

List of Figures

List of Equations

Abstract

This thesis describes the work involved in designing and fabricating a high-ambient pressure chamber for material testing. Using SolidWorks CAD software, an SAE AISI 4340 steel chamber was designed with a simulated design pressure of 60,000 psi and a proof pressure of 30,000 psi. Supporting air, electrical, and sensing systems were also designed for remote operations.

A proof-pressure test was performed where the system reached 30,000 psi and pressure was maintained for 30 minutes with no sign of deformation or failing. Following proof pressure testing, the dive of the DeepSea Challenger to Challenger Deep in the Mariana trench was simulated. Four each of two copper alloys and two aluminum alloys were pressurized in the chamber to 15,400 psi and dimensional measurements, microhardness, and surface images were compared between pretest and posttest data collection.

Analysis of the data indicated that there were statistically significant changes in microhardness averages for the copper alloys at an alpha level of 0.1 for both alloys and an alpha level of 0.05 for one. The aluminum alloys had no statistically significant changes in microhardness average but did have a significant change in variance at an alpha level of 0.1 for both alloys and 0.05 for one. The variance showed a narrowing of distribution around the pretest average data.

Imaging showed changes in topography at magnification greater than 2000x for the aluminum alloys indicative of a possible change in structure which would likely have a corresponding change in material properties but further research is required to confirm and quantify these changes.

Chapter 1: Introduction

1.1 Motivation

As more extreme environments are explored and high-pressure systems are needed in the search of energy reserves, it is important to understand how these environments affect the tools and materials we create for our investigations. These environments, such as those found deep in the ocean or pressurized hydrogen distribution systems, have high ambient pressures that may change how materials and designs perform. Can high ambient pressure derate the strength of materials, like high ambient temperature? Is there a way to detect and predict those changes? High ambient pressure differs from other loading cases as it provides uniform hydrostatic loading on all component surfaces. This uniformity and lack of physical restraint could cause intrinsic changes that engineers should consider and learn to predict through experimentation.

1.2 High-Pressure Chamber Purpose

A high ambient pressure chamber can be used in testing for both destructive and non-destructive High ambient pressure chambers can be used to simulate the ambient conditions found in extreme environments. Experiments using high ambient pressure chambers is more economical than sending and recovering systems from extreme environments for conducting post-exposure inspections, which are necessary to refine processes for studying the effects of extreme environments. This could enable the detection of damage or changes in properties prior to failure and create a derating standard for pressure and chemical exposure like that of temperature derating that currently exists for many materials.

With a high ambient pressure chamber rated at 30,000 psi, we can simulate pressures found at high natural environments such as those found at the bottom of the ocean or in deep down hole

drilling operations but also at pressures commonly found for storage of pressurized gasses and liquids, such a hydrogen and oxygen.

1.3 Problem Statement

How does an engineer or scientist test their design in high ambient pressures and what techniques may be used to analyze materials or components for residual changes in properties? High ambient pressure is defined as a high pressure caused by a liquid or gas. Liquids and gasses do not restrain movement of the component under test through physical means such as an anvil pressurization device. Anvil or direct contact applications of pressure do not allow the surface where force is being applied to move freely. This type of direct compression may mask the actual changes of structure in the materials that can occur in hydrostatic environments. Direct contact pressures are applicable for testing at geologic pressures where rock applies pressures to other rock with extremely high force. High ambient pressure however is more applicable to systems submerged in a fluid such as water or the dense atmosphere of a gas giant.

1.4 Thesis Goals

My thesis has four main goals:

1. Design a pressure chamber and test stand capable of creating a high-ambient pressure environment.
2. Demonstrate the functionality of the chamber by simulating a real-world scenario in which materials are subjected to high pressure.
3. Identify basic laboratory tests that can be used to determine if there have been mechanical or microstructural changes to the materials after the simulated dive.
4. Identify possible areas of further research for advanced engineering degrees, which may be of interest to the engineering community.

I chose to simulate the dive of the *Deepsea Challenger*, piloted by James Cameron on March 26, 2012, to Challenger Deep in the Mariana Trench near Guam [1]. This real-world scenario was chosen because it represents the area with the highest pressure explored directly by humans. Figure 1 details the two manmade dives to Challenger Deep and illustrates the pressurization cycle of the DeepSea Challenger: a three-hour pressurization cycle, a three-hour hold period, and then a one-hour depressurization cycle.

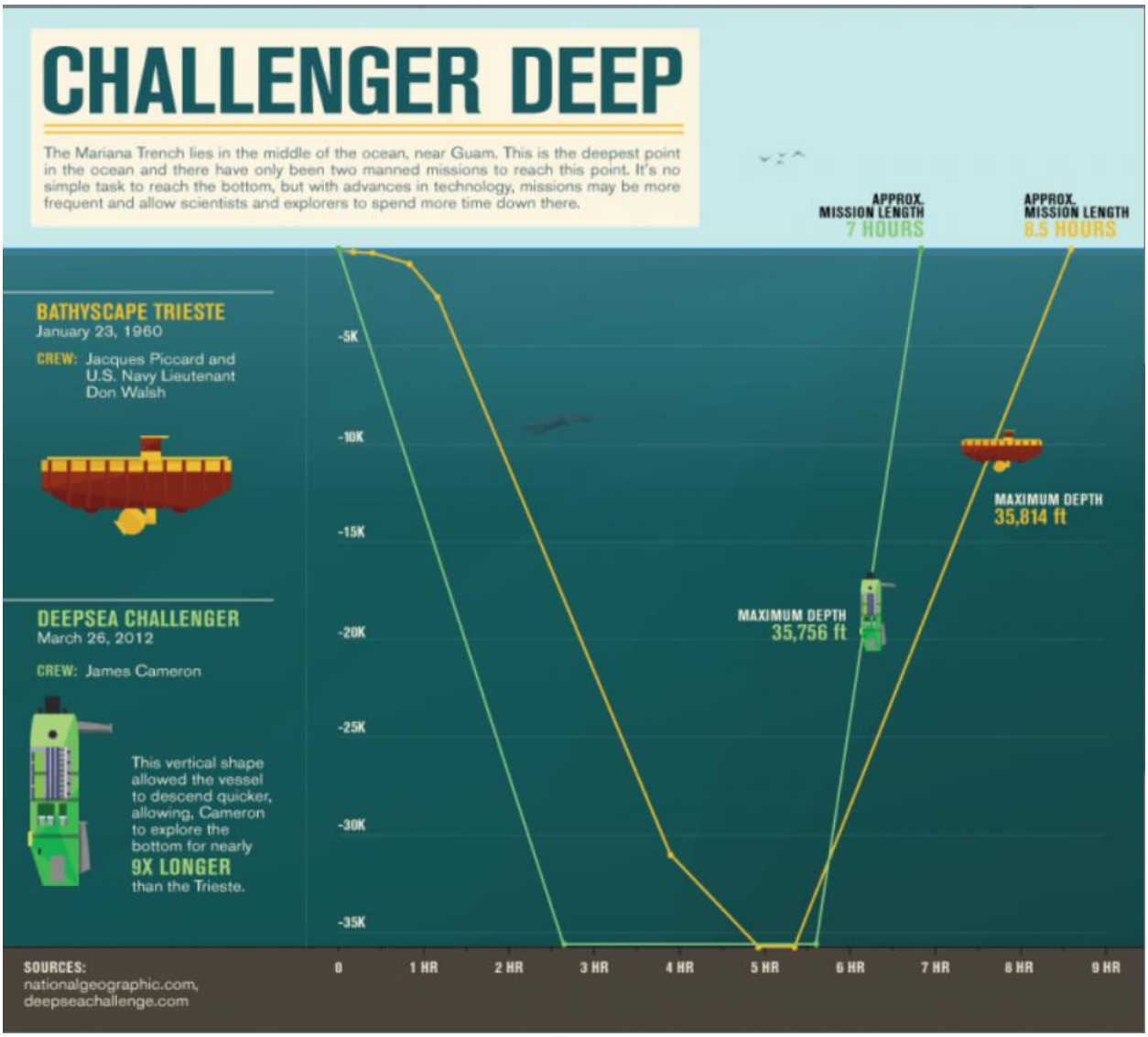

Figure 1: Dives to Challenger Deep [2]

For the chamber's demonstration testing I am assuming that high ambient pressure can have a measurable effect on material properties and leave residual traces once pressure has been returned to standard ambient conditions. Changes in mechanical properties or microstructure are indicators that at pressure the materials' properties would have also changed, possibly resulting in a change in performance of the design or use of the component. Any physical changes in dimensions, shape, grain size and orientation, hardness, or other physical characteristics can indicate that material properties have changed and should be considered when designing systems for high pressure environments.

This thesis is organized to present the following:

- Background information on material and high-pressure testing types and methods
- Design process used for the high ambient pressure chamber as well as the support systems
- A detailed account of the testing process and observations noted during the proof-pressure testing, demonstration testing preparation, and the demonstration testing execution.
- Testing analysis, which proves the proposed rating of the chamber design and demonstrates a possible application for research
- Suggestions for chamber improvements and further research

This thesis includes all technical data, such as models, drawings, schematics, procedures, raw data, and a final Bill-of-Materials (BOM) needed for future chamber use. Raw image files are available upon request from the author.

Chapter 2: Background Information on Material and Pressure Testing

2.1 Introduction

Material testing has been used by tool makers and users since the first efforts to create tools and weapons for survival. Initially, simple visual inspections and hand testing were the only methods available but technological advances have allowed engineers and scientist to categorize a wide variety of materials based on characteristics like yield strength, density, conductivity, corrosion resistance, and many other parameters.

Material testing is generally divided into two categories, destructive and non-destructive. Destructive testing applies a force in some way such that the material permanently deforms or is destroyed to categorize and understand how the material performs under actual loading. Some examples of destructive testing are the Charpy impact and dog-bone tensile tests. Non-destructive testing inspects and investigates materials using methods that do not cause permanent damage or changes to properties. Examples of these are microscopy and ultrasonic testing.

Part of the categorization and performance of materials is to apply pressure to simulate an environment with different ambient conditions. The first efforts to contain and control pressure can be traced back to Heron's Aeolipile, a steam-powered rotating ball [3]. Heron was a Greek inventor who lived approximately between 10 and 70 AD credited with creating many works on mathematics and engineering. Figure 2 illustrates how the Aeolipile used steam to produce mechanical work.

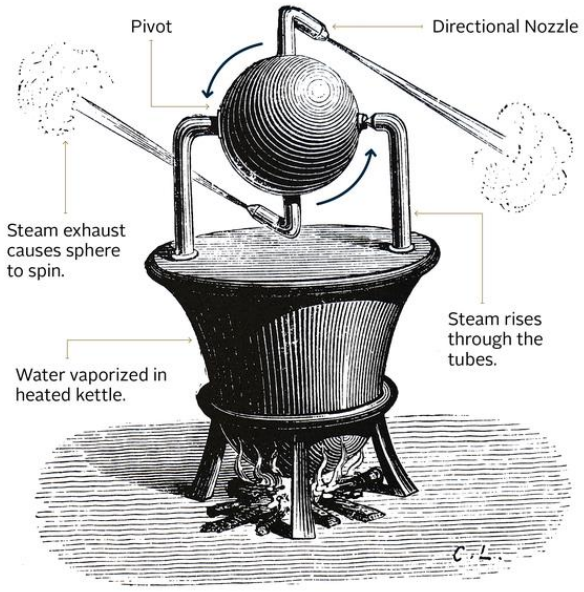

Figure 2: The Aeolipile (Artist's Rendering) [3]

Like temperature, pressure acts on the internal energy of a material. While temperature affects the behavior between vibrating atoms and their kinetic energy, pressure affects the atomic bonds of a material by compressing the distance of bonds. By manipulating these bonds, scientists have studied how minerals are created within the earth and created purely manmade materials that are super hard [4].

One of the first pressure vessel designs is described in Leonardo Davinci's Codex Madrid I and modern pressure vessels took form during the industrial revolution [5]. In the early 1900s, Dr. Bridgman, who would later receive the 1946 Nobel Prize in Physics, developed sealing techniques that enabled lab pressures above 30,000 atmospheres (440,879 psi) for fluids and solids [4].

2.2 Material Testing Methods

The fundamental areas of engineering mechanics are statics, dynamics, and the mechanics of materials [6]. Scientist and engineers must understand these areas for successful system design

and to understand the nature of why things work. Mechanics of materials is the study of a material's structure and how it relates to those materials properties. Material properties can be grouped into one of six categories: mechanical, electrical, thermal, magnetic, optical, and deteriorative [7]. Each of these properties can be changed by changing the physical structure of the material. Therefore, understanding how environmental changes relate to properties is crucial to ensuring a material and design performs properly. To gather data on these properties, testing is required to know the performance within each category.

Destructive testing is most often used when items are intended for large production runs such as stock material from a mill or a critical component of a larger assembly. In these cases, samples of the production run can be tested extensively to provided relevant statistical data for the end user with little impact to the cost of the run. Testing falls into categories of low strain rate tests such as tension or compression test, high strain rate tests such as shock and impact, or cyclic tests such as vibration or cyclic fatigue use tests. Actual performance data for multiple parameters can be determined from each test run. For example, in ASTM E8/E8M *Standard Test Methods of Metallic Materials* [8], standard dog-bone tension test can provide yield and ultimate tensile strengths, elongation, crack propagation, etc. Impact testing is a method of high strain rate testing that determines how a material or design will respond to a sudden, violent absorption of energy. Materials often respond differently depending on the rate at which energy must be absorbed. A material that is very strong and resilient at low-strain rates, may become hard and brittle at high strain rates. Cyclic testing is used to determine the performance of a material over time.

Non-destructive testing is used for inspection of products that may continue to be used for their intended functions as well as investigating failure without further damaging the component. Quality assurance for production or inspection for in-service components are examples of

situations that might use non-destructive testing. Some non-destructive tests are used to identify fatal flaws without imparting additional flaws as part of the testing. For example, the use of ultrasonic inspection can identify subsurface or microscopic cracks that may not be visible through normal visual inspections. By using the ultrasonic inspection method, the inspector can be certain that the testing process itself was not the cause of the flaw. If a destructive method had been used, such as pull test to determine if the component had lost strength, the test itself would impart flaws that would not have been present under normal operations. Non-destructive testing also includes inspection with the naked eye, microscopy, dye penetrant, and basic physical measurements.

I was particularly interested in hardness testing. The hardness of a material is dependent on the chemical makeup as well as the structural organization. Graphite, for example, exhibits low hardness in one direction where the planes of carbon atoms can move laterally with respect to each other but high hardness where the atoms form hexagonal bonds within the plane. If the carbon is forced under sufficient pressure and heat, a diamond can be formed. For this reason, a change in the structure of a material, even at the atomic or molecular level, can affect its mechanical properties and hardness [9].

Hardness testing can be broken down into two categories: indentation and non-indentation testing. Indentation testing uses an indenter of high hardness material, which is pressed into a surface and the resultant indentation is analyzed based on force used, indentation depth, and other surface reactions. This testing is considered destructive because it creates a permanent indentation on the surface of a part. The shape of a standard Vickers and Knoop hardness impressions is shown in Figure 3. Other indentation shapes exist for the other hardness scales.

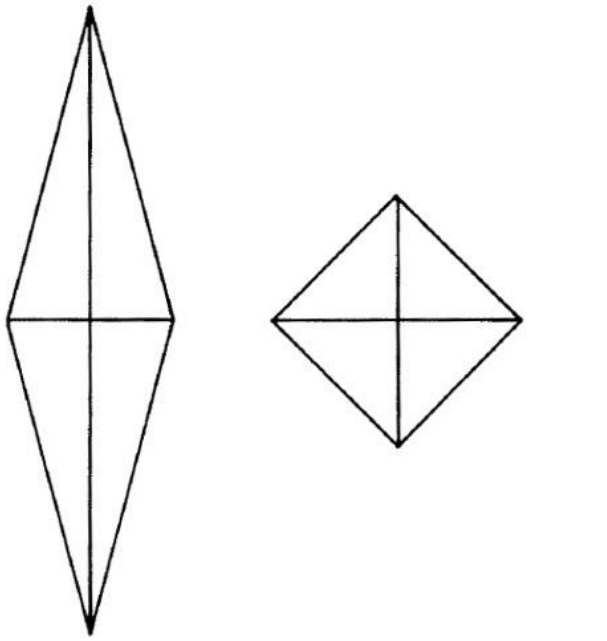

Figure 3: Comparison of Indentations Made by Knoop and Vickers Indenters [10]

The Vickers indenter penetrates deeper into the surface during testing and is therefore less sensitive to surface conditions than the Knoop indenter. However, because the Knoop indenter has longer diagonals, it has less sensitive to measurement errors. The Knoop indenter can also be oriented to follow surface characteristics such as grain lines and structure but is less useful when calculating an average hardness across the surface [10].

Non-indentation testing is much less common in industry but is used where low cost and speed is required or when hardness must be determined without permanent damage to a component is necessary. One example of non-indentation hardness testing is the 10-step scratch hardness test developed by Friedrich Mohs in 1822. This method uses tools or coated paper of known hardness between talc and diamond to scratch a surface. The surface will only be scratched if it is softer than the tool being used. If a surface can only be scratched with diamond, it is given a hardness of

10; if talc was sufficient the hardness was is one or less. Varying minerals were used to bound the hardness of the surface of interest on Mohs scale [9].

Hardness scales range considerably for soft plastics to diamond and carbides. The larger the scale, the less likely small changes in the hardness of a material will be detected. Microhardness testing will be necessary in my testing to detect these small changes. Microhardness is functionally like normal indentation hardness tests but uses smaller forces during the indentation process. Normal Rockwell hardness tests normally use loads between 22 and 330 pounds while the Vickers microhardness tests will use uses loads of two pounds or less depending on the material being investigated [11].

The Vickers microhardness test uses a precision ground, diamond indenter to create an indentation from a specific load, like a normal indentation test. Other than the magnitude of the load, the main difference between a standard Vickers hardness test and a Vickers microhardness test is that the microhardness is evaluated by measuring the area of the indentation left by the indenter instead of the depth of the impression made on the surface [10].

2.3 High Ambient Pressure Research

There are two main methods for transferring pressure to a material, component, or system. The first is to use direct contact of force between two materials with similar density, like applying a load from a piston directly to a rod or squeezing a sample between anvil forms. This method enables the generation of incredibly high levels of pressure. The second method is to place an item in a chamber and pressurize a lower-density fluid, such as air or oil, to a pressure that applies uniform hydrostatic pressure to all surfaces of the item. This method is often used to simulate environmental conditions such as submergence pressure in the ocean or non-standard atmospheric conditions.

One example of high-pressure research where an anvil setup is used as the pressure source is Darul, Lathe, and Piszora's research into the properties of Mn3O4 under high pressure and temperature [12]. The research team investigated how high temperature and pressures affected the stability, polymorphism, and elastic properties of the material. The maximum temperature and pressure used in the research were 1873 F (1273 K) and 1,044,272 psi (7.2 GPa). Using x-ray diffraction equipment, they showed that nonlinear compression occurred along both crystallographic axes and that some of the phases observed under pressure was not preserved upon the release of pressure. Figure 4 is the phase diagram that shows the changes in the crystal structure.

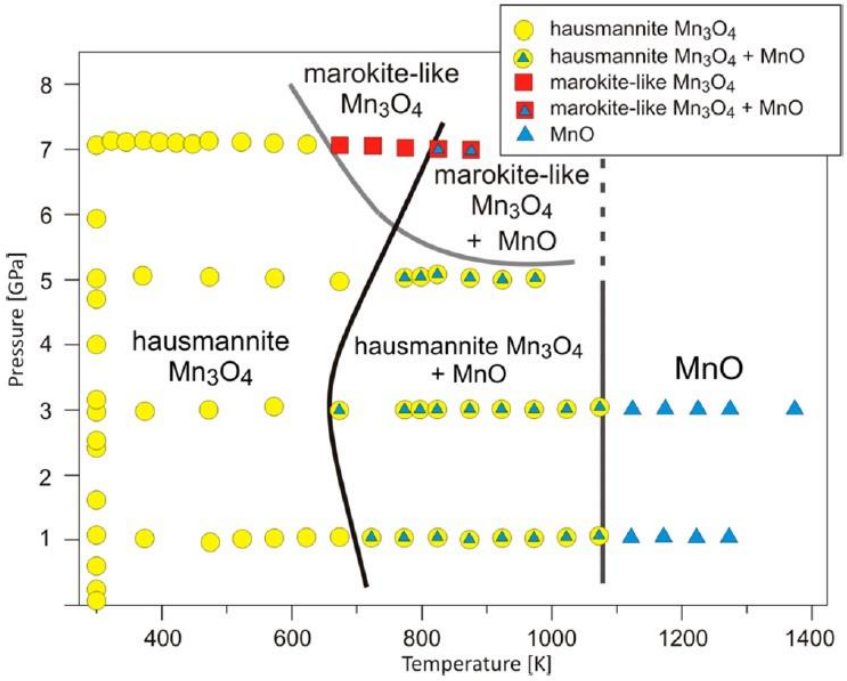

Figure 4: Phase Relations in Mn3O4 Based on the Present High-Pressure High-Temperature Experiment [12]

This environment was useful during their investigation into mineral creation and changes within the earth, but was well above the ambient conditions relevant to my research. The pressures achieved for the experiment were typical of the pressures obtained with the use of anvil pressurization devices. The x-ray diffraction method that was used could have been a useful

nondestructive method of investigating structure, but it was beyond the scope of my research at this time.

My research used hydrostatic pressure so that the materials under investigation were not constrained by a harder material. The materials were therefore more likely to move and to have surface deformation. An example of hydrostatic pressure testing of materials where hydrogen is the pressurization fluid is the work completed by Gaddam, Hornqvist, Antti, and Pederson. In their experiment, the research team investigated low-cycle fatigue and fatigue crack growth properties in cast titanium alloy [13]. In their experiment, ambient temperature and hydrogen up to 2,176 psi (15 MPa) was used to create an elevated pressure environment. Their findings indicated that the low-cycle fatigue life was significantly reduced, and higher strain rates had an even larger effect. They also showed that the cracks grew through different categories of grain colonies when exposed to hydrogen when compared to the use of air.

In Gaddam et al experiment, they demonstrated how hydrostatic pressure can be used, but the goal of their research was to determine how hydrogen affects the material, not necessarily the pressure. Hydrogen creates structural damage to materials even at low pressures. This is due to monatomic hydrogen diffusing into the crystal lattice, which can cause decohesion, localized plasticity, and other damage, which can affect material properties [14]. Because it can change in material properties, the use of hydrogen was not applicable to my attempts at determining pressure-related changes. The experiment showed that there are methods for creating a high-pressure environment utilizing a machine that can perform fatigue, tension, and compression testing. Though it was not useful in my initial investigation, these fatigue testing methods may be useful if the research expands beyond static experiments. The pressures used in this experiment also fall below the range of pressure I will be investigating.

My investigation into high ambient pressure testing of materials revealed very few applicable scholarly sources of similar research. When searching the University of Oklahoma Library catalog, the query for '*High Ambient Pressure' Material Testing* returned only two results, neither of which were applicable. The query for *'High Ambient Pressure' Metals* returned 20 results, but only one result was related to my testing.

Without the focused search for '*High Ambient Pressure'*, the results numbered in the thousands because of the commonality of the three words in academic research. Other phrases such as *High Pressure*, *Mechanical Properties*, and even phenomenon such as *Stacking Fault Energies* proved ineffective at identifying other research using the pressure and methods that my research intended to employ.

The most promising search within the University of Oklahoma Library catalog was *Mechanical Behavior Metal Hydrostatic Pressure*, which returned approximately 500 results. Without the term *high* or *ambient* it was more difficult to find research at significantly elevated pressures. Kathavate, Pawar, Bagal, and Adkine investigated the mechanical behavior of metals under hydrostatic pressure and low temperature. The temperatures and pressures used for the investigation were 39 F (4 C) and 8702 psi (600 bar) [15]. The team used ANSYS simulation, tension testing, and V-notch Charpy testing to investigate the effects high pressure and low temperature have on material performance. One of their goals was to properly model the Bauschinger effect, which is necessary for determining the proper spring-back of metals when they are subjected to high static and dynamic loading conditions. The Bauschinger effect is an observed material property where a material exhibits a softer stress response under reverse loading conditions, for example transitioning from tension to compression, after a material experiences plastic strain as compared to the stress response when loaded similarly to how the initial plastic

deformation occurred [16]. The team showed a correlation between the simulated results and experimental results for steel and aluminum. For steel, the high pressure and low temperature showed a large reduction in ductility. For aluminum, the same conditions had a small effect on the performance of aluminum which remained ductile and stiff. They theorized that steel's body-centered cubic structure and aluminum's face-centered cubic structure play an important role in the performance difference.

This research was interesting because it was the nearest to the pressure range for my experiment but the additional variable of low temperature masks the effect pressure played in the actual performance of the materials.

The reason for the absence of research in this field could fall into three categories as I see it. First, there is nothing of interest in this area. But I would expect there would be some discussion on why such investigations are not useful. The use of safety factors in high-pressure system design and the practice of simply making components thicker or stronger could be masking the actual understanding of the phenomenon at play. Second, the verbiage and keywords used by researchers is different than the words used in my searches. More technical terms or more descriptive terms may be used that I have not been able to identify for searches. Or third, no one has investigated this area of the material understanding and valuable information exists in this field of research.

Chapter 3: Test Stand Design

3.1 Introduction

Designing and manufacturing the pressure chamber and selecting support equipment required a careful examination of the requirements for testing at the high ambient and practices found in industry. Drawing on my experience of hydrostatic pressure testing with various water, oil, and gas systems for the United States Navy, I incorporated intrinsic safety into the design. This intrinsic safety included a large safety factor and components such as relief valves that are dedicated to ensuring the safety of testing. Cost and availability of material and process was also considered to ensure that the funding was used efficiently.

3.2 Design Philosophy

Before investigating options for my experimental design, I defined my project requirements and my design philosophy. My approach to designing has always revolved around simplicity and reliability. As components and systems become more complex, the risk of unknown complications and interactions increases. This is often unnecessary as most problems do not require overly complex solutions.

First, as this chamber is intended for a broad range of testing beyond my initial demonstration experiment, I incorporated as much flexibility as possible. I selected standard fittings and connections that did not require any significant changes for the addition of sensors or other testing devices. These commercial-off-the-shelf (COTS) item interfaces simplified the manufacturing process by reducing time and costs. I decided to make the pressure chamber large enough for a variety test apparatus that could be handled and assembled with normal hand tools and methods. For static material testing, such as aging or exposure to a pressurized environment, the chamber cavity only needed to be large enough to accommodate the coupon. However, to

perform more advanced material testing—including dynamic tests where a component must move—the cavity must be large enough for the coupon and a dynamic test holder.

The dynamic test holder was a test setup that was inserted into the chamber to perform an action. These actions include flexing or applying a known load on the coupon at pressure, which could be directly compared to the same test preformed at ambient pressures.

The motive force behind this holder only needed to rely on intrinsic properties that do not change in an extreme environment. The assumption was that mechanical properties, like spring constants and densities, change under pressure and cannot be known. With a sufficiently large cavity, a dynamic load or stress could be applied at pressure, and the reaction of the design and material could be compared directly to the same load or stress applied at ambient pressure.

The second requirement for my design was to produce it with normal machining practices. The manufacturing machines were large due to the weight and size of the chamber billet, but I did not rely on more complex and expensive processes. While designing my component, I used design for manufacturing principles to minimize the number of machine setups and tooling changes to reduce time and costs.

The last and most important requirement for my design was that it could be fabricated and used safely. The design needed to be intrinsically safe and not rely on additional safety features, such as relief valves except as backup protection. I selected a design pressure limit above my proof and normal working pressures. Design pressure is the value I will use for computer models and simulations as well as calculations and COTS component selection. I chose my design pressure by first selecting an initial working pressure. Challenger Deep is the deepest parts of the Mariana Trench, so I selected the pressure found at this point. At approximately 36,000 ft, the ambient pressure to creatures and vessels is approximately 16,000 psi. Working backward, I chose to proof

test my chamber at 30,000 psi. Proof pressure is the pressure to which I will test the chamber so I can prove the survivability of the as built chamber and connected systems. During my time as a test engineer, the standard operating procedure for hydrostatically tested components was to test at 150 to 200% their normal working pressure except in highly critical systems which had much larger safety factors. This provided a high degree of confidence in the quality of the design and manufacturing processes used in the system's fabrication. I doubled my selected proof pressure again to 60,000 psi for a normal safety factor of four for my design pressure. I selected appropriately-ranged pressure gages and relief valves so that the normal working pressure lands from 25% to 75% of the range, ensuring the gage is not over ranged or fails during normal use. The middle span of gages is considered the most reliable for accuracy. I also used gage that exceeds the maximum pressure capable from the pressure source as a backup, giving me the ability to observe the pressure in the system and asses if design limits were exceeded and if system must be evaluated for continued use if an over-pressurization occurs. The relief valve setting was 107% of the normal working pressure expected. This is also a common hydrostatic testing practice and allows for normal working pressures to be maintained with the pressure source while not lifting the relief valve. Continued lifting of relief valves can eventually cause the relief valve setting to change. The relief valve was also sized to relieve the full volumetric flowrate of the pressure source.

After selecting my main design limit and research goals, I investigated industry testing techniques, beginning with the roots of pressure testing. Autoclaves and hyperbaric chambers have large volume capacities but do not operate near the pressures at which I wanted my chamber to operate. Companies like HIP offer custom pressure chambers, but purchasing a chamber from a company did not seem in the spirit of learning for my research.

To begin my designing effort in SolidWorks, I noted ratios and general features for equipment used at my pressures. I observed a general 1-to-1 ratio of wall thickness to cavity diameter for pressure ratings of approximately 60,000 psi. For example, if I had three-inch diameter void, I would need roughly three-inch wall thickness. This was only a starting point for my design, and the final version was driven by finite element analysis (FEA). I also noted the highly-polished mating surface finishes and large radii, which combat crack initiation and growth and stress risers.

Next, I selected a material with well-established strength and toughness properties that could be machined by a normal machine shop. Knowing that costs may prohibit me from using materials like maraging steels or super alloys, I focused my efforts on selecting a standard steel alloy. Reflecting on my industry experience, I selected SAE AISI 4340 steel as my main chamber material. 4340 is a medium carbon, low alloy steel combining deep hardenability, high ductility, toughness, strength, and high fatigue and creep resistance [17]. Toughness was required to reduce the chance of catastrophic chamber failure caused by cyclic stress. It can be purchased in large billets from most suppliers and machined using normal machining practices. 4340 can also be heat treated using several methods to further increase strength and toughness from its normally delivered levels.

3.3 Chamber Design

The chamber design had two distinct stages of development. The initial design was based around a large, vertical loading chamber to maximize the number of coupons and volume available for testing. This design proved cost prohibitive, so a second stage was needed where I designed a smaller, horizontally-loaded chamber sized to utilize a 4340 billet more readily available than the vertical loading chamber and thus cheaper to procure. The material, treatments, support systems,

and the general functionality of each chamber was as similar as possible other than this design criteria.

3.3.1 Vertical Loading Chamber

To create a large chamber, I reviewed standard large billet sizes that were readily available. My searches revealed that 16.5 inch round billets of 4340 were used in the fabrication of valve bodies. After selecting this billet and using the design criteria of wall thickness (equal or greater than the diameter of the chamber), I selected a five-inch bore hole as the starting point for my design. Figure 5 shows my initial chamber body design.

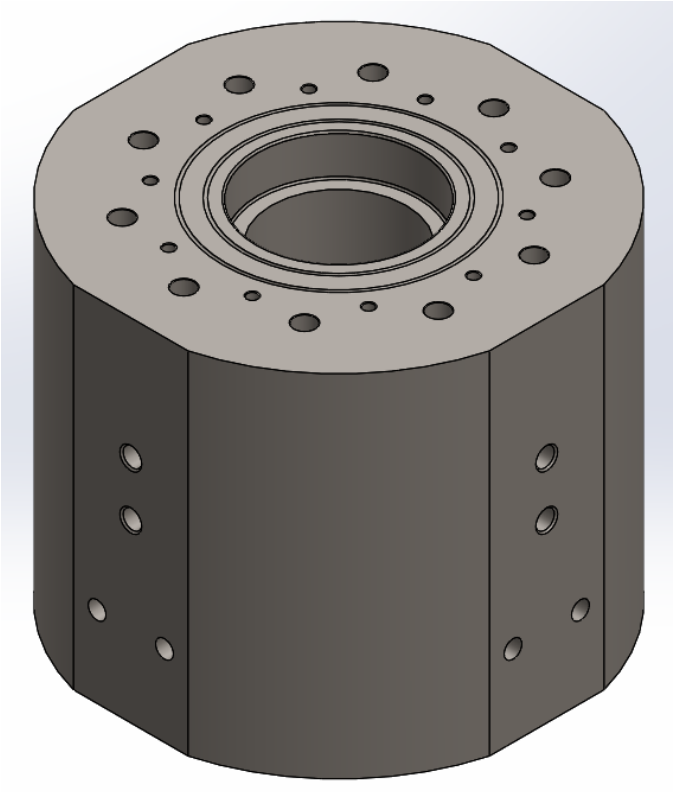

Figure 5: Initial Chamber Design

The five-inch bore was six inches deep providing a void volume of almost 120 cubic inches. The high-pressure ports for sensors and other piping connections were placed at 90-degree intervals around the central axis on machined flats. To maximize ports for experiments I would

place two on each flat, one above another. In Figure 5, the pressure ports are the two upper ports on the flats and the two lower holes are bolt holes for brackets to secure the chamber to a surface if desired.

The lid would also be made of 4340 and five inches thick at the point of pressure. Ten, 3/4-10 thread, Grade 8 bolts would secure the lid to the base. Ten fasteners will ensure a firm and even contact of the sealing surface and resist the significant levels of axial stress during the pressurization sequences. I do not intend to stretch the bolt upon tightening so they can be reused several times. Shear pins were used to take the radial load caused by the outward displacement at the base to lid interface boundary. In Figure 5, the smaller, inner ring of holes are for the 0.375-inch shear pins and the larger, outer ring of holes is for the bolts.

At my test pressures, I was unable to rely on traditional primary seal. Only exotic sealing materials can be exposed to my proof pressure and were cost prohibitive for initial research purposes. However, my research showed that many high-pressure components use a metal-to-metal surface to provide a pressure boundary. I selected a lapped, steel-on-steel interface as my primary seal. This is identified with a red arrow in Figure 6. I selected four o-rings and a second lapped interface as my secondary sealing method. A channel between the o-rings on the horizontal surface was to act as a tale-tale chamber with an attached gage to provide indications of pressure leak by.

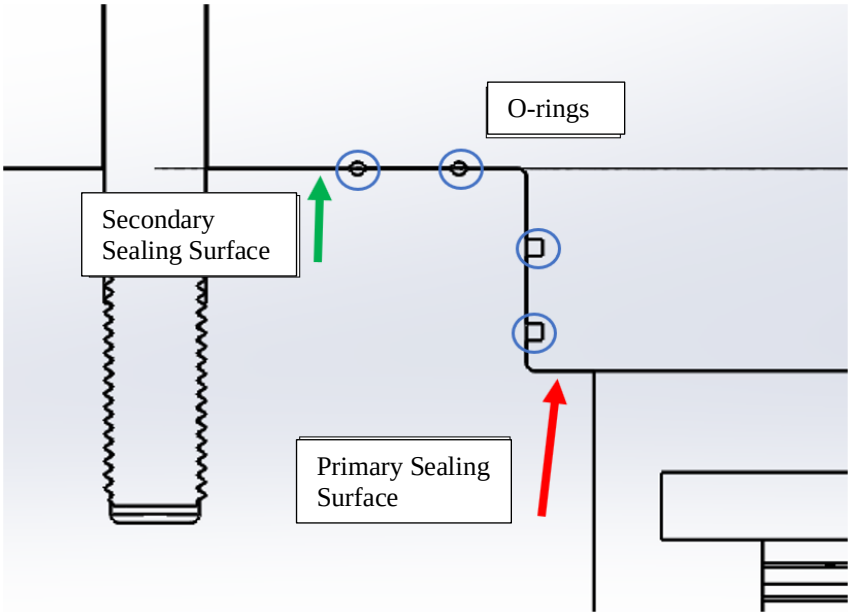

Figure 6: Initial Chamber Sealing Methods

No welded joints were used for attaching components to the chamber because of the uncertainty of welded connections. Additional safety factor is often added when using welded components to account for irregularities found in welds. The test manifold was designed to provide both positive and negative (vacuum) pressure so that the chamber could be evacuated of air between pressure cycles. This helped in reducing condensation within the chamber at pressure. All fittings and connections to the test chamber were in the base structure so that the lid could be removed and reinstalled without affecting the integrity of the test fittings. Figure 7 shows the initial design layout for the high-pressure components of my test stand.

On the inlet side of the chamber, a 0-30,000 psi gage was used as the primary pressure indicator for demonstration testing but would require removal for the proof-pressure test. The 0-50,000 psi gage was the primary pressure indicator for the proof-pressure test as well as act as the backup gage for all demonstration testing. It is a good practice to have an unisolable gage capable of reading the full discharge pressure of the pressure source for all testing. The 0-30,000 psi gage

on the top of the chamber was to act as a tale-tell in case pressure is leaking by the primary and backup seals.

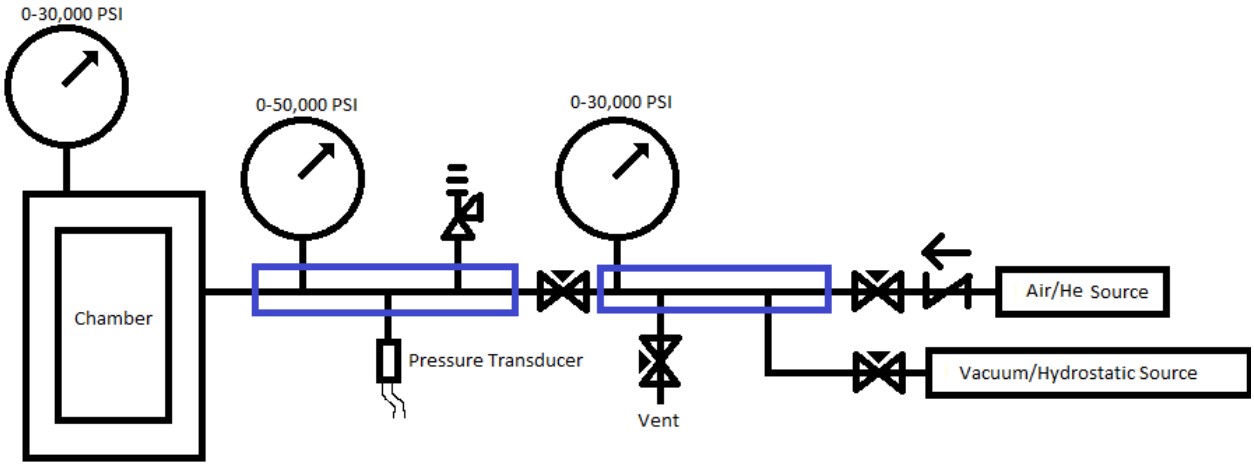

Figure 7: Initial High Pressure Component Setup

The lid was the only part of the setup that was intended to be removed regularly. After each removal, the test chamber was to be resealed and incrementally pressurized so that leaks could be detected at lower pressures. Surges in pressurizations were not desired because of the risk of crack initiation and failure increases associated with rapid load changes.

3.3.2 Revised Vertical Loading Chamber

Further discussions of the design with fellow engineers and manufacturer led me to redesign the main sealing surface from a horizontal interface to a 60-degree tapered interface. Figure 8 shows the revised design.

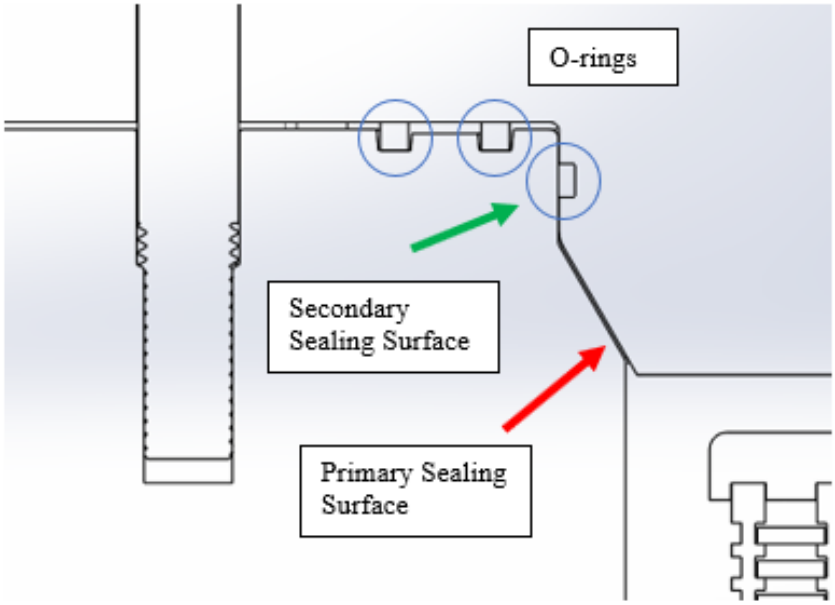

Figure 8: Revised Chamber Sealing Surface Design

The 60-degree interface was based on the HIP fitting seal design scaled up. I decided to leave a gap between the horizontal surfaces of the lid and base of the chamber so that the 60-degree tapered surfaces could be forced together. If the horizontal surface touched and the tapered surface did not fully seal, both surfaces would have to be honed to improve the seal. With a gap, only the tapered surface would need to be honed or lapped. The taper reduced the space available for two bore backup seals. I contacted American High-Performance Seals Inc. and worked with their engineers to pick an appropriate seal and modify my design to provide the pocket necessary for their seal cross-section. Because the chamber bore was a standard size American High-Performance Seals Inc. had a seal available to function as a backup. I modified the seal recess in the lid to accommodate the seal.

After completing the initial design of the pressure chamber, I modeled all the HIP fittings to be used so I could review possible interferences in the virtual environment before purchasing components. When modeled, I identified one interference that required a revision to the design. I had ordered custom manifolds from HIP, but when I modeled the manifolds and components, I

found that the spacing between the pressure gauge and relief valves was insufficient. I needed to increase the distance between the ports to allow for proper installation and function. I contacted HIP, and they increased the length of the manifold by four inches to accommodate my test setup desires.

I also asked HIP about a functional concern I had for their gauges. I intended to draw a slight vacuum prior to each pressurization to remove as much moisture as possible and help draw the pressurization fluid into the chamber. The pressure gauges I chose are rated for high pressure and not vacuum. I was concerned that drawing a vacuum on these gauges may affect their performance and calibration over time. HIP engineers assured me that drawing a slight vacuum on the gauges will not take them out of calibration or affect their performance. I would not be able to read the vacuum on the gauges but this is not necessary for my planned usage. Vacuum gauges can be added in the future if desired.

Discussions with the prospective manufacturer led to changes in the design to improve manufacturability and presentation. To support a simpler machining process and better product, first, they suggested leaving the chamber round except where necessary. This reduces the machining time and improves the appearance of the lid and chamber when mated together. The second modification was to put a single threaded hole in the center of the lid for removal. The lid was to weight approximately 200 pounds. It the lid needed to be forced off for any reason, pulling along the center axis would greatly reduce the chance of marring the mating surfaces. Threaded holes in the side of the lid were to assist in general handling of the lid. Figure 9 shows the revised vertical loading design and CAD model of the high-pressure COTS components.

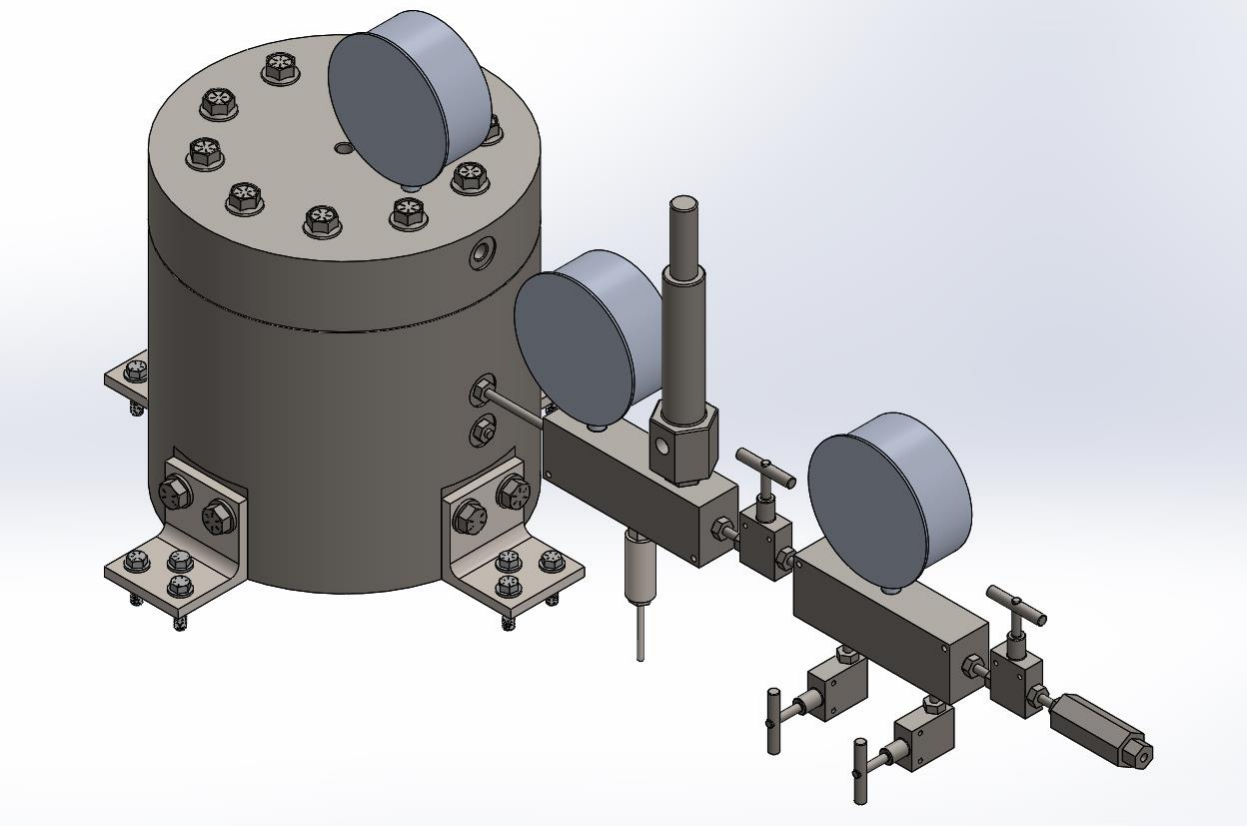

Figure 9: Initial High Pressure Test Setup

With the finalization of the chamber design, I proceeded to simulate pressurization of the chamber to determine if the expected stresses warranted design changes. For an initial stress estimate, I used Solidworks Simulation to perform my analysis. Solidworks Simulation does not allow for as fine a mesh control or assembly features as the more powerful ANSYS software but for simple geometry and loading conditions, Solidworks returns valid simulation results and allows for much quicker iteration in design. I iterated various radii and port hole sizes and eventually settled on a final design.

Figure 10 shows the color map of the 60,000-psi simulation. The scale of von Mises stresses is in ksi. The maximum stress returned by the simulation is 152 ksi. This is well within the heat treatment strength capable for 4340 which can be treated to >200 ksi strengths and retain significant toughness. I do not want to increase the strength more than necessary though as this

affects the toughness of the material. I want the chamber to be very tough and resistant to fracture and fatigue.

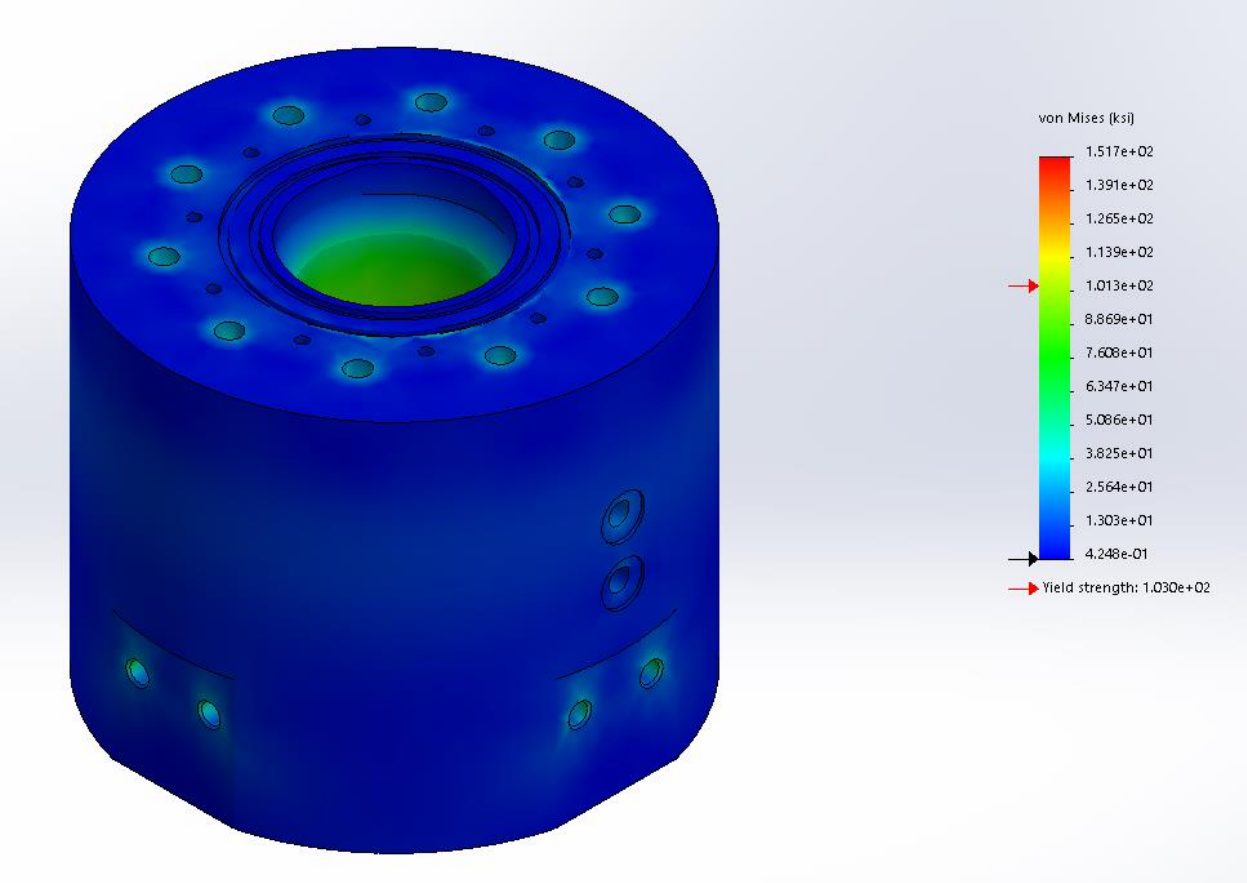

Figure 10: Pressure Chamber Stress Simulation

Figure 11 and Figure 12 below show isometric clipping of the simulation results at 120 ksi. Less than 1% of the total material volume is above 120 ksi in the simulation. The rapid increase within the last few percentages of material is often an indication of high stress risers returned as an artifact of the simulation meshing process.

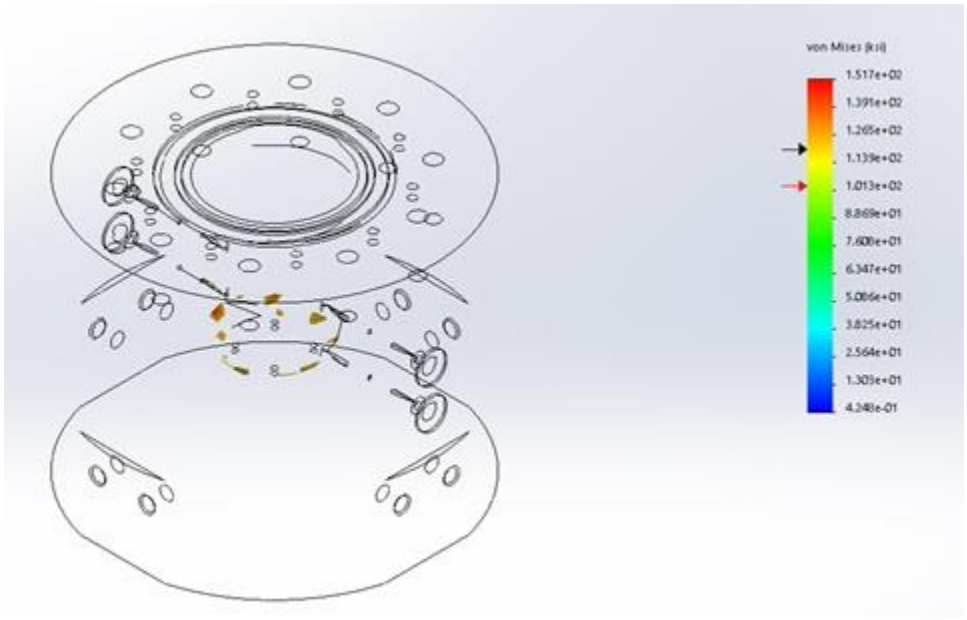

Figure 11: Isometric Clipping of Stress Results at 120 ksi (Full View)

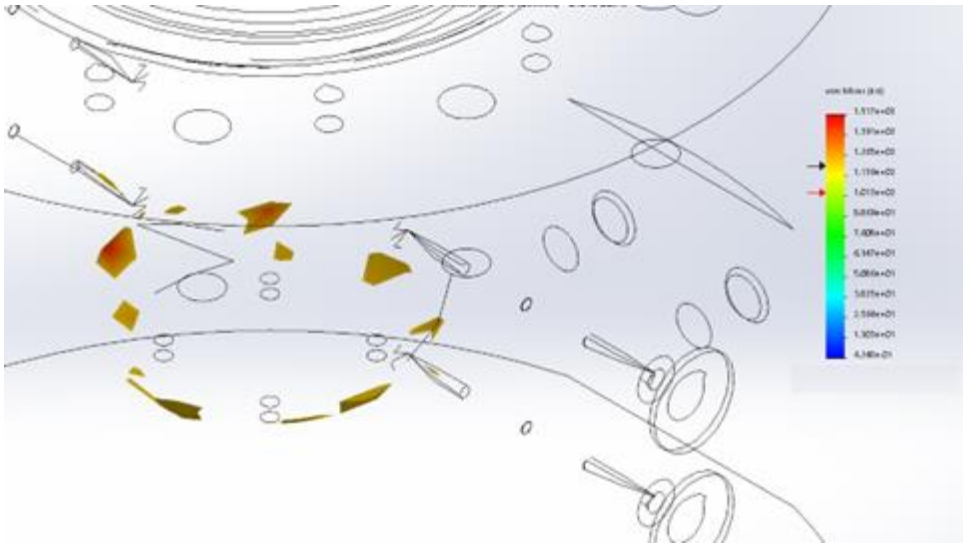

Figure 12: Isometric Clipping of Stress Results at 120 ksi (Up Close)

Manufacturing drawings of each component to be manufactured were created using SolidWorks 2019 with a custom template and detailing materials and critical manufacturing requirements. Step files would also be delivered to the manufacturer to be used with their Computer Aided Manufacturing (CAM) software and automated manufacturing processes. Appendix A provides the first revisions of these drawings.

The final design hurdle to overcome was to determine the best method for heat treatment. Traditional heat treatments heat the steel to an austenitic forming temperature, usually around 1600^{o}F, and then hold it there to dissolve all the carbide and alloying elements in the steel. The material is then be rapidly quenched to "freeze" the crystal structure with a primarily austenitic structure. This creates a very strong matrix of alloying elements and locks in the grain structure producing a strong and rigid steel. The drawback for making very strong and rigid steel is that it is more susceptible to rapid crack initiation and propagation. To minimize the risk of rapid crack propagation, I focused on treating the steel for the chamber to have as much fracture toughness as possible. This was done by researching methods to improve the ductility of the steel while maintaining a high strength which will allow the material to flex slightly before crack initiation.

Researching available methods for heat treatment of 4340 and discussing my project with several materials scientists, I selected the process of Austempering. This process has been used for sheet metal by the automotive industry for many years but has only recently been tested on thicker material. The process of Austempering is illustrated by the Time-Temperature-Transformation (TTT) diagram, which is shown in Figure 13.

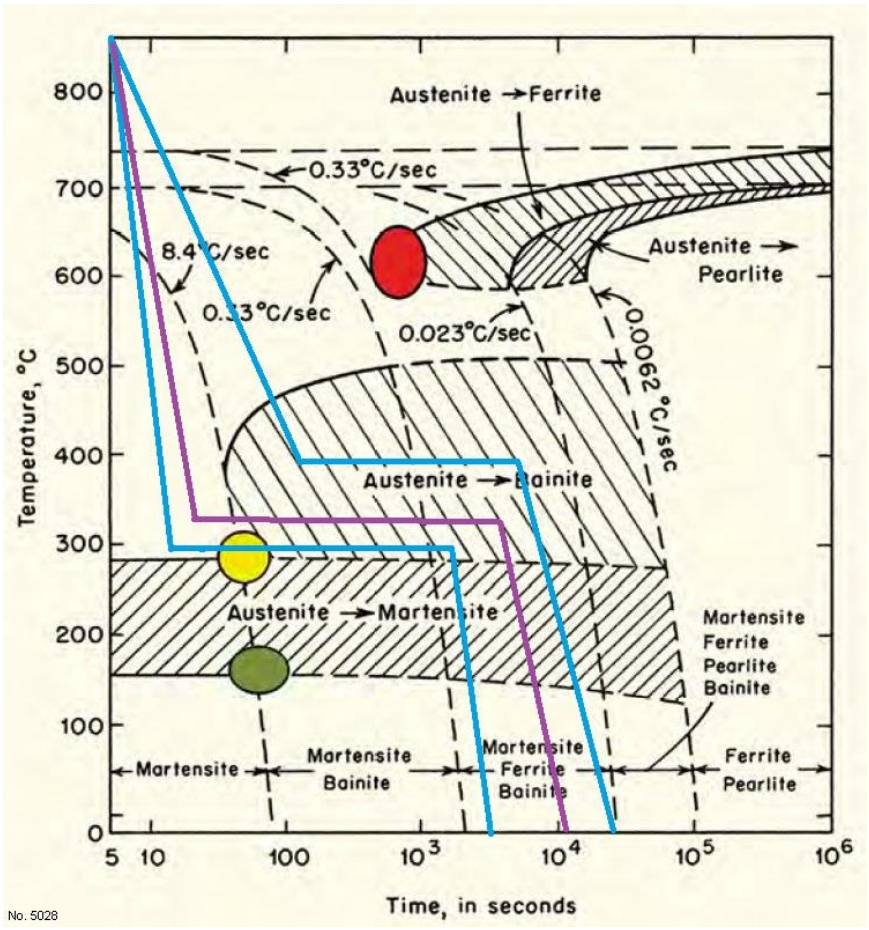

Figure 13: TTT Diagram for 4340 Steel with Austempering Track Overlay (Modified) [18]

This diagram shows the steel phase grain formations that occur at various temperatures and times through the cooling process from austenitic temperatures. The goal of Austempering is to increase the quantity of Bainite while reducing the quantity of Martensite and cooling before Pearlite formation begins [19]. Pure martensite is very hard and fractures quickly like glass but has a high strength. Pearlite is a very fine form of Cementite that is spread through a Ferrite matrix. These fine grains do not resist crack propagation and therefore allow for fast failure. Bainite are large formations of Cementite in a Ferrite matrix. The Ferrite absorbs stress and strain to slow the spread of cracks and the Bainite formations increase the hardness and strength of the steel. The small amount of Martensite that forms when cooling in the Martensite-Ferrite-Bainite zone improves ductility. The purple line shows the desired cooling path for the steel. The blue lines

represent the bounds of the cooling path for a successful Austempering. After a long soak at austenitic temperatures (but not so long that coarse grain structures begin to form) the steel is quickly quenched in a salt or oil bath at a temperature of approximately 600^{o}F. The quench must be fast enough to miss the ferrite formation "knee," shown by the red dot. This drastically changes the microstructure of the steel and significantly reduce its strength. The steel is then held in the heated bath until it enters the Martensite-Ferrite-Bainite zone and then removed from the bath and allowed to air cool. The steel does not require a second tempering process like other heat treatment methods. The expected hardness of this process was between 41 and 47 on the Rockwell C hardness scale. The expected yield strength was >160 ksi with improved toughness over a similarly hardened steel using traditional methods.

3.3.3 Horizontal Loading Chamber - Redesign

After completing the initial design and acquiring quotes for manufacturing, I redesigned my chamber. The material costs for a 16.5 inch 4340 billet and the Austempering process of such a large chamber made the design cost prohibitive. The design will be kept in reserve in case a larger chamber in needed for research at a later date.

I redesigned the chamber to be much smaller and simpler to manufacture. I first performed additional market research to find a more common but sufficiently large 4340 billet that was used in industry. I found that 8.5 inch diameter round stock was common and approximately 75% less expensive due to the weight reduction.

To redesign the chamber, I looked at the pressure chamber cavity-to-wall thickness relationship. In my first iteration, I used Austempering heat treatment to improve the maximum strength and toughness of my design to maximize the void size. This heat treatment was difficult to perform due to the weight of the chamber and the limited number of facilities with experience

in Austempering bulk material. The objective of the new design was to ensure that the stresses imparted on the chamber could be handled better by untreated 4340 to reduce costs while ensuring the chamber safety factor was 2 or greater. The new chamber was to be 2.1875 inches in diameter based on loading simulations using SolidWorks Simulation. Figure 14 shows the new design.

Figure 14: Horizontal Loading Pressure Chamber

To finalize the design, I obtained a material test report from Bauman Machine for the 8.5-inch billet that was used for the chamber. This manufacturer's testing report, included in Appendix A, showed the forged billet of 4340 had a yield strength of approximately 136 ksi. The clipping of the stresses of the chamber when loaded at 60,000 psi at this value, returned less than 0.25% of the material volume was above this value. Figure 15 and Figure 16 show the locations of the highest stresses returned by the simulations. These locations are at corners of the model and are therefore likely artifacts of the simulation. With the small percentage of volume above the yield

and the location indicating a simulation artifact, I am confident that the chamber would perform at the expected pressures of 30,000 psi and below.

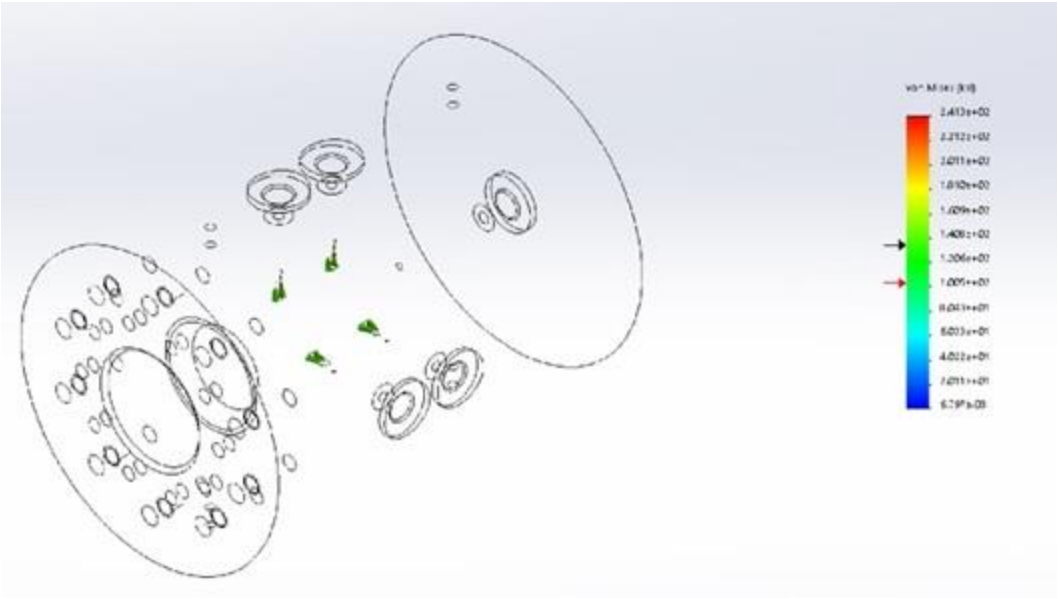

Figure 15: Horizontal Loading Pressure Chamber Simulation Results

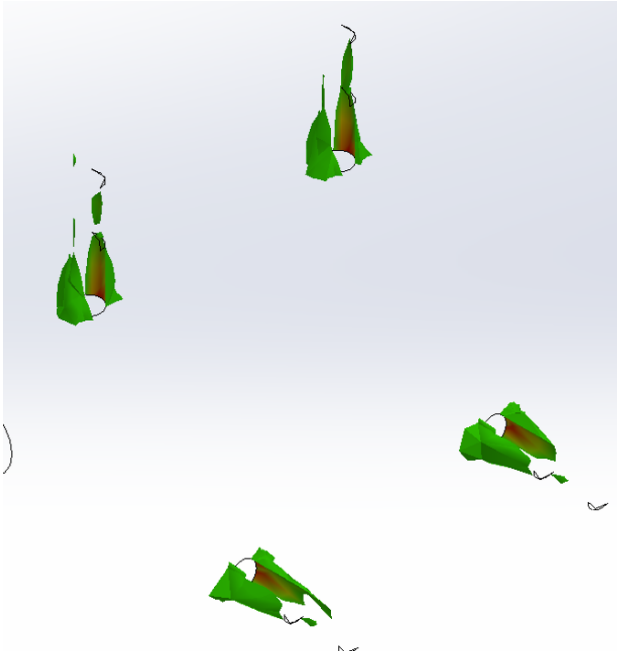

Figure 16: Horizontal Loading Pressure Chamber Simulation Results (Focused)

Figure 17 and Figure 18 show side-by-side images of the vertical loading and horizontal loading chambers. For reference, the original design was 16.5 inches tall and the new design was 12 inches tall.

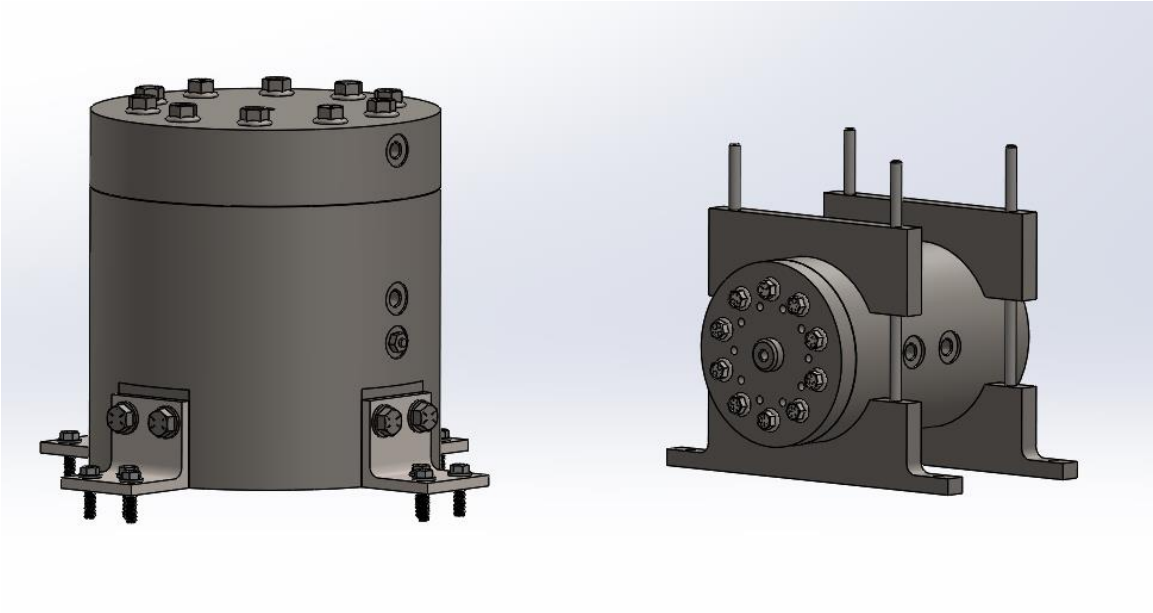

Figure 17: Vertical Loading Chamber (Left) vs Horizontal Loading Chamber (Right)

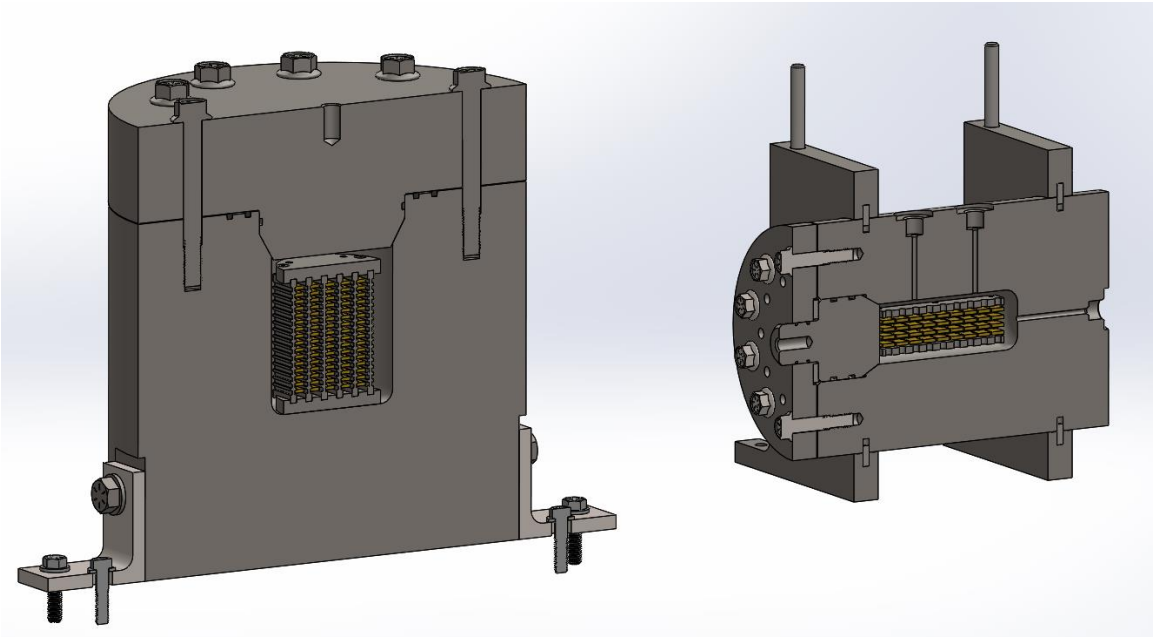

Figure 18: Vertical Loading Chamber (Left) vs Horizontal Loading Chamber (Right) Cutaway

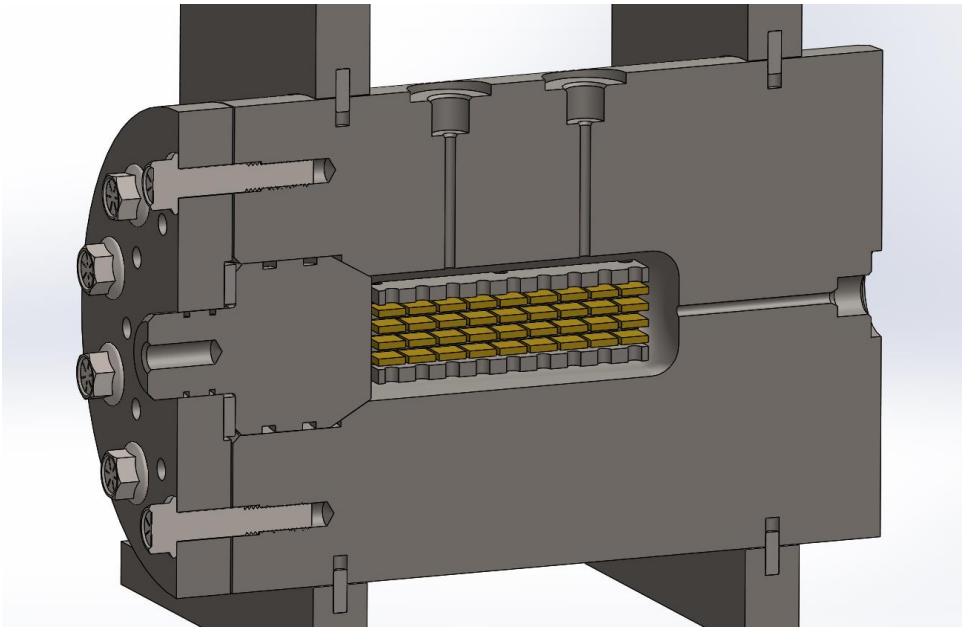

Figure 19: Horizontal Chamber Cutaway (Focused)

Figure 19 shows the internal features of the new pressure chamber design. The lid was designed to apply force to the plug through a large crush washer. The horizontal chamber was to use a 60-degree mating surface with two backup seals like the vertical design. Two low pressure seals provide low pressure sealing between the plug and the lid for the purpose of protecting the metal surfaces from marring each other and to better center the plug while the lid bolts were being torqued down. If significant lapping is required to the 60-degree taper sealing surface, a thicker washer could be installed to ensure proper force application. The purpose of separating the lid into a lid and plug on the horizontal design was to allow for easier maintenance and repairs if the mating surfaces require additional lapping. A single piece design like the vertical loading design would require a much larger piece of equipment to rotate and handle the material. The separation also allowed for redesigned plugs for different applications to be used at significantly reduced material and machining costs. The plug-to-bore radial clearance is approximately 0.005 inches and the backup seals were required to be crushed for installation. This results in a significant amount of

force to be needed to pull the plug out of the chamber, and the threaded hole on the outside of the plug allowed for the use of a slide hammer to remove the plug.

The mounts for the chamber included locator pins to ensure that the high-pressure connections were properly orientated for use. There were five high pressure ports (three shown) designed to accept the 3/8 High Pressure connection type as described by High Pressure Equipment [20] and rated to 60,000 psi. The rear facing port was to provide an easily-accessible port for installation of venting components. Venting should be focused at a wall or other rigid surface for safety. Ten Grade 8 bolts and ten ground shear pins were used on the lid-to-chamber interface. This was like the vertical loading chamber but used smaller threads and diameters. Figure 20 shows the exploded view of the major components of the horizontal chamber. Appendix A provides the revised drawings.

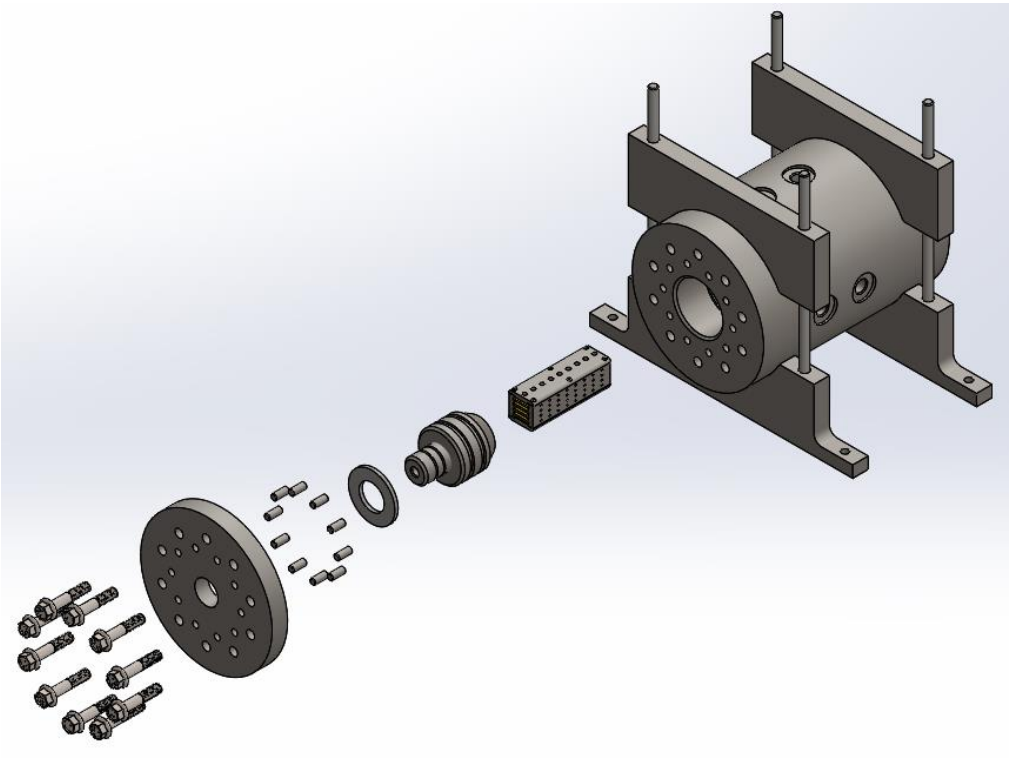

Figure 20: Horizontal Chamber Exploded View

(See Drawing PMR-MS2-10R0 in Appendix A for Component Identification)

I focused on the manufacturability of each component to reduce costs. First, the chamber was 75% lighter than the original design to reduce setup time and to expand the number of machines capable of turning the material. Second, I limited the number of times required to reposition the workpiece for machining. I attempted to have only one setup if possible. The lid and plug could both be fabricated without reorientation and the chamber will require one lathe operation and 2 or 3 milling operations depending on the machine used.

The seal selection proved to be difficult due to the size and pressures expected. The first company I was working with to create the seals declined the project for unknown reasons. After speaking with Eric Healy, an expert in sealing applications with Performance Sealing Inc (PSI), I found COTS seals that were suitable for our application. The seals were rated below my proof pressure of 30,000 psi, but the rating was based on the seal being designed for rotating shafts at elevated temperature. Though the manufacturer could not provide an estimated new rating for my low temperature, non-rotating design, they felt that the seal would likely provide sufficient backup sealing but may exhibit plastic deformation after each pressurization, requiring seal replacement after each cycle. The cost of the seals is less than $10 each, and the number of cycles was less than five initially, so the costs was acceptable. During the proof pressure test, the performance of the seals was carefully monitored. Figure 21 shows the position of the high-pressure and low-pressure seals on the plug.

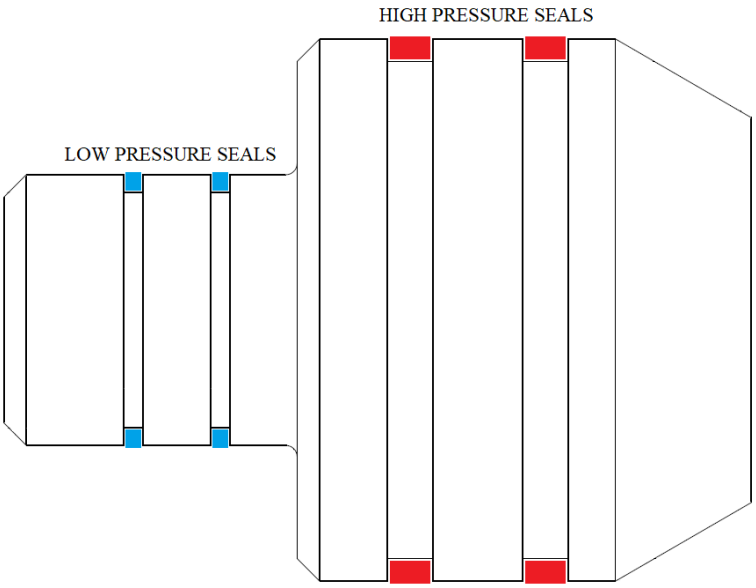

Figure 21: Redesigned Chamber Plug Seals

3.3.4 Horizontal Test Chamber Fabrication

Following the completion of the prototype design and drawings, Bauman Machine was hired to produce the Pressure Chamber, Plug, Lid, Mounts, and coupon holder components. The mounts and coupon holder were not fabricated out of 4340 as they would not be subjected to high amounts of stress. Figure 22 shows the components as delivered by Bauman Machine and prior to coating.

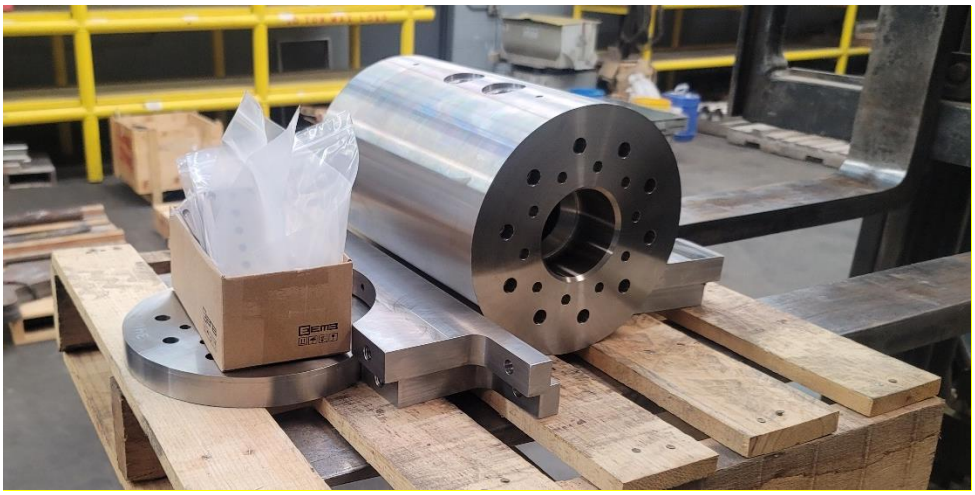

Figure 22: Uncoated Final Pressure Chamber Manufactured Components

To protect the chamber from corrosion, I investigated coating that would adhere to the steel surfaces and provide corrosion protection but not interfere with the fitment of the components. After investigating coating types I selected a Cerakote coating. Cerakote coatings are advanced coating like that of traditional gun bluing which has been used for centuries to protect steel in high-wear environments. They are known to have a very thin adhesion film thickness. The specific coating selected was P-109 Microslick, a dry film lubricant designed to provide low friction for metal-on-metal surface contact and superior protection against high wear, galling, and corrosion by the manufacturer [21]. None of the coatings investigated had any specification details about performance in high pressure environments, so I was mindful to observe the performance of the coating within the pressure boundary closely. Figure 23 shows the pressure chamber after coating and Figure 24 shows the assembled chamber.

Figure 23: Pressure Chamber with Cerakote P-109 Coating Applied

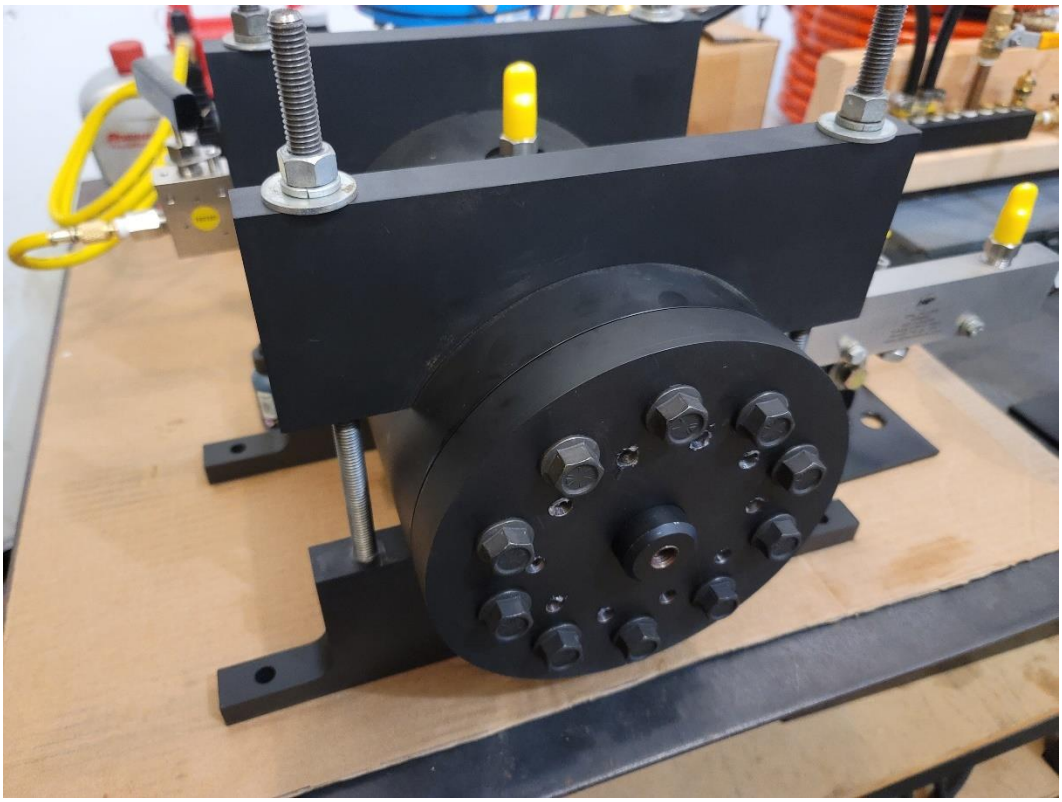

Figure 24: Pressure Chamber Assembly with Cerakote P-109 Coating Applied

3.4 Support Systems

Two support systems were required to operate the pressure chamber safely. The first was a dry air distribution system to operate the air-operated valves that provide isolation and venting of the high-pressure system. The dry air was also used as the motive force for the hydrostatic test pump (Sprague Pump) and the gas intensifier. The second support system was the electronic monitoring and control system. This was used to operate electronic solenoid valves for controlling the air flow remotely. The electronic monitoring and control system was to also provide power for electric control valves, sensors, and act as an interface location for the data acquisition system (DAQ).

3.4.1 Air Distribution Manifold

The air operated valves, hydrostatic (Sprague) pump, and gas intensifier all required filtered, dry air to operate. The facility's air supply had insufficient air cleaning and. The air-operated valves also had a maximum operating pressure below that of the facility air compressor. To ensure optimal performance, I designed a simple air distribution manifold to clean, dry, and regulate the air. The manifold was to provide overpressure protection by means of a relief valve that would relieve pressure prior to the manifold exceeding the valve's design limit. The pressure regulator selected has an integrated filter, water separator, and regulator to prepare the air. Orifices were used to ensure that the air valves do not operate too quickly which may cause damage. Manual isolation and vent valves allowed for proper ventilation and isolation as necessary. The air pressure was not considered high energy and is therefore safe to operate locally. A COTS distribution block, shown in Figure 25, provided a stable platform to attach the components together and had spare ports for expansion in the future if desired. Figure 26 shows the final schematic of the control air manifold.

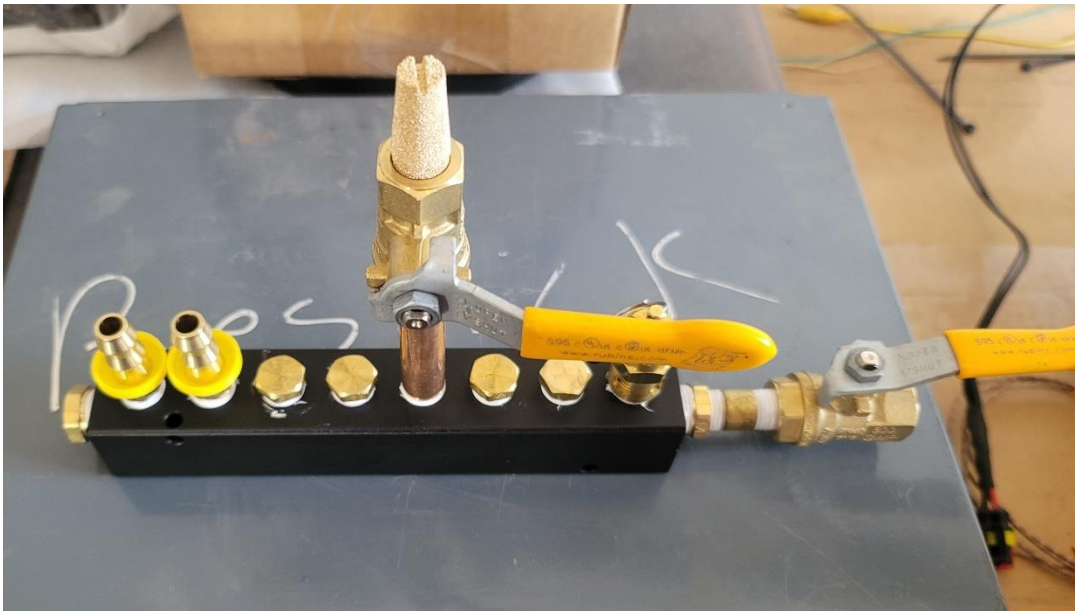

Figure 25: Control Air Distribution Block

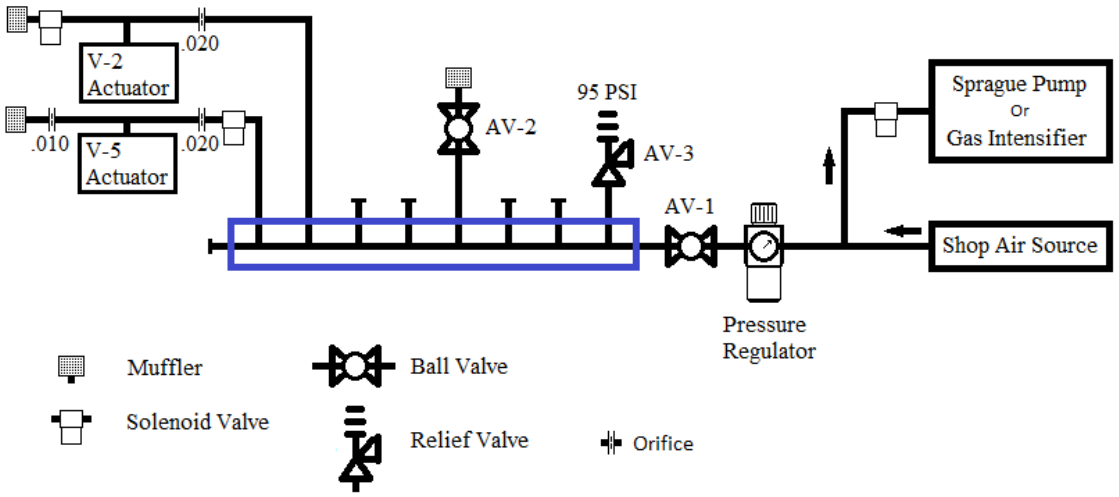

Figure 26: Control Air Manifold Piping Schematic

Additional air distribution components were necessary for the Sprague pump and intensifier. However, these systems were built in accordance with the manufacturer's recommended setups for control and overpressure protection. Both the Sprague pump and intensifier use throttled air valves to provide motive force to pistons to pressurize a fluid.

3.4.2 Electronic Control System

To control the solenoid valves, intensifier pressure regulator, and DAQ remotely I designed a means of providing electrical power and control signals to the various components. Two voltages were necessary to provide power. The solenoid valves that provided air to the air-operated valves required 24 VDC. The intensifier pressure regulator requires both 24 VDC operating power and a 0-10 VDC control signal. The pressure transducer was capable of operate between 9 and 32 volts; however, the DAQ could only operate safely with 10 VDC signal input. Figure 27 shows the functional schematic of the electronic control system with major elecrical components identified.

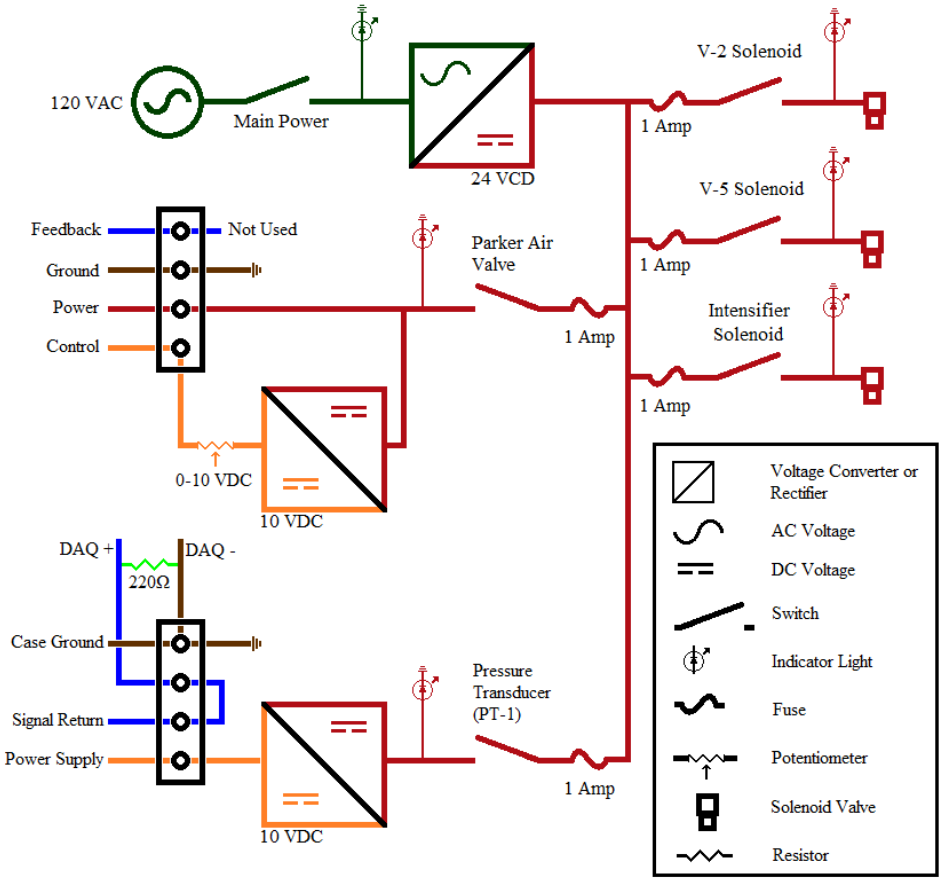

Figure 27: Electronic Control System Functional Schematic

3.4.2.1 Test Stand Control Panel

To condition, distribute, monitor, and control the components of the test stand, I built a physical control panel instead of a computer interface. Through testing experience, I have learned that physical controls are safer, more reliable, and enable quicker responses to problems than computer interfaces. After testing and verifying the expected system responses associated with the components, automation could be added through a dedicated Programmable Logic Control (PLC) or a DAQ.

The design for the control panel was to house power converting and protection components internally with switches, indicators, test points, and connectors secured to the lid or sides. I used connectors instead of hardwiring cables for circuits with known system responses, such as the

solenoid valves, to enabled easy assembly and disassembly of the controls. Also, if a cable needed to be replaced or altered, I would not have to disturb the contents of the box. Test points accessible from the outside enabled the use of a multimeter for troubleshooting of the more sensitive intensifier air regulator valve and pressure transducer. As part of the setup of the system and prior to connecting the components, the test points allow for me to check the circuit voltages prior to actual hookup and to also monitor the signals if necessary.

Figure 28 shows the internals of the control panel. The 120 VAC to 24 VDC power supply is in the upper lefthand position. DC power sources were not available in the North Campus bunkers, so incoming power was required to be conditioned from the available AC power to DC power. The component fuse block is located immediately to the right and below the power supply. This protected the wiring and components from over current damage in the event of a problem or short circuit. The fuses were sized based on the gage of wiring used and component specifications.

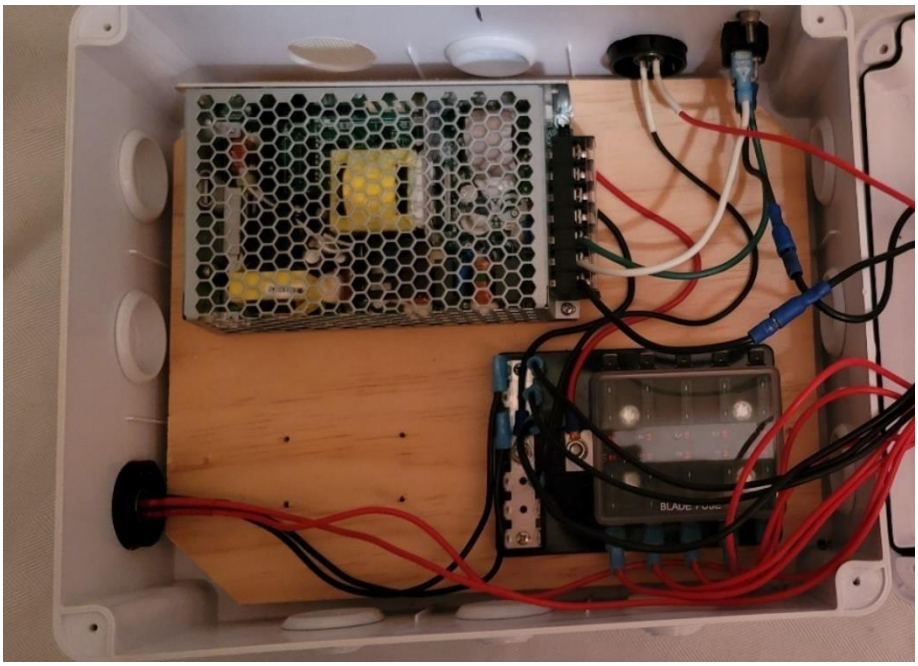

Figure 28: Test Stand Control Panel Internals

The lid of the control panel will support the control switches, indicator lights, terminal blocks for the sensitive components, test points, and breadboards for the creation of custom signal conditioning and controls. Green lights will indicate the presence of AC power input, and red lights will indicate an energized DC circuit. Standard 2-position toggle switches were used because they provide good circuit protection when open over other types of switches and are more readily available for the voltages and current requirements.

The lid of the control panel is shown in Figure 29. Each of the three solenoid valves and each breadboard circuitry has a dedicated toggle switch.

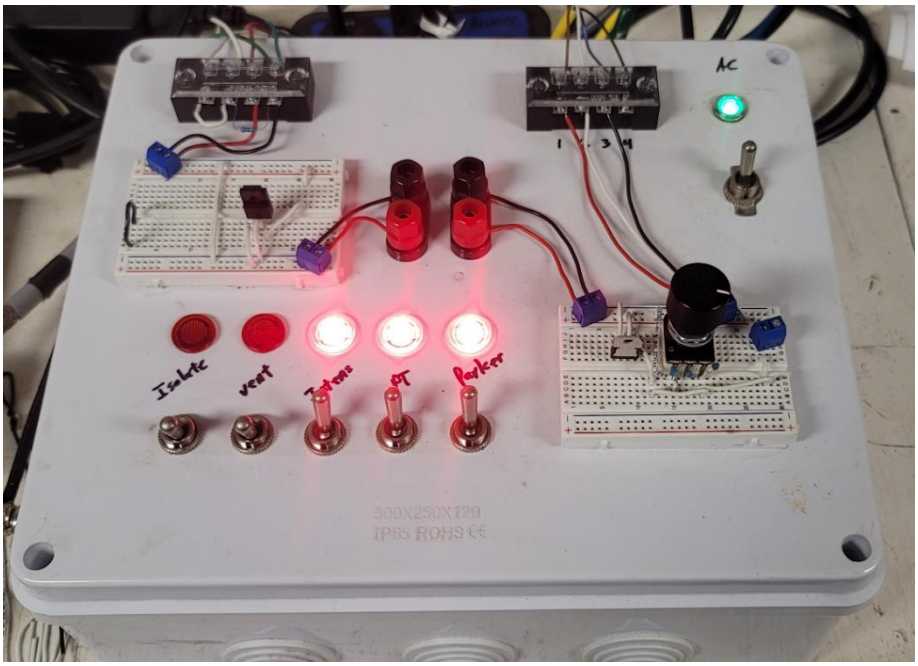

Figure 29: Test Stand Control Panel Top

The breadboard in the upper left of Figure 29 was used to condition the 24 VDC to 10 VDC for the pressure transducer. Because of the large range of the pressure transducer, the driving current required for the full range of pressures could not be provided by the NI-6343 DAQ alone. The 24 VDC power supply was more than capable of providing the driving current, but the voltage needed to be reduced so the DAQ was not damaged. This was accomplished by using a solid state

7810 voltage regulator, which steps the 24 VDC to 10 VDC. The 7800 series voltage regulator is a common board and circuit mounted regulator for converting a wide range of input voltages to output voltages with consistent and stable output.

The breadboard in the lower right of Figure 29 was used to condition and control the power for the intensifier's air pressure regulator valve. This air pressure regulator regulated the incoming motive force for the movement of the intensifier's internal pistons. The amount of pressure required depended on the amount of pressure downstream of the intensifier. As system pressure increased, air pressure was required to increase to drive the pistons. The regulator valve required 24 VDC power for the magnets and internal circuitry, but the actual position of the valve internals was controlled by a separate 0-10 VDC control circuit. The breadboard provided a location to connect both the 24 VDC power and connect and control the 0-10 VDC signal. To step the 24 VDC down to 10 VDC, a 7810 voltage regulator was again used, and then this 10-volt control signal was adjusted using a 10k potentiometer manually. I selected manual controls because I was unsure of the intensifier's sensitivity to the control circuit settings and wanted to adjust as necessary during my first rounds of testing. Following the completion of my testing, a feedback program could be written to adjust the circuit as necessary for a given rate and pressure.

3.4.2.2 Data Acquisition System

The DAQ used for my testing was a National Instruments DAQ X Series system, Model NI-6343. The NI-6343 is a multifunction, analog and digital signal system with 32 analog input, four analog output, and 48 digital input/output channels [22]. These channels are capable of being reconfigured for use with different current and voltage signals as necessary through National Instruments software. I used DAQExpress, a free software suite, for controlling the basic functions of DAQ systems. It is built on the more powerful LabView architecture, which enables used to

program channel monitoring and controls. My testing only required one channel for the pressure transducer, so the LabView Virtual Instrument was basic. It monitored a signal channel for amperage between 4 and 20 milliamps. This value corresponded to a system pressure which was also displayed. The testing did not require a high sample rate because it was not expected for the pressure to change rapidly. One sample every second was adequate and reduced the data file size. This was important for the test as it would run for eight or more hours. Figure 30 shows the LabView Virtual Instruments that were created.

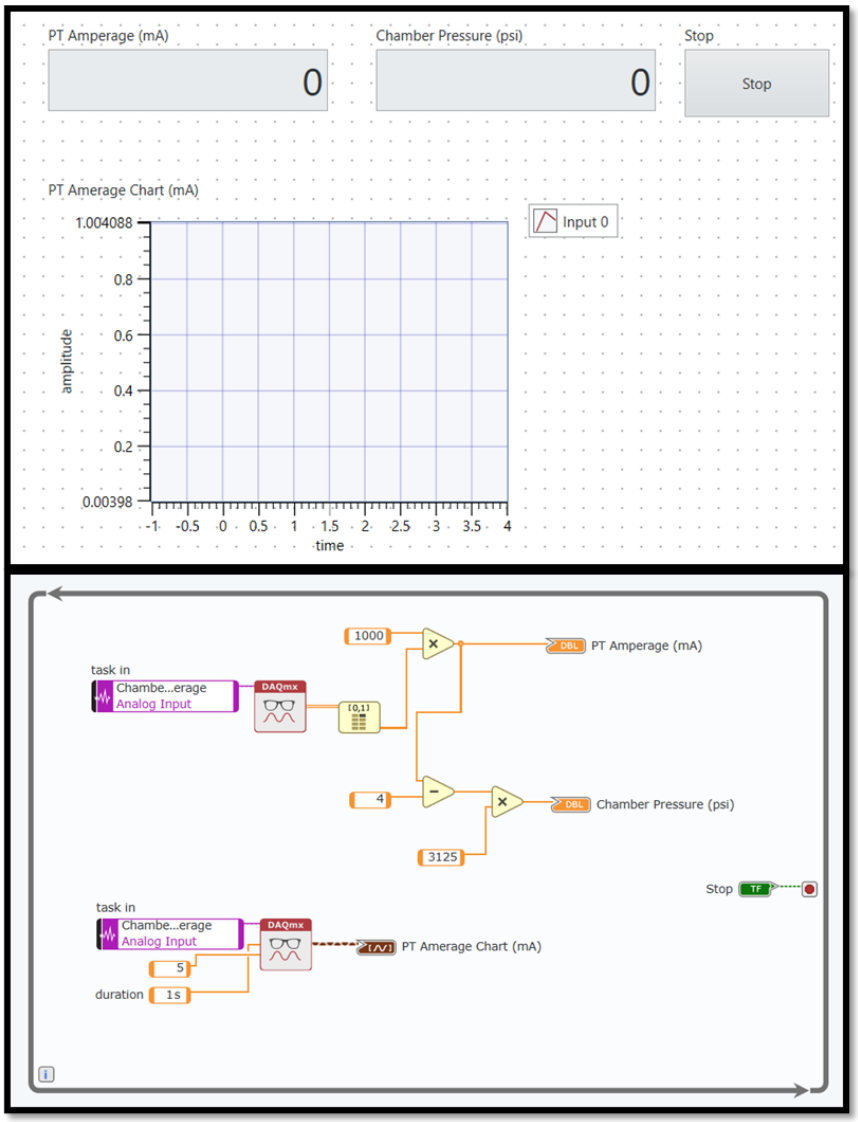

Figure 30: Pressure Transducer LabView Virtual Instruments

3.4.2.3 Pressure Transducer

A Honeywell Model TJE pressure transducer was selected for my test stand. The Model TJE is a welded stainless-steel sensor built for industrial applications. It can be configured to provide pressure ranges between 1 psig/a to 60,000 psig/a, be internally amplified, and output either voltage or ampere signals [23]. I selected a configuration with a range of 1 to 50,000 psig/a to match the range of my backup gauge. Unlike mechanical gauges, pressure transducers do not require to be sized to have the normal working range of pressure fall within the middle of the gauge. This allows for the same transducer to be used for both my proof pressure test at 30,000 psi and my demonstration test at 16,000 psi. I selected an internally-amplified sensor to eliminate the need for external amplification circuitry and an output signal of 4 to 20 mA. 4 to 20 mA is a common output signal for sensors and easily read by the NI-6343. Figure 31 shows the pressure transducer.

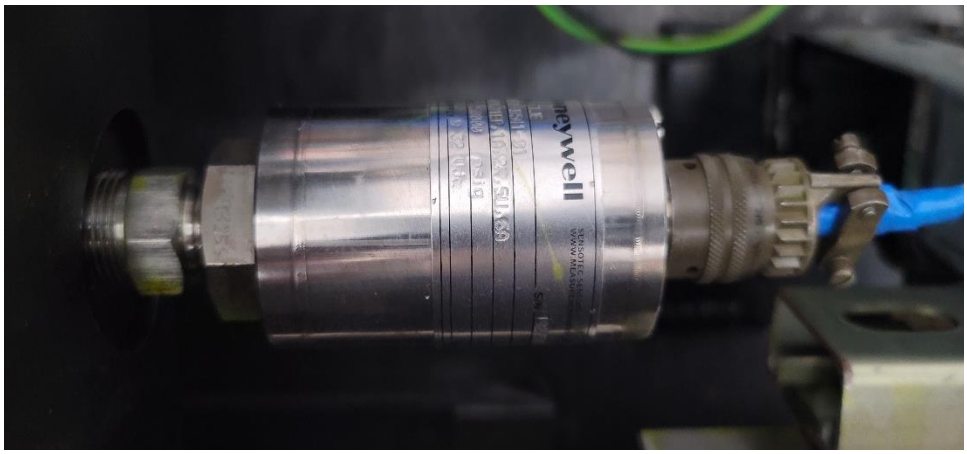

Figure 31: Honeywell Model TJE Pressure Transducer Installed

3.5 Final Test Stand Arrangement and Setup

The test stand was assembled and used in one of the University of Oklahoma Aerospace and Mechanical Engineering department bunkers at North Campus. The North Campus research facility is located at Max Westheimer Airport in Norman, OK. The bunkers are of solid concrete

construction with separate control areas for research performed within each bunker. The concrete construction provides protection for the high energy testing being performed on site.

The test stand was assembled on a welded steel table already on site. The size and location of the table required modifications to my intended setup. Figure 9 shows the control valves and components assembled as one large manifold and then attached at a single port of the chamber. This was initially selected for the vertical loading chamber; however, because the horizontally loaded chamber ports were closer to the deck of the table, the valves on the underside of the manifolds would not be in a good location for normal operations. More space was required for the air operated valves than initially intended; if the assembly was all on one side, it would exceed the length of the table. I rearranged the fluid control components to fit the available space. Figure 32 shows the revised component schematic.

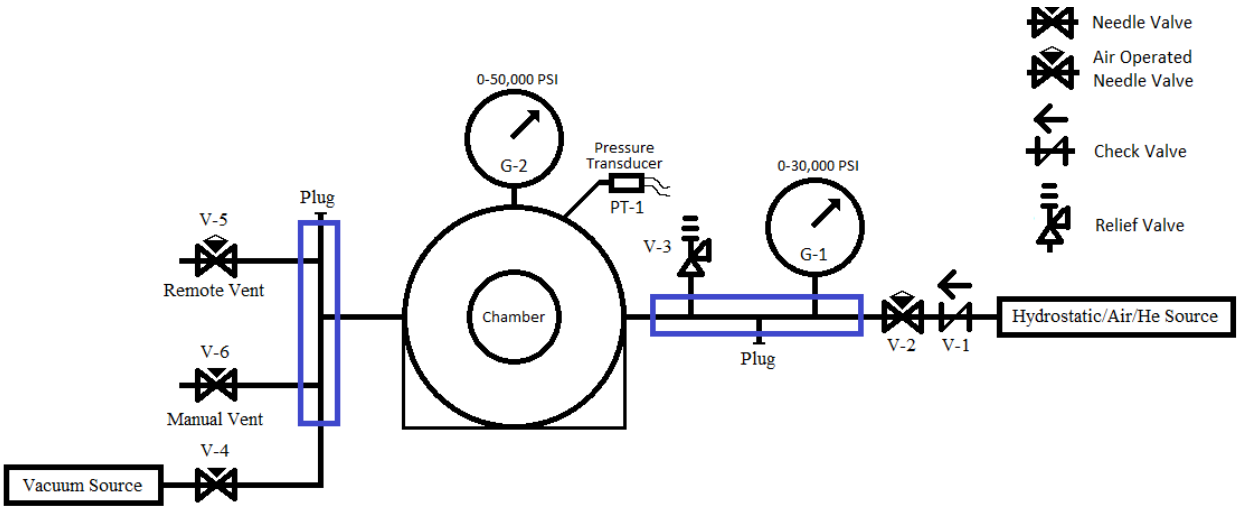

Figure 32: Test Stand Fluid Control Functional Schematic

The pressure source, relief valve, and primary pressure gauge remained attached to the side of the chamber with all fluid sources utilizing the same fitting. As different fluids will never be needed at the same time, separate fitting for air, water, or helium are unnecessary. Figure 33 shows the as-built setup of the inlet side of the chamber. The relief valve and gauges were unisolable

from the chamber so there was no condition where the pressure in the chamber could be isolated from the gauges and the relief valve. This would remove proper pressure indications and also remove the chamber's overpressure protection.

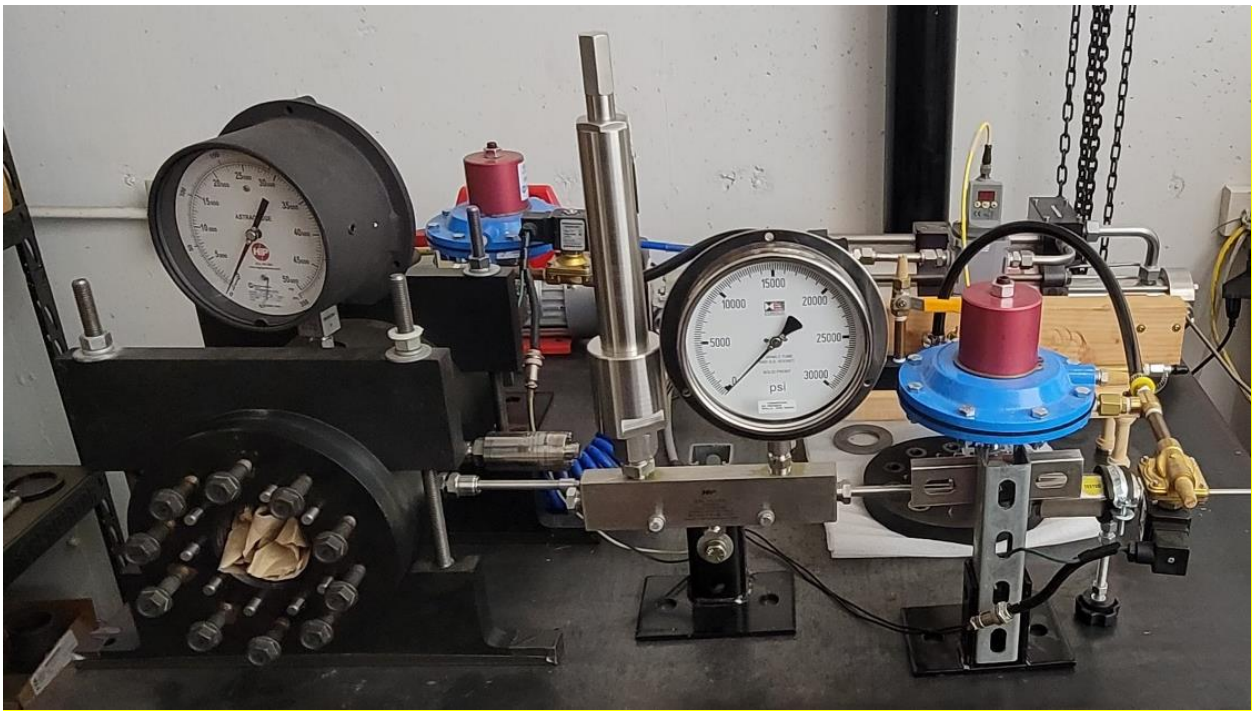

Figure 33: As-Built Test Stand - Inlet Side

The pressure sources for testing would be connected upstream of V-1 shown in Figure 32. The proof-pressure test involved incrementally pressurizing the chamber with filtered water using a positive displacement, air driven Sprague pump. As shown in Figure 34, low-pressure air is used to drive a large area piston attached to a small area piston. This pressure amplification allows the pump to pressurize systems to significantly greater pressures than the available air pressure [24].

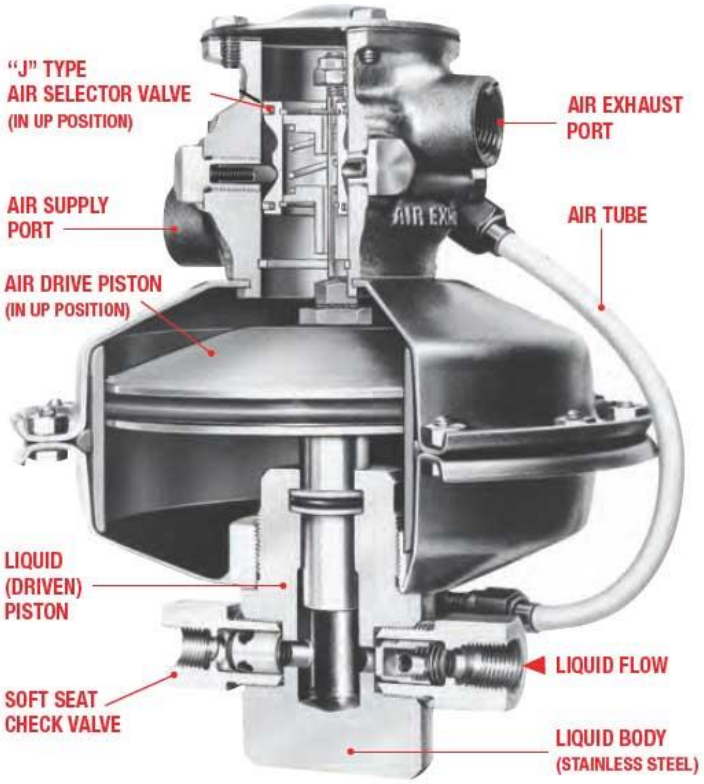

Figure 34: Typical Sprague Pump Cutaway [20]

The selected pump (Sprague Pump, Model S-216-JN-300) had a 300:1 pressure amplification ratio and was capable of 32,000 psi liquid discharge pressure. Sprague pumps do not require an electrical power source and only rely on air pressure to function. They also keep the fluids separate so there is no risk of mixture or aerating the high-pressure fluid.

To control the pump, along with the normal setup, an airline was run into the control area and then back out to the pump. A throttle valve in the middle of this line was used to control the operation of the pump. Manual valves are a best practice when hydrostatically testing a system for the first time or when the system is in an abnormal condition or arrangement. Automatic valves can cause significant fluid leakage if a leak begins as the circuitry attempts to compensate for the

lowering pressure with further pump cycles. By manually controlling the pump, I could immediately stop pressurizing the system and act if a major leak occurs.

The Control Air Manifold was positioned behind the inlet side of the test stand and is shown in Figure 35. The air manifold was elevated on a wooden structure to provide adequate space for proper function of the automatic water drain valve of the pressure regulator. The blue hose in the photo was for initial Sprague pump and intensifier functional testing but does not provide full air pressure at elevated levels for testing. The Sprague pump and intensifier are connected directly to the building air compressor for actual testing.

Figure 35: As-Built Test Stand Control Air Manifold and Intensifier

The vent valves and vacuum source isolation valve were attached to one of the custom manifolds fabricated by High Pressure Equipment and connected as a single assembly to the rear of the chamber. The vents are directed toward the bunker wall and not toward where an operator might be positioned. Figure 36 shows the discharge side of the chamber.

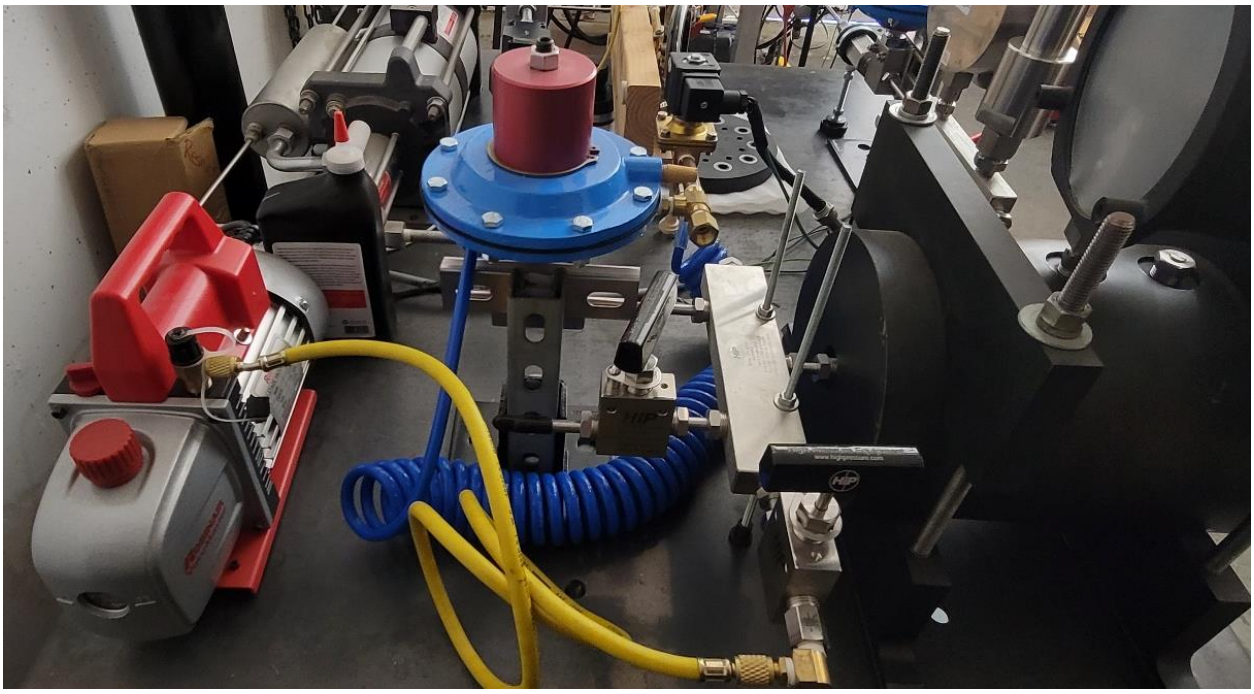

Figure 36: As-Built Test Stand - Discharge Side

Cabling and air lines required for operations were run along the back of the test stand table and along the ground under drop-over cable protectors to ensure the cables and lines are not damages by foot traffic or other equipment rolling. The bunker walls had pass-throughs that allowed for safe transitioning from the bunker area to the control area. Figure 37 shows the final remote operator and monitoring station.

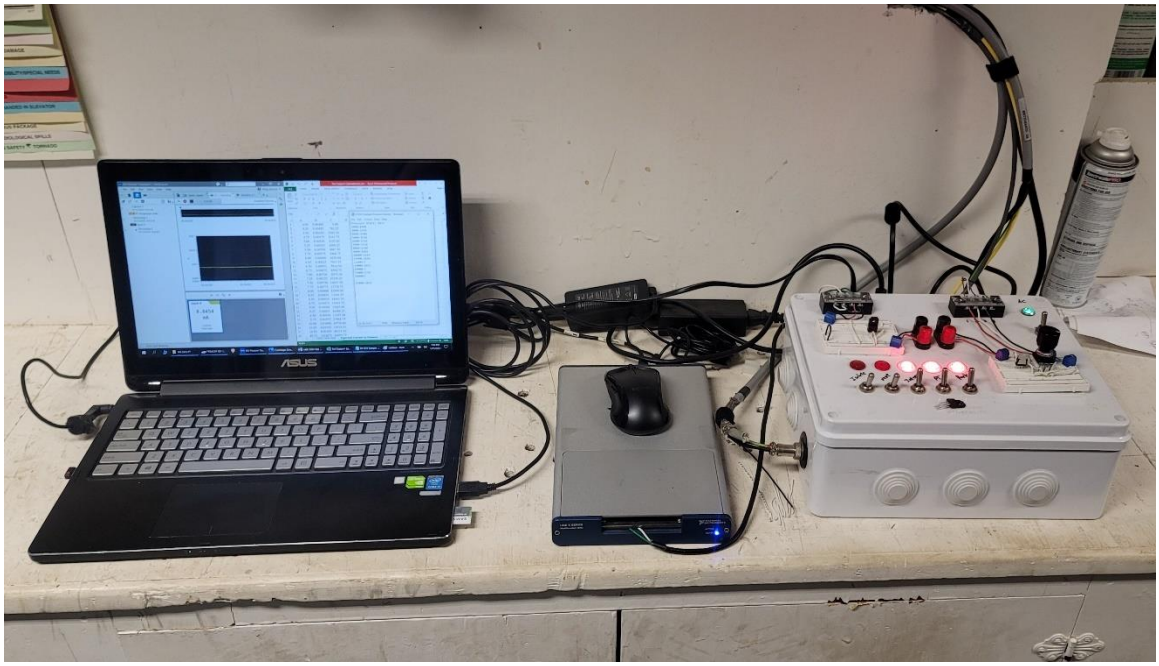

Figure 37: Remote Operator and Monitoring Station

3.6 Demonstration Specific Design

To demonstrate the function of my test stand design, I investigated the pressure effects on materials and methods of observing these changes when the materials are no longer exposed to the pressures. I chose to simulate a dive to Challenger Deep, mimicking the duration and pressures experienced by the DeepSea Challenger submersible used in 2012 by James Cameron. To perform this test, I needed to design a coupon holder and select materials.

3.6.1 Material Coupon Holder

For my demonstration testing, I investigated the effects of high-pressure on material properties. During the initial design phase, I intended to utilize a large, vertical loading chamber and designed a coupon holder capable of holding up to 160 samples at once. This large number enabled the collection of data from many samples even if multiple different materials were tested simultaneously. Testing materials simultaneously reduces the number of cycles and times required for data gathering. The coupon holder was sized to hold coupons with rough dimensions of 0.5 x

1 x 0.125 inches. This size was selected to provide large samples so multiple tests can be performed on the same coupon and still enable the coupon to be embedded into an acrylic puck for machine polishing. The coupons had a 1/8 inch gap between each other, enabling movement and equal pressure on all sides. Additional testing on larger or smaller samples can be performed with a redesigned coupon holder or apparatus. Figure 38 shows the original design of the coupon holder.

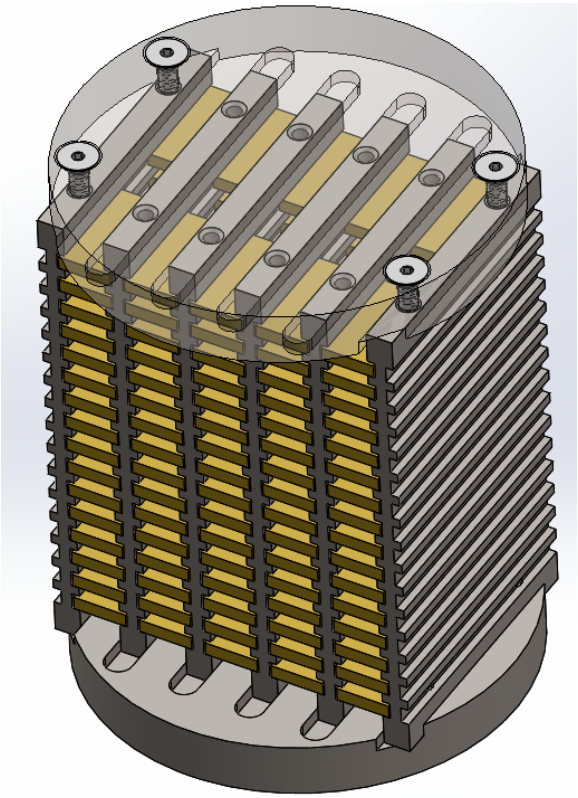

Figure 38: Initial Coupon Holder

The smaller chamber necessitated a smaller coupon holder and number of coupons that can be tested at one time. The number of individual components of the coupon holder went from eight to four pieces. The number of coupon slots was reduced from 160 to 36. This will increase the number of pressurizations required for large data sets but still provides many slots for specimens. Figure 39 and Figure 40 show the original and new designs. For reference, the original design is 5.5 inches tall.

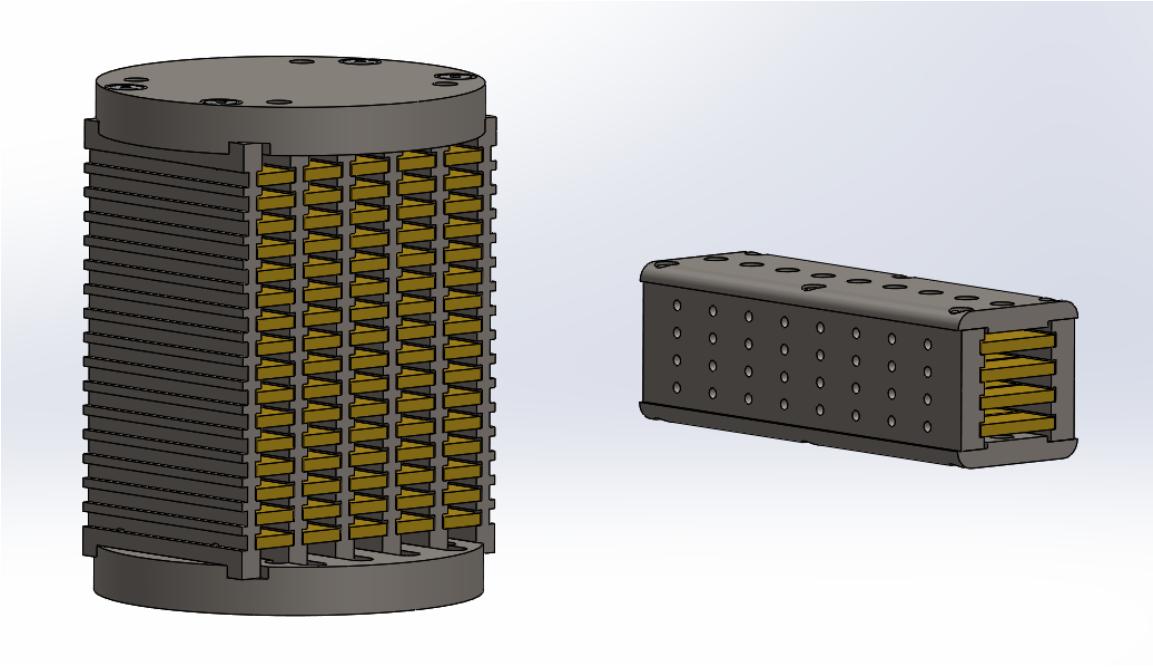

Figure 39: Initial Coupon Holder (Left) vs Redesigned Coupon Holder (Right)

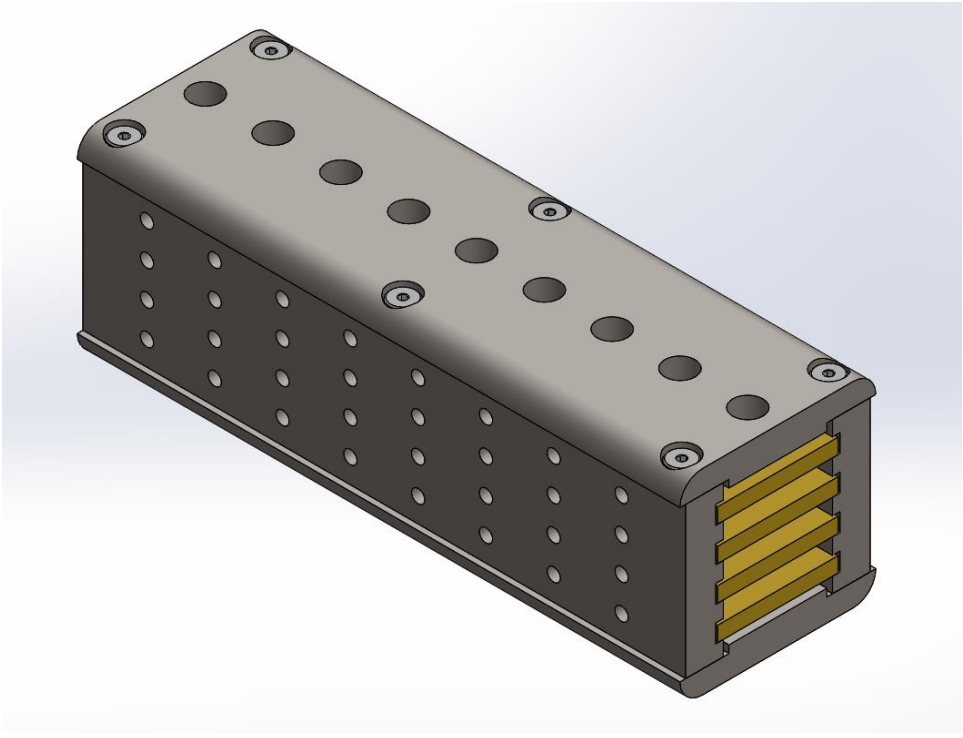

Figure 40: Redesigned Coupon Holder Closeup

For demonstration testing, the coupons were loaded into the holder and supported only by a narrow shelf on the edges. This provided minimum contact between the holder and coupon and

enabled the coupon to move freely. It was possible that the material would deform at pressure if not restrained. Figure 41 shows the coupon loaded with coupons for testing.

Figure 41: Coupon Holder Loaded with Material Coupons for Testing

3.6.2 Material Selection

The initial concept of material testing with the larger vertical loading chamber enabled the potential use of a wide range of materials. I planned to test eight samples of a variety of steels, aluminums, coppers, and composites with a variety of alloying compounds, tempers, and coatings. I selected COTS material stock because I wanted to see how normally procurable materials reacted.

When revising my experiment to utilize the smaller chamber, I reduced the material selection to four alloys and planned to reduce the number of initial samples to four samples of each to reduce costs. Two of the alloys selected were 110 multipurpose coppers in the annealed and half-hard temper. I selected copper because it is used in underwater cabling and subjected to large hydrostatic pressures. It is also possible to work harden copper. By pressurizing the alloys, I believed I could increase the hardness values of the annealed samples toward the half-hard samples. If the copper can be shown to harden under hydrostatic pressure, it may be a possible

reason for the failure of underwater cabling. The other two alloys selected were 1100 and 2024-T4 aluminums. I selected to see if alloys of the same base element but with different alloying compounds affected changes in the grain structures. The softer alloys were also selected over steel and other harder materials because they provided a better chance of showing change following the pressurization and allow me to determine whether normal methods of inspection could be used to find pressure-related changes.

Each material required different chemical stains and processes to reveal the grain structures. These stains could be wiped on the coupon surface or the coupon could be partially submerged and left to react. Acid neutralizer was used after the recommended reaction time to stop the reaction from continuing and over staining the surface. The copper alloys used a 50ml H_2O to 50ml NH_4OH + 10ml 3% H_2O_2 (immersed for 10 to 15 seconds) solution, which produces copper amines that are water soluble and washed away as part of the staining and polishing process. The lines this etches into the surface follow grain boundaries and are interpreted as boundary lines when viewed under a microscope. Other stains, like Klemm's Reagent, exist and can create colors on the grains but are not as common.

The aluminum alloys used a 100ml H_2O + 1 gram NaOH + 4 grams $KMnO_4$ (immersed for 45 seconds) solution, which produces Aluminum Hydroxide $(Al(OH)_4)^-$ and Manganese Dioxide (MnO_2). The MnO_2 forms films on the surface of the aluminum. Different thicknesses and concentrations appear as different colors along the grain surfaces and boundaries. Like copper stains, the color of these stains change based on orientation from the surface with relation to the viewing angle; therefore, if the surface topography changes, the colors will also change.

3.7 Summary

The test stand design represented most of the time spent for my research. A significant redesign from a vertical loading chamber to a horizontal chamber added time but created a less expensive, more easily handled and utilized chamber. Using common components, such as standard fittings and bore sizes, enabled me to purchase replacement parts and adapt the pressure chamber for additional experiments more easily. The remote operator capabilities protected the tester from dangerous high-energy failures. Safety was instrumental in the design of the chamber and was maintained throughout its use.

Chapter 4: Testing

4.1 Introduction

Preparing the laboratory for my experimental setup required repurposing a heavy-duty steel table already in the bunker to support the weight of the test chamber and equipment, which would exceed 500 pounds. The steel table also offered a readily available grounding point for electrical circuits if necessary.

To control the operations of the chamber for testing, a test procedure was written. The test procedure dictated the required equipment, safety precautions, prerequisites, casualty procedures, installation of the test stand, specific testing steps, data recording, and other pertinent information for the successful performance of test. The test procedure also allowed me to document my activities in case of repeated testing is desired by myself or others. During the pressurization cycles, personnel are not be allowed to enter the test bunker without appropriate Personal Protective Equipment (PPE) worn at all times. Appendix C provides the test procedure.

This chapter presents the general methods, processes, and details I used to execute my thesis testing. This chapter also provides my observations and findings from testing.

4.2 Goals

There were two main unknowns regarding the chamber's performance that needed to be resolved. First, during the initial pressurization, I needed to verify that the backup seals I selected would work sufficiently with the primary sealing surface to maintain pressure. My goal of the proof pressure test was to reach and maintain 30,000 psi for 30 minutes to allow time to make slow leaks visible. The goal was not to have a zero drop in pressure as a hold or tightness test might require, but it was to ensure that the pressure source could sufficiently maintain pressure. If this

goal was achieved, then I could state that the chamber is rated for pressures up to 30,000 psi for future testing.

The second unknown was the sensitivity of the intensifier needed for the material testing demonstration. As I mentioned, my intention was to mimic the dive of DeepSea Challenger. This required the ability to pressurize at a rate of approximately 100 psi/min. I had never operated this style of intensifier or had pressurized such a small volume to such a high pressure before, so I was uncertain if such a slow rate could be achieved.

My goal of the material testing demonstration was to show that the high-pressure chamber could be used to investigate the properties of metals post exposure and to develop techniques for comparison.

4.3 Proof Pressure Test

The purpose of the proof pressure test was to ensure the test stand design could safely operate at the selected high pressure. The testing followed Paragraph D.3 of the test procedure after the actions of Paragraphs D.1 and D.2 were completed to assemble the test stand systems and perform a low-pressure air test to prove component functionality. For the setup of the proof pressure test the relief valve is installed and unisolable from the chamber. The relief valve setpoint is set at 32,100 psi or approximately 107% of the test pressure. As previously mentioned, this is an industry practice to enable short surges in pressure from the pressure source near the test pressure without risking damage to the system. The relief valve is also sized such that it can discharge the full cycle volume of the pressure source.

In accordance with my test procedure, water was supplied to the system through pump and air was vented by opening the vent valves until water issued and then a plug at the top of the chamber was loosened until water began to issue and then retightened. This removes as much air

from the system as possible to enable a steadier pressurization as air is compressible but water is generally considered not. The system was then pressurized to 250 psi and checked for leaks after a short hold period. Any leaking joints can be tightened at this pressure without risk of damage. Following a successful hold at this pressure, pressure was increased in 500 psi increments and held for 5 minutes until 30,000 psi was reached. As leaks were found during the 5-minute hold, pressure was relieved to below 250 psi before tightening the joint and then repressurized. Joints under pressure, specifically threaded joints, can be damaged if manipulated under high pressure. The common practice for initial system pressurizations is to take special care to ensure none of these joints is damaged and can be proven to hold pressure.

During this pressurization I observed that the pressure transducer was no longer tracking with the mechanical gauge. The mechanical gauge was my primary testing instrument, so I did not need to stop testing. The pressure appeared to stop tracking around 15,000 psi, and I believed this was due to the inability of the power source to output the required amperage for the pressure transducer to function properly at the elevated pressures. This required modifications to the transducer power supply circuit (previously described in Section 3.3.4) which proved to be successful during the performance of my demonstration material testing.

At 30,000 psi, the system was held for 30 minutes to enable small droplets to form from joints as well as for deformation of components to reach an observable amount. I selected a 30-minute hold based on my experience in hydrostatically testing water distribution systems. Figure 42 shows the primary test gauge during this hold.

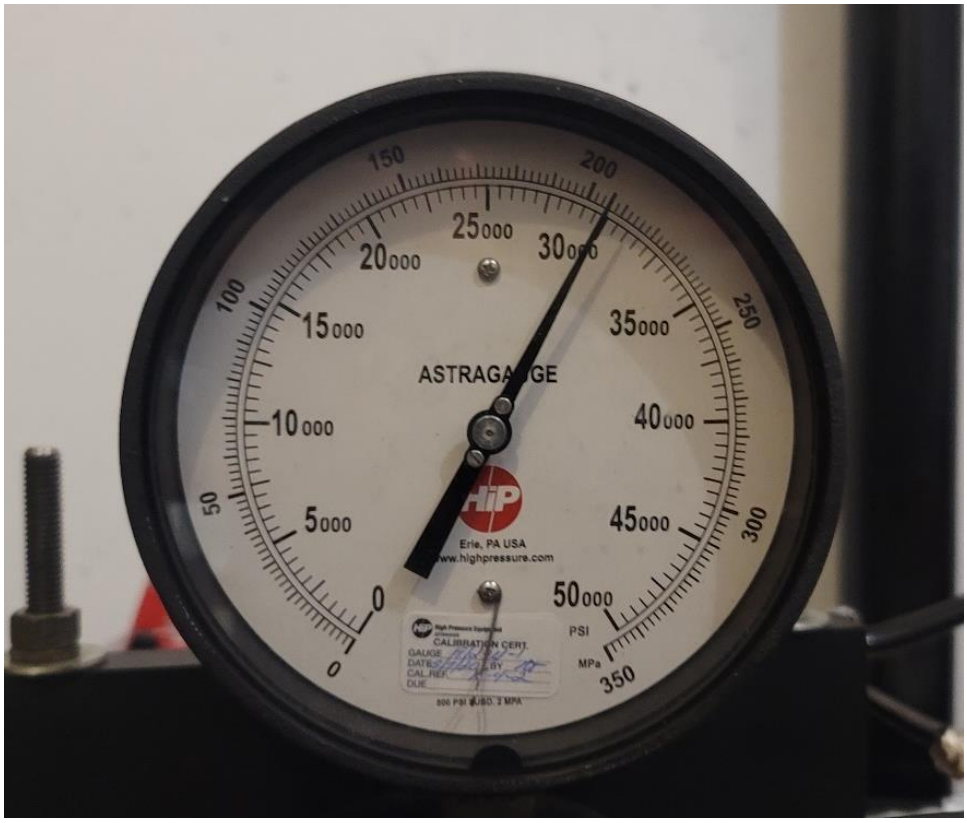

Figure 42: Proof Pressure Test Primary Pressure Gauge at Test Pressure - 30,000 psi

During the performance of my proof pressure test, small mechanical joint leaks were observed at 3,500 psi and 15,000 psi that required depressurization and tightening but the test stand was able to reach and maintain pressure easily at 30,000 psi with no signs of significant leakage or deformation of components.

Following the 30-minute hold, pressure was slowly depressurized at approximately 500 psi/min until the system was at atmospheric pressure. The system was then drained, and the lid and plug were removed. At this time, a very small amount, an estimated 3 drops or water, were identified trapped between the lid and chamber body. The surface tension of water appeared to have been sufficient to hold the drops in the small gap until the lid was removed. As mentioned previously, this is an acceptable leak by as the leak rate was well below the pressurization rate capable from the pressure source. However, this finding does require that I investigate other

sealing methods for improvements to the chamber and confirms the backup seals being used have a pressure rating below 30,000 psi. As mentioned in Section 3.3.3, this was a known possibility because the manufacturer rated the seals for a lower pressure. However, the pressure rating was based on a rotating sealing surface and elevated temperatures. I was comfortable using the seals for future testing because the failure was not catastrophic and no damage to the equipment or danger to the operator appeared to be a result of the leak by.

Further internal and external inspection of the chamber and components did not indicate and permanent deformations or failure of components from the test, meaning the chamber was safe to operate at 30,000 psi for future tests.

4.4 Coupon Preparation

After successfully completing the proof pressure test and receiving approval to conduct the chamber demonstration test, I prepared the coupons of my selected materials. Each alloy was given a material designator, and each sample was labeled with a combination of the designator and sample number, *XX-YY*. *XX* represents the material designator, and *YY* represents the sample number. The test procedure outlines the coupon preparation, which can be replicated in the future. The material for the coupons was purchased from a supplier's normal stock without any special treatments or conditions. The material stock was two inches wide x 24 inches long and a stock thickness of 0.125 inches. The coupons were then cut into their final shape of 0.5 inches x 1 inch x 0.125 inches +/- 0.020. Figure 43 shows the final shape and size of the coupon.

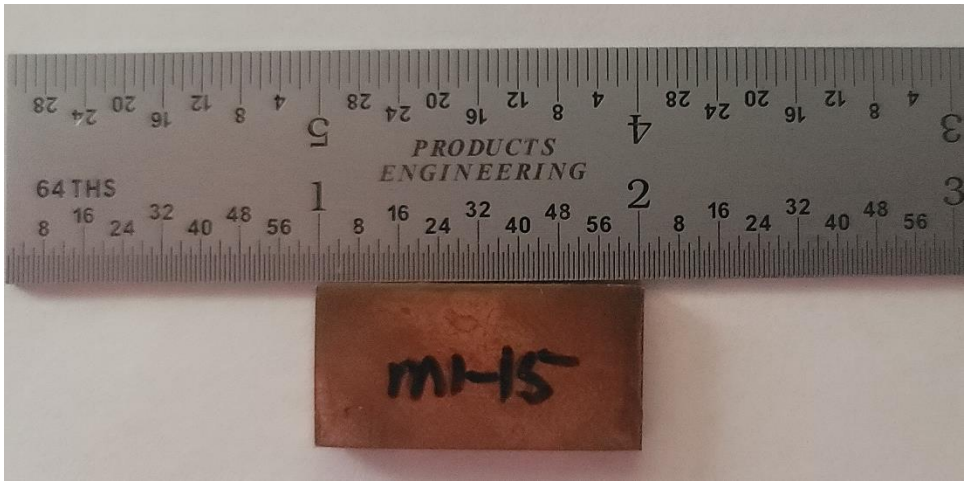

Figure 43: Test Coupon Shape and Size

One long edge was selected to be the polished surface and then sanded progressively from 220 grit to 10,000 grit. Final polishing and staining, as described in Section 3.6.2, were performed by Element Labs in Tulsa Oklahoma. The four coupons for each allow were encased in an acrylic puck for polishing, staining, and microhardness testing. Figure 44 shows this setup.

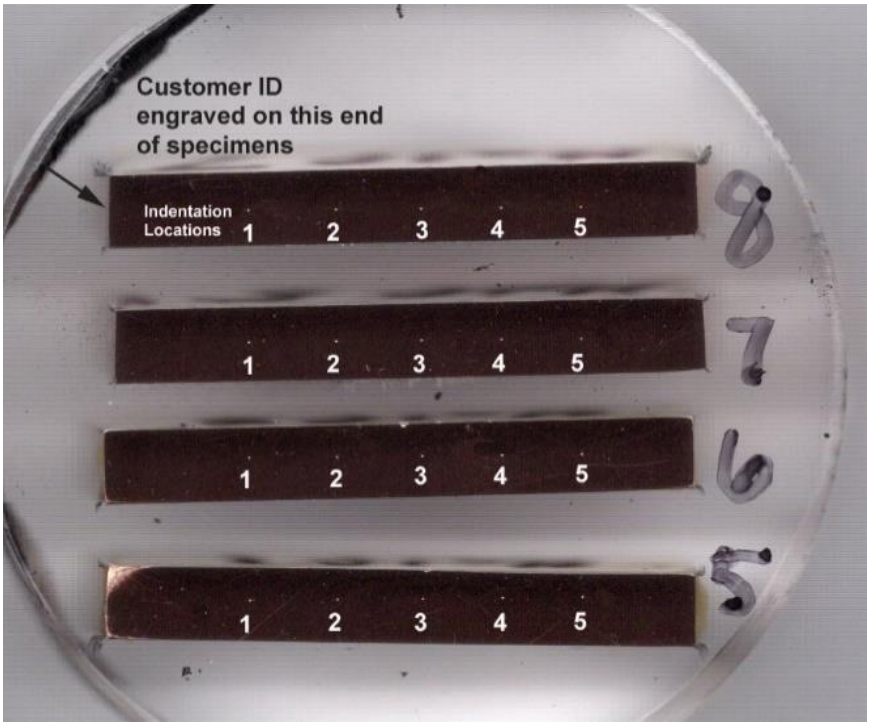

Figure 44: Coupons Encased in Acrylic Puck (Copper 110 – Annealed Shown) Pretest

Figure 45 shows the 220-grit surface of the copper and aluminum that were sanded, polished, and etched.

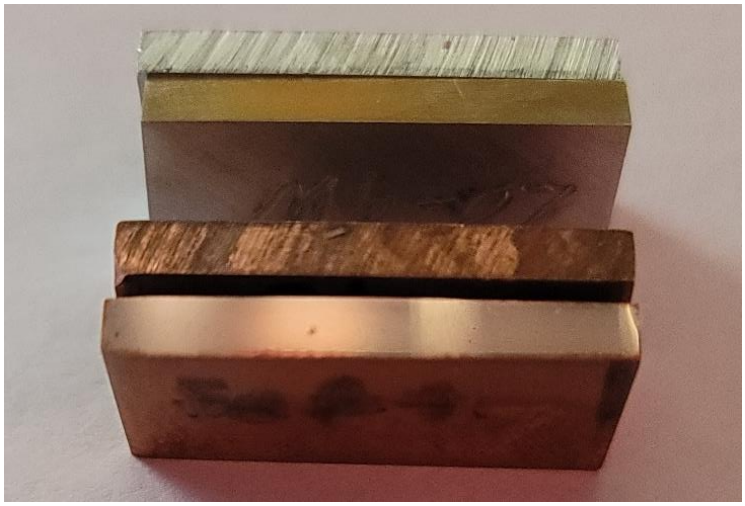

Figure 45: Comparison of 220-Grit Sanded Surfaces and Polished and Etched Surfaces of Aluminum (Top) and Copper (Bottom)

A Struer's TegraPol-31 Auto Polisher was used to polish the pucks using a specific force and duration as dictated by the manufacturer's recommendations for each alloy. Figure 46 shows the polisher.

Figure 46: Struer's TegraPol-31 Auto Polisher - Stock Photo [25]

To support maintaining cleanliness and the integrity of the polished surface, several coupon holders were designed to hold and organize the coupons. The holders were 3D printed in black PLA filament and are shown in Figure 47.

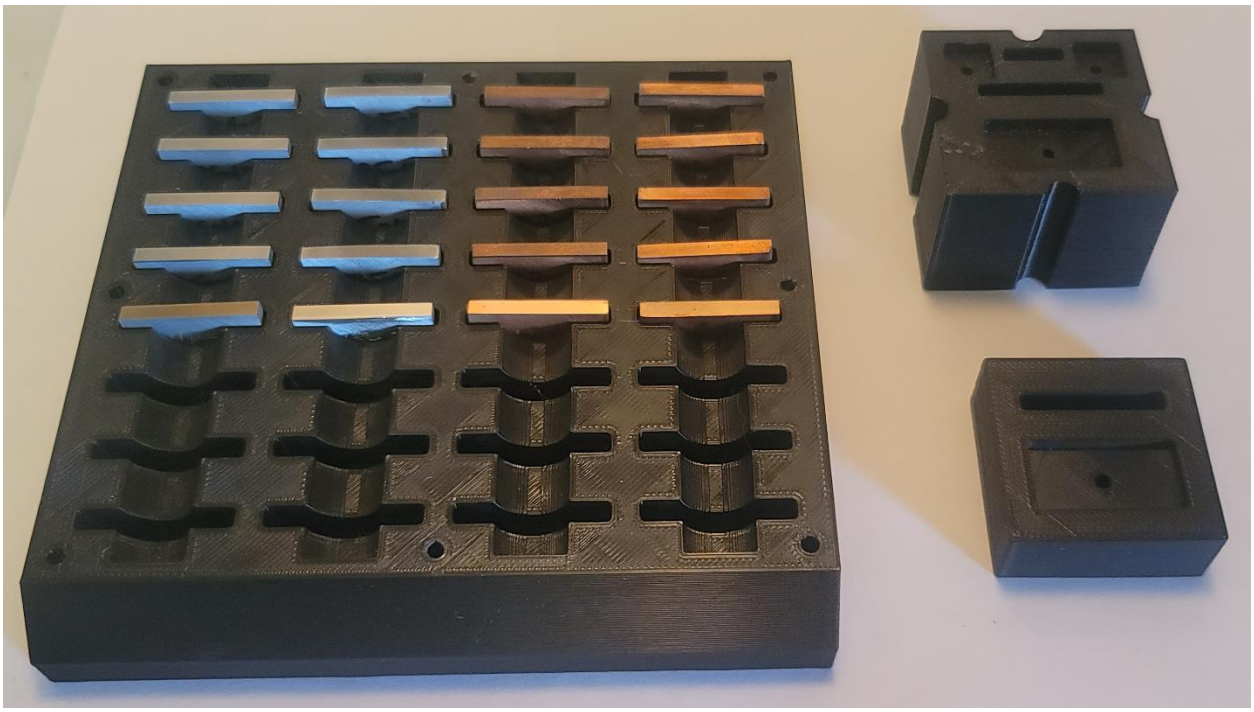

Figure 47: Coupon Holders

The larger holder held sets of coupons and had a protective lid that can be secured over the coupons to protect them from surface damage and moisture. The taller square holder could be used to image any side of the edges of the coupons as desired. The shorter, holder can be used for imaging the large flat side and long edge side only. The shorter holder used less material and was easier to produce.

4.5 Microhardness Testing

Microhardness was performed before and after pressurization IAW ASTM E384-17, Standard Test Method for Microindentation Hardness of Materials. I selected a Vickers microhardness indenter as is standard practice in industry when the materials are not brittle.

Five indentations were made across the surfaces of each coupon to provide an average hardness for each sample as well as five data points for direct comparison posttest. These indentations can be seen in Figure 44 above. Later these indentations were used for location marking during imaging to provide a point of reference for inspection of the same area of the surface before and after pressurization. Figure 48 shows the shape of the Vickers indentation tip.

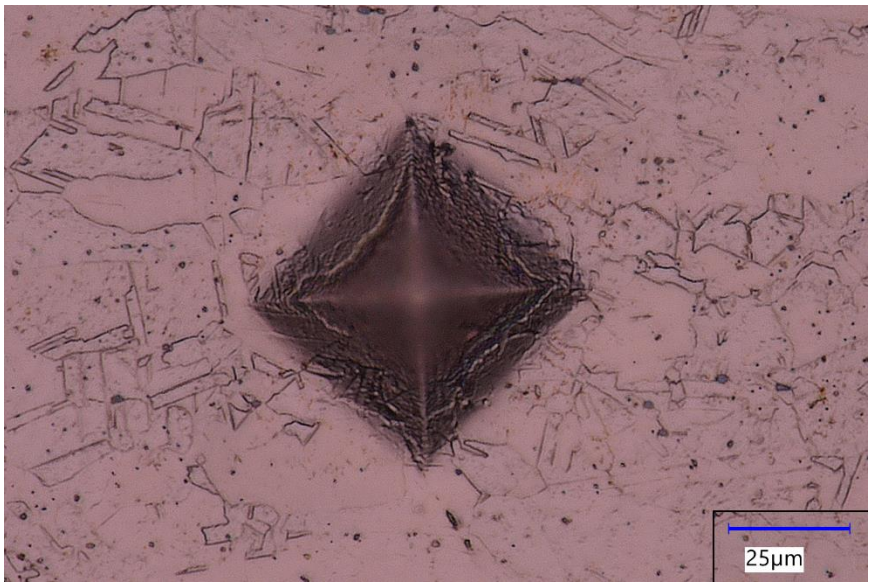

Figure 48: Vickers Hardness Indentation at 1000x (110 Multi-Purpose Copper - Annealed (M1) Shown)

For the microhardness testing, Element Labs utilized a Affri Wiki 200 JS 2 Indenter and Clemex Software. Figure 49 shows the indenter.

Figure 49: Affri Wiki 200 JS 2 Indenter - Stock Photo [26]

The indentations from the pre pressurization test indentations were lost following polishing for the post pressurization indentations however using computer mapping they indentations are in the same relative vicinity for both rounds of testing. One change that occurred following the pressurization test was that only three coupons of each alloy was retested so that one coupon for each alloy can be used for detailed 3D topographic comparison. The topography was altered during the polishing process and therefore a direct comparison or before and after surface features would not be possible. Chapter 5 discusses the data obtained from microhardness testing in detail.

4.6 Imaging

Following the pretest microhardness testing, each sample was imaged to capture the stained grain structure and 3D topography. The goal of this imaging was to determine if imaging could identify changes in material structure following pressurization. A change in grain structure or surface topography may indicate that at pressure the mechanical properties and performance were changed. Like how elevated temperatures change the design ideologies for proper function, a change in performance due to elevated pressure may require a similar change in design ideology.

Imaging was performed at the Samuel Roberts Noble Microscopy Lab (SRMNL) on a Keyence VHX-7000 ultramicroscope. The SRMNL houses several different pieces of equipment including Advanced Light - Confocal Microscopes, Scanning Electron Microscopes (SEM), Transmission Electron Microscopes (TEM), and Specimen Preparation Equipment. The VHX-7000 is a fully automated optical digital microscope with magnification from 20x to 6000x. The companion computer setup provides software for detailed picture analysis and comparison at any level. Figure 50 shows the ultramicroscope.

Figure 50: Keyence VHX-7000 Ultramicroscope - Stock Photo [27]

To limit the amount of surface to be imaged, I focused on the area around the center Vickers hardness indentation. This marker would most likely survive the pressurization cycle even if there is significant deformation or changes of surface topography. As magnification is increased, I selected regions with easily-identifiable characteristics to improve the chance of locating the same location for posttest imaging. Figure 51 shows one imaging set for example. All the images taken are orientated in the same way. The x-direction corresponds to the lengthwise direction of the

coupon and is perpendicular to the rolling direction of the stock material. The y-direction corresponds to the thickness direction and is also perpendicular to the rolling direction of the stock material. The z-direction (perpendicular to the images) is parallel to the rolling direction of the stock material.

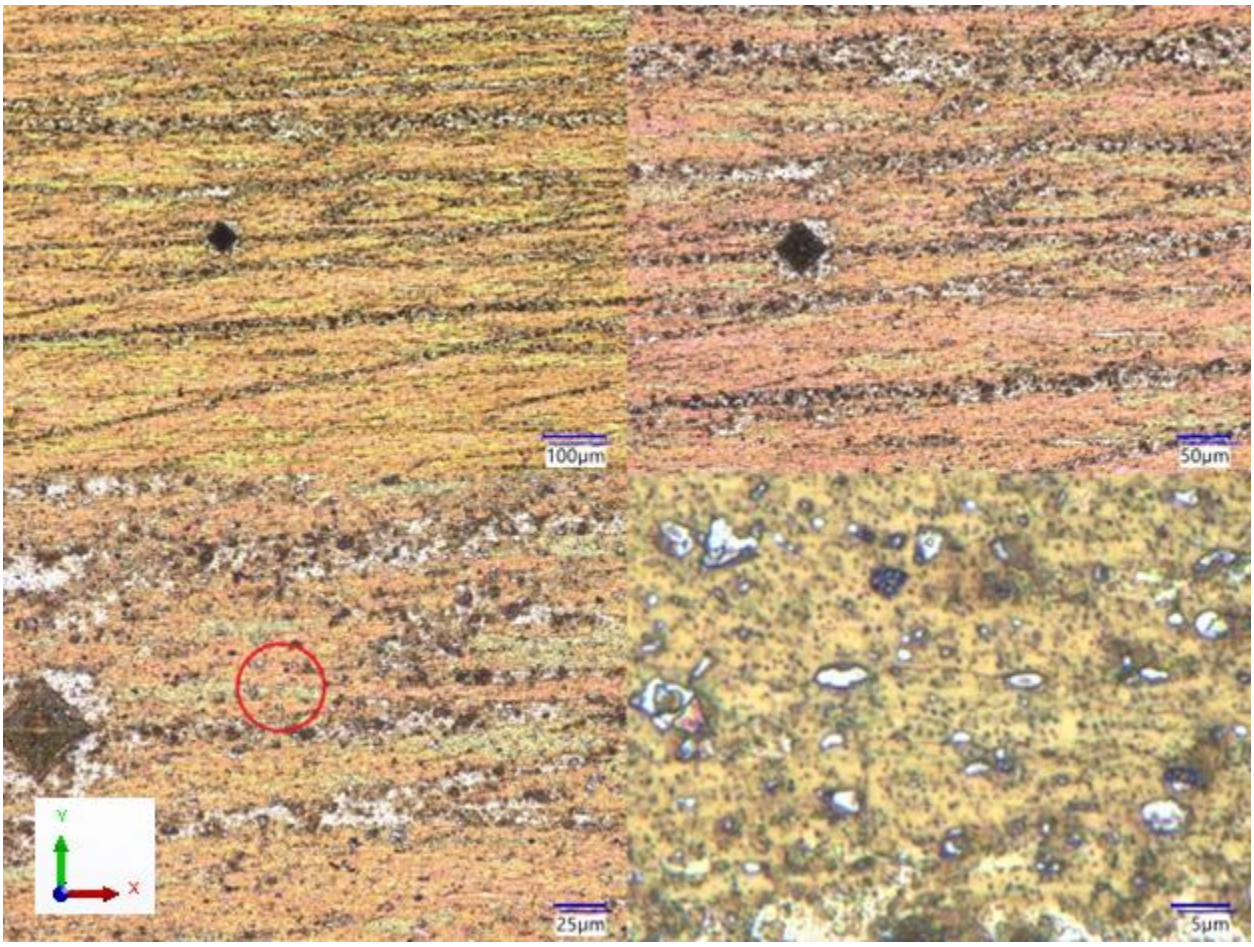

Figure 51: 2024-T4 High Strength Aluminum (Sample M6-07) Pretest Coaxial Imaging Steps

This image set for 2024-T4 Aluminum alloy prior to testing shows the progression of imaging from 300x to 500x, 1000x, and finally 6000x. These images show the colored areas created by the stain and reveal grain structure. The colors are based on light angle, thickness of the film, and topography. The changes in color resulted from the light intensity on specific areas

increasing in tandem with increasing magnification. The elevated white surfaces were most likely surface plateaus of aluminum that did not react with the stain.

Figure 51 shows the specimen under coaxial light, meaning the light on the specimen was being emitted through the lens itself. Figure 52 shows the specimen illuminated by a full ring light method where the lighting is from a ring of light emitting diodes (LED) arranged around the outer edge of the lens. The coaxial light revealed the stains more clearly, but the full ring light showed the surface topography more effectively. The images in Figure 52 are of 110 Copper in its annealed state pretest. The top image is using the coaxial light and the bottom image is the full ring light.

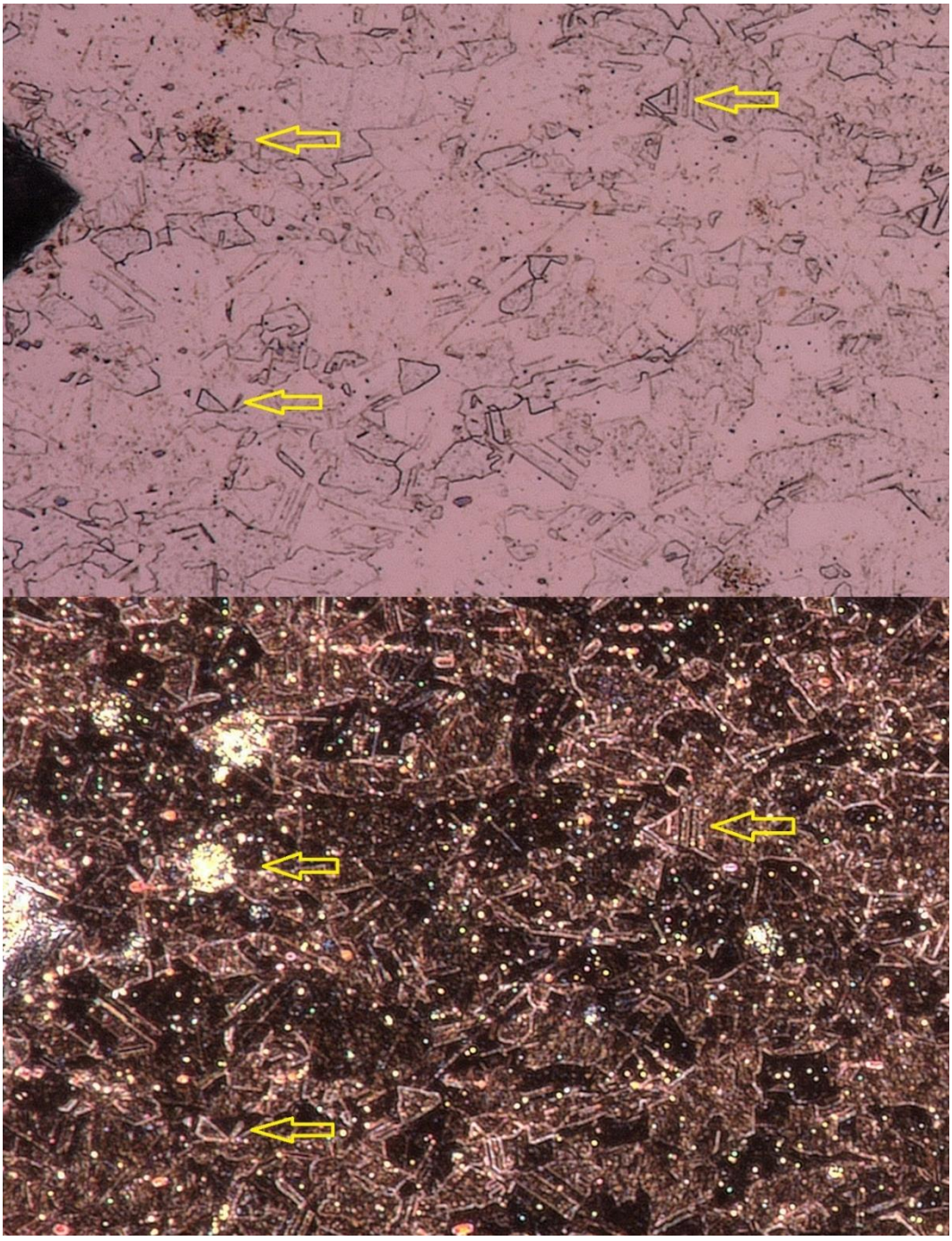

Figure 52: 110 Multi-Purpose Copper - Annealed (Sample M1-07) 500x Pretest, Coaxial Light (Top) and Fully Ring Light (Bottom)

2D images of each of the 16 sample coupons were crated before and after pressurizing at 100x, 300x, 500x, 1000x, 2000x in both coaxial and full ring lighting as well as at 4000x and 6000x in coaxial lighting only. The higher magnification is only available in coaxial lighting. 3D

images were also taken of one of each alloy coupon sets at 6000x. I compared each coupon's surface before and after testing to identify if optical light imaging could be used as a method of identifying changes in the grain structure which would indicate possible material property changes. Chapter 5 discusses the findings of the image analysis.

4.7 Chamber Demonstration –Dive Simulation High Pressure Material Test

As stated in Chapter 1, to demonstrate one possible use for my pressure chamber, I simulated the dive of the DeepSea Challenger submersible to the bottom of Challenger Deep on March 26th, 2012 on my selected materials. I then attempted to determine if there were any changes to material properties after completing the dive indicating a possible change in material properties while the material was at test pressure. This is based on the assumptions that if a materials structure changes, there is a good probability of property changes and if there is a residual change with no pressure, there must have been a related change at the elevated pressure.

The operation of the test stand through the dive was controlled using the steps listed in Paragraph D.4 of my thesis test procedure. The setup is identical to the proof-pressure test except I included the 0-30,000 psi gauge as my primary pressure indicator and the primary relief valve was swapped out to one that is set at 17,100 psi. My target simulated depth was 35,756 feet which equated to a pressure of approximately 15841.9 psi. As described in Section 1.4, my goal was to perform a 3-hour descent followed by a 3-hour hold at test pressure and a one-hour ascent. My target descent rate is 100 psi/min and my target ascent rate is 250 psi/min. The mechanical gauge is incremented at 200 psi so these rates are only goals and not requirements for a successful test.

After loading the chamber with my materials and sealing the plug and lid in accordance with my procedure I prepared to pressurize my chamber. Helium was used as my high-pressure fluid instead of air because ideal gasses are more effective as pressurization mediums than mixed

gases such as air. This is due to their predictable compressive properties and moisture. Other mixed gasses do not precipitate out at pressure. Ideal gasses are also non-reactive with metals. Surface reactions could interfere with the posttest inspection methods used.

Control air and Helium sources were supplied to the test stand systems, and the pressure of the chamber was increased to 250 psi. A brief leak inspection with water and soap spray revealed no leaks. Pressure was then increased to 500 psi, and another inspection was performed. It is common for manned submersibles to dive to a shallow depth for a period of time and ensure nominal operations of all systems prior to continuing to deeper depths. I then began to pressurize the system to simulate the descent at approximately 100 psi/min. This rate was achieved with one cycle of the intensifier piston at lower pressures so I was forced to operate the intensifier for one cycle and then wait on the next cycle of pressure would have increased too quickly. One of these pressurization periods lasted approximately three seconds for a cycle of the intensifier and 57 seconds of waiting. This means the pressurization was not a truly constant rate but I believe it is an acceptable simulation given the limitations of how intensifiers operate.

The 0-30,000 psi gauge, designated G-1 in the test procedure and Figure 32, was my primary pressure indicator however the pressure transducer was tracking with the gauge for the duration of the dive with one exception. The pressure transducer signal was not steady whereas the gauge showed no signs of fluctuations in pressure such as a bouncing needle. The milliamp signal read by the DAQ fluctuated steadily around the value shown by the manual gauge. The range of fluctuation appeared to be +/- 300 psi with each one hertz reading being different. At lower pressures this is significant but at higher pressures this is a small deviation. I believe the fluctuation was caused by noise in the signal from the pressure transducer. The wires from the control panel to the pressure transducer passed close to power and other signal cables to pass

through the concrete walls. This can cause noise that I did not account for. Better cable shielding can mitigate this in the future. Noise may also be attributed to the power supply or the voltage regulator used to step the voltages down from 120 VAC to 24 VDC and then to 10 VDC for use by the transducer. It is possible that the current fluctuates due to these processes. A better and dedicated 10 VDC testing power supply may be used in the future to help as well. However, even with the fluctuations, the pressure transducer tracked with the manual gauge and recorded the entire dive simulation sufficiently.

The raw data track from the pressure transducer for pressure is shown in Figure 53. The raw data was sampled at one Hz by the DAQ resulting in approximately 32000 data points over a 9-hour period. The data has clear pressurization, hold, and depressurization stages. The thickness of the graph line is caused by the noise fluctuation in the signal. The green portion of Figure 53 corresponds to the graph in Figure 54. The details span of Figure 54 makes the pressure fluctuations more apparent and the nominal +/- 200 psi fluctuation around a centralized trend line is visible.

Figure 53 shows above 12,000 psi there is a steady rise and fall of the average pressure. This corresponds to the main facility air compressor cycling on and off due to overheating and thermal tripping of the internal motor thermal protection switches. The fact that the pressure did not hold as required for a hold test is likely due to small leak by of the sealing surface and backup seals or leakage in a location that I could not identify with soap bubbles. Helium has a very small molecular size and no viscosity compared to water so some leakage was expected but the intensifier should have been able to compensate and maintain pressure had the facility air compressor not been thermally cycling. As the motor cycled on and off, the chamber pressure trend would cycle up and down. There was no solution for this during the dive and I chose to continue

with the test to complete the experiment. I believe the average pressure is still sufficient for my purposes of determining if pressure affects material performance. It can also be seen in this data that I was unable to reach a sustained pressure of approximately 16,000 psi. While the noise in the pressure transducer signal made it difficult in the identify a definitive maximum pressure, the mechanical gauge, shown in Figure 55, read approximately 15,400 psi for most cycles prior to the air compressor cycling off. I consider this sufficiently close to my goal pressure to be consider a successful dive pressure and I am confident with a different air compressor with higher performance capabilities I would have been able to reach my target pressure. 15,400 psi represents approximately 34,750 ft below sea level.

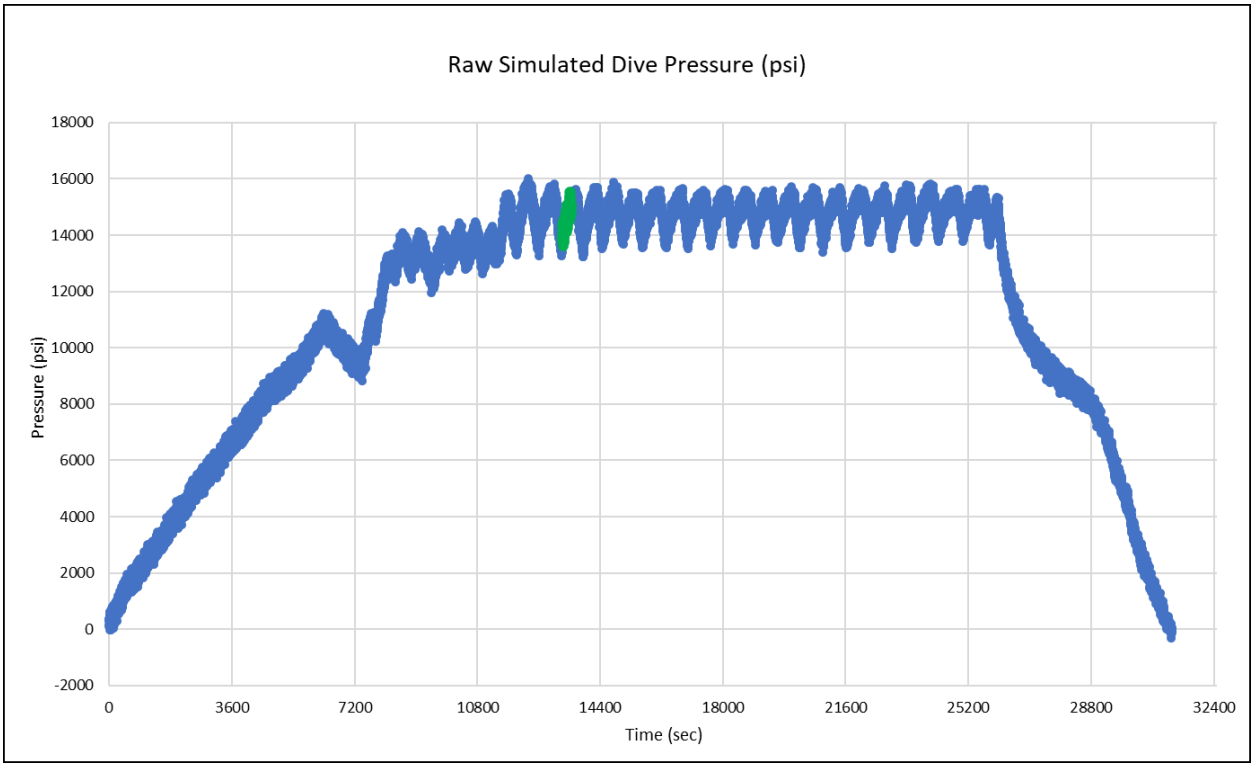

Figure 53: Raw Simulated Dive Pressure (psi)

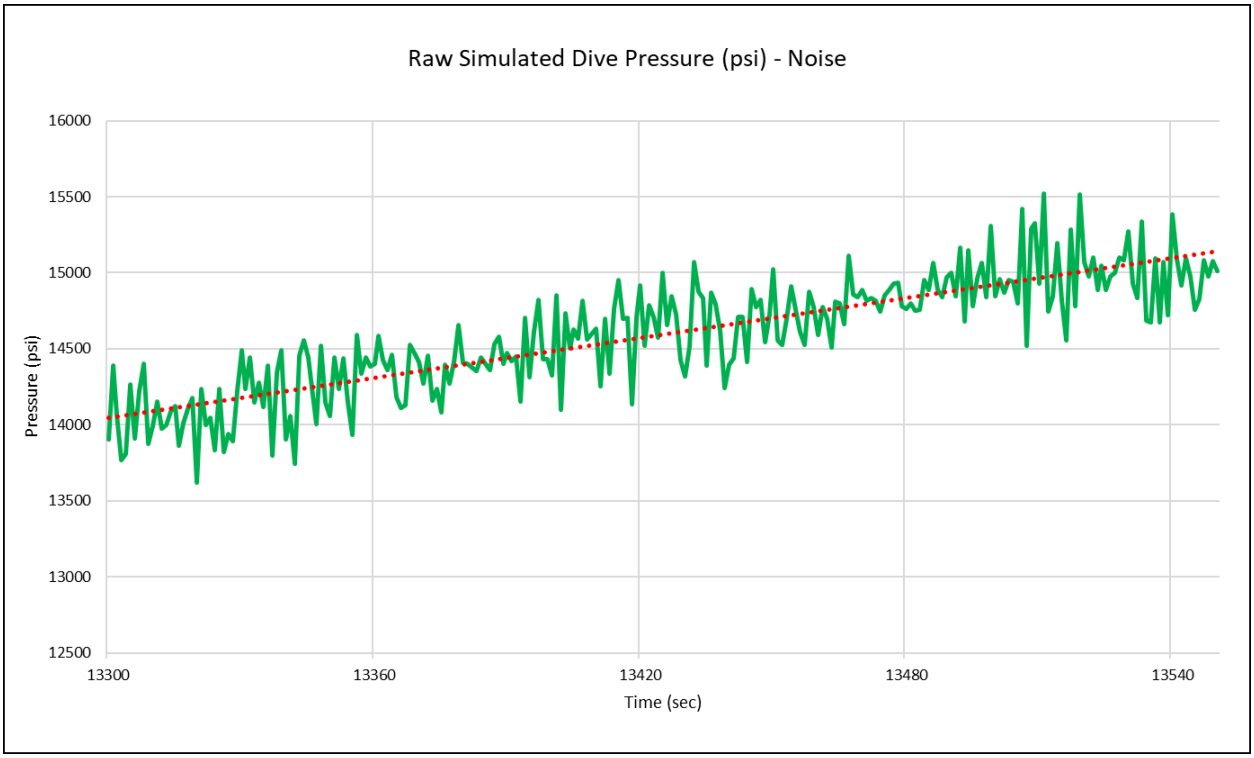

Figure 54: Raw Simulated Dive Pressure (psi) - Noise

Figure 55: Mechanical Gauge Estimated Maximum Pressure

Section 5.2 analyzes how the simulated dive compared to my actual testing goals.

4.8 Summary

My pressure chamber and test stand were able to complete testing and show its usability for providing a high-pressure environment for testing. My proof-pressure test experimentally proved that the chamber can be used safely used for maintaining hydrostatic pressures up 30,000 psi. I demonstrated methods of testing material samples and simulated a dive to Challenger Deep showing that the chamber can be used to duplicate real-world conditions and situations. Several areas of improvement were identified with regard to improving the quality of the pressure transducer signal and the sealing methods for both liquids and small molecular gasses such as Helium but I did not identify any fundamental flaws in the chamber design or test stand that cannot be addressed with simple modifications. Chapter 6 will discuss these modification and possible ways forward with the chamber.

Chapter 5: Demonstration Test Results and Analysis

5.1 Introduction

I gathered data on the performance of my pressure chamber and test stand as well as during the demonstration test to determine if methods can be used to identify if high pressure has a lasting effect on material properties. Appendix D contains the Excel spreadsheets with the raw data and calculations discussed here.

5.2 Pressurization Performance Analysis

To determine if my chamber succeeded as an apparatus for high-pressure testing, I performed two different pressurization cycles. During the proof-pressure test I successfully reached and maintained a pressure of 30,000 psi. An inspection of the test stand and chamber at pressure revealed no indications of deformation or precursors to failure. Following depressurization, I removed the plug and inspected the primary sealing surface and backup seals for signs of damaged or failure. Though a small amount of water was able to leak by my sealing components, no evidence of permanent failure or damage was observed, but the Cerakote coating on the 60-degree taper surfaces had lost adhesion. Cerakote has no pressure rating, so this failure was not concerning. The removal of the coating would enable joints to be lapped together again, creating a more effective metal-to-metal seal. The backup seals showed no signs of nicks or permanent deformation when compared to an unused seal. Some changes in mechanical properties may exist; however, none were observed with the methods at hand. The seals were inexpensive and could be replaced after each pressurization cycle if desired. There were no indications of thread deformation on any threaded fastener.

The demonstration test consisted of a simulated dive to Challenger Deep and its effect on materials. To better understand and analyze the performance of my simulated dive and test stand, I separated out five distinct sections of my test sequences. The sections are based on manual notes taken and activities that were required by me to complete the test. Figure 56 shows the sections color coded with their associated trendlines for reference.

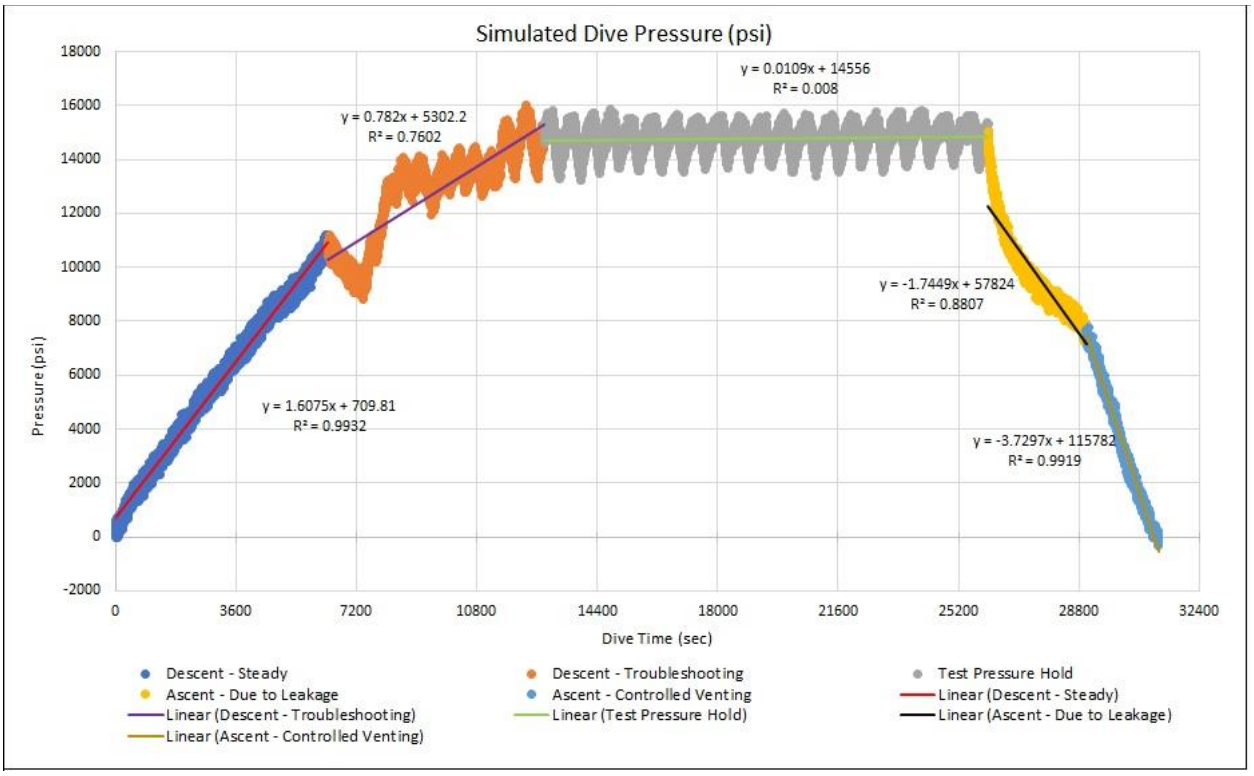

Figure 56: Simulated Dive Pressure (psi) - Separated Sections

The dark blue section between start and approximately 6,000 second is the initial pressurization sequence where I maintained a pressurization rate of approximately 100 psi/min. The start of the orange section between 6,000 and 12,500 seconds indicates when I observed a small leak in the video feed of my chamber as indicated by bubble formation on a joint. The leak came from one of the mechanical joints on the upstream side of the manual vent valve. Pressurization was secured, and the pressure source was isolated remotely. I did not vent the system due to the risk of ruining the samples for comparison. Wearing ear, and face protection, I

entered the bunker and placed a wooden board between myself and the joint to be tightened, tightened the joint at pressure. The main risk of this process was reducing the life of the threads, not catastrophic failure. Since fittings could be replaced and failure would cause the pressure to be vented away from where I stood, I determined that the risk of component failure and injury was low enough to proceed to preserve the integrity of the test. After retightening the joint and rechecking the joint for leakage, I returned to the remote operator station and recommenced pressurization. The pressure increased until the air compressor began thermally cycling, as indicated by a small plateau around approximately 13,000 psi. I allowed pressure to cycle around this point and began troubleshooting the cause and determining possible solutions. The facility air compressor pressure regulator was set well below its normal maximum operating pressure. After adjusting the pressure regulator up, the pressure rose and the cycle stabilized around approximately 14,500 psi as indicated by the average of the pressure transducer with a maximum indicated at approximately 15,4000 psi by the mechanical gauge.

The gray portion between 12,500 and 26,000 seconds of Figure 56 indicates my hold period. The hold period was approximately 3.5 hours as opposed to three hours due to pressure cycling away from the maximum level during the hold. The yellow section beginning at 26,000 seconds is the start of my simulated ascent sequence. I secured the intensifier and allowed the leak present in the test stand to allow pressure to drop. I did this to determine approximate point where pressure may stabilize indicating leakage stopped and because I did not want to restart pressurization periodically to slow the depressurization as this could mask my attempt at determining when the leakage stopped. The leak rate was slower than my goal ascent rate and tracked as you would expect a normal leak rate to track with a high rate of leakage that slowed as pressure is released. Pressure began to stabilize at approximately 8,000 psi so I began controlled

venting of the system indicated by the light blue section starting at approximately 29,000 seconds. My controlled venting attempted to vent at a rate of 250 psi/min and my average rate of controlled venting was 225 psi/min. My ability to vent at a rate close to my goal indicated that my setup is capable of controlled venting when operated properly.

When pressure had returned to ambient, air pressure was secured to the air operated control valves, the Helium source was secured, and the coupons holder and coupons were removed from the pressure chamber in accordance with my test procedure.

The problems with the support systems and unknown leakage prevented the demonstration from matching the intended rates of pressure change or durations. However, the pressurization cycle achieved demonstrated the possible chamber uses for future experimentation as shown in the comparison of the dive track in Figure 57. The approximated real-world dive for the DeepSea Challenger is shown on the left as a green line and the calculated simulated depth from my pressure transducer is shown in blue on the right. The dive tracks have similar rates of changes, trends, and overall timeframes.

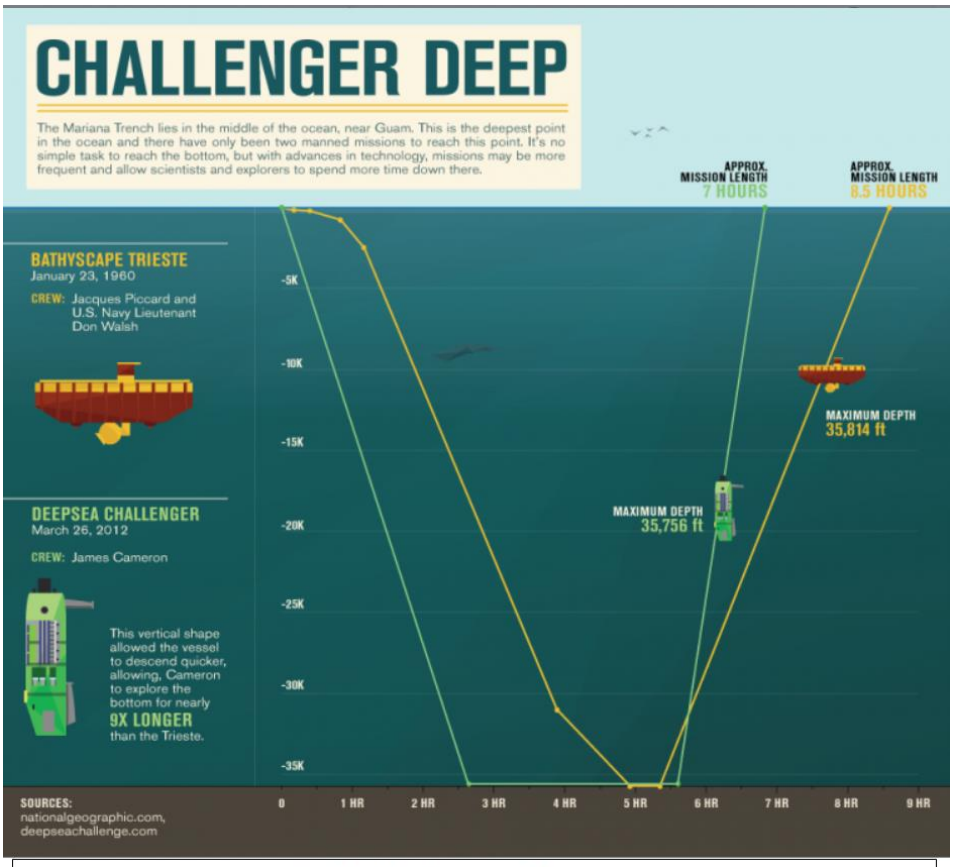

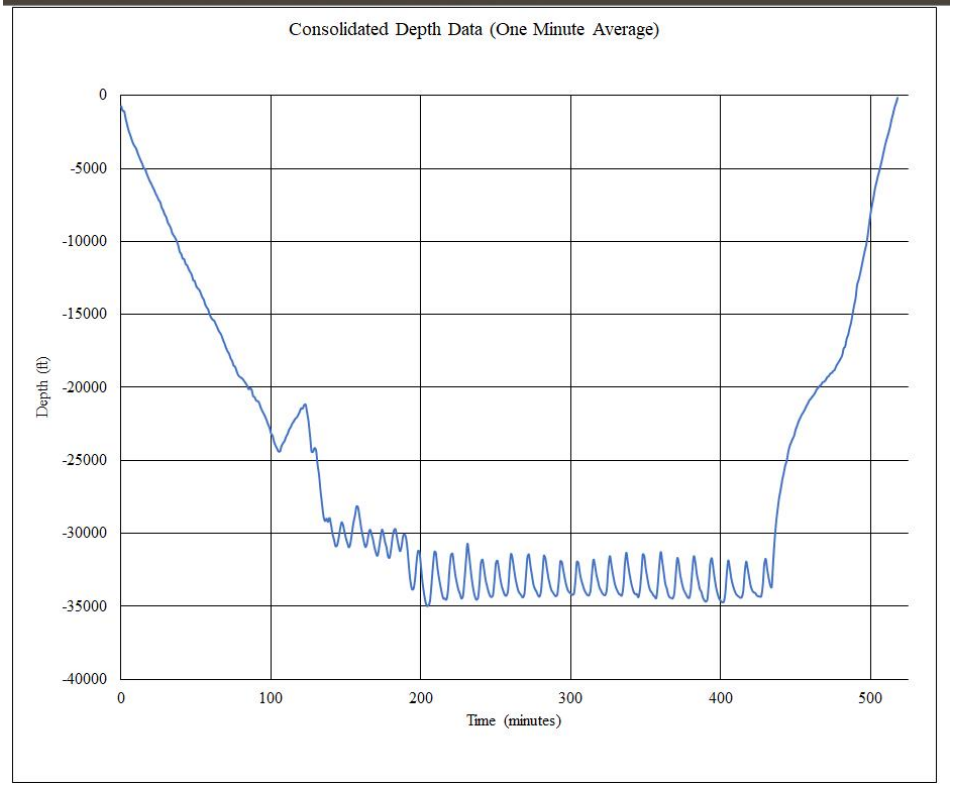

Figure 57: Dive Track Comparison [2]

An inspection of the components of the chamber and test stand following the simulated dive showed no signs of failure or permanent deformation. The slow leak that could not be found will need to be addressed for future experiments and may need to be addressed with improvements described in Chapter 6.

5.3 Manual Measurements Analysis

I used four-inch Mitutoyo calipers (Model 505-629) to measure basic dimensions to detect structure changes in the coupon samples. These calipers are incremented in 0.001 inches, which enabled estimates to 0.0005 inches. The error for such hand calipers was approximately 0.002 inches; however, I used them because they are very common in industry inspection tools. I measured the length (L), width (w), and thickness (T) in the same manner and in the same location for each coupon before and after pressurization. A total of three measurements taken on four unique specimens of each alloy provided 12 data points for my analysis of each material. Table 1 through Table 4 list these measurements.

Table 1: 110 Multi-Purpose Copper - Annealed (M1) Dimensional Data

Designator	M1								
Material	110 multi-purpose copper - Annealed								
	Pre-Test			Post-Test			Difference		
Sample Number	L	W	T	L	W	T	L	W	T
01	1.0015	0.5140	0.1250	1.0015	0.5140	0.1250	0.0000	0.0000	0.0000
03	1.0005	0.5130	0.1250	1.0005	0.5125	0.1250	0.0000	-0.0005	0.0000
05	0.9970	0.5190	0.1245	0.9970	0.5195	0.1250	0.0000	0.0005	0.0005
07	1.0020	0.5185	0.1255	1.0020	0.5170	0.1255	0.0000	-0.0015	0.0000

Table 2: 110 Multi-Purpose Copper - 1/2 Hard (M2) Dimensional Data

Designator	M2								
Material	110 multi-purpose copper - 1/2 hard								
	Pre-Test			Post-Test			Difference		
Sample Number	L	W	T	L	W	T	L	W	T
01	1.0010	0.5075	0.1255	1.0015	0.5075	0.1250	0.0005	0.0000	-0.0005
03	1.0025	0.5070	0.1260	1.0025	0.5065	0.1260	0.0000	-0.0005	0.0000
05	1.0050	0.5150	0.1260	1.0050	0.5145	0.1260	0.0000	-0.0005	0.0000
07	1.0040	0.5180	0.1255	1.0035	0.5155	0.1245	-0.0005	-0.0025	-0.0010

Table 3: 1100-H14 Hardened Easy-to-Form Aluminum (M5) Dimensional Data

Designator	M5								
Material	1100 Aluminum								
	Pre-Test			Post-Test			Difference		
Sample Number	L	W	T	L	W	T	L	W	T
01	1.0045	0.5000	0.1250	1.0050	0.4995	0.1250	0.0005	-0.0005	0.0000
03	0.9990	0.5075	0.1245	0.9990	0.5065	0.1260	0.0000	-0.0010	0.0015
05	1.0000	0.5115	0.1245	0.9990	0.5085	0.1235	-0.0010	-0.0030	-0.0010
07	0.9915	0.5060	0.1250	0.9920	0.5050	0.1250	0.0005	-0.0010	0.0000

Table 4: 2024-T4 High Strength Aluminum (M6) Dimensional Data

Designator	M6								
Material	2024 Aluminum								
	Pre-Test			Post-Test			Difference		
Sample Number	L	W	T	L	W	T	L	W	T
01	0.9990	0.5065	0.1250	0.9990	0.5065	0.1255	0.0000	0.0000	0.0005
03	1.0020	0.5040	0.1245	1.0020	0.5040	0.1240	0.0000	0.0000	-0.0005
05	1.0005	0.5090	0.1250	1.0005	0.5085	0.1250	0.0000	-0.0005	0.0000
07	1.0015	0.5135	0.1250	1.0005	0.5135	0.1250	-0.0010	0.0000	0.0000

Only two specific pairs of measurements exceeded the 0.002 inches error of the calipers; however, I wanted to perform a Repeated-Measures t-test on the values assuming the measurements were correct to test the methodology.

Fewer statistical tests were performed on the hand measurements compared to the hardness test (discussed in Section 5.4) because the error involved in hand measurements and the limited number of data points for each coupon does not support strong statistically-significant findings. The methods are shown here to demonstrate them for future research. The hardness tests are performed with metrology grade equipment to approved standards; therefore, I spent more time analyzing that data as the results were more significant. If physical dimensional measurements can be taken with metrology grade equipment, the techniques and methods discussed for hardness testing can be applied to the physical measurements as well.

A t-test was used to determine if there was a statistically-significant change in population means. The key assumptions were that the values measured were random and indicative of the actual population, the population is homogenous, the distribution is normal, the data collected is continuous, and the sample size is sufficiently large to represent the population. For the purposes of demonstrating the technique, I considered all these assumptions were true for the dimensional data collected. If normality was not assumed, distribution tests like the Anderson-Darling test would need to be used to first determine the distribution and then an appropriate population mean test would need to be selected. The larger the sample size, the more powerful the t-test results. I was limited on sample size due to cost, but I believe 12 dimensional measurements is sufficient to test the methodology. I am also assuming that the variances are approximately equal so I can utilize the student's t-test distribution instead of the Welch's t-test to demonstrate the methodology of this form of analysis.

Using Microsoft Excel's Data Analysis add-on and the built in *T-Test: Paired Two Sample for Means* function, I obtained the t-statistic for each material's set of dimensions shown in Table 5 through Table 8. The yellow highlighted block is the determined critical value for the t-test based

on the degrees of freedom with a significance level (alpha) of 0.1. This is a common significance level for initial testing but alphas of 0.05 or 0.01 are more powerful for identifying significant change. Because the values could have increased or decreased from the original, a two-tailed confidence interval critical value was used.

Table 5: 110 Multi-Purpose Copper - Annealed (M1) Dimensional Excel T-Test Results

	M1 Pretest	*M1 Posttest*
Mean	0.5471	0.5470
Variance	0.1398	0.1398
Observations	12	12
Pearson Correlation	1.0000	
Hypothesized Mean Difference	0	
df	11	
t Stat	0.5606	
P(T<=t) one-tail	0.2931	
t Critical one-tail	1.3634	
P(T<=t) two-tail	0.5863	
t Critical two-tail	1.7959	

Table 6: 110 Multi-Purpose Copper - 1/2 Hard (M2) Dimensional Excel T-Test Results

	M2 Pretest	*M2 Posttest*
Mean	0.5469	0.5465
Variance	0.1406	0.1408
Observations	12	12
Pearson Correlation	1.0000	
Hypothesized Mean Difference	0	
df	11	
t Stat	1.8898	
P(T<=t) one-tail	0.0427	
t Critical one-tail	1.3634	
P(T<=t) two-tail	0.0854	
t Critical two-tail	1.7959	

Table 7: 1100-H14 Hardened Easy-to-Form Aluminum (M5) Dimensional T-Test Results

	M5 Pretest	*M5 Posttest*
Mean	0.5433	0.5428
Variance	0.1396	0.1396
Observations	12	12
Pearson Correlation	1.0000	
Hypothesized Mean Difference	0	
df	11	
t Stat	1.2832	
P(T<=t) one-tail	0.1129	
t Critical one-tail	1.3634	
P(T<=t) two-tail	0.2258	
t Critical two-tail	1.7959	

Table 8: 2024-T4 High Strength Aluminum (M6) Dimensional T-Test Results

	M6 Pretest	*M6 Posttest*
Mean	0.5446	0.5445
Variance	0.1402	0.1401
Observations	12	12
Pearson Correlation	1.0000	
Hypothesized Mean Difference	0	
df	11	
t Stat	1.1489	
P(T<=t) one-tail	0.1375	
t Critical one-tail	1.3634	
P(T<=t) two-tail	0.2750	
t Critical two-tail	1.7959	

For the t-test results to show significant change, the absolute valve of the t-statistic must be larger than the related critical value. A large t-statistic indicated that we should reject the null hypothesis, and we should accept the alternate hypothesis. In my test, my null hypothesis stated that the dimensional change is zero and the alternate hypothesis stated that the change was not zero. Any changes in a physical property could indicate material property changes, though it does not rule out other causes.

The results of the t-test showed that the annealed copper (M1) and both aluminum sample sets (M5 & M6) showed no significant change in dimensional measurements. These values of the test statistic are highlighted in red for these materials. The 1/2 hard copper alloy (M2) showed a statistically significant change in dimension. The value of this test statistic is highlighted in green for these materials. The reason that this alloy showed significant changes and not the other alloys is unknown and may simply be a result of inaccurate measurements or error. Additional research with more care taken for measurement precision and accuracy is necessary to verify the results. Higher accuracy and precision measurement tools could identify more subtle changes in dimensions.

Excel's t-test function also shows the variances for each material is approximately equal. If they had been significantly different, more than a ratio of four is a common rule [28], I would have been required to perform a variance analysis to determine if the assumptions were valid.

Though the data does not show significant changes in dimensions for all alloys the method does show that simple hand measurements and statistical testing of differences may be able to show physical changes in the materials which would indicate some property change has occurred.

5.4 Hardness Test Analysis

The second method I used for determining material property changes is a Vickers microhardness test. The test was administered at five points across the polished surface of the test coupons. This would provide an average hardness as well as five points for paired comparison. A total of five measurements taken on three unique specimens of each alloy provided 15 data points for my analysis of each material. Table 9 through Table 12 show the raw hardness testing data from Element Labs. The "07" sample in each sample set was initially tested. Following pressurization, I chose to preserve one coupon of each alloy in its undisturbed posttest condition.

The hardness data from these coupons cannot be used for posttest comparison except for material averaging and is primarily provided for completeness.

Table 9: 110 Multi-Purpose Copper - Annealed (M1) Hardness Data

Designator	M1									
Material	110 multi-purpose copper - Annealed									
	Pre-Test					Post-Test				
Sample Number	Hardness 1	Hardness 2	Hardness 3	Hardness 4	Hardness 5	Hardness 1	Hardness 2	Hardness 3	Hardness 4	Hardness 5
01	68	66	68	73	68	67	64	68	68	74
03	91	92	87	85	82	82	87	81	78	78
05	66	68	74	72	78	72	75	68	68	70
07	73	74	68	74	68					

Table 10: 110 Multi-Purpose Copper - 1/2 Hard (M2) Hardness Data

Designator	M2									
Material	110 multi-purpose copper - 1/2 hard									
	Pre-Test					Post-Test				
Sample Number	Hardness 1	Hardness 2	Hardness 3	Hardness 4	Hardness 5	Hardness 1	Hardness 2	Hardness 3	Hardness 4	Hardness 5
01	98	98	99	106	106	99	101	96	104	100
03	98	101	103	102	102	94	99	102	100	102
05	97	98	100	101	99	96	99	96	99	98
07	103	102	99	102	104					

Table 11: 1100-H14 Hardened Easy-to-Form Aluminum (M5) Hardness Data

Designator	M5									
Material	1100 Aluminum									
	Pre-Test					Post-Test				
Sample Number	Hardness 1	Hardness 2	Hardness 3	Hardness 4	Hardness 5	Hardness 1	Hardness 2	Hardness 3	Hardness 4	Hardness 5
01	45	46	44	44	44	44	43	45	45	44
03	45	43	45	46	46	44	45	45	46	45
05	42	43	42	45	45	43	43	44	44	45
07	44	47	46	44	43					

Table 12: 2024-T4 High Strength Aluminum (M6) Hardness Data

Designator	M6									
Material	2024 Aluminum									
	Pre-Test					Post-Test				
Sample Number	Hardness 1	Hardness 2	Hardness 3	Hardness 4	Hardness 5	Hardness 1	Hardness 2	Hardness 3	Hardness 4	Hardness 5
01	144	140	139	142	145	141	142	140	139	142
03	137	140	144	145	143	145	141	139	140	142
05	138	136	136	137	147	140	141	137	139	142
07	140	140	138	138	146					

To determine if there were statically-significant changes with regard to distribution, average, and variance, I performed basic statistical testing. Other methods exist and may be used for future research.

5.4.1 Hardness Values Normality Analysis

Unlike the dimensional analysis discussed in Section 5.3, I believed it was prudent to check that the hardness data collected followed a normal distribution. To perform a t-test to determine if the average hardness changed for each alloy, the data was assumed to be normally distributed. If it was not, other methods are required and may not provide the same strength of results as the t-test.

I used the Shapiro-Wilk test for normality to analyze the hardness data collected for my alloys. This test was not a built-in function within Excel. The Shapiro-Wilk test uses Equation 1 to calculate a W statistic, which is then compared to tables found in statistic resources.

$$W = \frac{(\sum_{i=1}^{n} a_i x_i)^2}{\sum_{i=1}^{n} (x_i - \bar{x})^2}$$

Equation 1: Shapiro-Wilk (W) Test Statistic [29]

In this equation, x_i are the individual hardness values and $\bar{x}$ is the sample set average. The coefficient vector of the weights is represented by a_i and is determined from number of samples and is symmetrical so only positive values are provided in the tables. The values of the dataset are

sorted from low to high and then the calculation can be made. If the W test statistic and related p-value are larger than out selected p-value then there is not statistical evidence to reject the null hypothesis which states the data are normally distributed. Table 13 is a summary of the normality test p-value results.

Table 13: Hardness Data Shapiro-Wilk Normality Test P-Values

	Shapiro-Wilk P-Value	
Material	Pretest	Posttest
M1	0.0399	0.3582
M2	0.0830	>0.5
M5	0.0969	0.0505
M6	0.3261	0.4561

By selecting a critical p-value of 0.05 and comparing these results, the only dataset that does not meet the normality test is the 110 Multi-Purpose Copper - Annealed (M1) coupons pretest. The reason for this discrepancy could be due to the small sample size or some other unknown factor. A Tukey test to compare the means between the three individual coupons showed that the -03 coupon was statistically different from the others. Removing these data points passed the Shapiro-Wilk normality test. The pretest distribution remained skewed to the right.

For my analysis, I assumed that the data was normally distributed. With a small sample size, it would not be uncommon to use a very small critical p-value to reject a normal distribution assumption. If I had selected a p-value or 0.025, all the datasets would have passed the normality test.

5.4.2 Hardness Values Frequency Analysis

The Shapiro-Wilks test is a frequency test but does not analyze the data from a graphical standpoint, which can also be a powerful method of investigating normality and any changes in distribution. To analyze the frequency, I created comparative frequency column graphs with both pretest and posttest frequencies for direct comparison. I also overlaid a randomly-generated normal

distribution curve based on the average and standard deviation for pretest and posttest data to show the approximate normal trend of data. This curve was for visualization purposes, and quantitative information should not be interpreted from its shape or values.

Figure 58 is the frequency chart for the 110 Multi-Purpose Copper - Annealed (M1) hardness data set. We can see in the data the right-skewedness discussed in Section 5.4.1. The data has a large right tail from single values of hardness, increasing from the large distribution around 68.

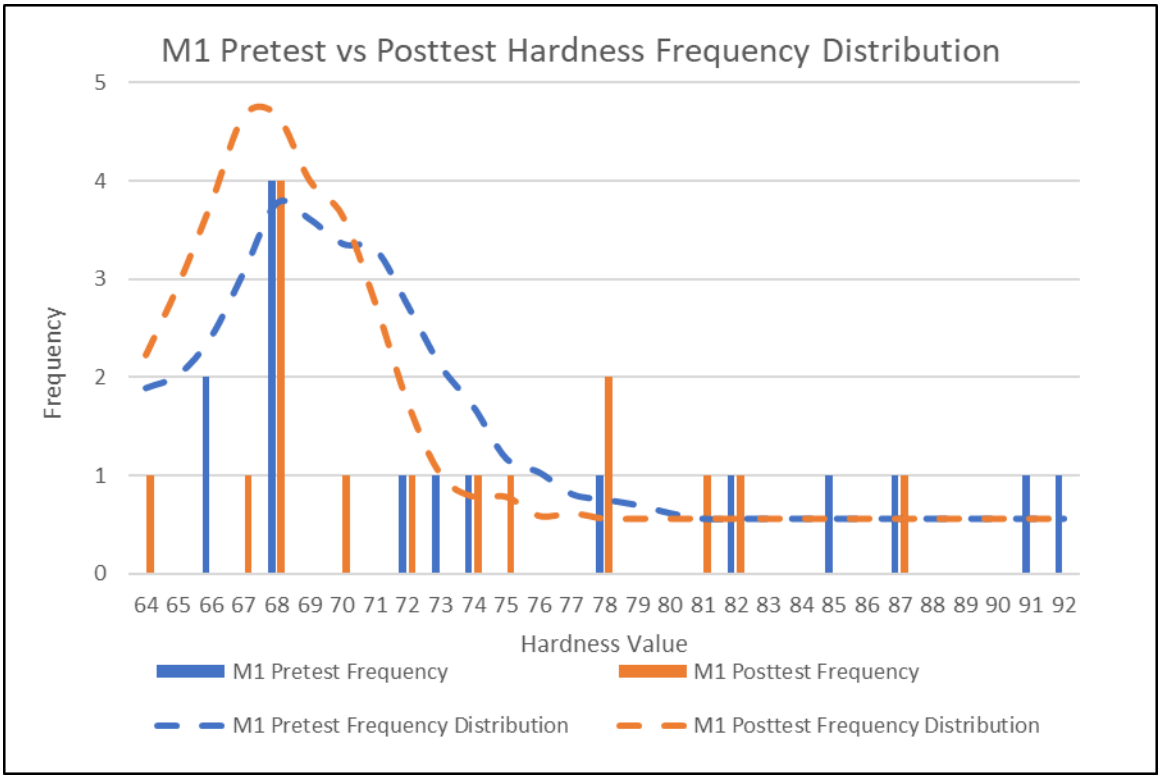

Figure 58: M1 Pretest vs Posttest Hardness Frequency Distribution Chart

Analyzing this data, we can see that the hardness frequency shifted slightly lower however the mode of the data remained constant at 68 and the distribution range is similar.

Figure 59 is the frequency chart for the 110 Multi-Purpose Copper - 1/2 Hard (M2) hardness data set. The distribution for this is visually more normal than the annealed copper but the pretest data are also more skewed to the right than the posttest data.

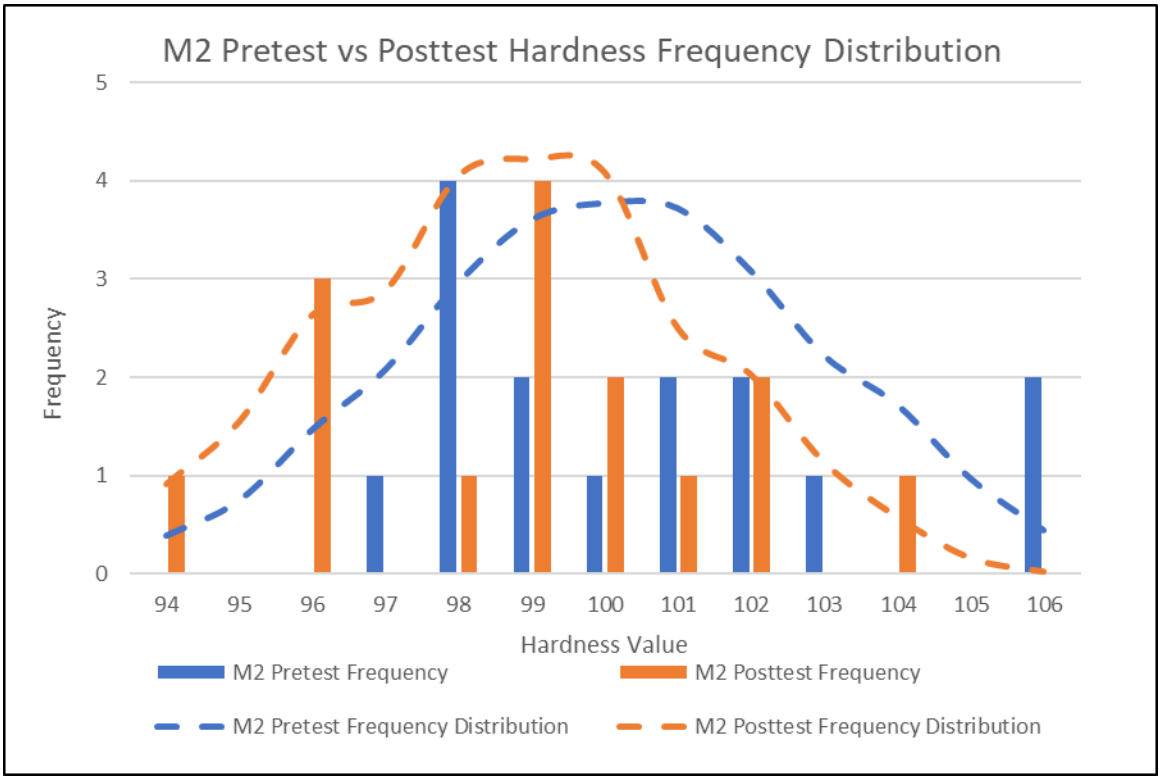

Figure 59: M2 Pretest vs Posttest Hardness Frequency Distribution Chart

Analyzing this data, we see that the hardness frequency distribution shifted lower slightly following the pressurization cycle. The mode increased slightly but the range remained similar.

From the visual frequency analysis of the copper, we see that the frequency of hardness results shifted slightly lower slightly with similar ranges. This could indicate a uniform change in hardness for copper alloys shifting in the direction of the alloys becoming softer. The statistical significance and the exact cause of this is unknown but further analysis could be performed with a larger sample set for each coupon and a larger number of coupons to better show frequency changes.

Figure 60 is the frequency chart for the 1100-H14 Hardened Easy-to-Form Aluminum (M5) hardness data set. These data sets had a smaller range but appeared to have a normal distribution.

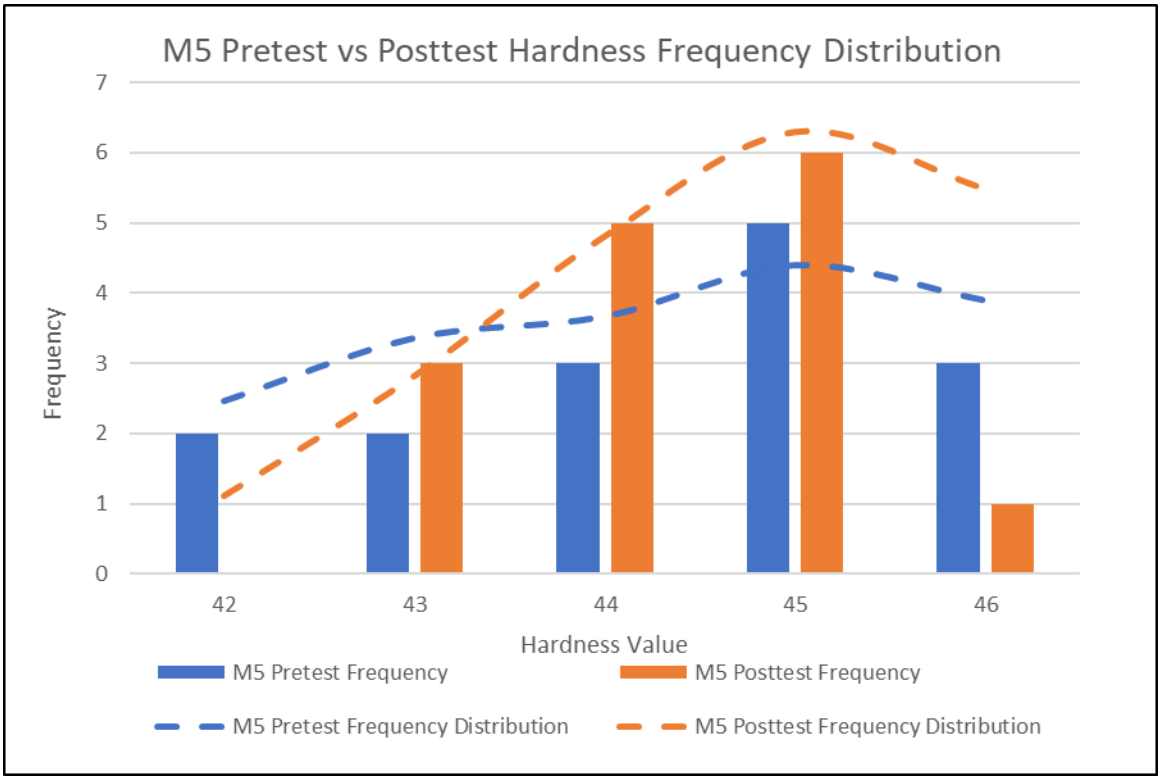

Figure 60: M5 Pretest vs Posttest Hardness Frequency Distribution Chart

Analyzing this data, we see that the average hardness values pretest and posttest does not change but the distribution narrows slightly around the average.

Figure 61 is the frequency chart for the 2024-T4 High Strength Aluminum (M6) hardness data set. Though both data sets passed the normality test with large p-values, the pretest data looks more uniform than normal. The posttest data has a distinctly normal distribution.

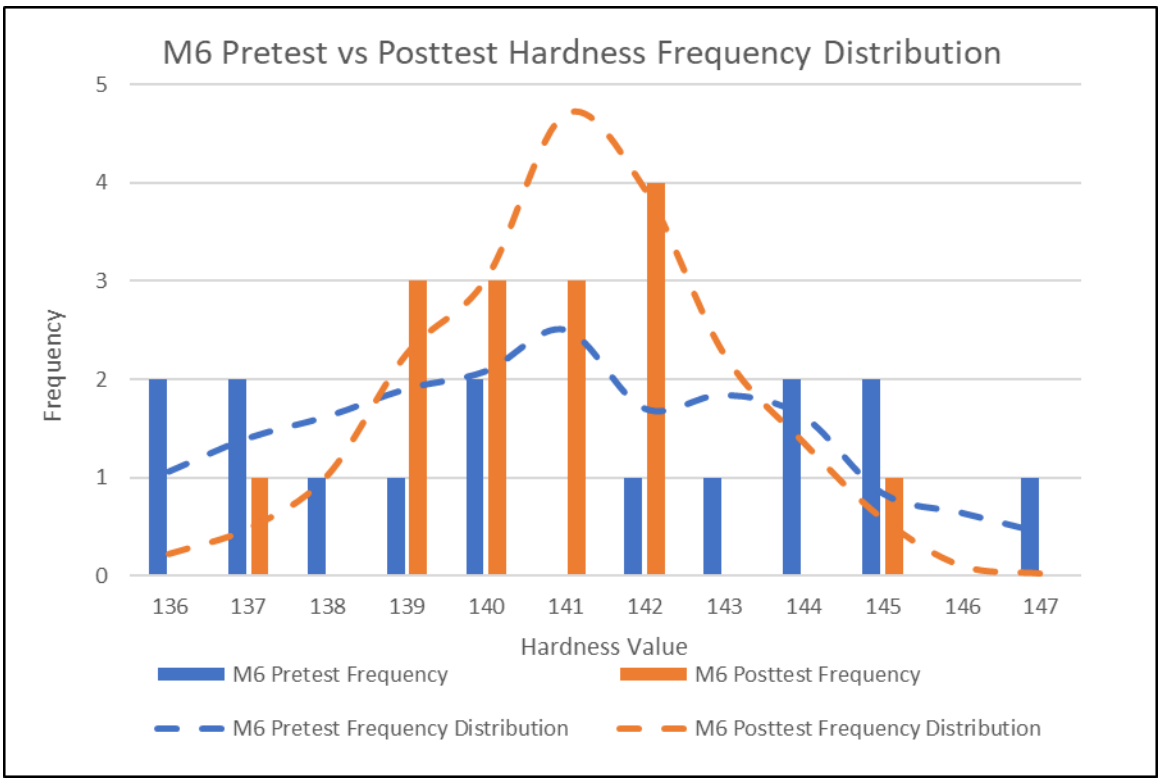

Figure 61: M6 Pretest vs Posttest Hardness Frequency Distribution Chart

Analyzing this data, we see a narrowing distribution without a change in average hardness. Though the aluminum coupon sets were not be directly compared because they were not the same alloys, both alloys showed a narrowing of the distribution around a steady hardness value. This could indicate that the hardness of the material was more uniformly distributed across the surface around an average that may be a result of the manufacturing process. A more uniform hardness can improve predictability for some designs, though hardness is only one of the material properties that goes into design analysis. More testing is required to understand this phenomenon and determine possible applications for such a process.

The visual frequency analysis showed possible changes in material hardness for all alloys, which may have appeared as a reduction in hardness averages or a change in distribution. If hardness changed following the pressurization cycle, material property changes at depth may have

affected material performance. Statistical tests were used to determine if the changes observed in the visual analysis were statistically significant for average hardness and variance.

5.4.3 Hardness Values T-Test Analysis

The t-test used for the hardness testing analysis is described in Section 5.3 for the dimensional analysis.

I tested against significance values of 0.1 and 0.05 for hardness but used the same methods and assumptions. The hardness values between coupons within an alloy were compared directly because they were all manufactured from the same material stock and cut from this stock near each other. This is a guiding principle for general design processes. Only high performance and precise designs require determining and comparing hardness values for each part. For my purposes, I assumed that the values returned from anywhere on the material stock was from the same population of values. The larger sample size provides a stronger statistical test.

With this assumption and again using MS Excel's Data Analysis add-on and the built in *t-Test: Paired Two Sample for Means* function, I obtained the t-statistic for each material's set of hardness values shown in Table 14 through Table 21. The yellow highlighted blocks are the determined critical value for the t-test based on the degrees of freedom with significance levels (alphas) of 0.05 and 0.1.

Table 14: 110 Multi-Purpose Copper - Annealed (M1) Hardness Excel T-Test Alpha = .05 Results

t-Test: Paired Two Sample for Means (alpha = .05)		
	M1 Pretest	*M1 Posttest*
Mean	75.8667	73.3333
Variance	86.2667	44.3810
Observations	15	15
Pearson Correlation	0.8377	
Hypothesized Mean Difference	0	
df	14	
t Stat	1.8889	
P(T<=t) one-tail	0.0399	
t Critical one-tail	1.7613	
P(T<=t) two-tail	0.0798	
t Critical two-tail	2.1448	

Table 15: 110 Multi-Purpose Copper - Annealed (M1) Hardness Excel T-Test Alpha = .1 Results

t-Test: Paired Two Sample for Means (alpha = .1)		
	M1 Pretest	*M1 Posttest*
Mean	75.8667	73.3333
Variance	86.2667	44.3810
Observations	15	15
Pearson Correlation	0.8377	
Hypothesized Mean Difference	0	
df	14	
t Stat	1.8889	
P(T<=t) one-tail	0.0399	
t Critical one-tail	1.3450	
P(T<=t) two-tail	0.0798	
t Critical two-tail	1.7613	

Table 16: 110 Multi-Purpose Copper - 1/2 Hard (M2) Hardness Excel T-Test Alpha = .05 Results

t-Test: Paired Two Sample for Means (alpha = .05)		
	M2 Pretest	*M2 Posttest*
Mean	100.5333	99.0000
Variance	8.1238	7.2857
Observations	15	15
Pearson Correlation	0.6685	
Hypothesized Mean Difference	0	
df	14	
t Stat	2.6235	
P(T<=t) one-tail	0.0100	
t Critical one-tail	1.7613	
P(T<=t) two-tail	0.0200	
t Critical two-tail	2.1448	

Table 17: 110 Multi-Purpose Copper - 1/2 Hard (M2) Hardness Excel T-Test Alpha = .1 Results

t-Test: Paired Two Sample for Means (alpha = .1)		
	M2 Pretest	*M2 Posttest*
Mean	100.5333	99.0000
Variance	8.1238	7.2857
Observations	15	15
Pearson Correlation	0.6685	
Hypothesized Mean Difference	0	
df	14	
t Stat	2.6235	
P(T<=t) one-tail	0.0100	
t Critical one-tail	1.3450	
P(T<=t) two-tail	0.0200	
t Critical two-tail	1.7613	

Table 18: 1100-H14 Hardened Easy-to-Form Aluminum (M5) Hardness T-Test Alpha = .05 Results

t-Test: Paired Two Sample for Means (alpha = .05)		
	M5 Pretest	*M5 Posttest*
Mean	44.3333	44.3333
Variance	1.8095	0.8095
Observations	15	15
Pearson Correlation	0.3738	
Hypothesized Mean Difference	0	
df	14	
t Stat	0.0000	
P(T<=t) one-tail	0.5000	
t Critical one-tail	1.7613	
P(T<=t) two-tail	1.0000	
t Critical two-tail	2.1448	

Table 19: 1100-H14 Hardened Easy-to-Form Aluminum (M5) Hardness T-Test Alpha = .1 Results

t-Test: Paired Two Sample for Means (alpha = .1)		
	M5 Pretest	*M5 Posttest*
Mean	44.3333	44.3333
Variance	1.8095	0.8095
Observations	15	15
Pearson Correlation	0.3738	
Hypothesized Mean Difference	0	
df	14	
t Stat	0.0000	
P(T<=t) one-tail	0.5000	
t Critical one-tail	1.3450	
P(T<=t) two-tail	1.0000	
t Critical two-tail	1.7613	

Table 20: 2024-T4 High Strength Aluminum (M6) Hardness T-Test Alpha = .05 Results

t-Test: Paired Two Sample for Means (alpha = .05)		
	M6 Pretest	*M6 Posttest*
Mean	140.8667	140.6667
Variance	13.4095	3.5238
Observations	15	15
Pearson Correlation	0.1593	
Hypothesized Mean Difference	0	
df	14	
t Stat	0.2017	
P(T<=t) one-tail	0.4215	
t Critical one-tail	1.7613	
P(T<=t) two-tail	0.8430	
t Critical two-tail	2.1448	

Table 21: 2024-T4 High Strength Aluminum (M6) Hardness T-Test Alpha = .01 Results

t-Test: Paired Two Sample for Means (alpha = .1)		
	M6 Pretest	*M6 Posttest*
Mean	140.8667	140.6667
Variance	13.4095	3.5238
Observations	15	15
Pearson Correlation	0.1593	
Hypothesized Mean Difference	0	
df	14	
t Stat	0.2017	
P(T<=t) one-tail	0.4215	
t Critical one-tail	1.3450	
P(T<=t) two-tail	0.8430	
t Critical two-tail	1.7613	

Analyzing these results, we see that there is no significant change in hardness for the aluminum alloys (M5 and M6). The copper alloys (M1 and M2) however both showed statistically significant hardness changes at a significance level of 0.1 and the 110 Multi-Purpose Copper - 1/2 Hard (M2) showed a significant change at a level of 0.05. This shows a possible relation to the

dimensional changes for M2 identified in Section 5.3 and may validate the assumption that any physical change will influence mechanical properties.

5.4.4 Hardness Values Chi-Square Test for Variance Analysis

The chi-squared test for variance is used to test if an estimated population variance is significantly different from a specified value. I planned to test the variance from the posttest hardness data against the variance from the pretest data as the specified value. The chi-squared test can be either single or two tailed depending on the required test. I looked for any changes in variance, so utilized the two-tailed test. Like the t-test, to use the chi-squared test, a hypothesis must be stated. My null hypothesis stated that pretest and posttest variances were equal, and my alternate hypothesis was that they were not equal. The chi-squared test statistic created from Equation 2 was then compared against a chi-squared critical value based on the selected alpha value and degrees of freedom. I again tested against alphas of 0.1 and 0.05.

$$T = (N - 1)\left(\frac{s}{\sigma_0}\right)^2$$

Equation 2: Chi-Square (T) Test Statistic [30]

In this equation, N is the sample size, s is the sample standard deviation, and σ_0 is the selected desired standard deviation which will be from the pretest hardness sample data. The test statistic was again compared to a critical value found in standard Chi-Square tables. The test statistic, T, was then compared to the critical region of the two-tailed distribution, and the hypothesis is rejected if it falls outside of the critical region.

Table 22: Hardness Data Chi-Square Test for Variance Test Statistic

	Chi-Square Test Statistic	
Material	Posttest	
M1	7.202	
M2	12.556	
M5	6.263	
M6	3.679	
Critical Value	Low	High
Alpha = .1	6.571	23.685
Alpha = .05	5.629	26.119

The test statistic returned for each coupon alloy is shown in Table 22: Hardness Data Chi-Square Test for Variance. The copper alloys fall between the test statistics for alphas of both 0.1 and 0.05 and we therefore must fail to reject the null hypothesis and should assume that the variance of each data set is equal. This matched the visual frequency analysis we performed in Section 5.4.2 where the distribution range and shape did not change significantly but was shifted slightly lower. The 1100-H14 Hardened Easy-to-Form Aluminum (M5) coupons showed a statistically significant change in variance at an alpha level of 0.1 but not at 0.05. This also matched the visual frequency analysis where the distribution narrows slightly. The 2024-T4 High Strength Aluminum (M6) coupons showed a statistically significant change in variance at both an alpha level of 0.1 and 0.05.

The small sample size for testing each coupon individually required a very strong indication of change to reject the null hypothesis. All the coupons had Chi-Squared test statistics that fell within the bounds of the critical values for alphas of both 0.1 and 0.05 except for coupon M6-05 which had a statistically significant change with an alpha level of 0.1.

5.4.5 Hardness Summary

The hardness data analysis showed that the materials that underwent hydrostatic pressurization had permanent material properties changes. The visual frequency analysis could be interpreted to indicate that the copper alloys shifted their average hardness distribution but the general shape of the distribution remained constant. This was also seen in the t-test and chi-square analysis, which indicated the average hardness for the alloys lowered, but the variance did not change in a statistically significant way. The same analysis of the aluminum alloys showed visual evidence that the average hardness did not change but, the distribution of hardness narrowed. This matched the findings of the t-test and chi-square analysis, which showed that average hardnesses did not change but the variance decreased for the samples.

These findings were significant because they indicated that the hardness of the materials changed at pressure. More research was necessary to determine how much hardness changed and if other properties, such as stiffness and strength, changed in a significant way.

5.5 Imaging Analysis

Imaging analysis is the most subjective form of material analysis. There are several industry standards to help create useful data, but the scale of change traditionally used for these standard tests are significantly larger than the changes I observed. I compared before and after images and the measurement tools available on the microscope in use. My previous analysis focused on presenting my methods for image analysis and attempting to find indications of surface and grain structure changes. The details presented here do not represent an exhaustive analysis of every sample or possible indication of surface topography change that may exist on my samples or in the data collected. Image analysis can take months for the smallest of samples and is beyond

the scope of this research. Further analysis may be performed on the 2D and 3D raw images as required to identify more findings.

5.5.1 General Image Analysis

My initial imaging task was to obtain photos of the surfaces in question in their raw form. This needed to be done before comparing each coupon image sets for changes. As previously mentioned, I took images using the middle hardness test indentation as a location marker. These images were at magnifications of 50x, 100x, 300x, 500x, 1000x, and 2000x, in both coaxial and full ring lighting and 4000x and 6000x in coaxial lighting only.

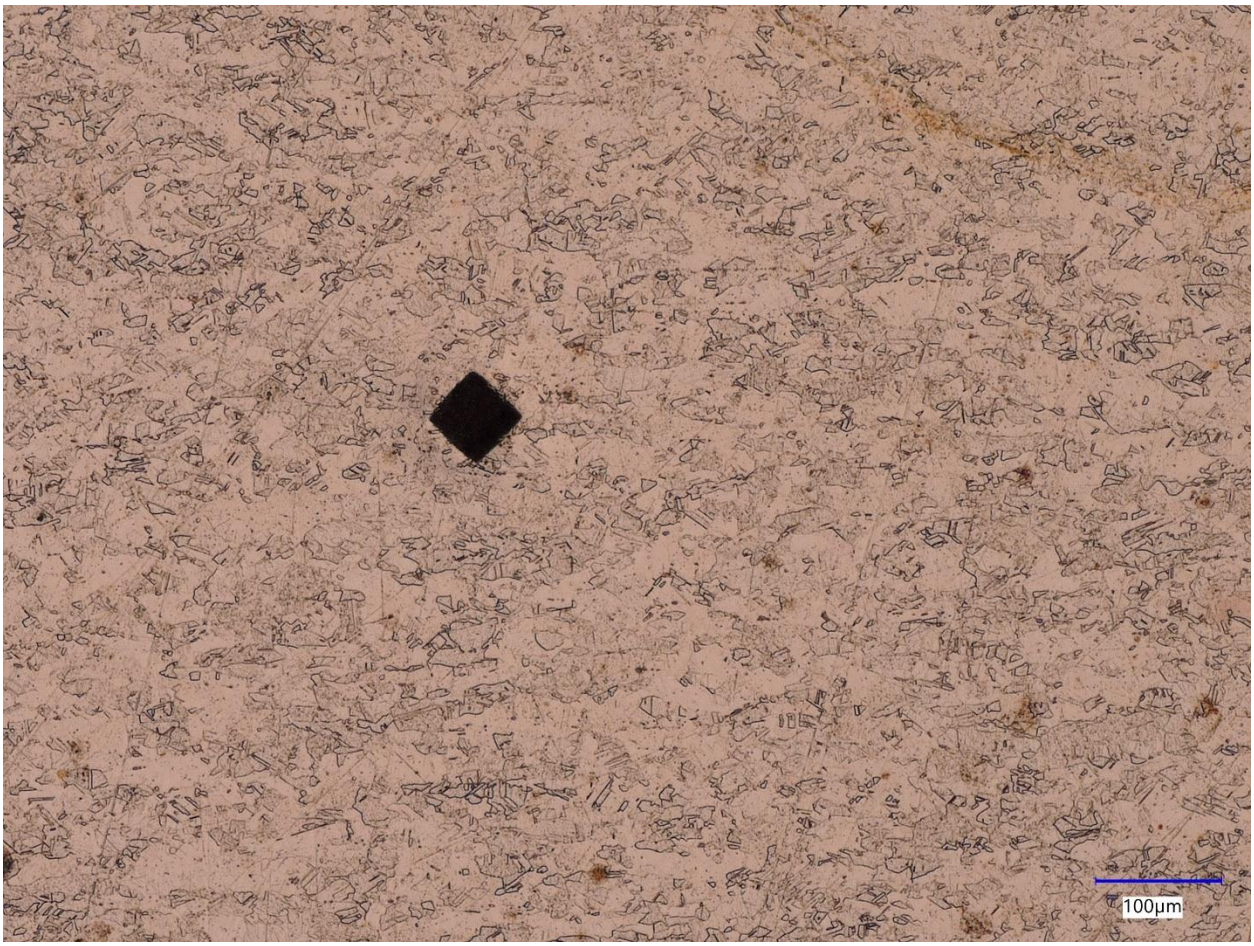

Figure 62: Pretest M1-07 300x Coaxial

Figure 62 shows one of the 110 Multi-Purpose Copper - Annealed (M1) coupons. At 300x magnification, we can easily distinguish the diamond-shaped hardness indentation and see the stain outlining surface features. Using coaxial lighting provided a better view of the stain but did not make the surface topography any clearer it only showed that it exists. Small red splotches on the surface are corrosion or contamination were visible at 300x. As magnification increased, these spots should be avoided or they may obstruct a clear view of the material structure. Very subtle scratches from the polishing process were visible but they were fine enough and few enough that as we increase magnification, we can also find locations of interest where these lines do not exist. The lines and surface corrosion can help locate points of interest, so removing them is not necessarily ideal.

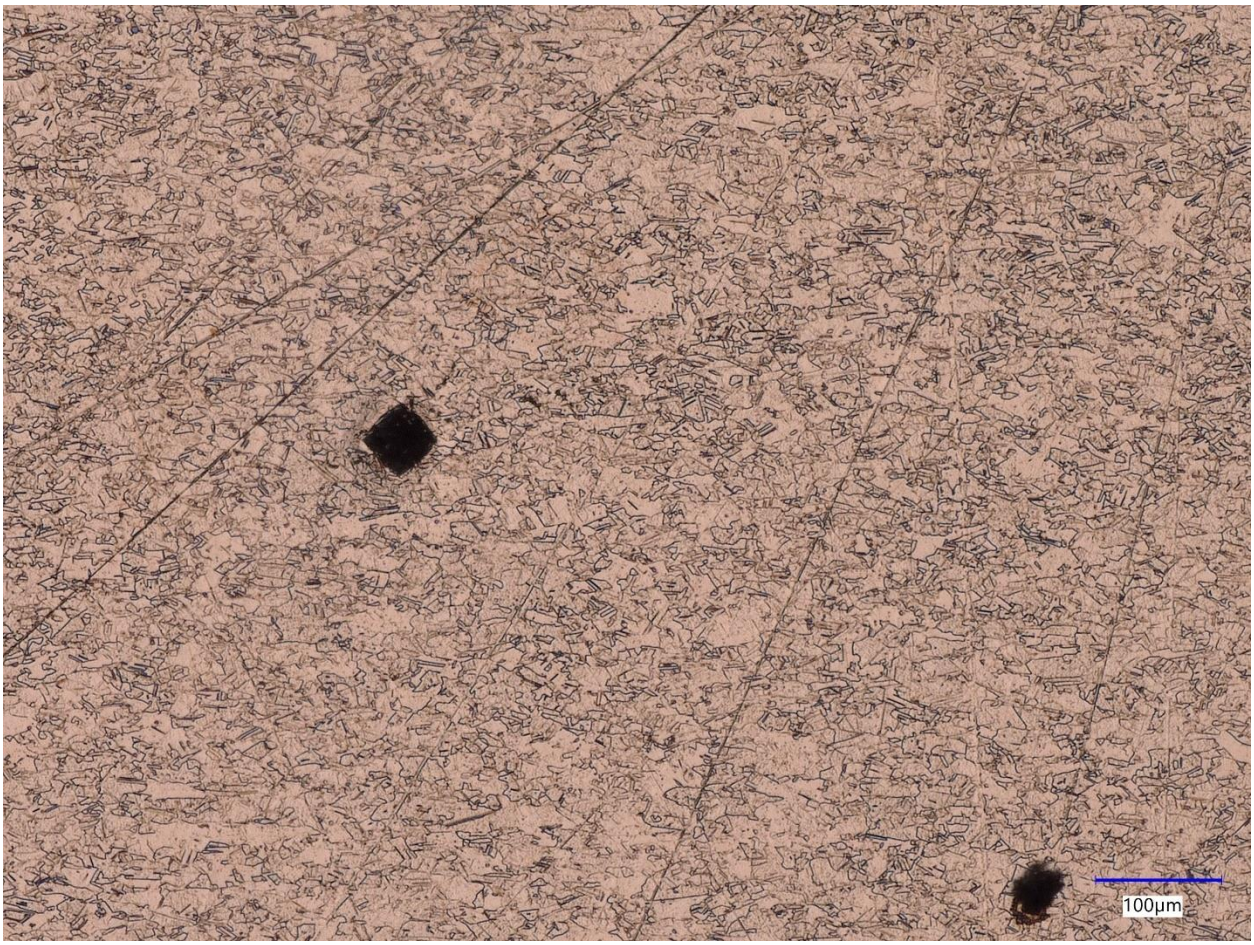

Figure 63: Pretest M2-03 300x Coaxial

Figure 63 shows a 110 Multi-Purpose Copper – 1/2 Hard (M2) coupon at 300x magnification with coaxial light. The polishing lines are more pronounced and run in a similar direction. Grain lines are unlikely to be straight and will travel in multiple directs based on their formation and the material processing techniques. The fact that these are straight and in similar direction these resulted from a polishing process and are a surface characteristic. If we were polishing by hand, once we are finished removing all the lines except those in the same direction at a particular grit, we can rotate the sample 90 degrees and proceed to the next step of polishing until these lines are gone. Going back and forth in that manner ensures that we are polishing the entire surface to a certain level before moving on to another polishing stage.

Figure 63 shows a surface that is more densely covered in stained surface features than the surface seen in Figure 62. This was as expected because you would expect more closely packed and smaller grains in a harder material.

Figure 64: Pretest M5-05 500x Full Ring

Figure 64 shows a 1100-H14 Hardened Easy-to-Form Aluminum (M5) coupons. At 500x magnification and in full ring lighting, we see a clearer picture of the indentation shape and see the high and low spots of the topography. The brown spots on this surface are obstructing the grain structure of the aluminum and are likely residual particles of the polishing compound or excessively reacted areas of the aluminum staining process. 1100 series aluminum is a pure aluminum and very soft. Particles and contamination often embed themselves in the surface unless

special care is taken to keep the surface clean. However, I will show later how the presence of this contamination in the pretest imaging helped identify that something occurred on the surface of the coupon during pressurization.

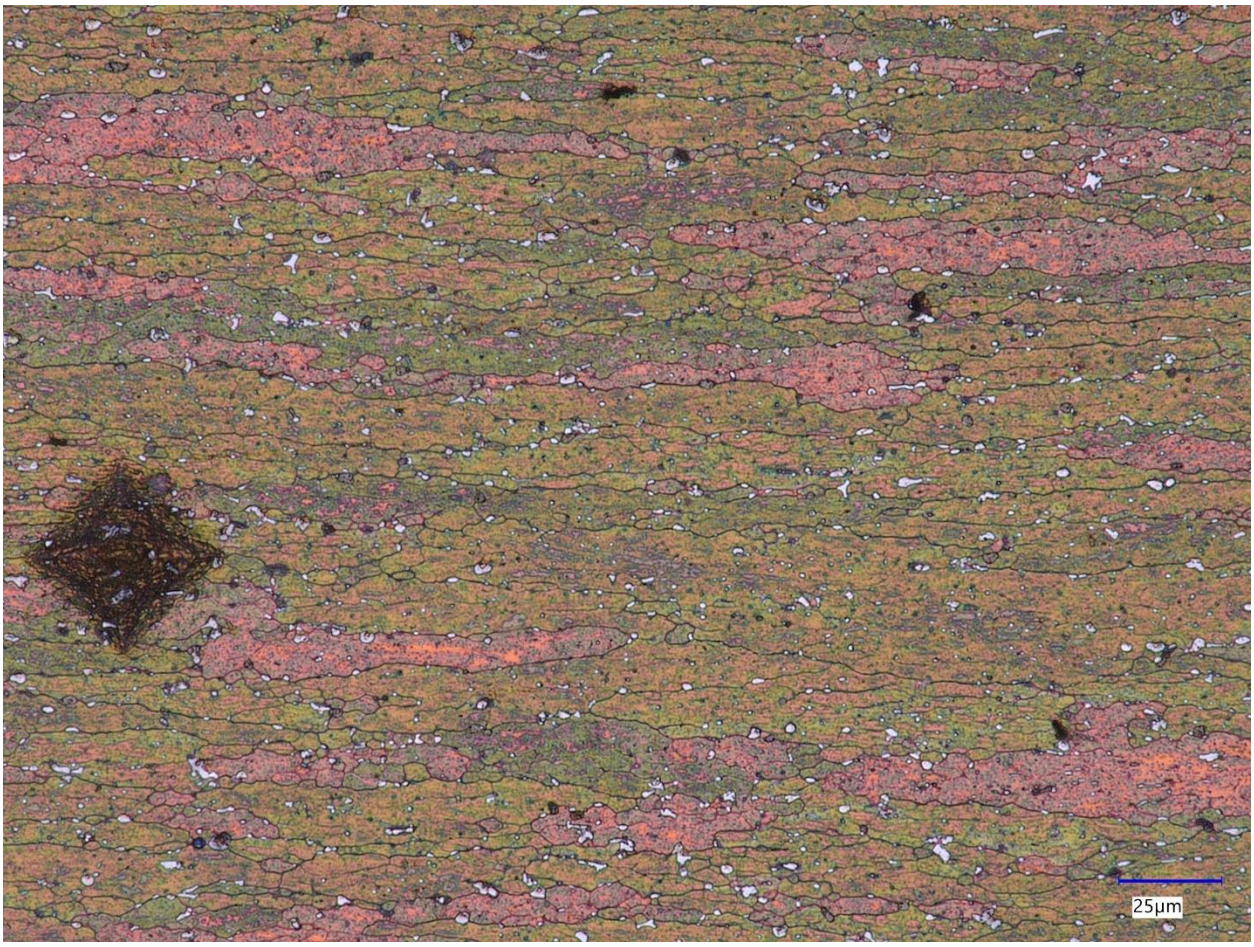

Figure 65: Pretest M6-01 1000x Coaxial

Figure 65 is a photo of one of the 2024-T4 High Strength Aluminum (M6) coupons. This image at 1000x magnification and in coaxial light better shows the stained surface of aluminum. The various colors are grains and the colors are caused by the thickness of the stain at that location. In this image we can see the flattened and elongated grains you would expect from a rolled product. The white spots are unreacted portions of the alloy and the darker spots are most likely surface contamination from polishing compound, corrosion, or some foreign particulate.

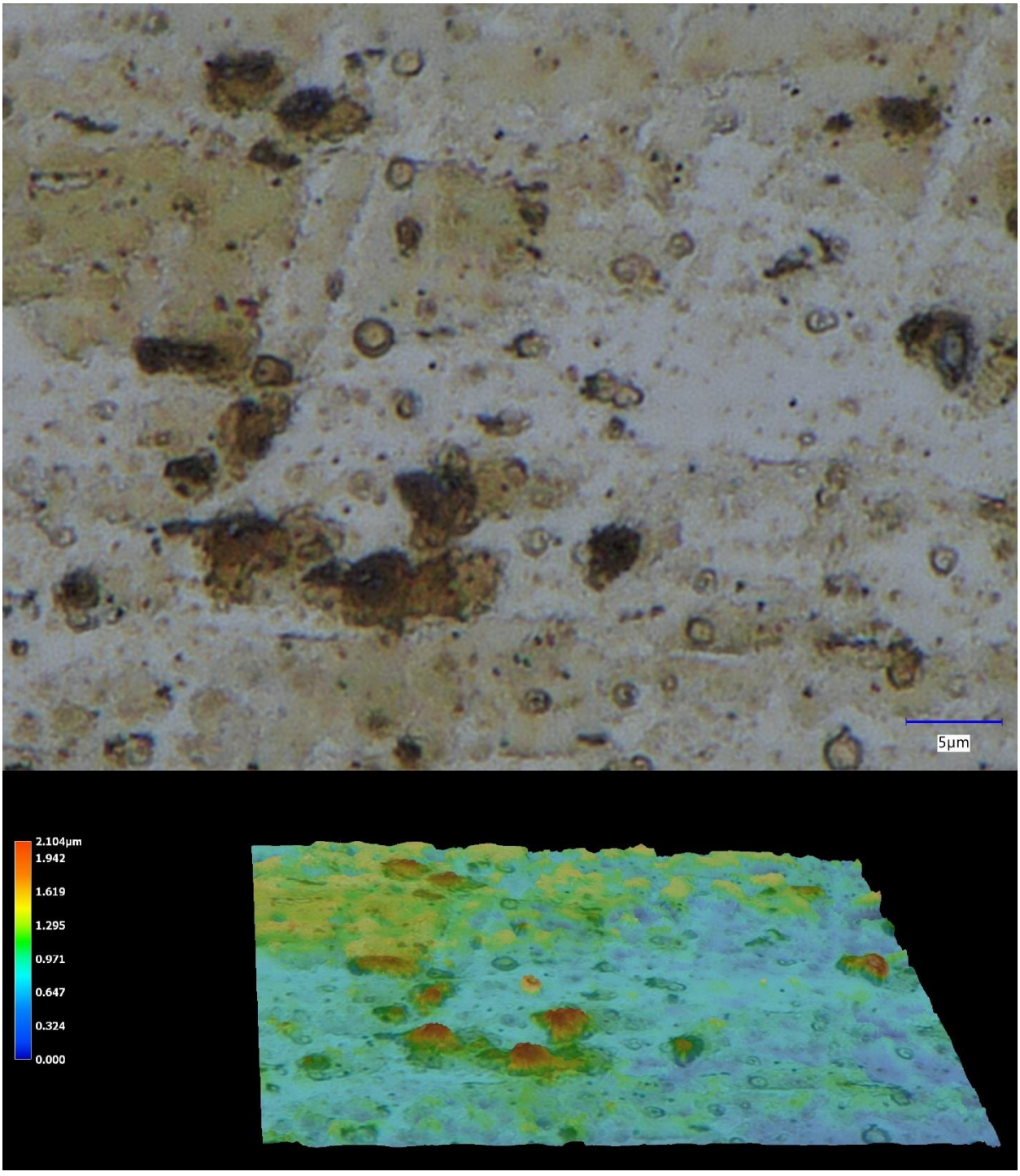

Figure 66: Pretest M5-07 6000x Coaxial 3D Side-By-Side

Figure 66 shows 2D and 3D views of one of the 1100-H14 Hardened Easy-to-Form Aluminum (M5) coupons at 6000x magnification. The top image is the standard coaxial light 2D image, which shows surface features and small amounts of stain however at this magnification the

normal grain detail is completely lost. The bottom image is a 3D topography color map generated by the Keyence VHX-7000 Ultramicroscope, which was used for all my experimental imaging. The color map allows us to relate the 2D image features to topography. The dark spots in the 2D image are shown as small plateaus of material in the 3D color map. We can also distinguish between those dark spots that have related topography changes and those that show as flat in the color map. The flat spots are more indicative of surface features than dirt or particulate, but this is not always true, and care must be taken when making assumptions. This was critical in identifying subtle surface changes following the pressurization cycle.

Following the individual image captures, I combined images to compare two different surface topographies and imaging options to better understand what is being shown. Figure 67 shows a coaxial and full ring light comparison of a 1100-H14 Hardened Easy-to-Form Aluminum (M5) coupon to be able to identify how features show up differently in different lights.

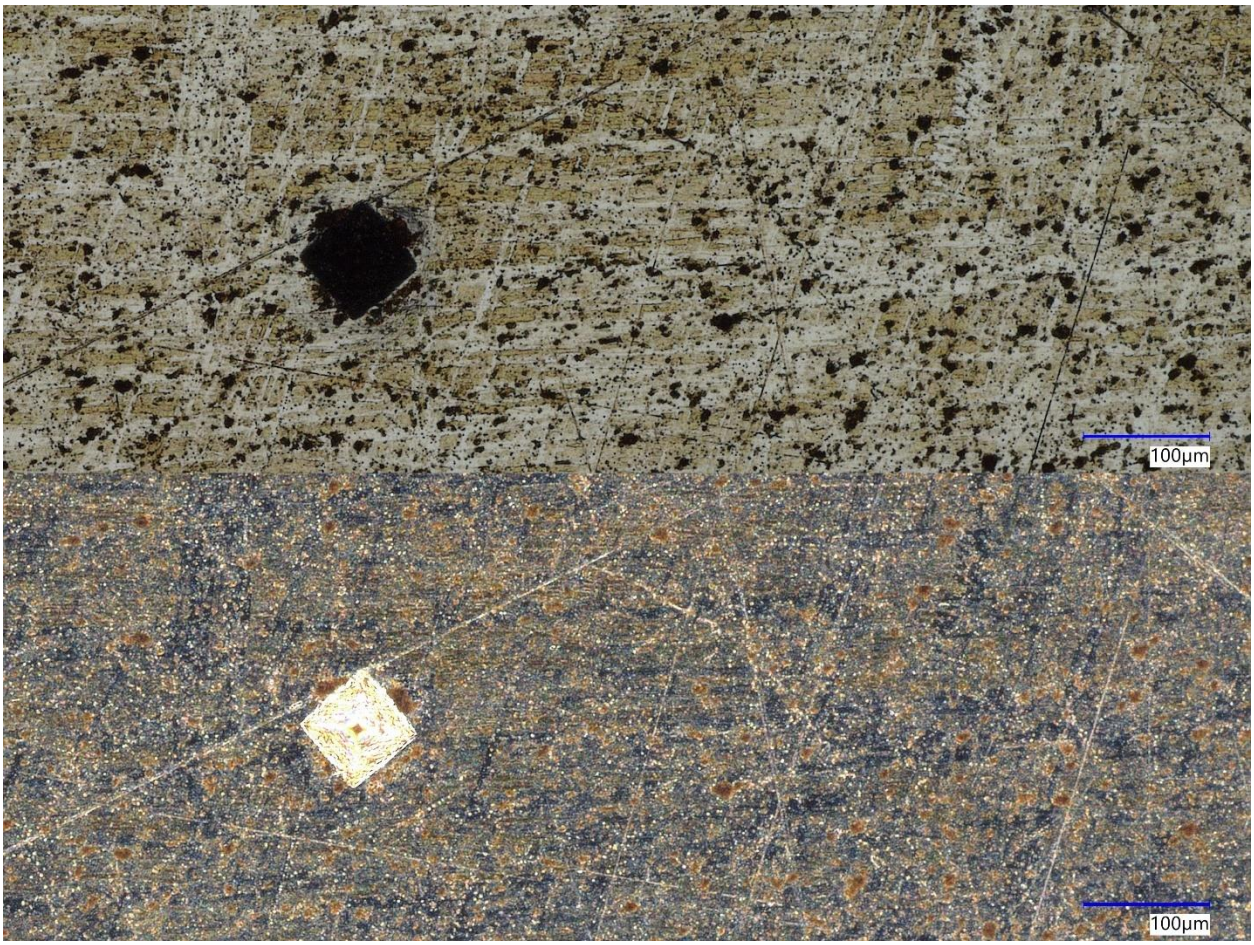

Figure 67: Pretest M5-07 300x Light Type Comparison (Coaxial – Top, Full Ring – Bottom)

The dirt inclusions shown in the full ring light show as black spots in the coaxial light. Scratches are more apparent in full ring than in coaxial light however the stain is more apparent in the coaxial lighting.

I also created quad images of three or four separate images to provide a means of location specific features as magnification increases. Figure 68 and Figure 69 show quad images for a 110 Multi-Purpose Copper - Annealed (M1) coupon with magnification stepped from 100x to 500x, 2000x, and 4000x. The coaxial light quads contain four images but the full ring light quads only contain 3. This is because the full ring light method is not available at 4000x and higher

magnification and to ensure simple direct comparison of quads I chose not to include an image that may confuse reviewers.

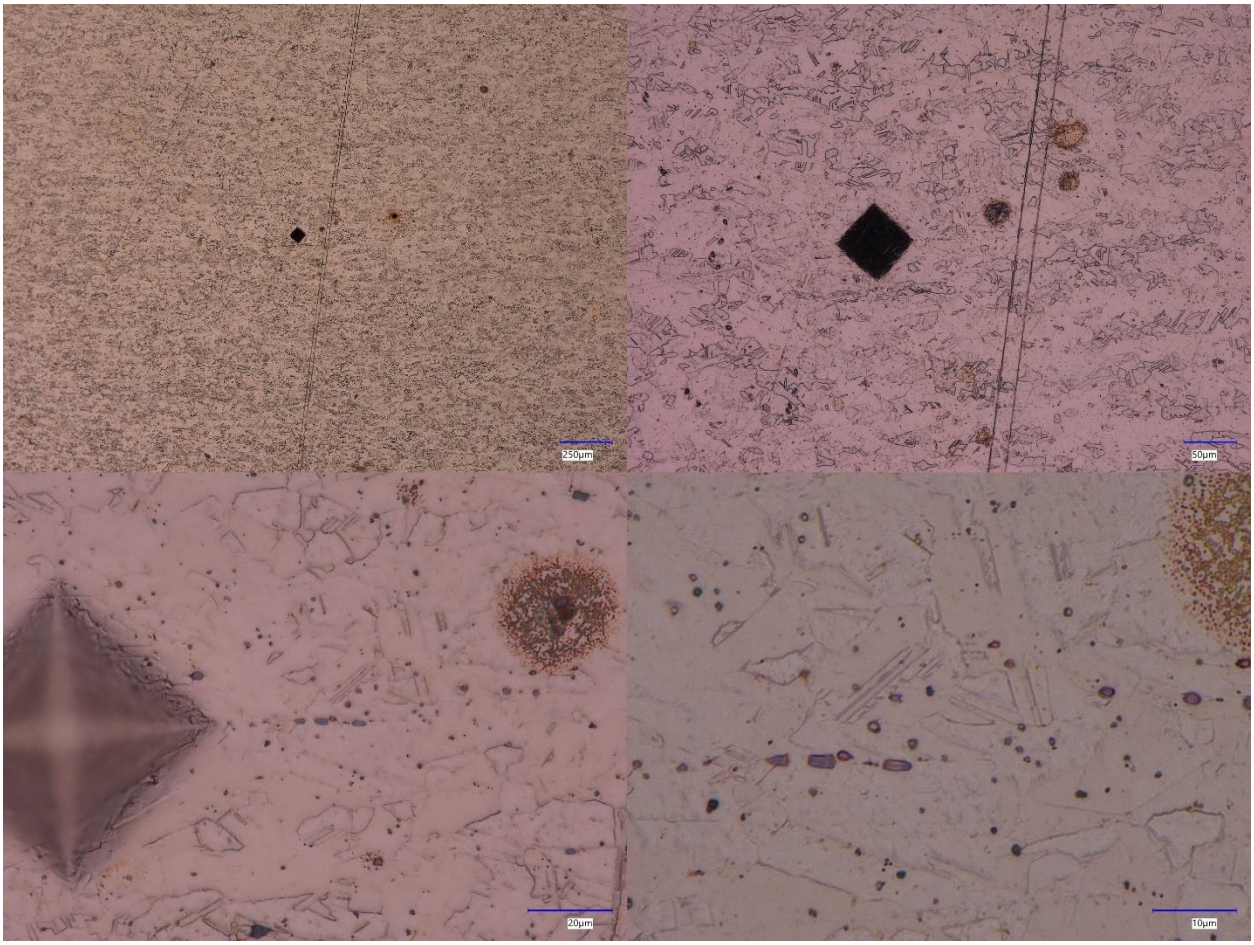

Figure 68: Pretest M1-01 Coaxial Quad

(Upper Left 100x, Upper Right 500x, Lower Left 1000x, Lower Right 4000x)

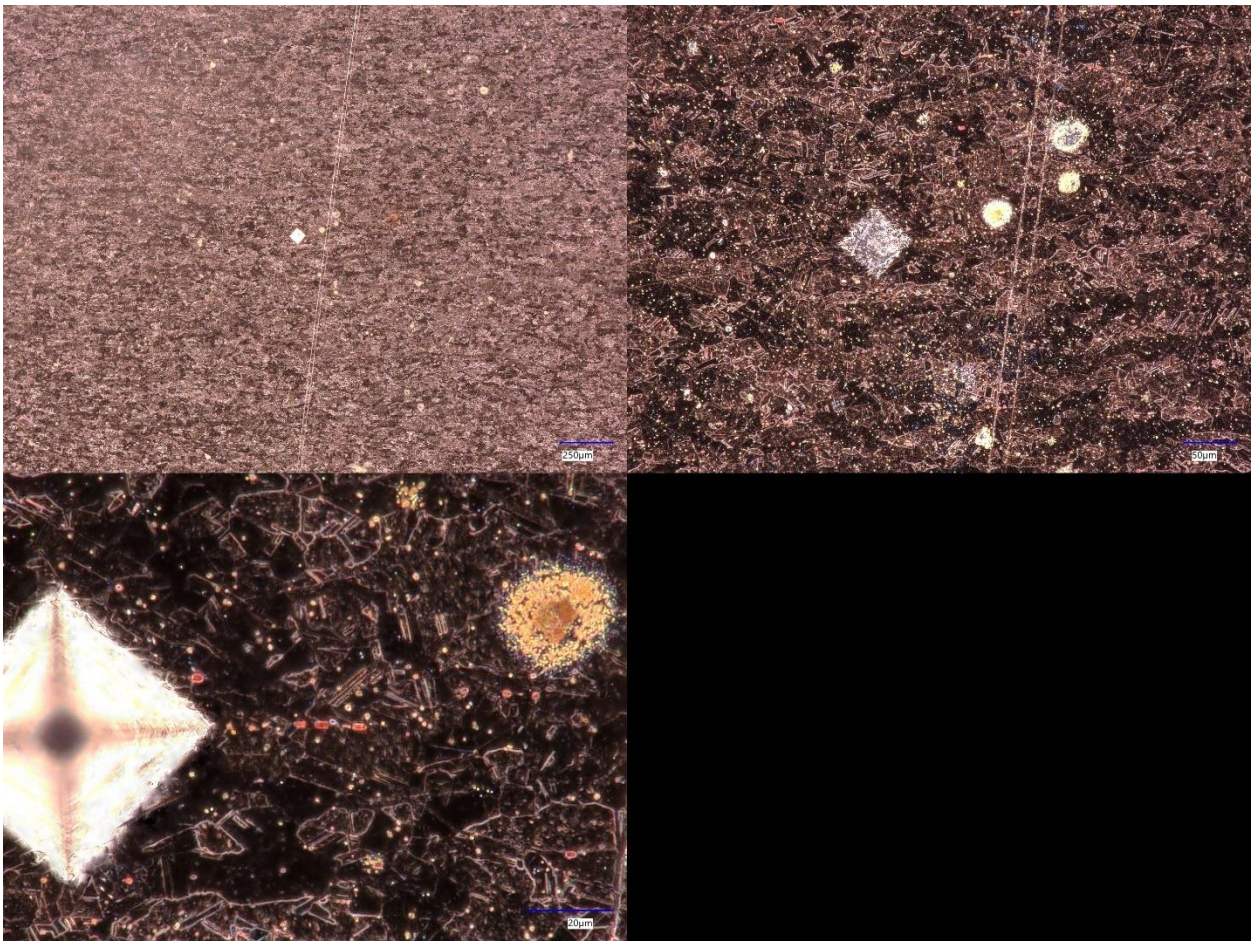

Figure 69: Pretest M1-01 Full Ring Quad

(Upper Left 100x, Upper Right 500x, Lower Left 1000x, Lower Right Intentionally Blank)

Following my pressurization cycle, I repeated the process of capturing individual photos as well as created new split and quad images to assist in comparison. The goal of these posttest images was to capture the exact same locations as the pretest so comparisons can be easily made. Figure 70 shows a pretest and posttest image comparison for a 110 Multi-Purpose Copper – 1/2 Hard (M2) coupon.

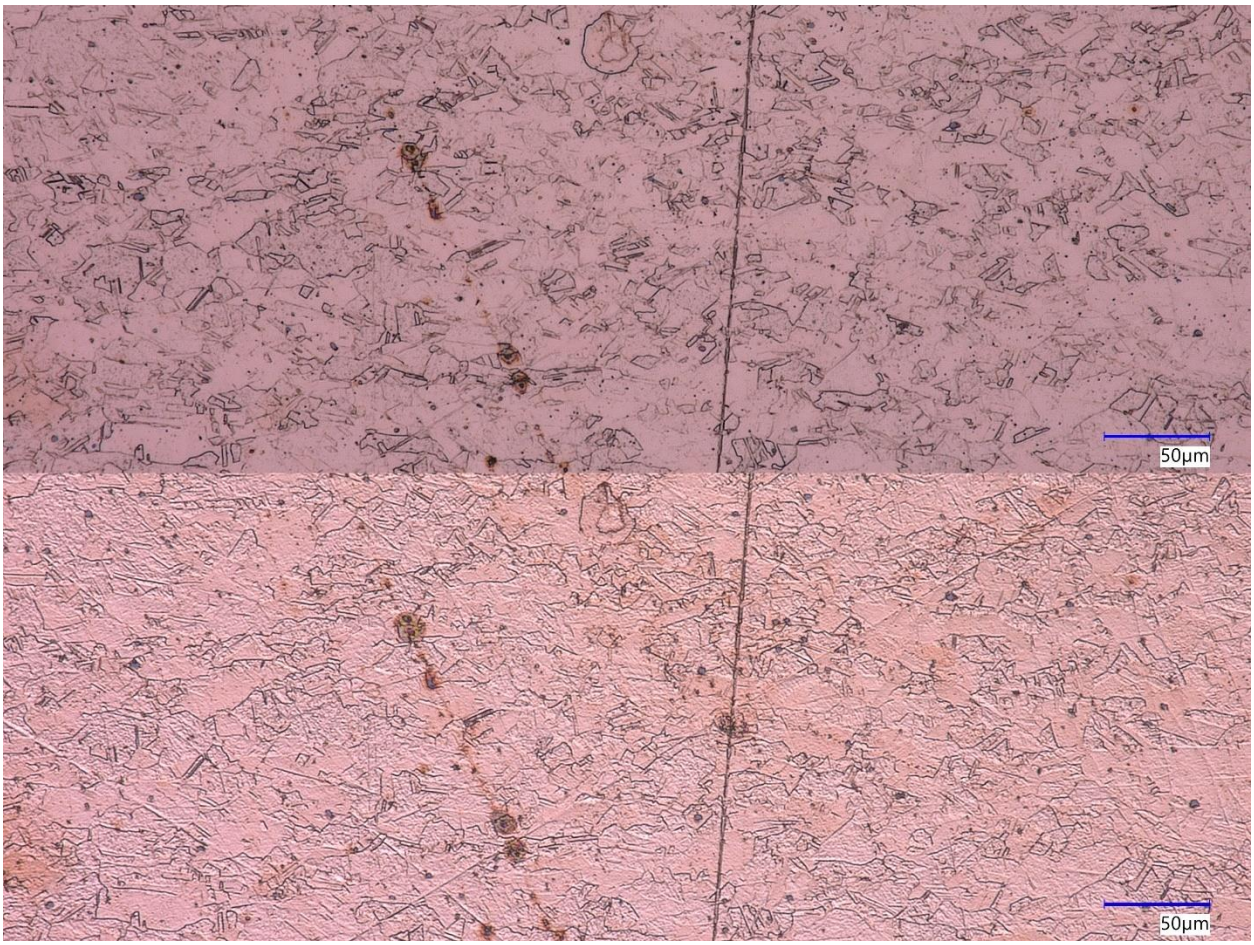

Figure 70: M2-07 Side-by-Side Pre_Post 500x

We can see in this side-by-side comparison that while the general surface topography did not change, there are indications of some event occurring due to the pressurization cycle. The slightly darker upper section is due to the changes in the brightness settings during imaging and is not a material characteristic. The next section will discuss additional differences.

5.5.2 Copper Comparative Analysis

With all the planned images captured and split and quad images created, the next step was to characterize the observed changes in general for each alloy. This was done prior to looking into detailed image analysis looking for unique and specific instances of surface topography changes.

Figure 71 and Figure 72 are representative comparative images for the 110 Multi-Purpose Copper – Annealed (M1) coupons. This is for only one coupon but the findings are similar for all coupons of this alloy. Only coaxial light images are presented here for the copper as the full ring images do not provide good comparative images. These images were created and are contained in the image library accompanying this thesis.

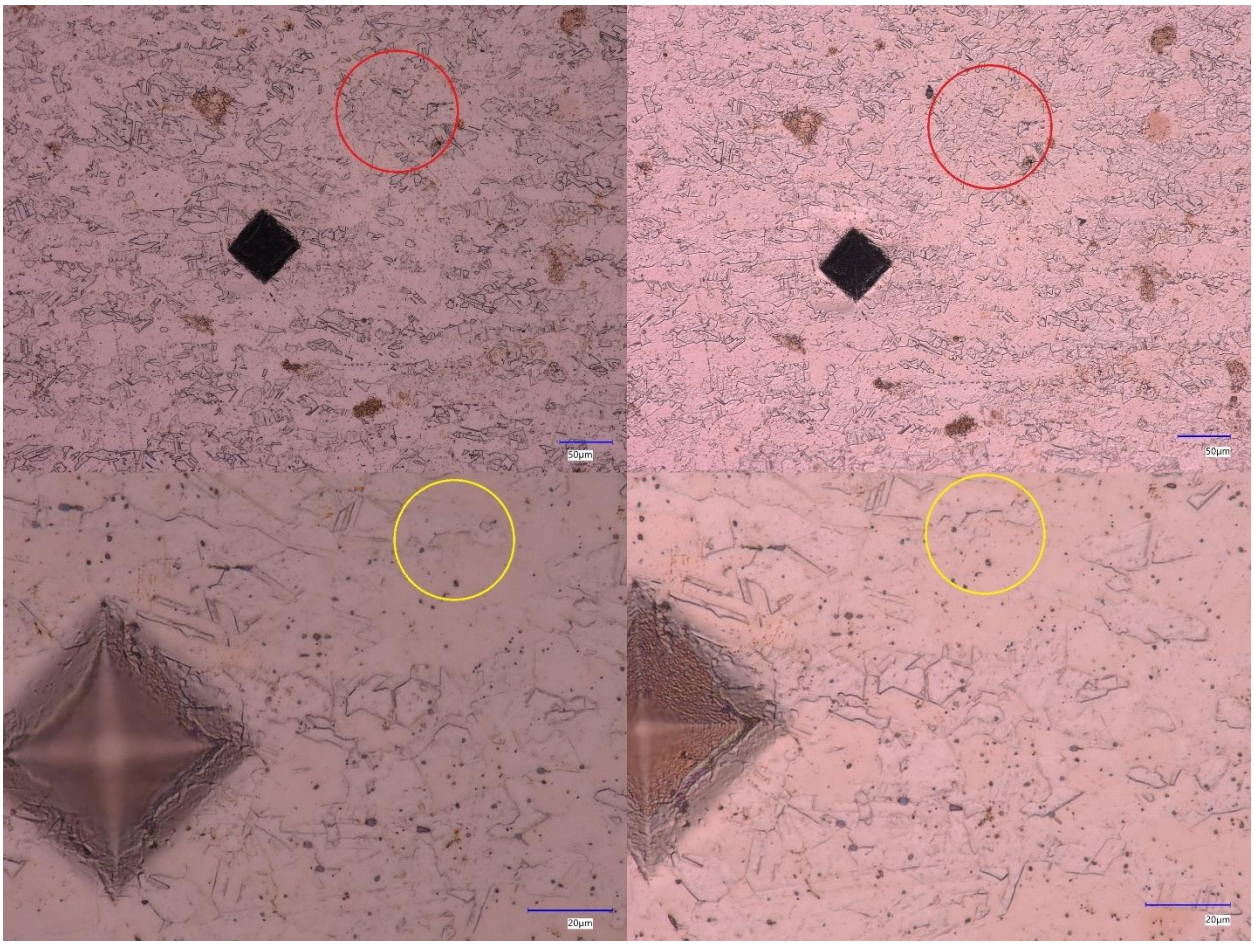

Figure 71: M1-05 Coaxial Comparative Quad 500x_2000x Pre_Post

In this quad image the pretest images are on the left and the posttest images are on the right. The upper two images are at 500x magnification and the lower two images are 2000x magnification. The surfaces of the annealed copper suggested signs of feature exaggeration after

pressurization. The red circles in the upper portion show similar feature topography however after pressurization the features are more pronounced as shown in the detailed view in Figure 72.

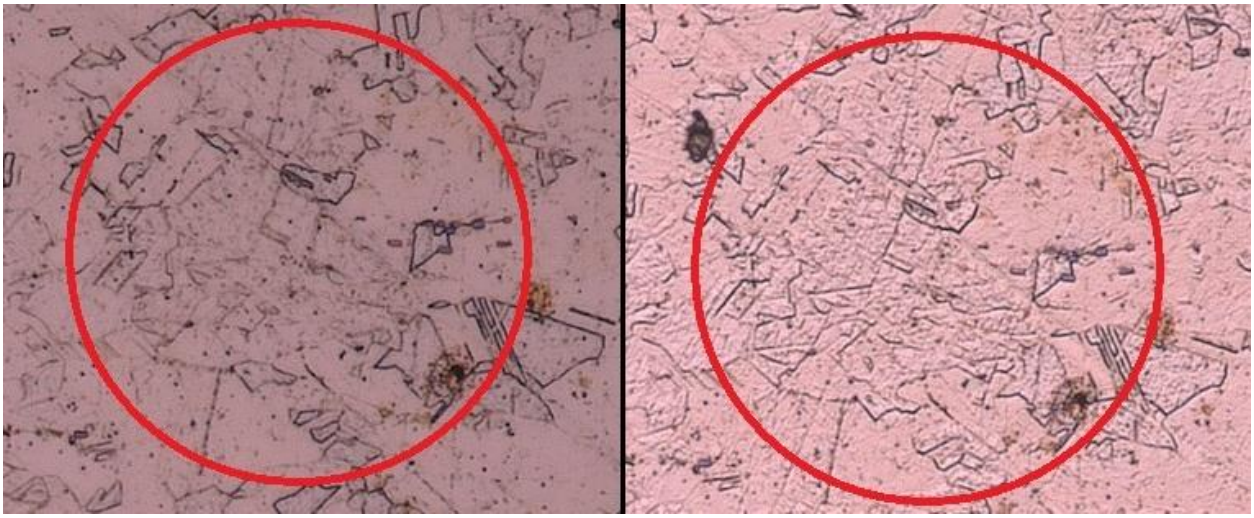

Figure 72: M1-05 Coaxial Comparative Quad 500x_2000x Pre_Post Red Circle Detail

At the higher 2000x magnification I have highlighted several features that are more pronounced after pressurization. These are the locations noted for additional investigation as possible indications of physical changes. My initial interpretation is that the surface became rougher from pressurization but further analysis is required.

Figure 73 and Figure 74 are representative comparative images for the 110 Multi-Purpose Copper – 1/2 Hard (M2) coupons. The images are organized similarly to the previous images for the annealed copper.

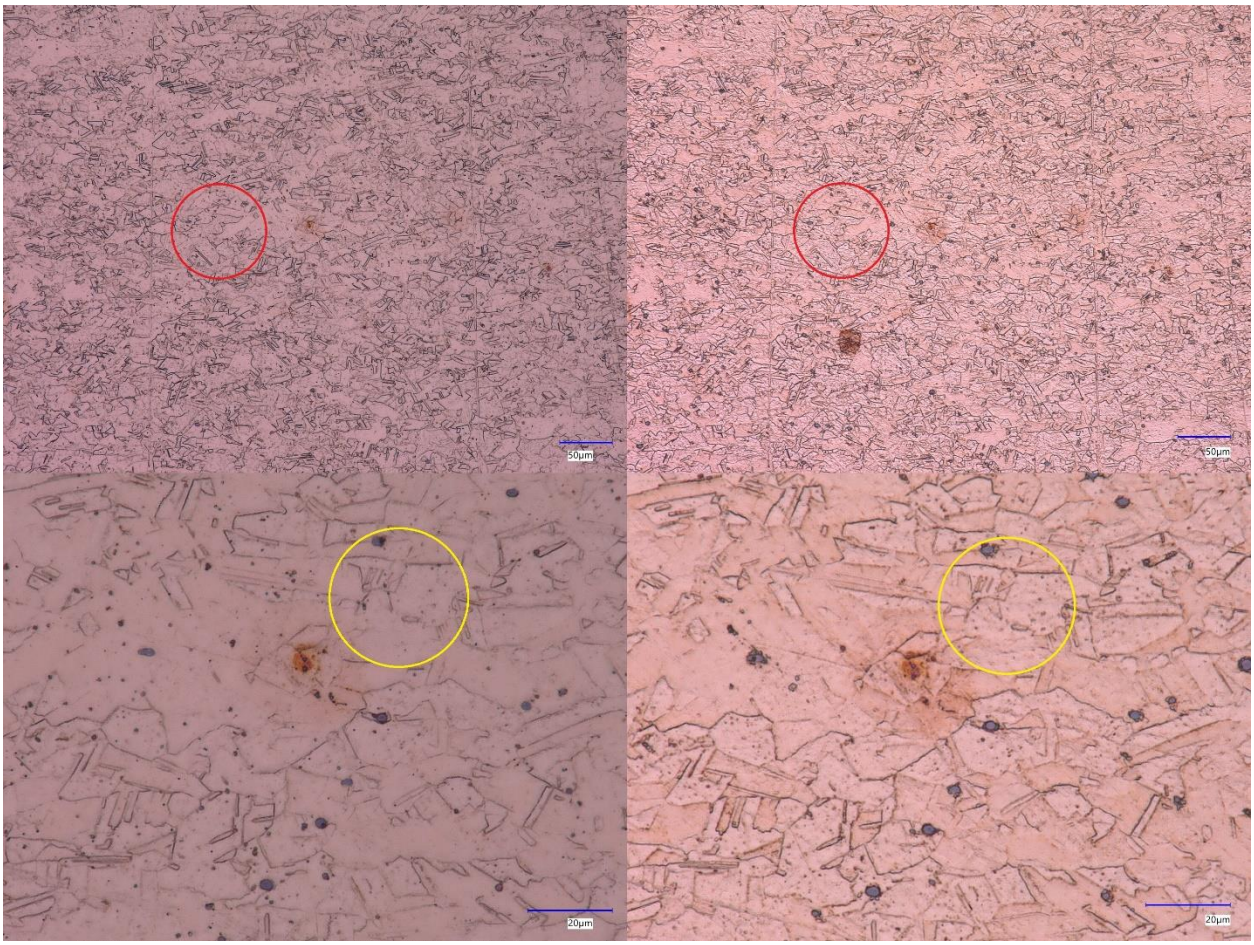

Figure 73: M2-05 Coaxial Comparative Quad 500x_2000x Pre_Post

The 1/2 hard copper has more tightly packed surface features making identifying areas of change more difficult. Again, focusing on small sections of the 500x magnification portions of the quads highlighted with red circles and shown in Figure 74, we see that the unique surface features are more pronounced and may indicate surface movement. The yellow circles also show more pronounced features at the higher magnification.

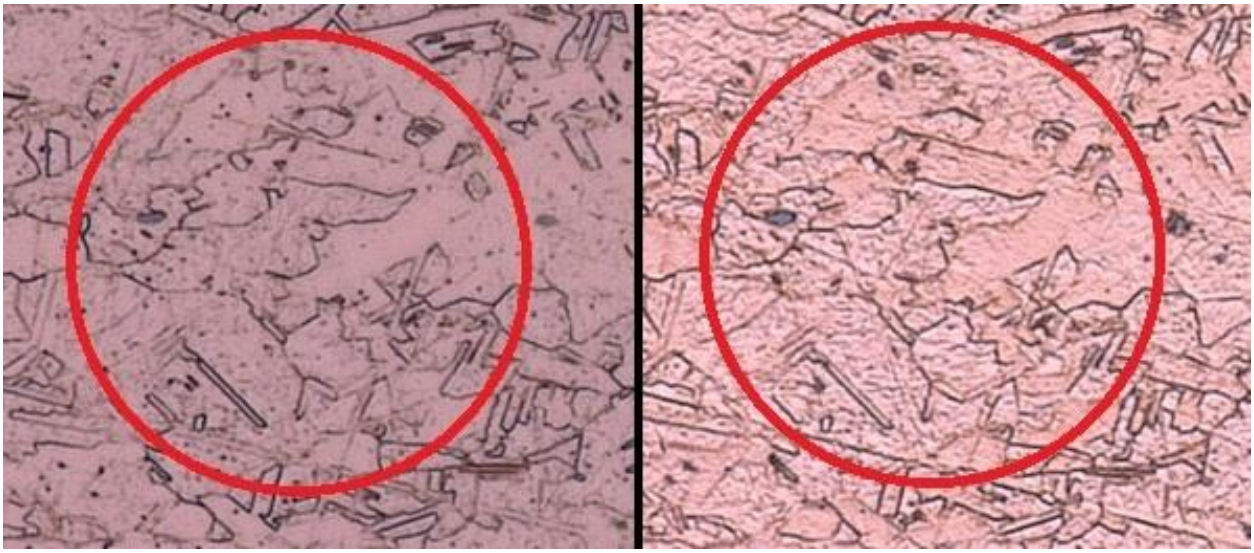

Figure 74: M2-05 Coaxial Comparative Quad 500x_2000x Pre_Post Red Circle Detail

Based on the initial image analysis of the copper alloys, there was sufficient justification for further analysis of the surface topography to determine if specific instances of change can be identified. Section 5.5.4 provides an example of this analysis.

One or both copper alloys showed statistically significant changes in physical dimensions and hardness means. The traditional ideology among material scientist is that if there is a change in hardness or physical properties, there should be a change in grain structure. The normal magnification to see these changes is 500x or less; however, there is evidence that these changes have occurred without a significant change in grain structure or size. This could represent a novel way of modifying hardness in a material, but further research is required to confirm and quantify the findings.

5.5.3 Aluminum Comparative Analysis

Unlike the copper alloys which are the same alloy but different manufacturing process hardness values, the aluminum alloys cannot be directly compared. 1100 and 2024 aluminum alloys have different alloying elements and intrinsic mechanical properties. Therefore, they would

not expect to have the same response to external forces or conditions. What may be observed in one alloy is not expected to be seen in the other.

Figure 75 and Figure 76 compare the 1100-H14 Hardened Easy-to-Form Aluminum (M5) coupons.

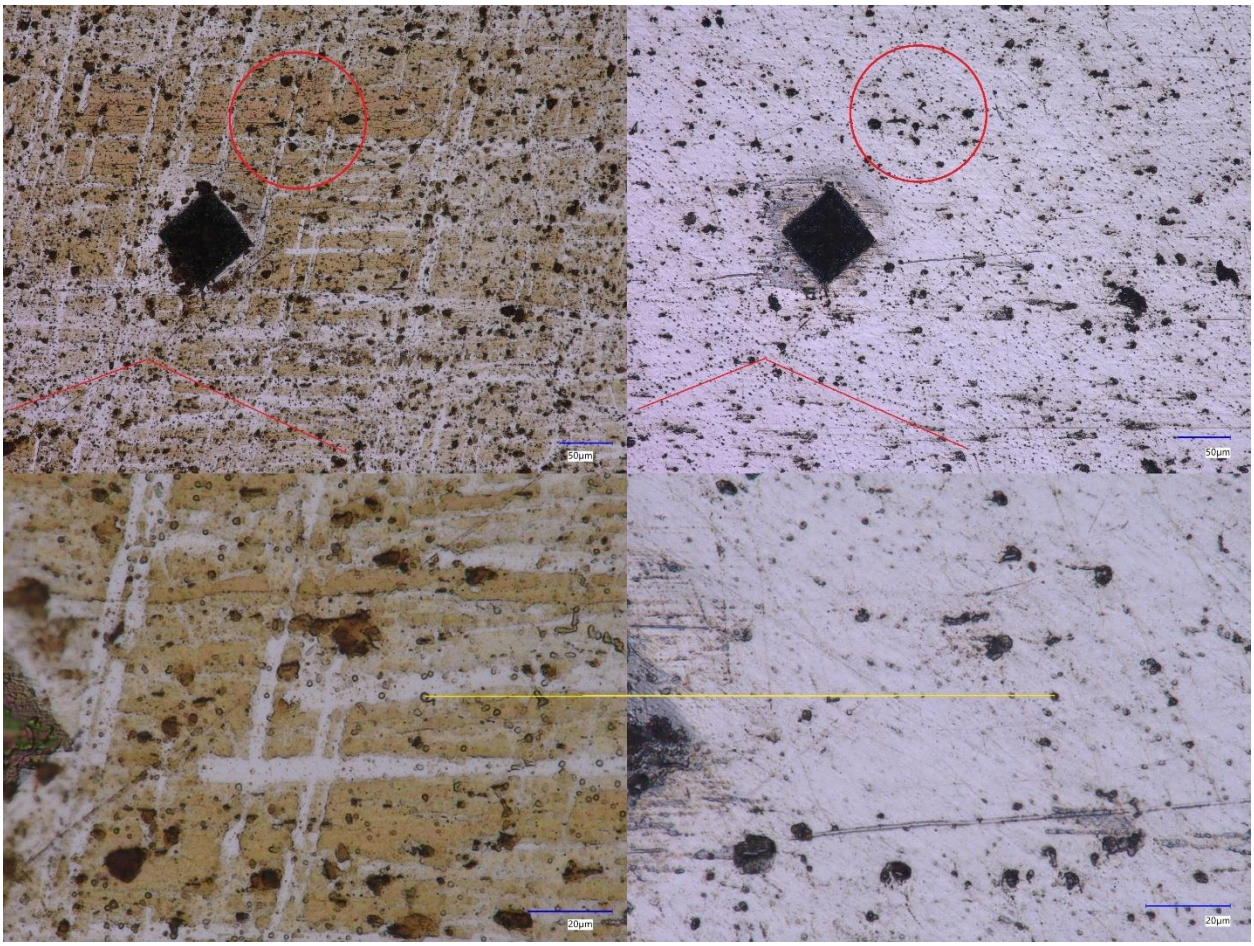

Figure 75: M5-05 Coaxial Comparative Quad 500x_2000x Pre_Post

The surface color change is not due to a lighting condition change. The stain or surface contamination appears to have been removed during the pressurization sequence for some unknown reason. Many of the surface features have also been removed or slightly altered in appearance. To assist in visualizing the locations I have used a red line in the 500x magnification images to trace a series of surface features that did not change. In the 2000x magnification section,

I have included a yellow line as a visual queue between the same spot before and after. The red circles detailing an area of the 500x magnification section is shown in Figure 76 and the general pattern of large surface features is clear when detailed in this way, but the feature shapes and surrounding areas has been altered.

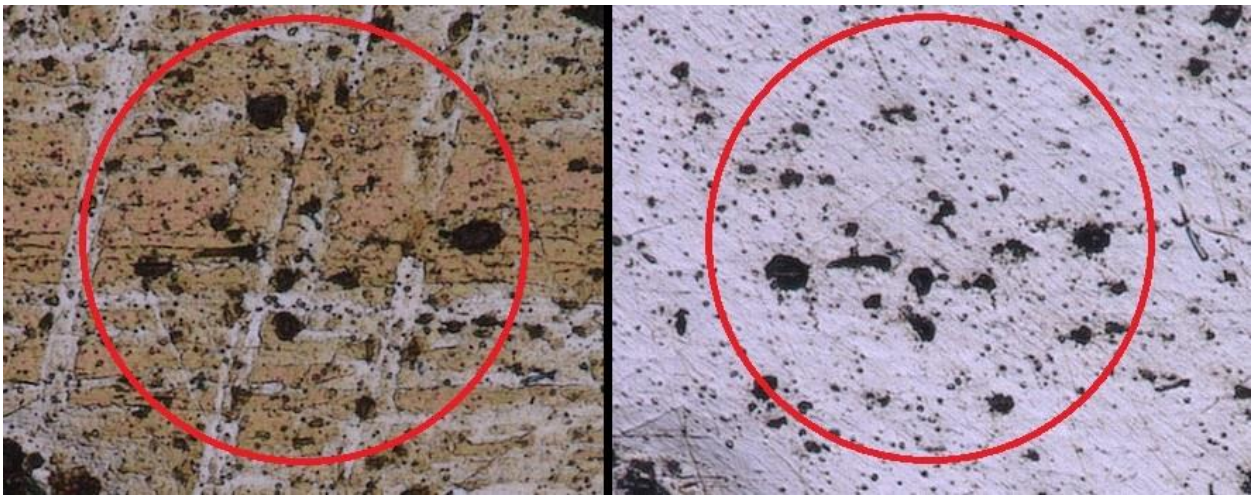

Figure 76: M5-05 Coaxial Comparative Quad 500x_2000x Pre_Post Red Circle Detail

The 1100 series aluminum had the most drastic surface appearance change but showed no signs of hardness or physical dimension changes. As can be seen in the images, the changes were so drastic that duplicating the locations for higher magnification images required additional steps. As discussed earlier, the full ring lighting showed the small particulate either from embedded polishing grit or contamination. However, the full ring comparison images in Figure 77 and Figure 78 show this surface condition appears to have been removed.

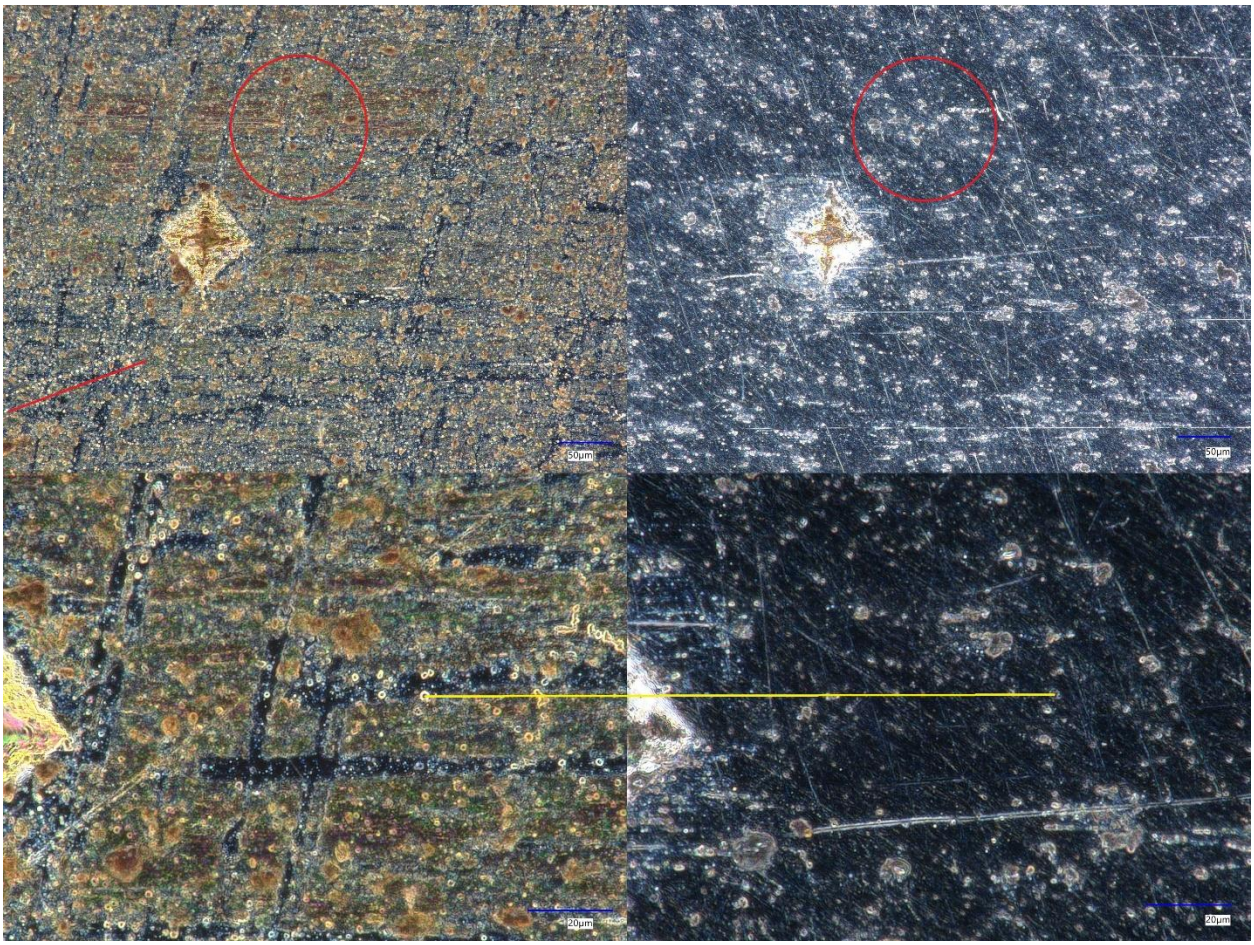

Figure 77: M5-05 Full Ring Comparative Quad 500x_2000x Pre_Post

I have included similar circles and lines as those used in the coaxial image comparison for visual reference and a detailed view of the red circled area. Remnants of the larger surface features remained posttest for locating key areas for further study. I would speculate that the widespread change in surface condition would point to a large deformation of the surface which caused the harder polishing grit or contamination to flake off the softer aluminum surface. The red circles detailing an area of the 500x magnification section is shown in Figure 78 and the general pattern of large surface features is clear when detailed in this way, but the feature shapes and surrounding areas has been altered.

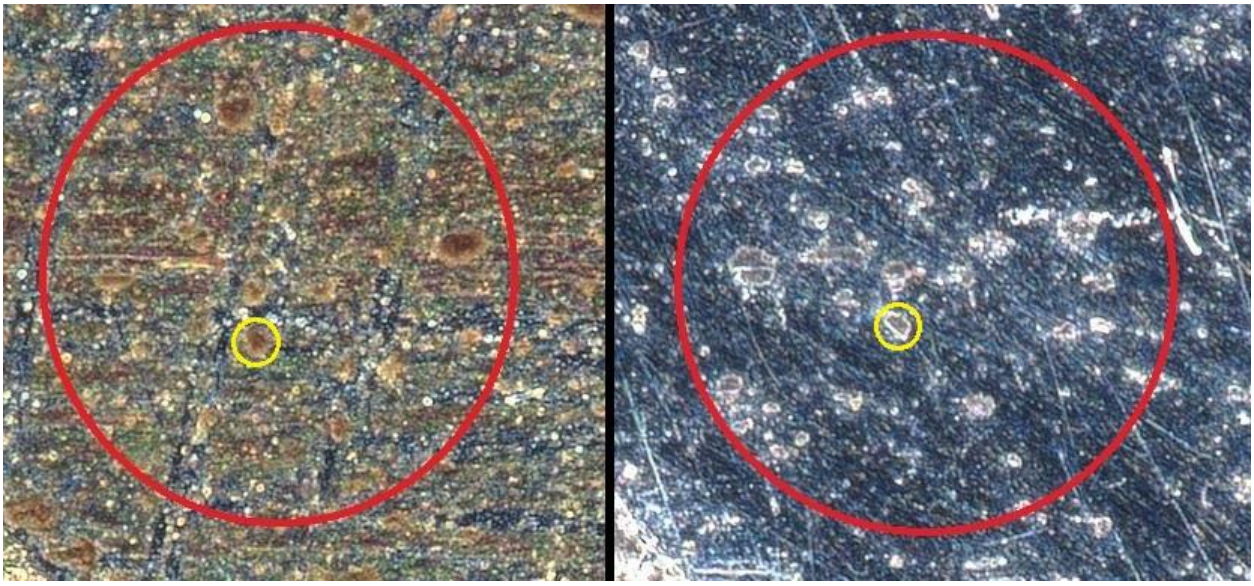

Figure 78: M5-05 Full Ring Comparative Quad 500x_2000x Pre_Post Red Circle Detail

With the removal of the surface contamination the surface topography is more clearly visible. The 1100 series aluminum showed no statistical change in average hardness or physical dimensions, but the distribution of hardness values narrowed. The posttest surface was not cleaned with a polishing cloth or treated in anyway other than normal handling. Further research and more stringent cleanliness and handling techniques will be required to understand this phenomenon.

Figure 79 through Figure 81 compare the 2024-T4 High Strength Aluminum (M6) coupons. My full ring 2024 images failed to reveal any indications of changes due to the uniform color of the material masking the stain. The analysis of the 2024 coupons used only coaxial light images though full ring images were captured for further analysis if desired.

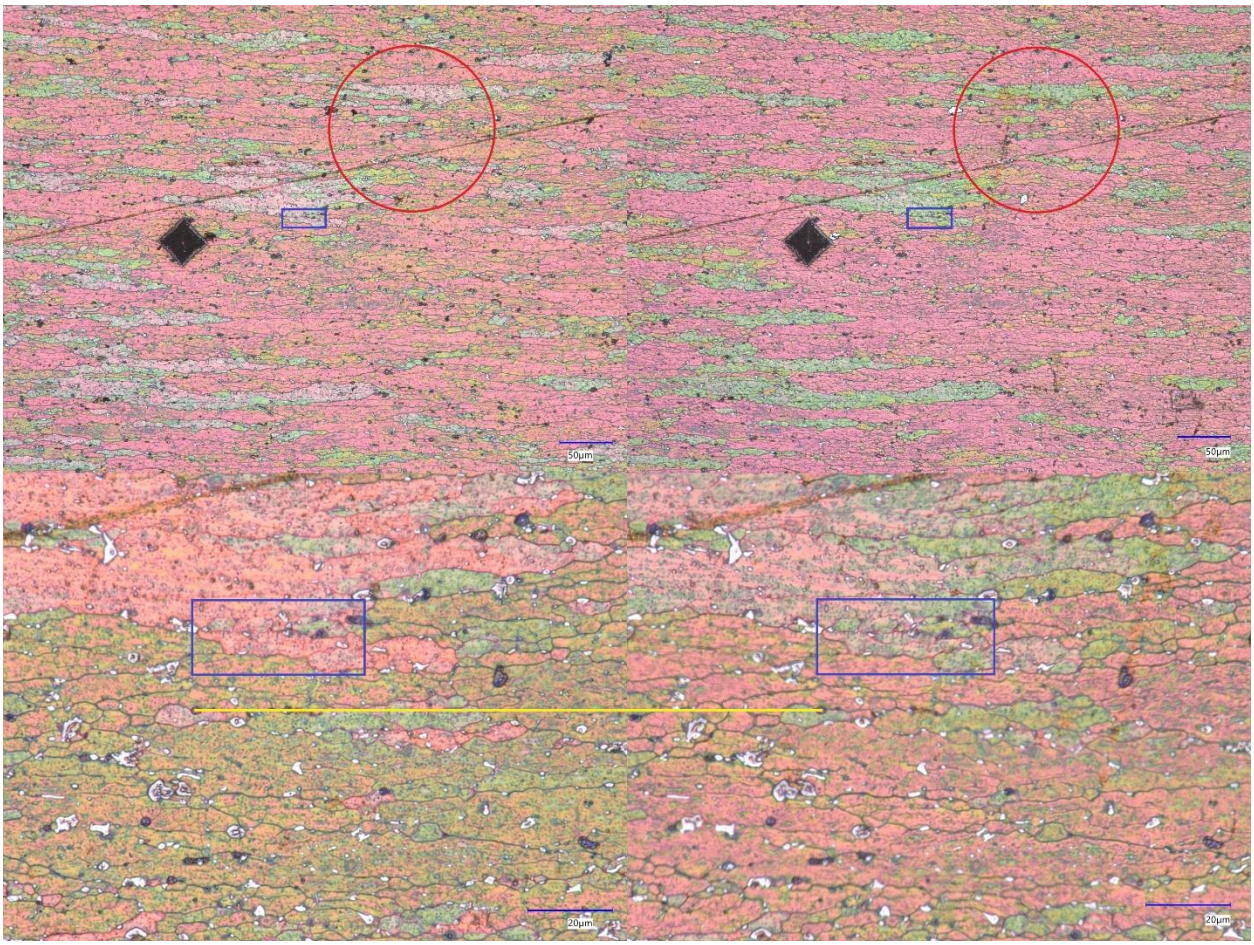

Figure 79: M6-05 Coaxial Comparative Quad 500x_2000x Pre_Post

The surface changes in the 2024 coupons were not as apparent as in the 1100 series alloy. The stain was much easier to see, and the general shape and locations of the grains remained constant. The color shift was not significant. The angle of light from the microscope, as well as other factors, such as oxidation and other surface conditions, cannot be stopped while exposed to air. Therefore, a shift from red to green did not immediately indicate a region of interest. I have added red circles to the 500x images in Figure 79 to show the same locations pretest and posttest and a yellow line from the same feature pretest and posttest in the 2000x portion. Figure 80 is a magnified view of the areas circled in red.

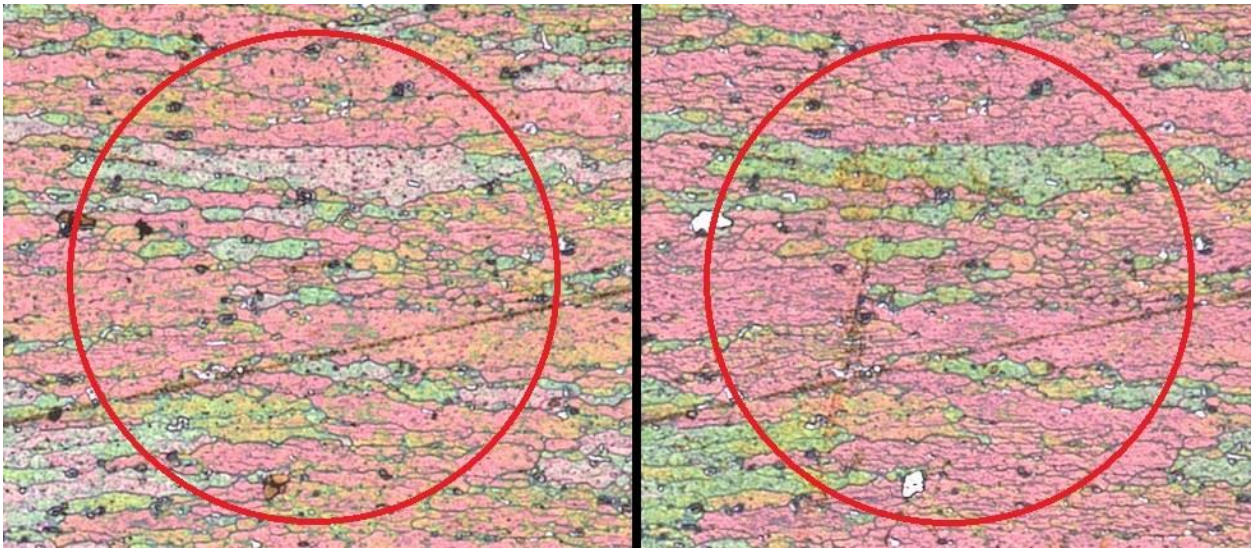

Figure 80: M6-05 Coaxial Comparative Quad 500x_2000x Pre_Post Red Circle Detail

Excluding the color shift on the surface of the 2024, there are not many changes at the 500x magnification that is traditionally expected for grain structure change. There are some instances where the boundary lines between grains have thickened but further analysis is required to determine if the lines represent actual surface changes or are artifacts of the lighting conditions.

At higher magnifications there were indications of surface grain structure changes. The purple boxes in Figure 79 are magnified to 4000x in Figure 81.

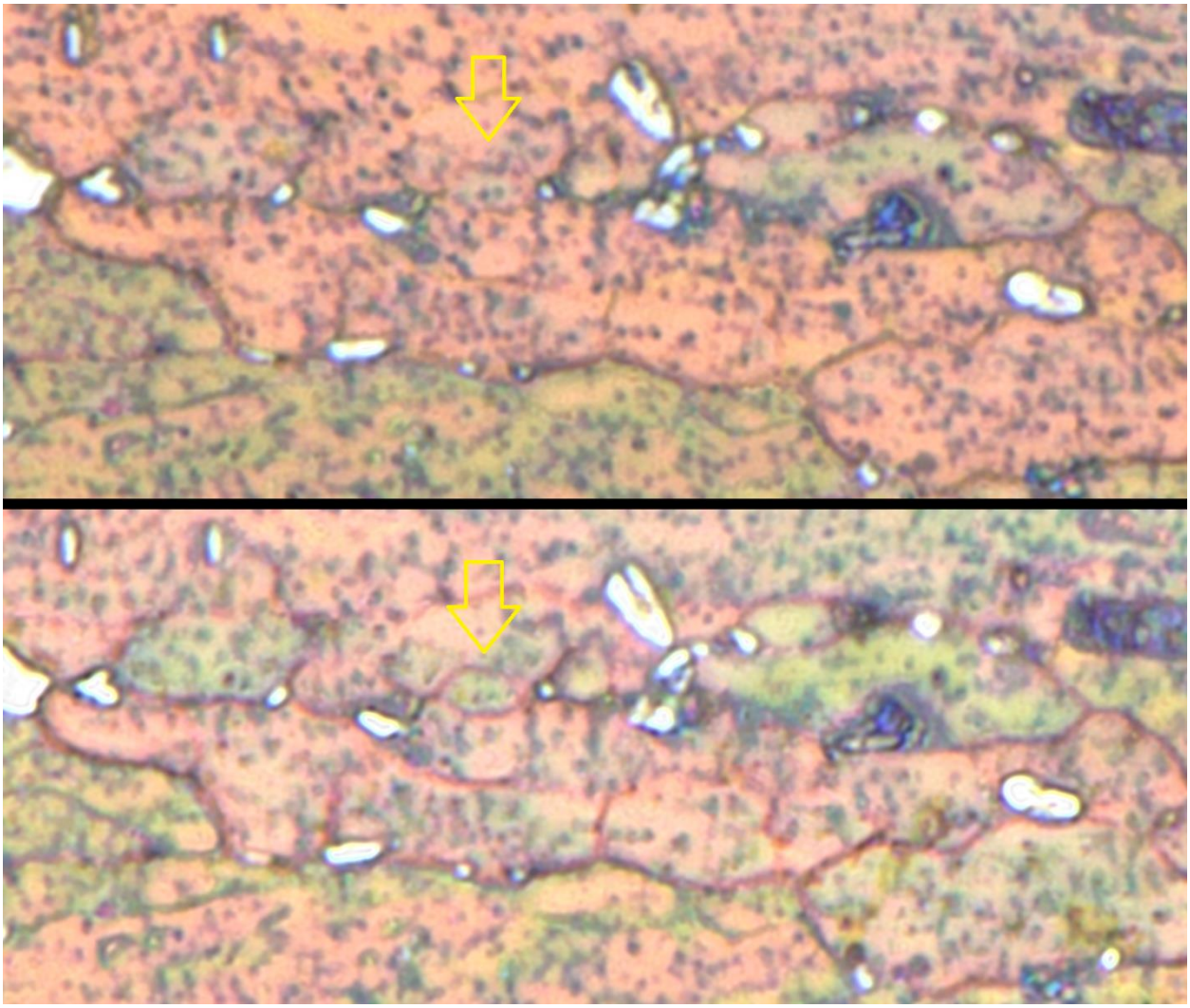

Figure 81: M6-05 Coaxial Comparative Split 4000x Pre_Post

In the top part of Figure 81, the pretest grain structure is more uniform in color. While some surface features are present, they do not indicate unique grain boundaries. The bottom portion, however, shows more pronounced grain boundaries and changes in surface features. The yellow arrow points at a specific region where a defined grain is present after exposure to high pressure. Other instances are visible throughout the surfaces in these images, but further analysis is required. The next section discusses details of the surface changes.

5.5.4 Detailed Indications of Surface Topography Changes

The Keyence VHX-7000 Ultramicroscope is capable of 3D imaging surfaces up to 6000x magnification. Taking advantage of this feature, I investigated several coupons from each alloy to determine how well this method worked for investigating surface changes, which may accompany material property changes. Light reflectance, angle, and other factors go into the detailed analysis capable from these scans, but the general topography and shape of features were expected to remain the same.

Beginning with the copper alloys, I noticed that the pretest copper images had a significant amount of noise, but I am unsure how this was caused. The highly-reflective surface may have affected the mapper's ability to gather data properly as the noise is less apparent in some darker, less reflective features and patterns than the rest of the surface. Figure 82 shows an angled 3D map for the 110 Multi-Purpose Copper - Annealed (M1) coupon M1-07.

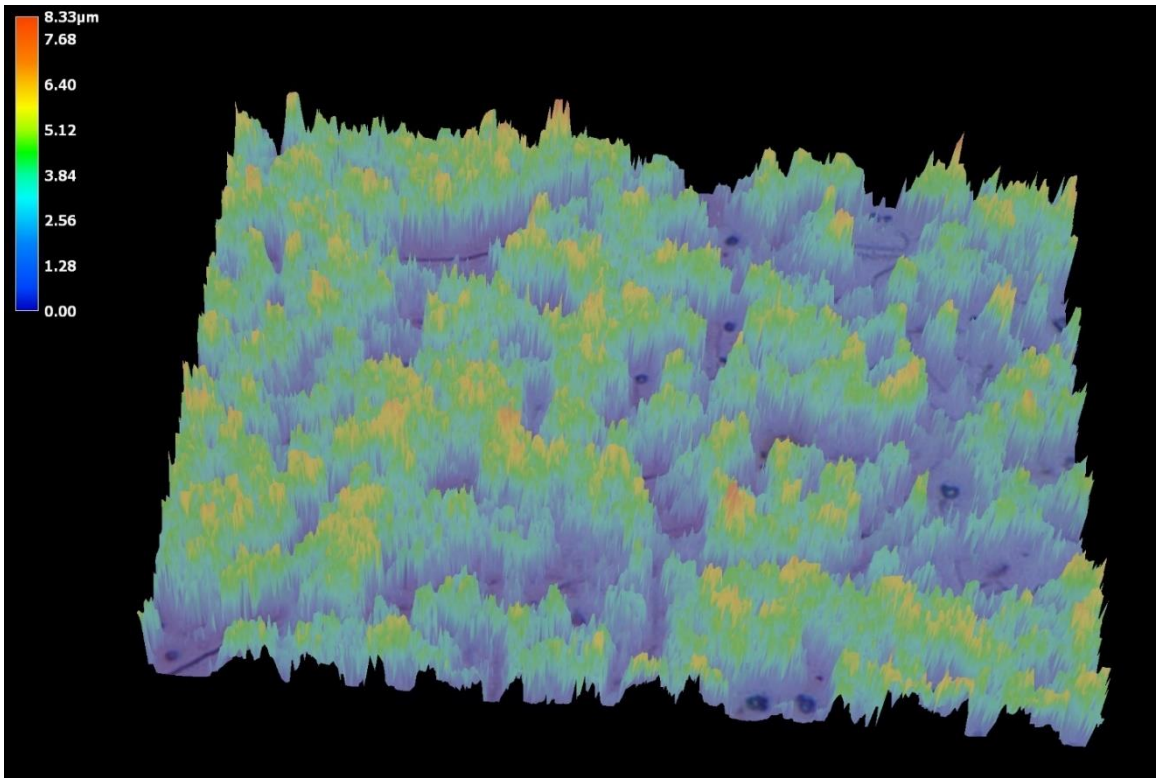

Figure 82: Pretest M1-07 3D Color Map 6000x

The significant peaks and valleys make it difficult to identify locations to perform comparative analysis and the 2D images showed few instances of apparent changes for the copper when compared to the aluminum. The changes described in Section 5.5.2 are better described as holistic and across the entire surface than specific instances. Figure 83 shows the same region of interest following pressurization.

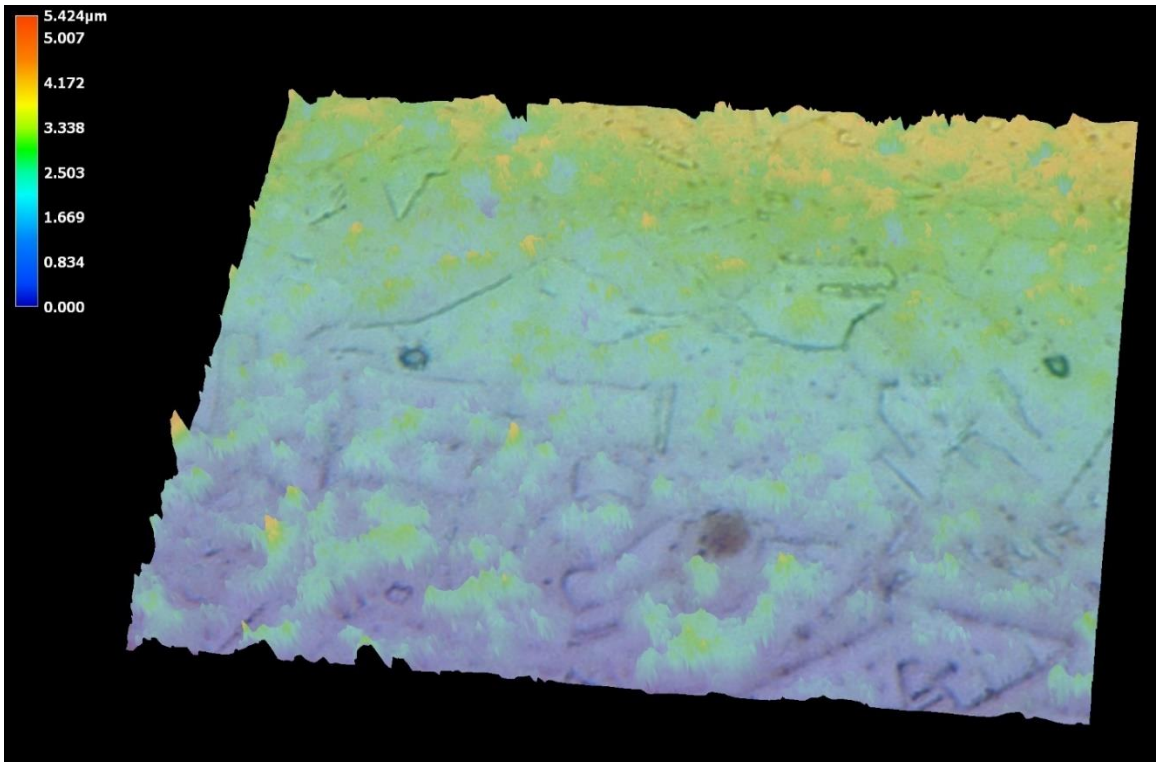

Figure 83: Posttest M1-07 3D Color Map 6000x

The consistent color shift from low too high in the post test images was caused by a slight tilt in the coupon surface in the holder. The original imaging was performed with the samples encased in acrylic, so the surface is more parallel with the surface of the microscope than the 3D printed holder used for posttest imaging.

There are similar peaks and valleys in the posttest image that are not as extreme. The exact cause is unknown, and further investigation and more careful surface preparation and care is

required to determine if such a holistic surface change is real or if it is an artifact of the 3D imaging process.

The 110 Multi-Purpose Copper – 1/2 Hard (M2) material also exhibited noise on the surface of the sample but not to the same extend as the annealed copper. Figure 84 shows the pretest surface of the M2-07 coupon, and Figure 85 shows the posttest surface.

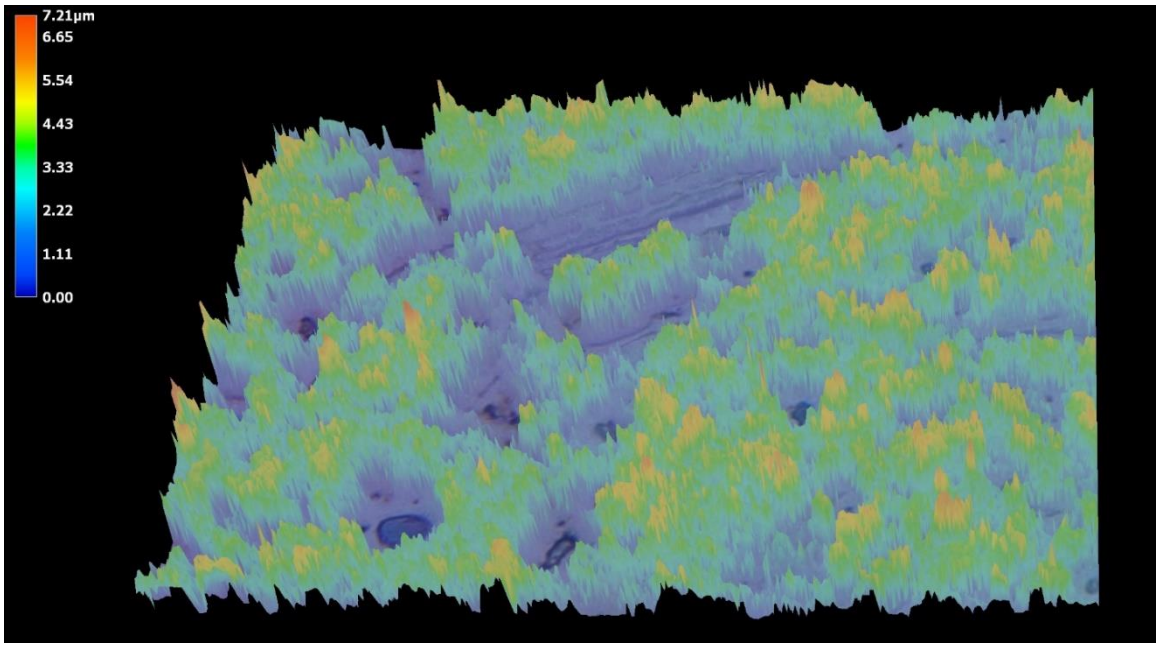

Figure 84: Pretest M2-07 3D Color Map 6000x

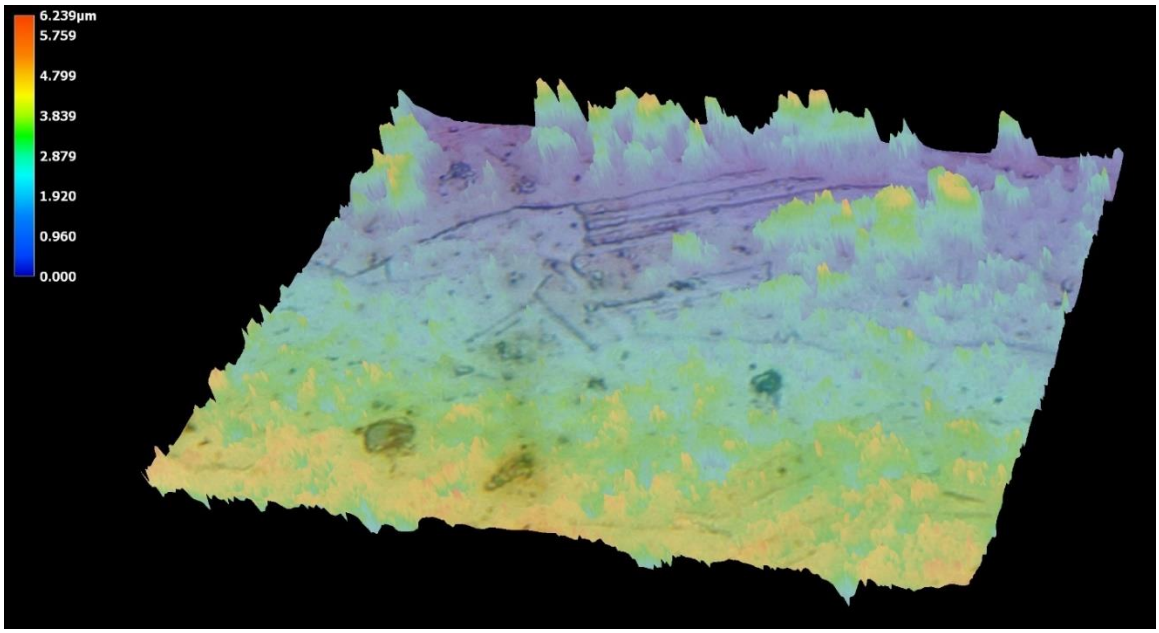

Figure 85: Posttest M2-07 3D Color Map 6000x

It is also difficult to distinguish and changes in these 3D images. To find if there were other means of investigating the surfaces, I used the 3D mapper topography track feature that shows the relative height of points on a given line, which I used to determine if changes occurred. I first identified two features that developed or become more prevalent. Figure 86 is the graph and related images created by the microscope on the pretest 3D surface. The horizontal red line to show how the surface image relates to the track chart.

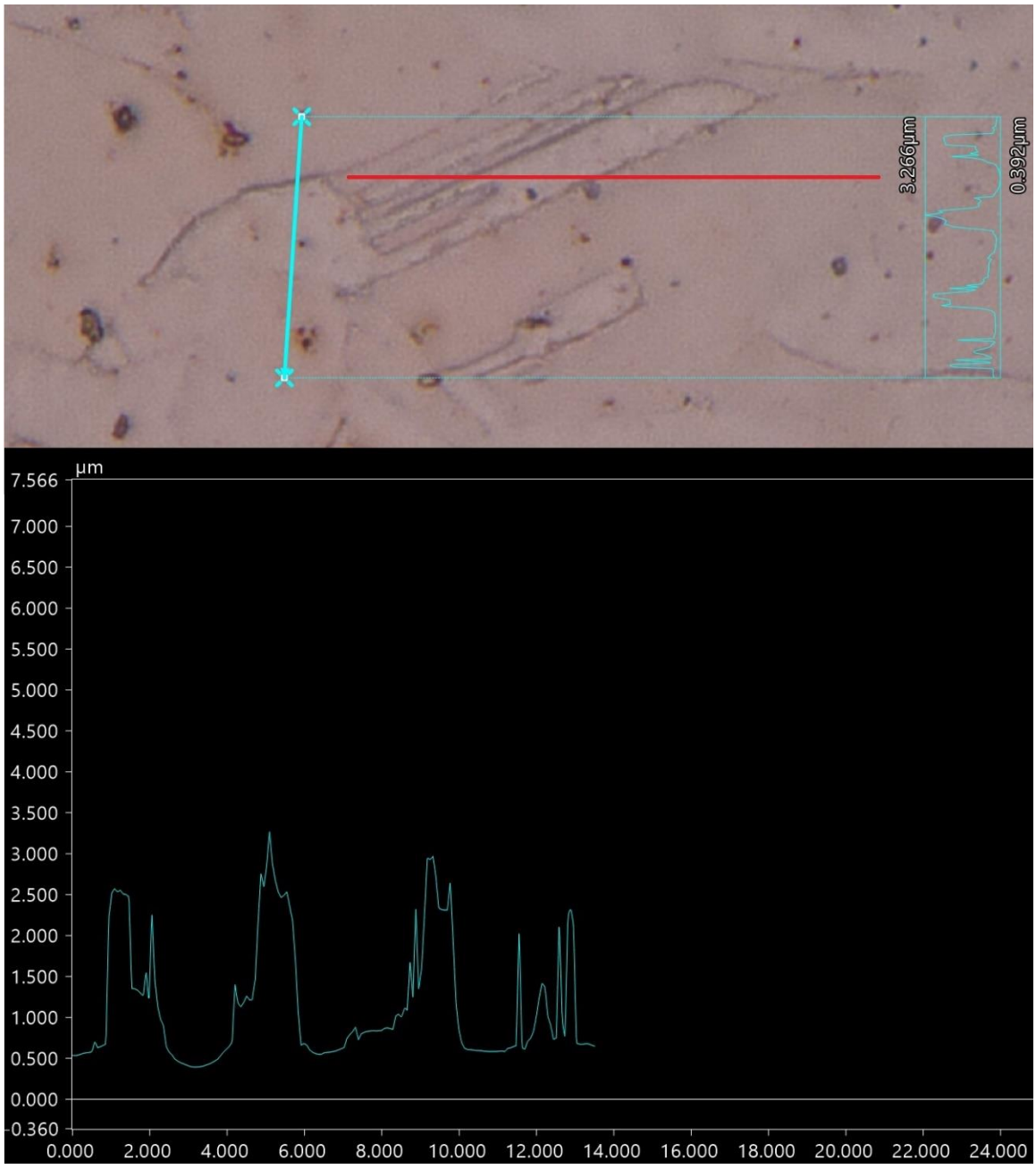

Figure 86: Pretest M2-07 3D Topography Track Chart 6000x

In this image, the line appears to be in a valley between two higher features. Other peaks and valleys are visible on the track chart, but their correlating features on the 2D image is difficult to discern. Because there were no full ring light images at this magnification, there was no other light angle to see features differently. I learned that lines are not always cracks. In some cases, they are simple surface feature transition zones, such as edges of uplifts.

Figure 87 is the posttest track chart of the same area. The line was between two surface feature points that appeared constant throughout testing.

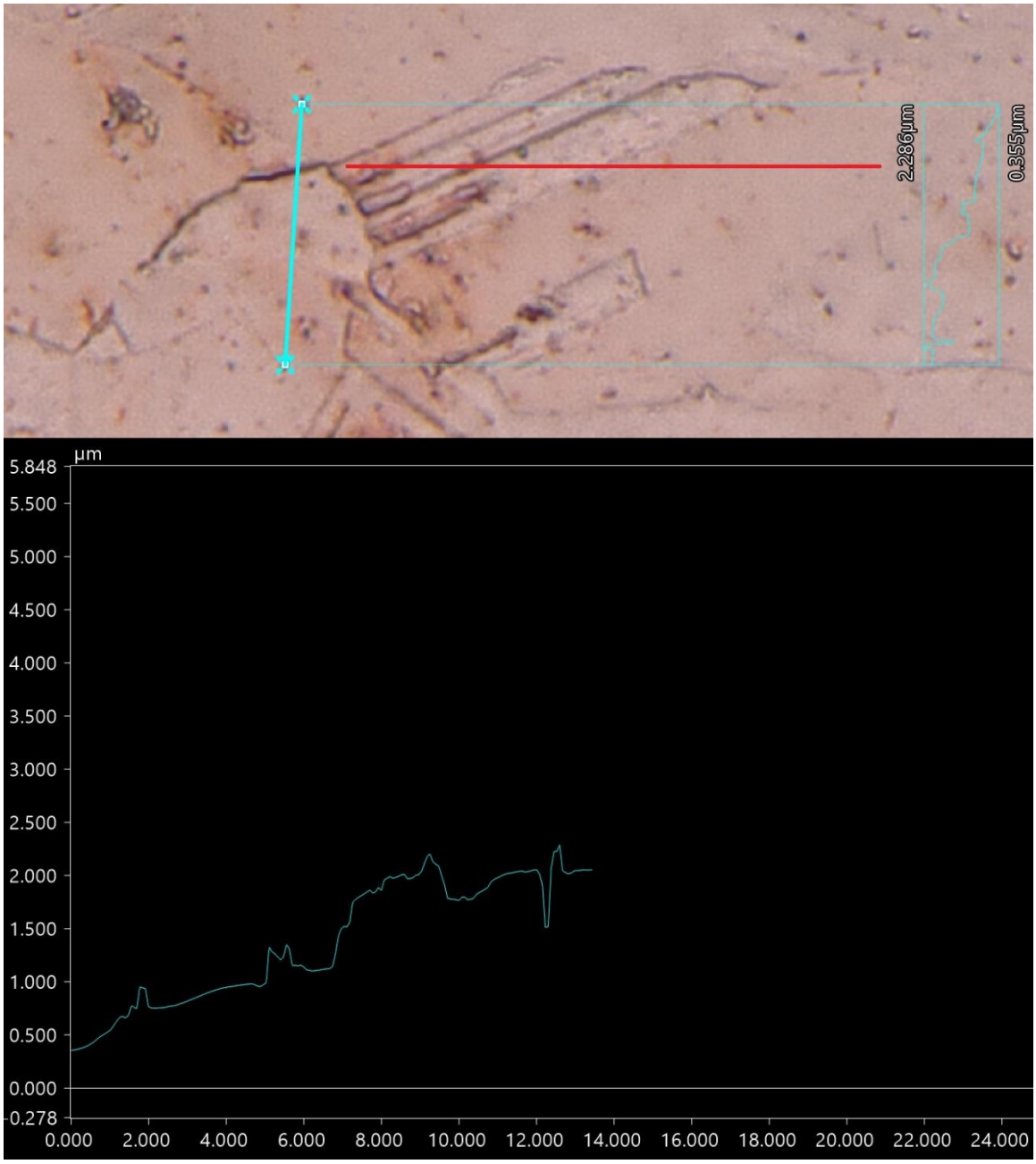

Figure 87: Posttest M2-07 3D Topography Track Chart 6000x

The track chart for the posttest surface is much smoother but still contains four areas of surface uplift. The line of interest in the posttest track chart is still between two uplift features, and the valley is wider, which could be the cause of the intensification of the line from the pretest

image. These could be the same features affected by the pressurization or artifacts of the imaging process, angle of the surface with respect to the lens, or possible loss of reflectivity on the posttest surface. Further investigation is required to determine the exact cause of change, but the method showed promise in revealing surface topography changes in detail if proper controls are used.

The two aluminum alloys tests had different surface changes. For the 1100-H14 Hardened Easy-to-Form Aluminum (M5), as discussed in Section 5.5.3, the surface imaging showed a complete change to the areas of interest following pressurization. Though the surface features were difficult to identify between the pretest and posttest image set, I endeavored to try and test the methodology of finding the same location and determining if the surfaces had changed under the 3D topography feature and if the significance could be determined.

I created Figure 88 to ensure I investigated the same location after pressurization. The top two images are the 500x and 2000x pretest surfaces with a brown surface stain or contamination. The bottom two photos are the same two regions after pressurization.

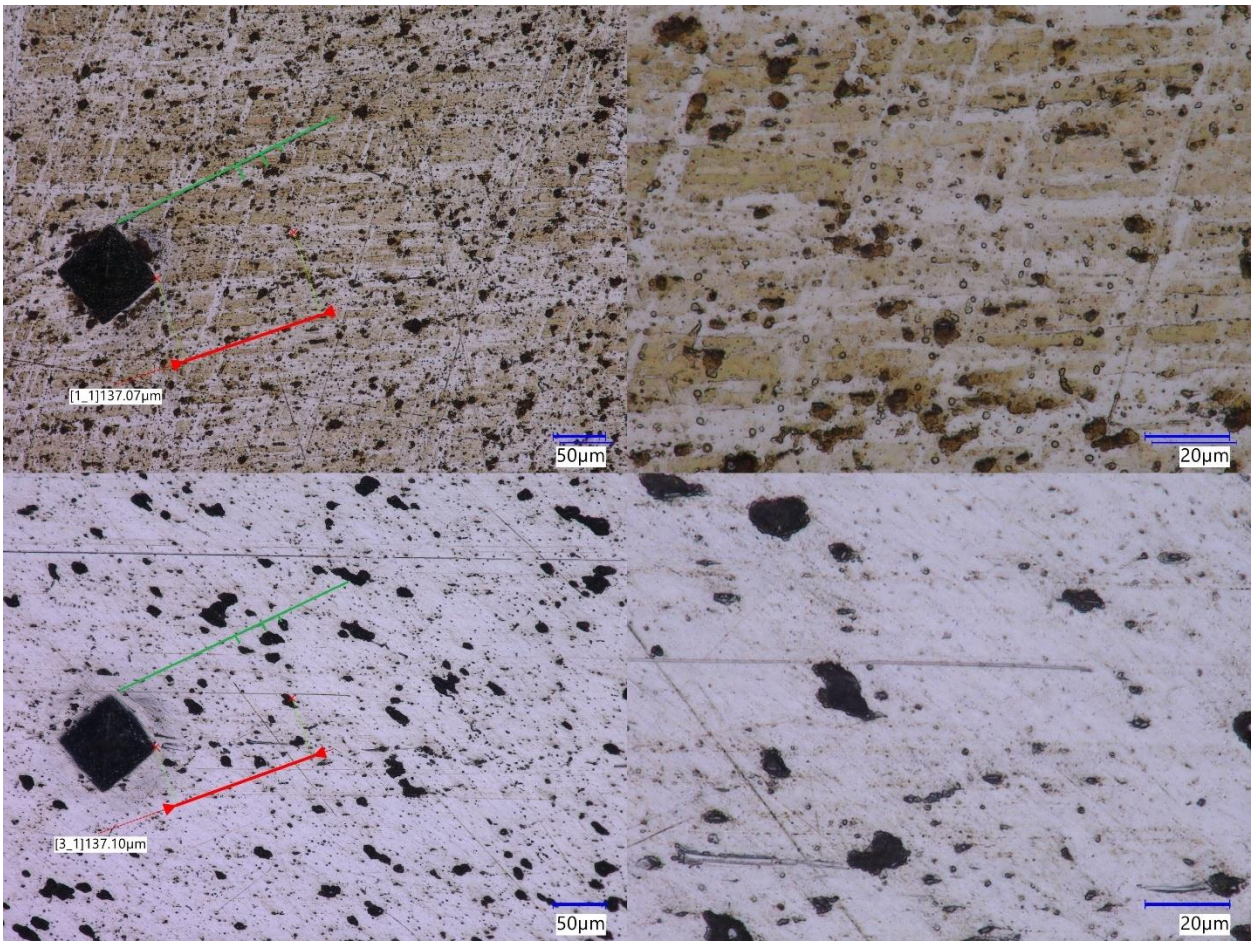

Figure 88: M5-07 Coaxial Comparative Quad 500x_2000x Pre_Post

Though their shapes may have changed, I assumed that major surface features would appear in the same location as a guide to find the same areas. I used a red measurement line from the closest point of the hardness indention to a major feature I knew was part of the pretest 6000x 3D area in the pretest image. I then attempted to find a corresponding major surface feature and found a new shape that I believed was the same feature, which had undergone some surface changes. Green lines were added to highlight common surface lines and three additional large features.

After determining I had located the same location and a major feature to reference, I created Figure 89 to further increase the image comparison from 2000x to 6000x before investigating the

3D data. At this much higher magnification, I observed smaller, features between the images. Green lines were added to several rows of circular surface features that appear to have persisted following the pressurization cycle.

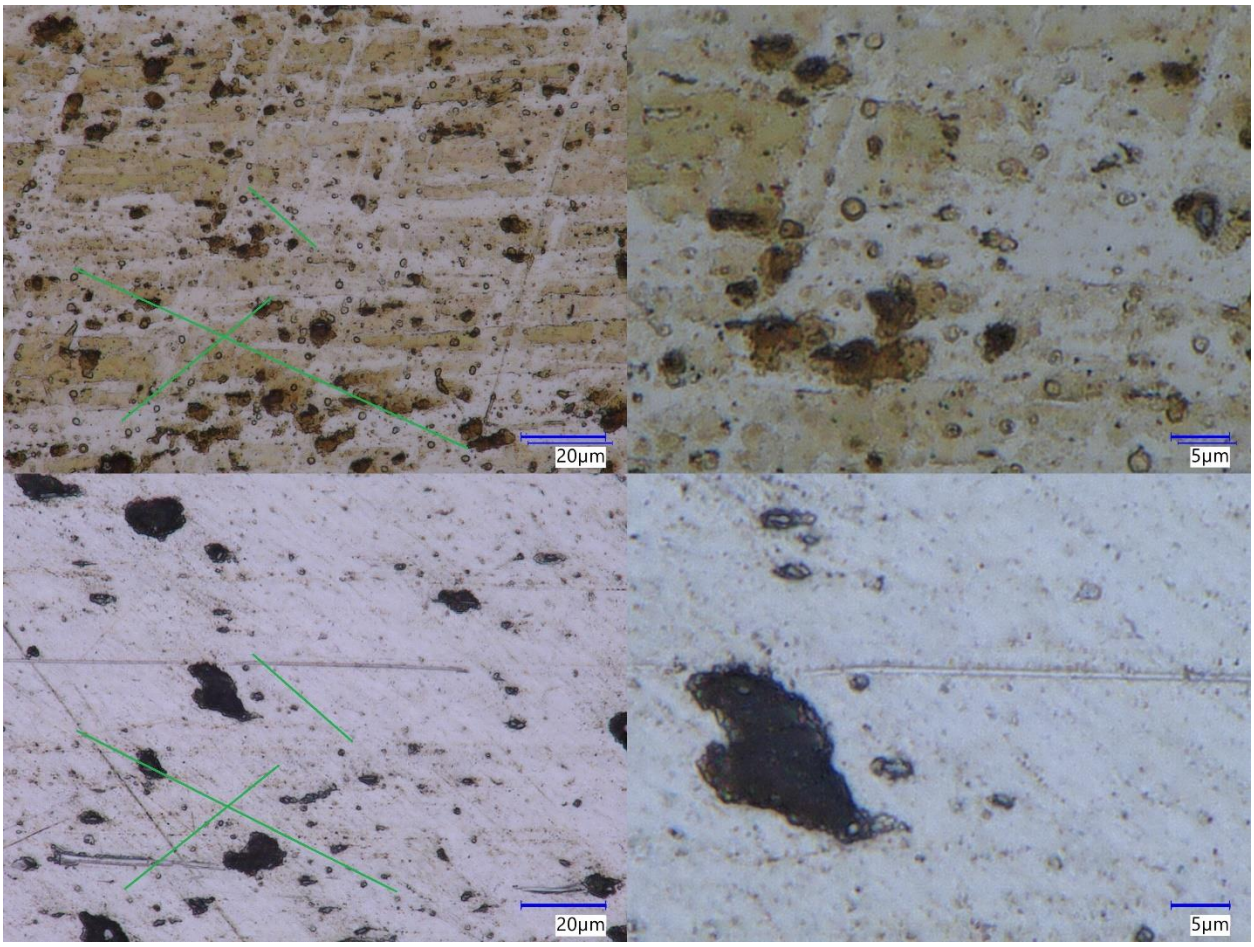

Figure 89: M5-07 Coaxial Comparative Quad 2000x_6000x Pre_Post

It was difficult to see similarities between the two 6000x images, but I assumed the regions were correct based on the measurement and comparison steps taken from the lower magnification images and then compared the two 3D color maps. Figure 90 shows the 2D region of interest and its corresponding 3D color map from pretest imaging. Figure 91 is the same composite image but from posttest imaging.

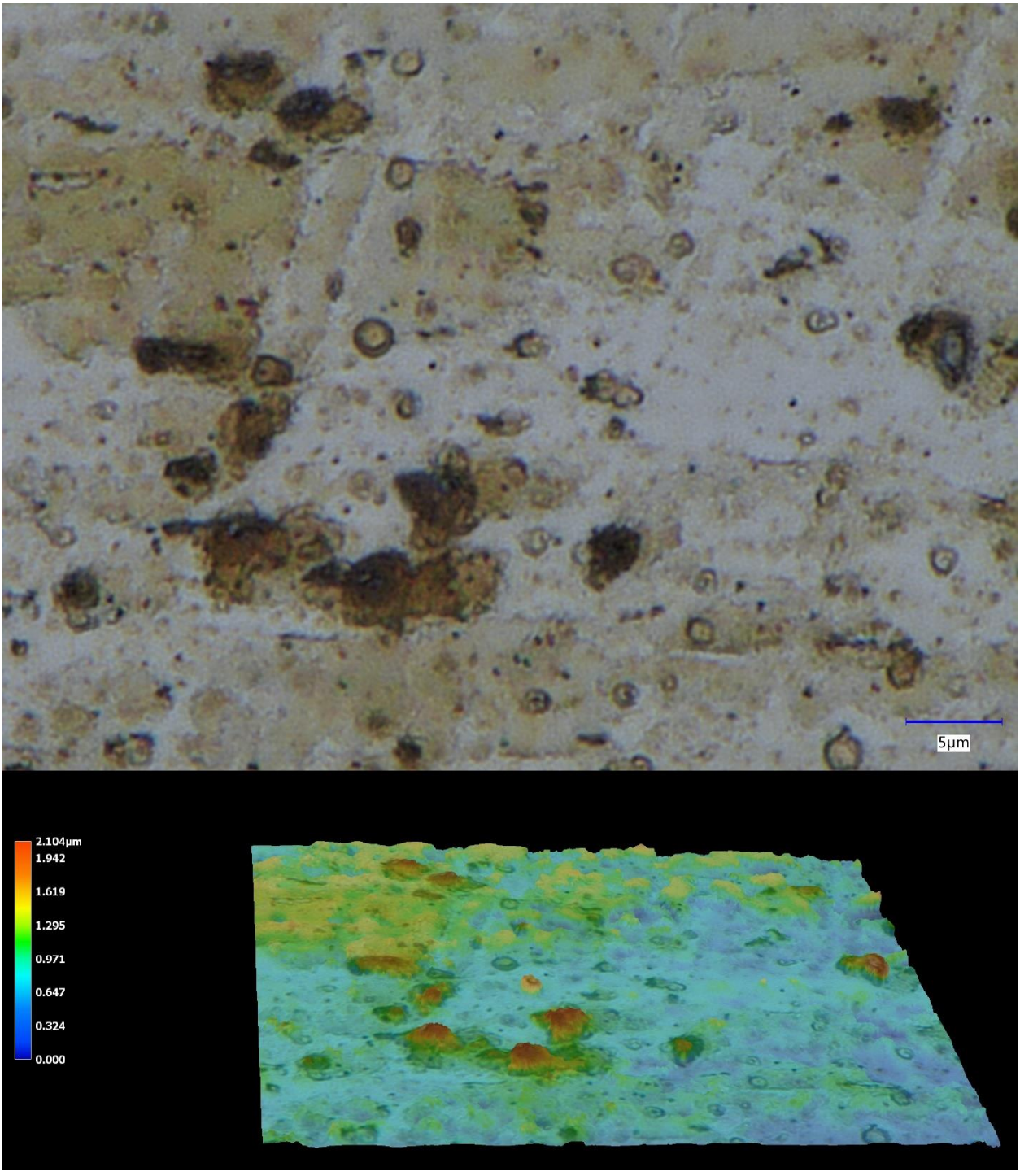

Figure 90: Pretest M5-07 6000x Coaxial 3D Side-By-Side

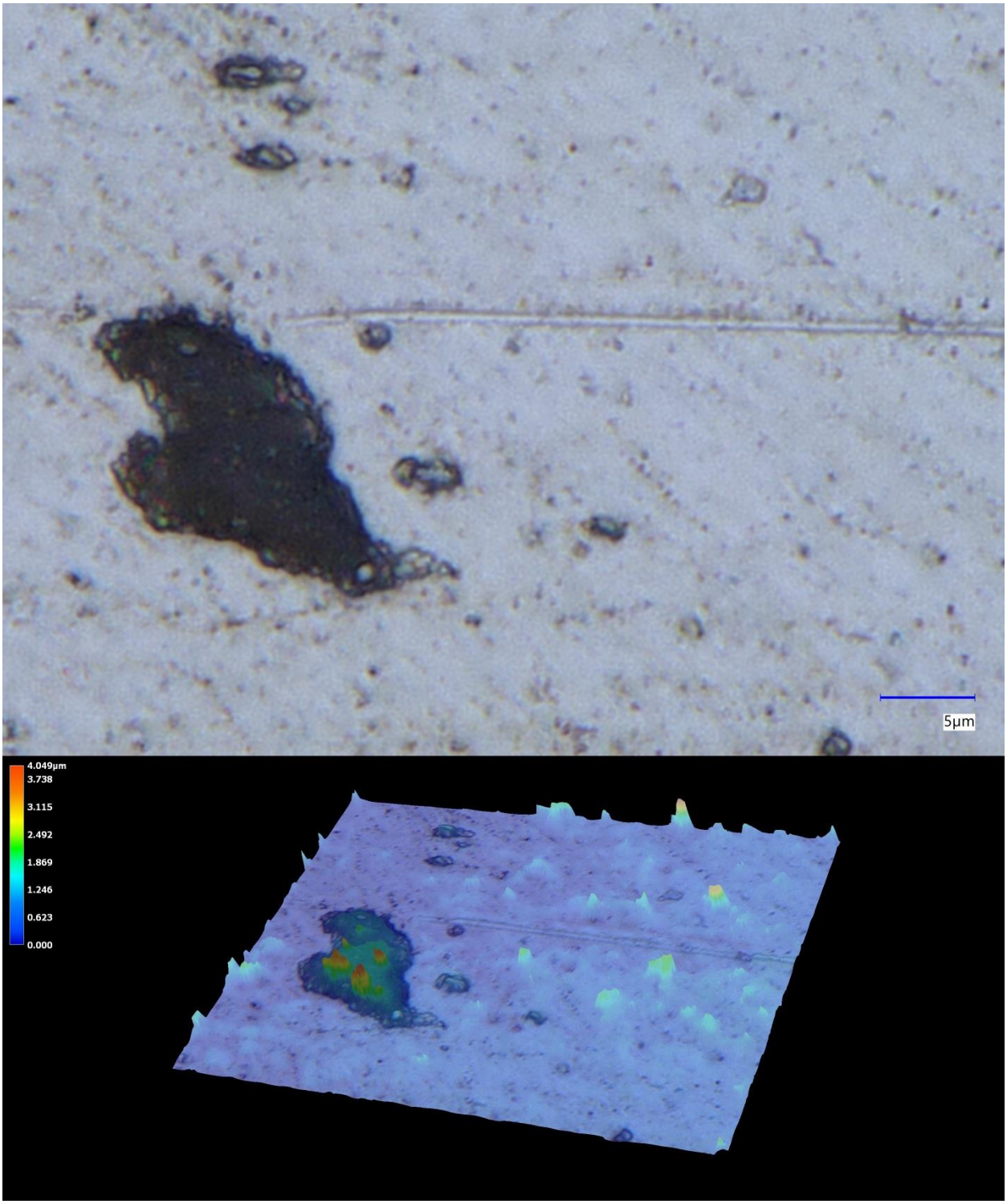

Figure 91: Posttest M5-07 6000x Coaxial 3D Side-By-Side

After comparing these images, I concluded that the surface deformed enough to sluff off most of the surface contamination particles that were in the pretest image. Unfortunately, this

meant that comparing the surfaces was impractical because no markers remained to provide quality points of reference. However, assuming the change cannot be attributed to some part of the experimentation process other than the pressurization cycle, it was certain that the surface had changed. This indicated that the change likely affected the mechanical properties of the material at pressure.

The final alloy investigated using the 3D imaging methods was the 2024-T4 High Strength Aluminum (M6). This alloy had the best stain and grain structure for analysis and therefore provided several locations of interest.

I returned to the area described in Section 5.5.3 and shown in Figure 81. This section showed a possible change to the grain boundaries on coupon M6-05 and therefore represented a good location for further investigation. Figure 92 and Figure 93 are the pretest and posttest color maps for the region of interest at 6000x magnification.

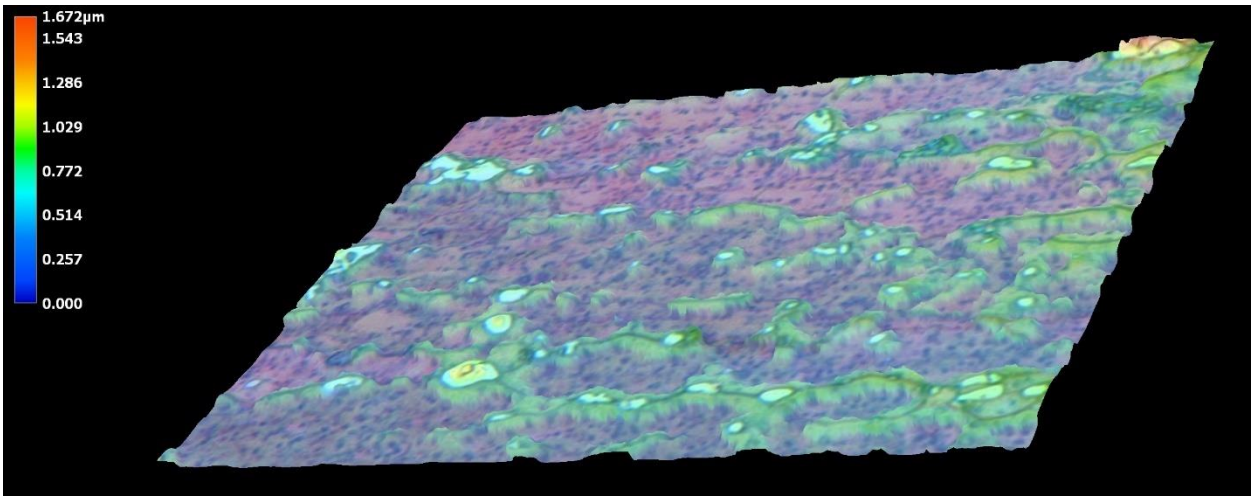

Figure 92: Pretest M6-05 3D Color Map 6000x

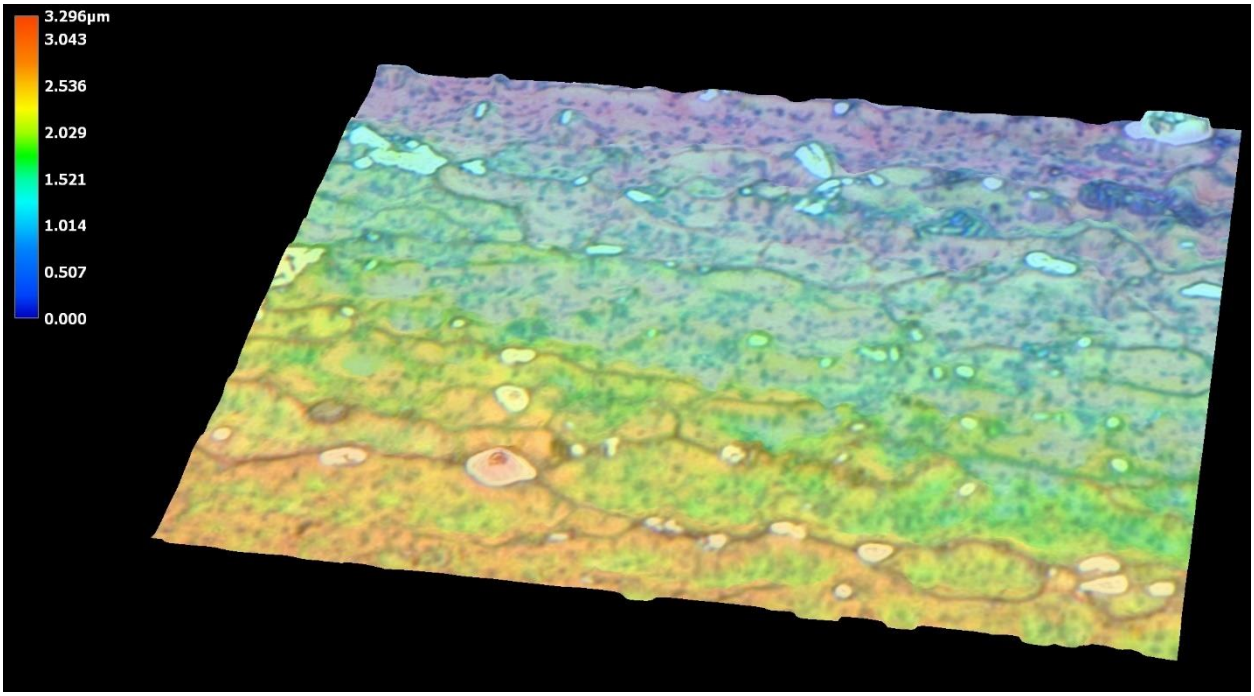

Figure 93: Posttest M6-05 3D Color Map 6000x

These images do not show the same extreme peaks and valleys as those of the copper alloys nor do the surface features appear completely changed. The major boundaries and features appear identical which allows for close inspection of the area of interest originally shown in Figure 81 but duplicated in Figure 94 again for ease of comparison.

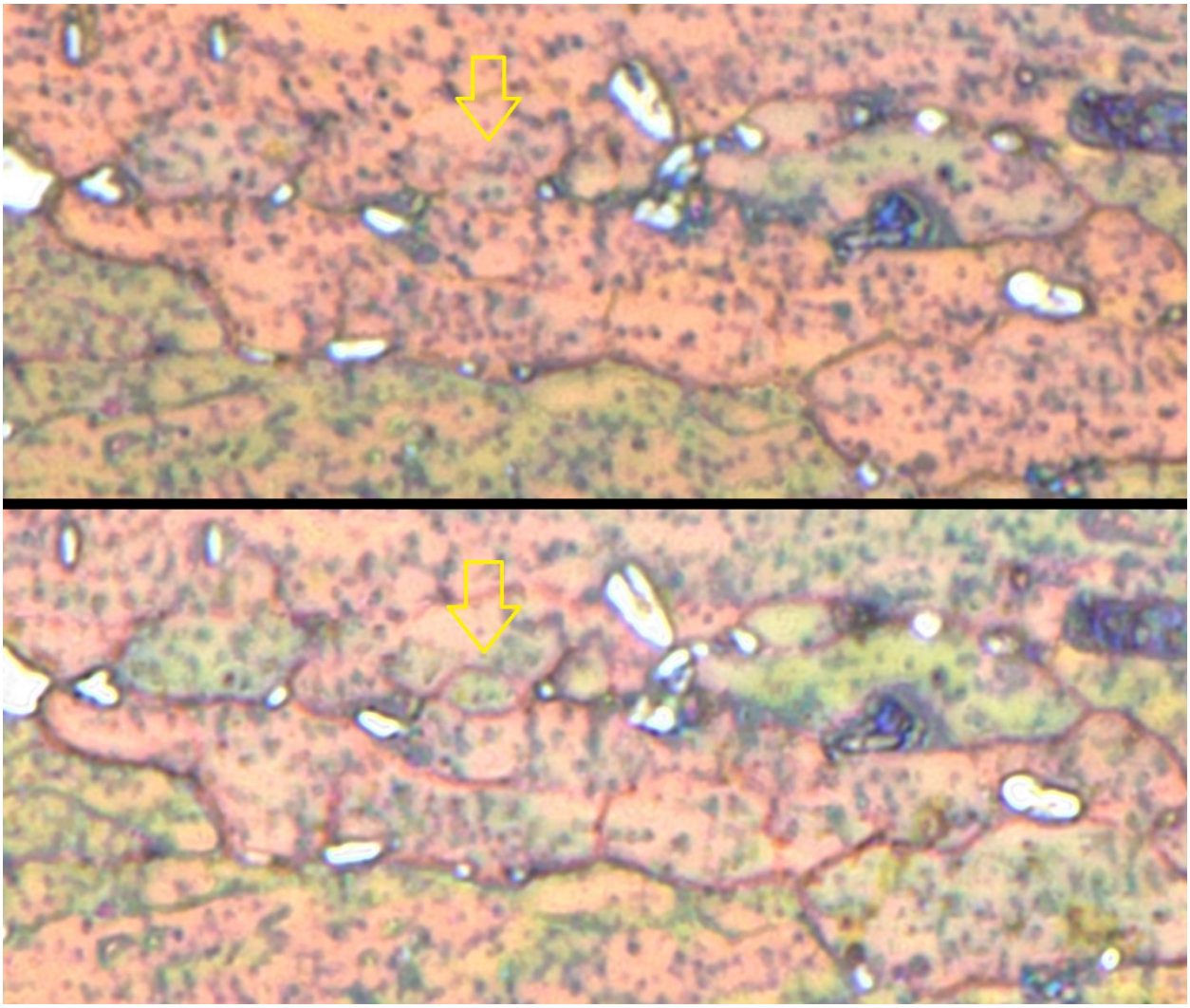

Figure 94: M6-05 Coaxial Comparative Split 4000x Pre_Post (Duplicate)

Close investigation of the area indicated by the yellow arrow reveals changes. While the change in color (from salmon pink to a light green) did not indicate a change had occurred, by itself, the inconsistent change in color showed that the topography around the area where the grain boundary lines became more pronounced has changed, meaning that the angle and possible thickness of the stain caused the change. Figure 95 compares the 3D topography identified with the yellow arrow.

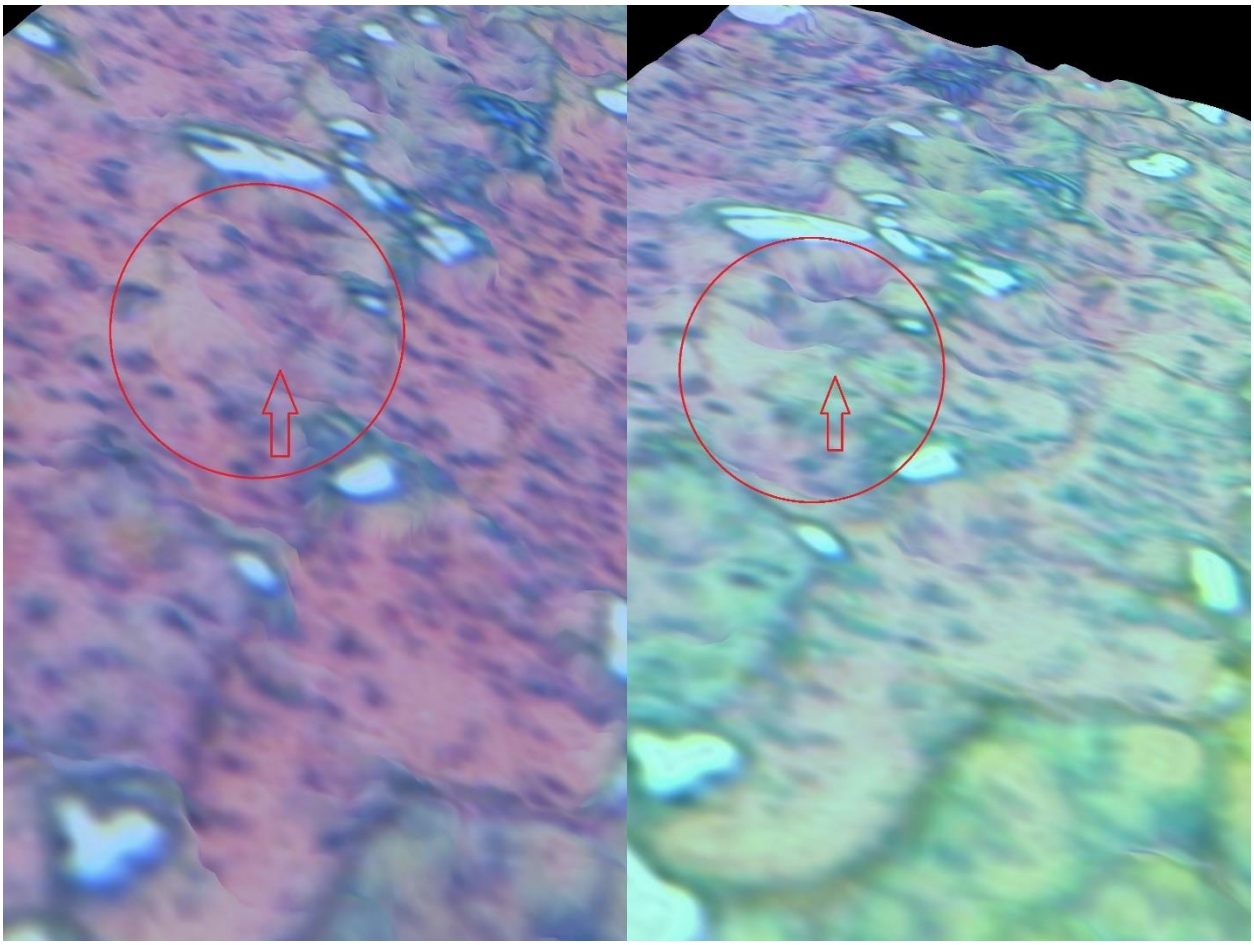

Figure 95: M6-05 3D Topography Area of Interest Detailed Image 6000x Pre_Post

The area within the red circles corresponds to the area of interest (the yellow area in Figure 94). The image on the left is the 6000x 3D color map of the pretest surface and the right image is the same area from the posttest imaging. Using clear markers points that remained constant between images we see that a bowl-like area has developed. Some features of the bowl's edges were present before pressurization but became more pronounced, and the region indicated by the red arrow developed from a smooth area into a clearly-defined updrift of material. These images showed that change in surface topography occurred and likely correspond to a change in physical properties at some level. It was unlikely that any process that I performed as part of my testing

would have caused such topography changes. Polishing and sanding would have smoothed the surface and would not have created an updrift of material.

Other areas of interest were identified on coupon M6-07 of the 2024 aluminum alloy. Figure 96 shows the pretest and posttest areas at 4000x magnification that were investigated using 3D topography.

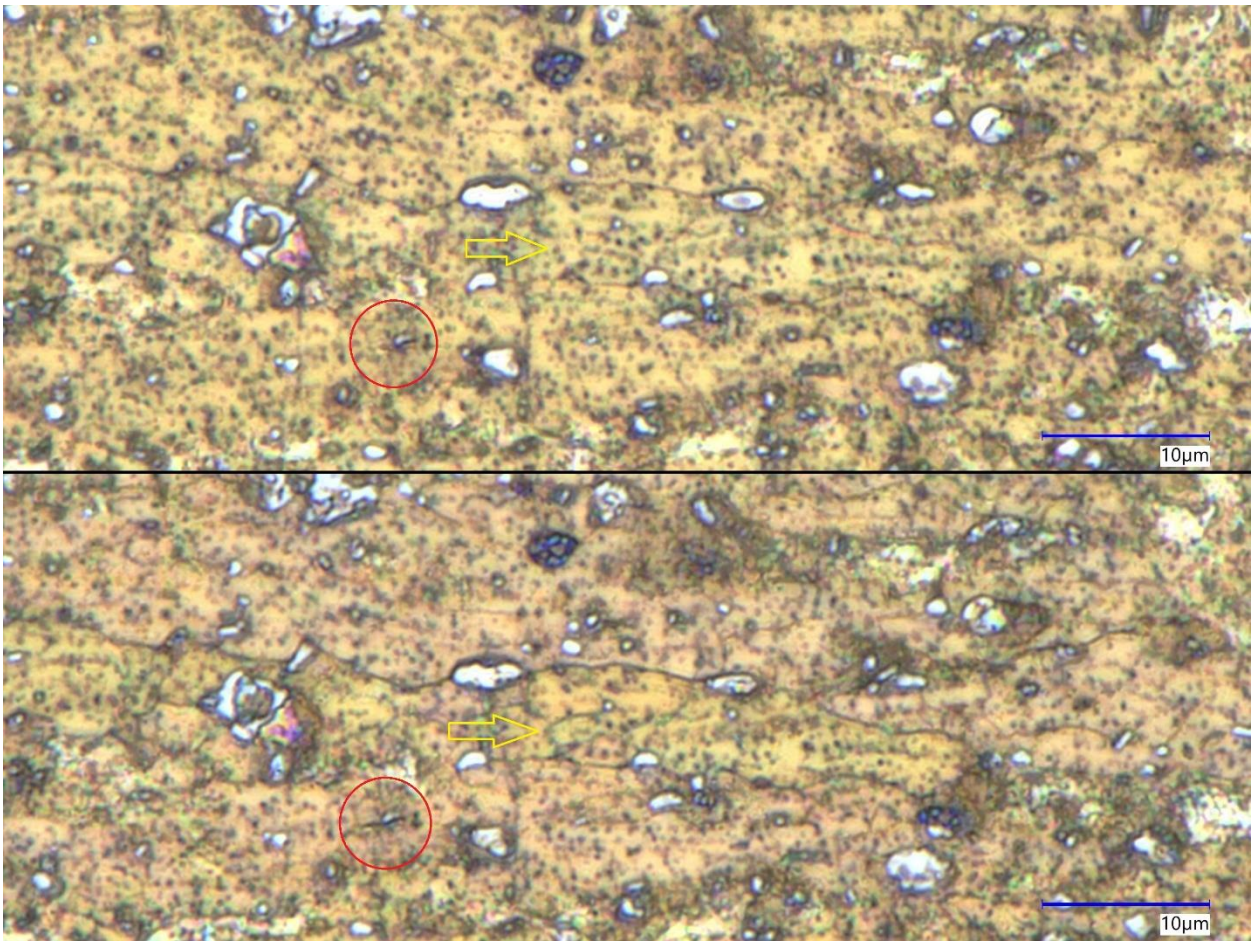

Figure 96: M6-07 Coaxial Comparative Split 4000x Pre_Post

There are several areas in this image that can be investigated further. There were instances of grain shift and development, like those discussed for M6-05 as well as several feature lines that became more distinct following pressurization. I identified two areas to investigate further (labeled

with a yellow arrow and red circle) but more analysis could be performed from the raw data image if desired.

Figure 97 compares the M6-07 coupon, 4000x data focused on the area indicated by the yellow arrow. Like the area on the M6-05 coupon, this area exhibited a color shift and boundary line development.

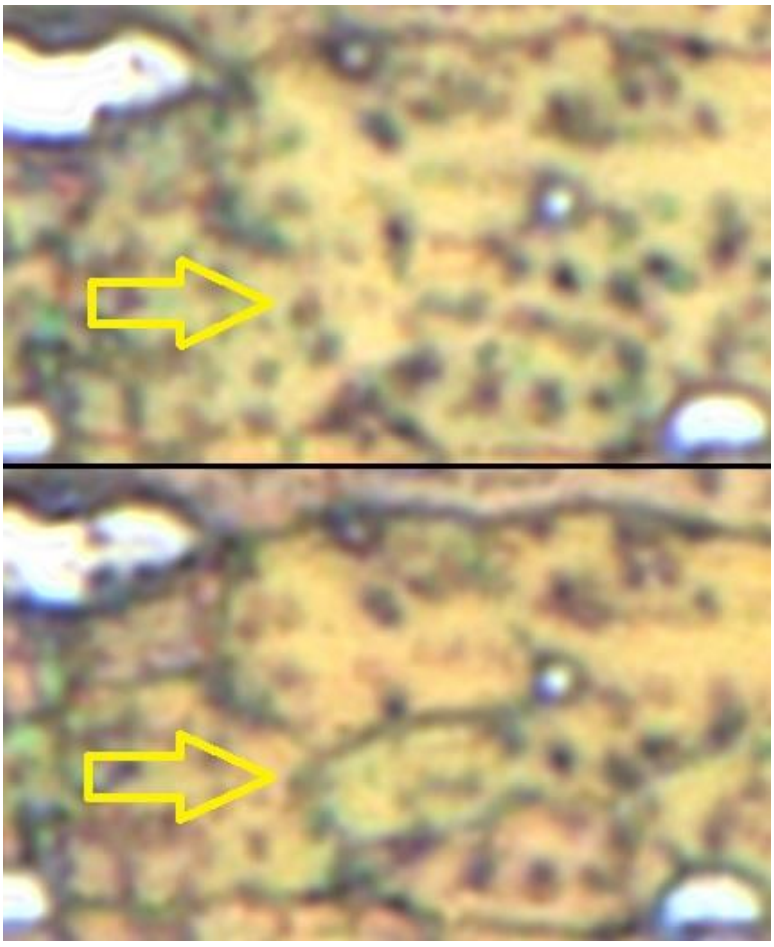

Figure 97: M6-07 Coaxial Comparative Split 4000x Pre_Post Area 1 Focus

This image shows a feature line that developed along the upper edge of the newly-formed area, connecting several smaller surface anomalies indicated by black dots. Within this area, the color shifted slightly from a lighter yellow to a tinted green, while the area outside it remained mostly light yellow. To further investigate this area, 3D topography images and surface track lines

were created. Figure 98 is a focused, angled image of this area and shows the changes identified in the 2D images.

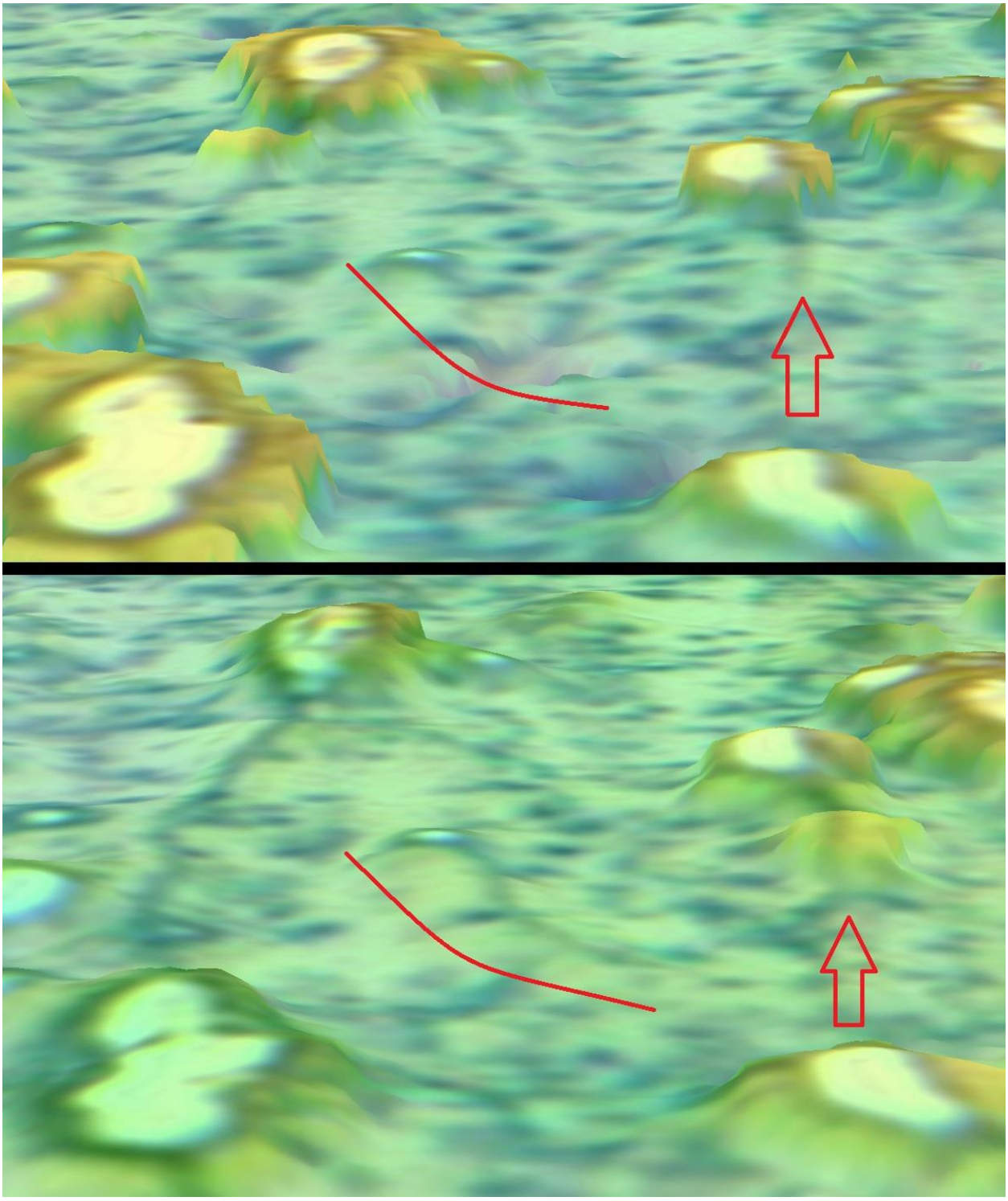

Figure 98: M6-07 3D Color Map 6000x Split Comparison Region of Interest 1

Several changes occurred in this area. First, several low valleys in the area disappeared. This could be due to the slight change in angle of the sample between pretest and posttest imaging, which have affected the light, or they could have been caused by movement in the surface material. Future testing should endeavor to maintain a more consistent surface-to-lens orientation to reduce the risk of this being and artifact of the imaging process. Second, as indicated by the curved red line, a ridge formed across the region corresponding to the new boundary line that can be seen in Figure 97. This ridge corresponds to the new feature line that can be seen in the posttest imaging and would indicate that when the material was subjected to pressure, the material was compressed sufficiently to cause plastic deformation resulting in a new updrift. The third change is indicated by the red arrow. Another more pronounced updrift of material appeared on the southern edge of the new grain area. Other updrifts can been seen in other areas of this color map as well. These new features provided a new region on the surface of the coupon and indicated that lasting changes to the physical properties have occurred.

Figure 99 and Figure 100 are the profile track charts that were created to analyze this new feature. The red horizontal lines were added to identify the features covered by the track line.

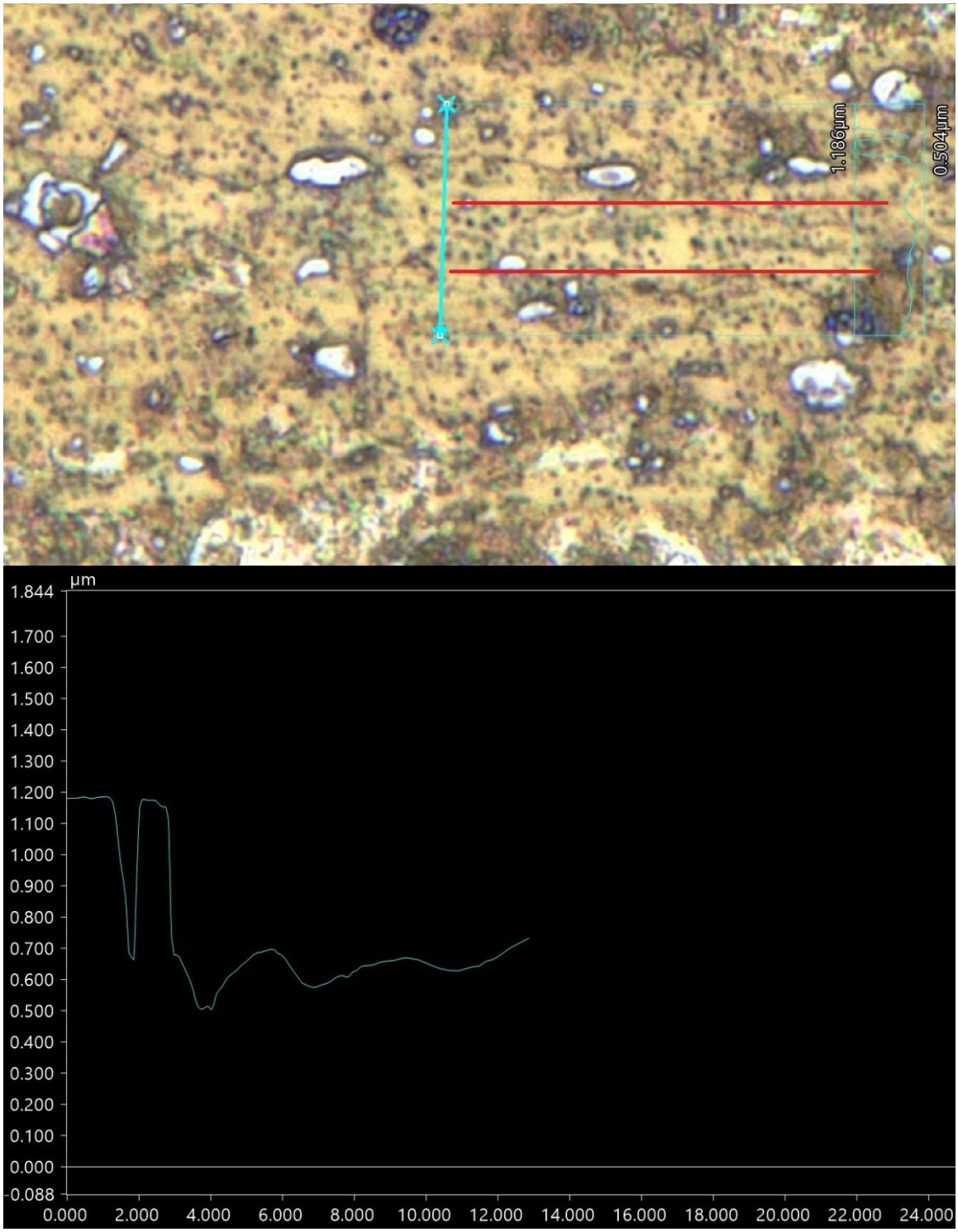

Figure 99: Pretest M6-07 3D Topography Track Chart 6000x Area of Interest 1

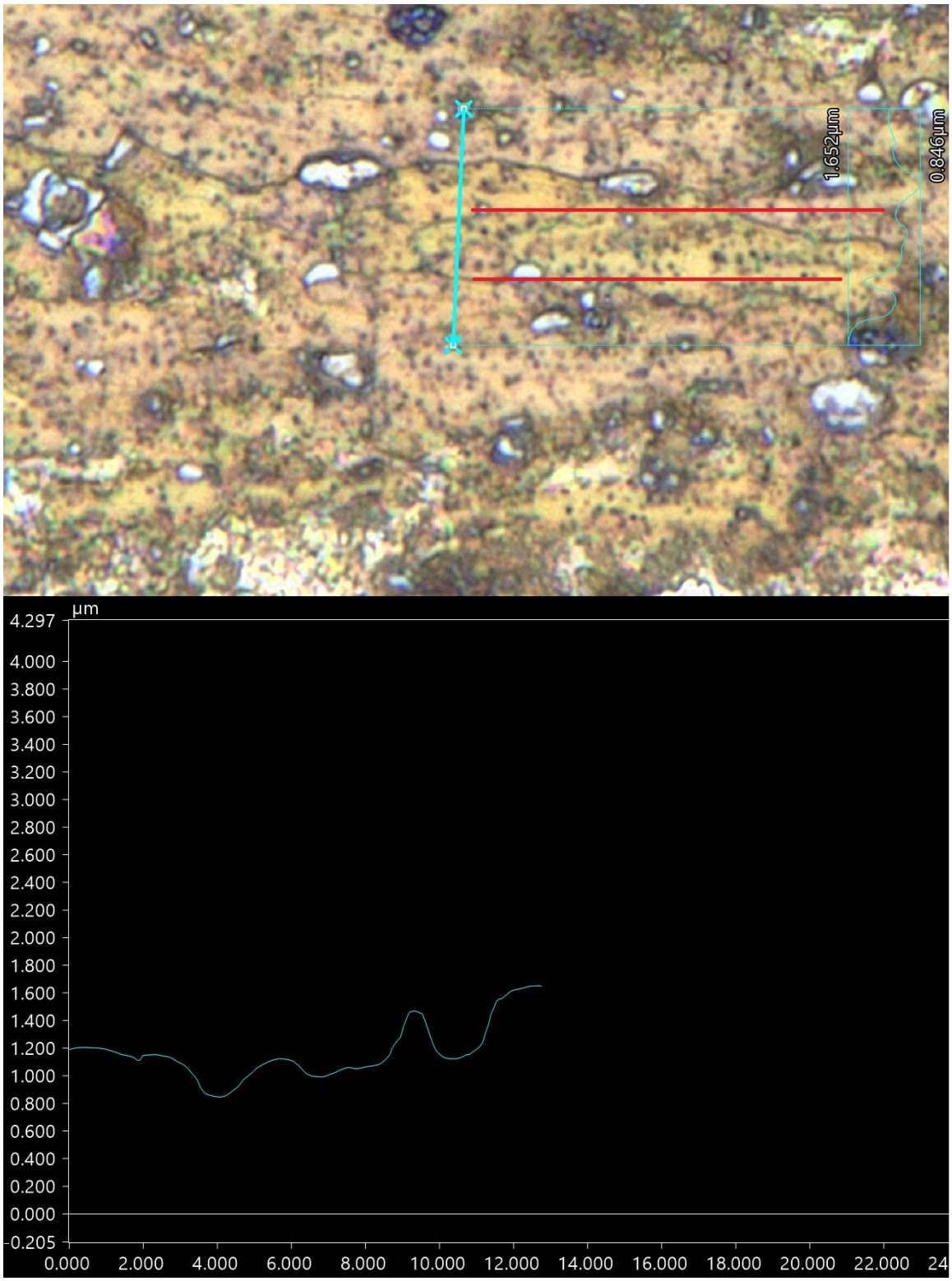

Figure 100: Posttest M6-07 3D Topography Track Chart 6000x Area of Interest 1

Analyzing these two track charts we see that though the magnitude of the features is less in the posttest surface, the general shape of the topography is similar enough to identify. Reading the chart from left to right, we see an initial uplift, followed by a valley, another uplift and then another drop in elevation with a subtle rise and lowering. Then the track ends with a final uplift. The additional feature that stands out in the chart on the posttest track occurs at nine μm in the track where a defined, narrow peak has developed. This may correspond to the uplift identified in Figure 98 on the lower boundary of the new grain region. The more pronounced lines in the 2D image are most likely transition zones that changed where an uplift of material has occurred and do not indicate cracks in the surface.

The second area of interest in Figure 96, indicated by a red circle, is a feature line that increased across the surface. Figure 101 shows the measured change in the feature of interest at 6000x magnification.

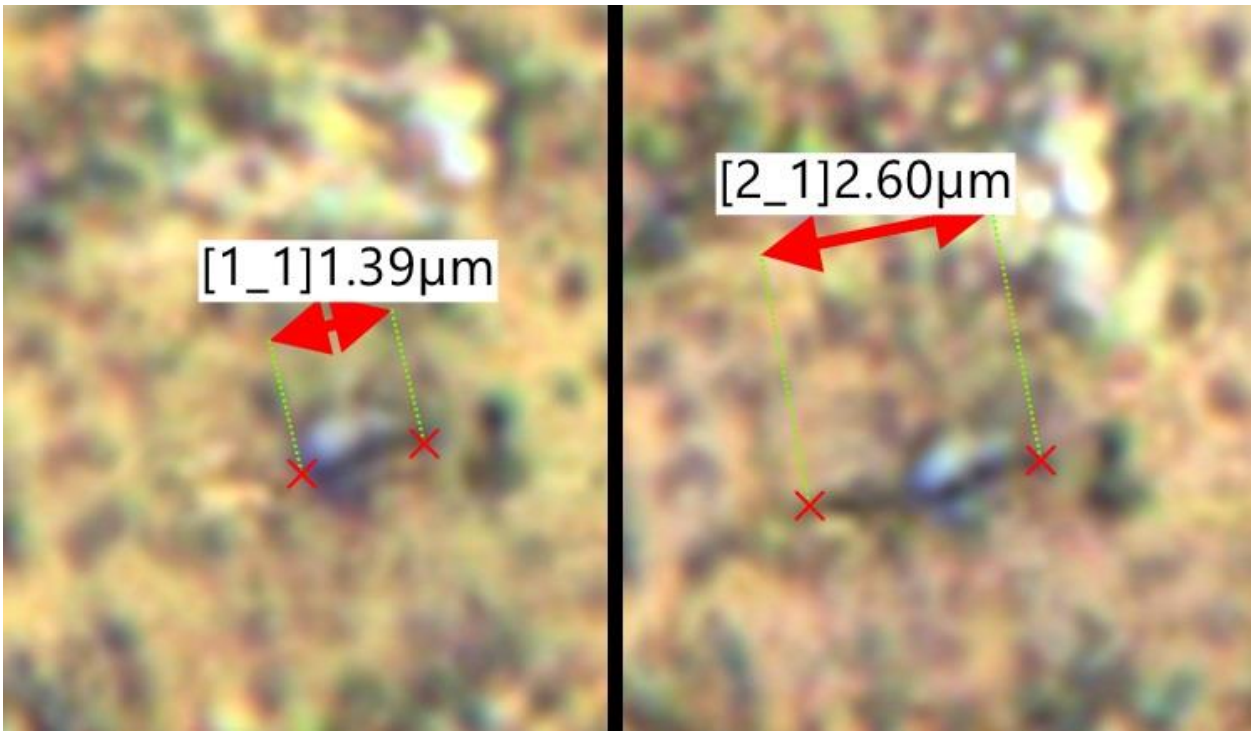

Figure 101: M6-07 Coaxial Comparative Split 6000x Pre_Post Area of Interest 2 Focus

The feature appears to extend from a previous feature and increases from approximately 1.39 µm to 2.60 µm. To determine if the feature is a crack or another feature boundary, Figure 102 was created to compare the 3D topographies of the surfaces.

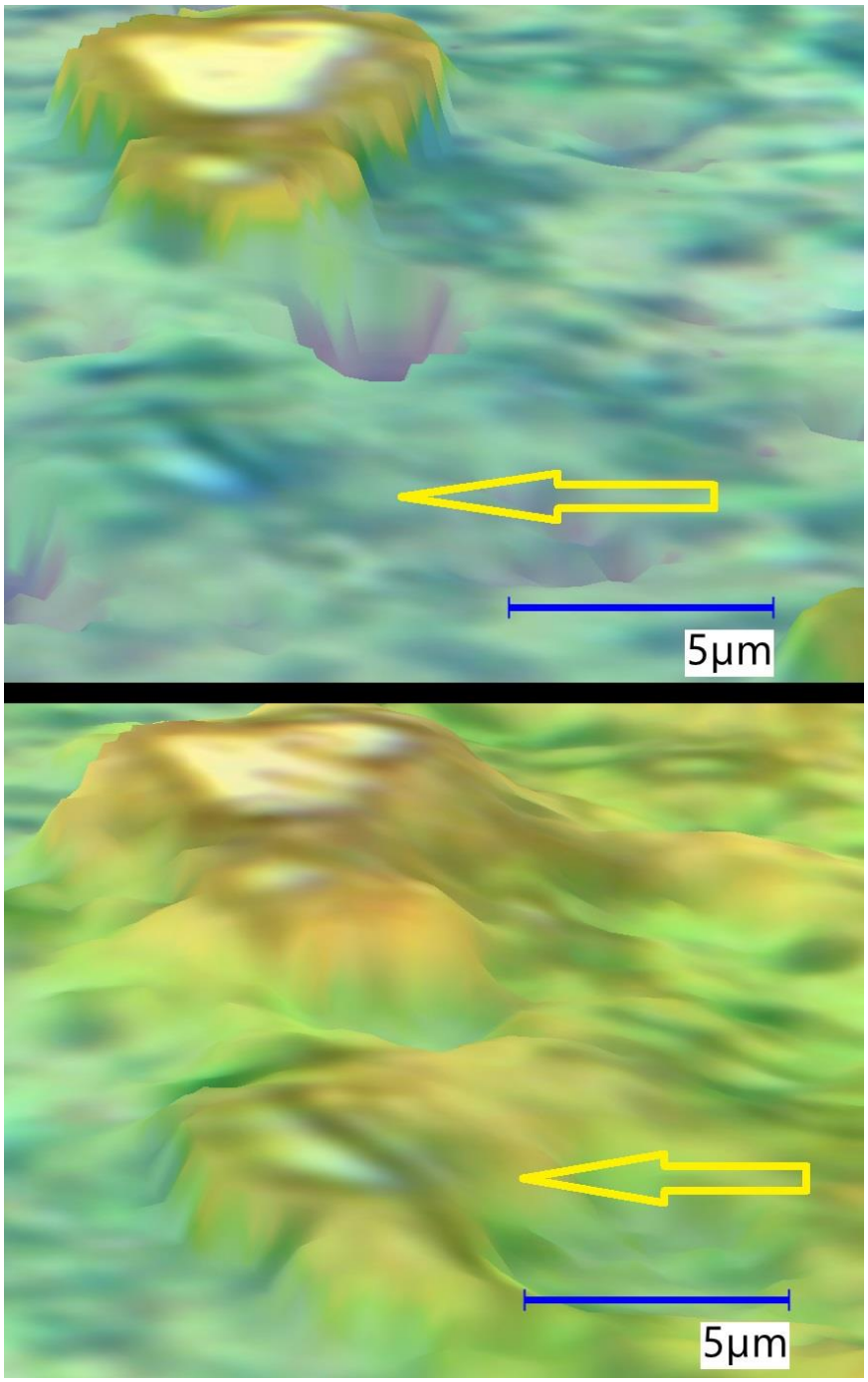

Figure 102: M6-07 3D Color Map 6000x Pre_Post Split Comparison Area of Interest 2

In these images, the line is a transition zone for an uplift of material that was not clearly present in the pretest imaging. Figure 103 and Figure 104 are track charts that were created for further analysis.

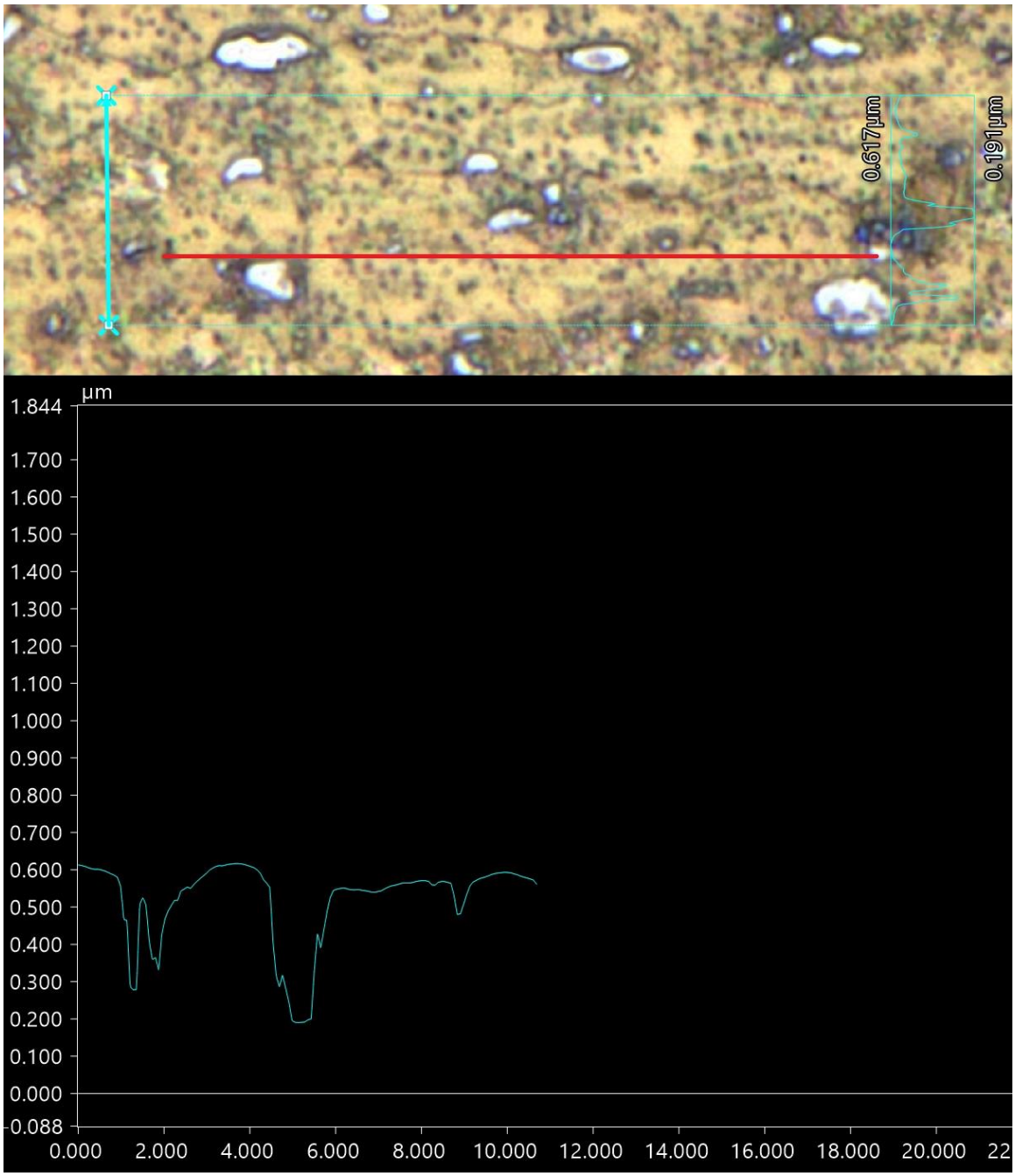

Figure 103: Pretest M6-07 3D Topography Track Chart 6000x Area of Interest 2

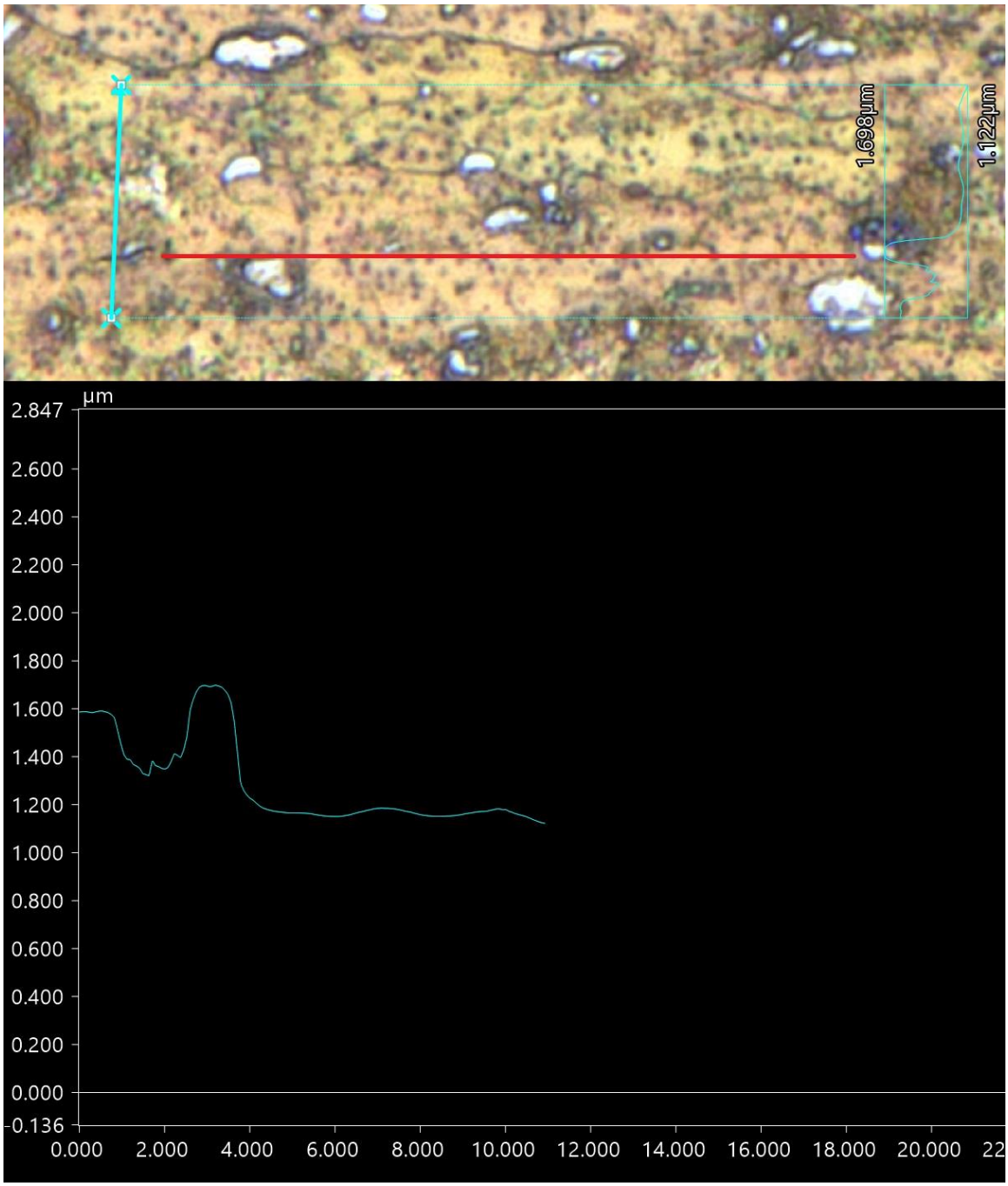

Figure 104: Posttest M6-07 3D Topography Track Chart 6000x Area of Interest 2

In these track charts, the creation of the uplift is visible. The feature line in the posttest image does not represent a new feature but is more clearly visible because of the uplifted material. There is a deep valley immediately above the area of interest that is no longer present. This valley may no longer exist because of deformation caused by the pressurization cycle. The uplifted

material may be interfering with the way in which the light is reflected off the image's surface and obstructing the presence of the valley.

5.5.5 Imaging Analysis Summary

The analysis of the coupons using common imaging techniques revealed several instances of surface topography changes. The scale of the changes was expected to be visible at magnifications of 500x or less in accordance with common grain structure analysis standards like ASTM E112-13 [31]. However, while some changes were visible at this scale, the more significant changes were identified at much higher magnifications by using the high-quality images from the Keyence Ultramicroscope. The images showed subtle surface feature changes in texture and grains with visual comparison, 3D color mapping, and 3D surface topography track charts.

Reflectivity of the surfaces caused problems with the ability to compare the pretest and posttest copper alloy coupons but there were indications of visible changes though further research and more careful handling controls are required to better understand and explain the actual phenomenon. The 1100-H14 Hardened Easy-to-Form Aluminum (M5) images showed a near complete change in the surface appearance and topography. The cause of this is also unknown but indicated that the material had permanent changes caused by the pressurization cycle. The images also demonstrated both methods for lighting surfaces, coaxial and full ring lighting, can show different changes and both are important for image analysis of materials. The 2024-T4 High Strength Aluminum (M6) had the most successful stain which allowed the identification of areas where grain structure and surface topography changes occurred.

5.6 Summary

The data collected during the use of my pressure chamber showed can perform high pressure testing up to 30,000 psi safely and can be used to simulate real world situations that

designs are expected to survive. The demonstration of this functionality was to simulate a dive to Challenger Deep to determine if hydrostatic pressure should be researched as a possible cause of material property change which may affect design performance. Following this pressurization cycle, using these physical measurements, Vickers microhardness testing, and imaging analysis, I was able to show statistically significant changes in material properties with common statistical analysis techniques. Though the cause and performance changes at depth cannot be predicted with the static testing that was performed, the presence of permanent changes in the materials indicated areas of future research that may be of interest to the engineering community.

Chapter 6: Way Forward

6.1 Introduction

The successful assembly and demonstration of the capabilities of my pressure chamber and supporting test stand show the possibilities for its continued use. However, during the design, assembly, and operation of my test setup I determined there were several areas for improving the design of my pressure chamber to work more effectively as a pressure chamber across a broader range of applications. A brief discussion on my findings and design changes are presented here; however, these have not been fully developed as solutions and if implemented will require further effort.

6.2 Sealing Improvements

Following the performance of my proof pressure test, I observed that a small amount of water had passed my primary and backup sealing methods. The chamber did not need to be drop-test proven; however, this was ideal.

Drop-tests are usually used in situations that involve low to moderate pressures and large fluid volumes, such as large water tanks. The tanks are pressurized, and then all inlet and outlet points are sealed. Pressure is noted and then held for a certain amount of time. If pressure drops at all, then the test is considered a failure and the welds, valves, fittings, and other possible leak points are inspected. The purpose of this kind of test is for components that may not be continuously monitored or where any leakage is undesirable. The practice also is used in situations where the volume cannot be practically tested to its working pressure in a normal condition such as a submersible craft. Large submersible crafts are sealed and then have the internal volume

pressurized and a drop test performed. Normally, pressure is exerted on the exterior, but pressure chambers this large are not economical.

My test stand was designed to maintain pressure but not hold pressure, which meant the pressure source was expected to compensate for small leaks. If the leak rate was below the capability of the pressure source, the chamber was functioning acceptably. However, several economical improvements can improve the sealing ability of the pressure chamber. This is critical when using fluids with smaller molecular sizes like helium and hydrogen. Water has a large surface tension and molecular size, so a water leak indicates that other fluids would leak at equal or greater amounts.

6.2.1 Increase Lid Thickness

A brief investigation into the leakage revealed that one possible cause was deformation of the lid at pressure. Though the lid was not at risk of failure due to excessive stress, according to my SolidWorks simulation results, the deformation at 30,000 psi may be sufficient to reduce the effectiveness of the primary sealing surface allowing leak by. The backup seals could not seal this pressure and thus a small amount of leakage occurred. The chamber still held pressure with minimal drop over the 30-minute hold during the proof pressure test.

Increasing the thickness of the lid may alleviate this problem. The current lid is 1 inch thick and increasing the thickness to 1.5 or two inches reduces the estimated deformation at 30,000 psi from 0.008 to 0.004 or 0.002 inches, respectively. The smaller gap will significantly reduce the amount of fluid that can flow from the pressure chamber to the backup seals. With high viscosity fluid, the gap may be small enough to stop all fluid movement. The only costs associated with this modification are the remanufacturing of the lid and longer bolts and shear pins.

6.2.2 Backup Seal Design, Utilization, and O-Ring Addition

In addition to increasing the thickness of the lid, better backup sealing methods can be incorporated. As mentioned in Chapter 3, the backup seals are not rated by the manufacturer for the pressure at which the chamber is capable. This is due to a combination of seal design, materials, and how they are used. Sealing product companies like Hercules Sealing Products can create custom sealing products for various applications. It is possible that a different material, seal design, or plug design that more properly loads the seal for optimal performance can be determined.

Figure 105 shows the cross section of the current seal. The black portion is a harder material. When pressurized, it pushes against the gray material, forcing it outward for better sealing. A change in the gray material may enable better resistance to leak by or a redesigned black material geometry may provide better contact with the sealing surfaces.

Figure 105: Hercules Sealing Products U12-2.75-25B – Cross Section [32]

To improve the function of the seal and better utilize the seal design, the seal pockets could also be improved. Figure 106 shows how the pockets could be changed. The seal pocket on the

right is the original design. The seal pocket on the left has an added chamfer that allows for pressure to better interact with the core of the seal, which should improve the performance of the seal design. This would require modification or remanufacturing of the plug.

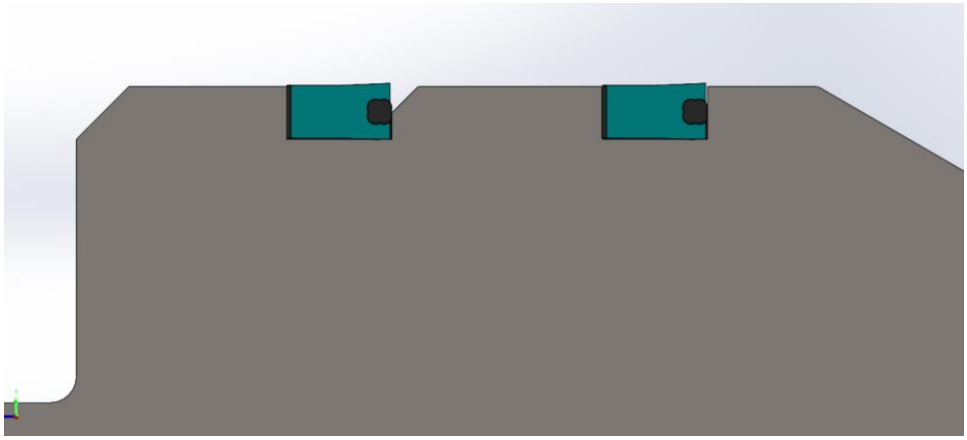

Figure 106: Seal Pocket Modification Option

Another sealing option that only requires minimal changes to the pressure chamber setup is the addition of a single use o-ring in the void between the plug taper and the chamber bore. Figure 107 shows a cutaway of the area from my SolidWorks assembly.

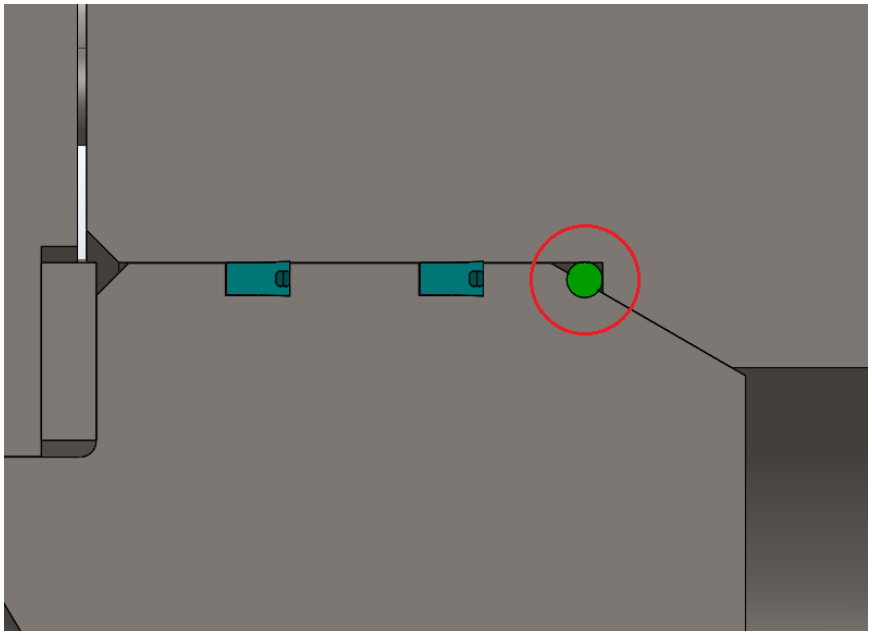

Figure 107: Optional O-Ring

The o-ring (bright green for visualization purposes) could be added to the bore of the chamber prior to the insertion of the plug. The taper of the plug would still be forced against the taper of the chamber but this force would also deform the o-ring to fill the void in the transition zone between the taper and bore. A material such as 90 or 95A urethane rubber could be used for the o-ring. This material has been used in other high-pressure applications. By filling the void, any pressure would have to first pass through the taper seal, then force its way through or past the crushed o-ring, and then past the two backup seals before escaping the chamber. This may improve sealing especially when using small molecular size fluids like helium and hydrogen. The o-ring would need to be replaced after each use due the deformation that would occur. Custom o-rings for the void and material are available from companies such as Hercules Sealing Products.

6.2.3 Gland Seal Plug Design

One of the more complicated design modifications is to redesign the plug to utilize a gland-seal method to improve seal performance. This method is common in rotating equipment that operate under high-temperature and high-pressure fluids like steam. Most polymer seal designs function on a differential pressure principle so if the pressure difference across the seal can be reduced, then the seals function more effectively. Figure 108 shows a redesigned plug that incorporates a gland-seal void.

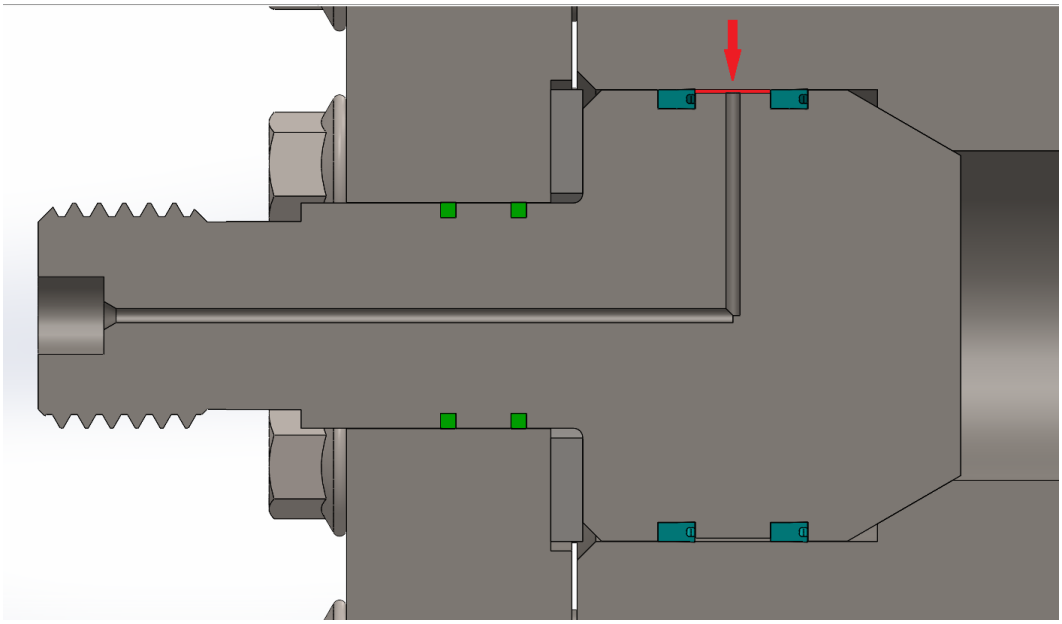

Figure 108: Modified Gland Seal Plug

The red arrow in Figure 108 points to a small void that can be pressurized through a pressure port integrated into the plug. The void is created by lowering the radial dimension between the seal surfaces to enable pressurization around the entire perimeter of the plug. To ensure proper function of the gland seal, as chamber pressure increases, the gland seal void would also be pressurized just below that of the primary chamber. The void should not be higher than the main chamber or it may become an unwanted pressure source entering the chamber. With this method, the differential pressure across the seal can be kept below its normal working pressure and thus enable proper operations. If the seal between the void and atmospheric pressure leaks by it does not affect the primary chamber with the goal of providing a more stable pressure within the area of the experiment. This would be the most complicated sealing modification because it would require a new plug to be manufactured and additional pressurization piping and components to provide the sealing pressure.

6.2.4 Packing Rings and Tell-Tale Pressure Port

The last sealing redesign I will propose is to utilize packing material instead of o-rings. Packing materials are softer, flexible materials that can be tightly formed around and against hard surfaces. They come in a wide variety of materials such as Teflon, rubber, and graphite and can also include fibrous material like glass, Kevlar, and cotton to strengthen the matrix. The method of use for packing material is to intentionally deform the material into a void like o-ring as described in Section 6.2.2. Packing is specifically designed to be used this way and is also significantly cheaper and can be fabricated from a wide range of materials to customize the setup more easily for specific applications where chemical interaction may be a concern. Figure 109 shows a possible redesign utilizing packing rings (from the top-down due to the placement of the tell-tale port).

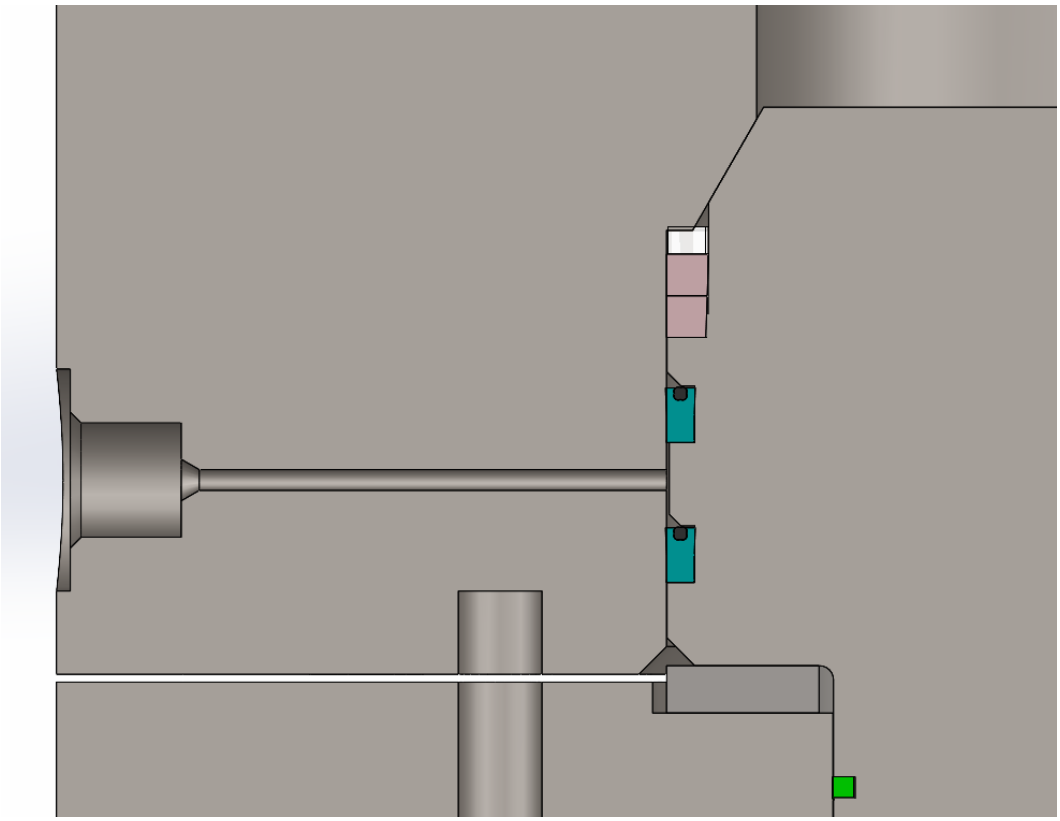

Figure 109: Redesigned Plug for Packing Rings and Tell-Tale Port

The packing rings are represented by the red square components. Upon installation of the plug, these rings are compressed against the shoulder of the plug by means of a nylon compression ring shown here as a white rectangle. As the packing is deformed, it will push against the bore of the chamber as well as the shoulder of the plug sealing the surfaces tightly. The primary sealing surface remains the 60-degree taper; however, this could be an equally effective sealing method and is in common use in pumps and valves.

Figure 109 also shows a tell-tale pressure port. Tell-tale pressure ports are used in pressurized systems on the low-pressure side of seals. If the seal begins to leak by, the pressure gauge connected to the port will begin to show a rise in pressure, and corrective actions can be taken. This port could also be used for gland sealing as described in Section 6.2.3. The advantage of having a tell-tale in this setup is in helping to identify leakage. If no pressure increase is observed on the gauge when leakage is known to be occurring, then efforts can be focused on identifying the leak elsewhere in the setup.

This solution would require remanufacturing of the plug and modification of the pressure chamber to add the port. Packing material would also need to be determined as well as the packing area revised as recommended by the packing manufacturers.

6.3 Operational and Testing Capability Improvements

Several test stand and test chamber modification can be made to improve the ability to perform and expand testing data collection.

6.3.1 Pressure Transducer Signal Improvement

As discussed in Chapter 4, the pressure transducer signal suffered from fluctuations that were caused by induced signal noise in the cable or fluctuation in the power supply amperage and conditioning circuit. To address this, the test stand signal wires for the transducer should be

replaced with shielded cable and connectors and then routed to the control panel in such a way that it is not closer than six inches to power circuity and cables. This will reduce the risk of the signal from the transducer being interfered with by induced voltages. A dedicated 10 VDC, low-noise power supply, like the Keysight E36150 series power supply shown in Figure 110, could be incorporated to provide a known, low-noise power to the transducer. This could also be used temporarily to determine if the current system is the cause of the fluctuation.

Figure 110: Keysight E36150 Series Autoranging Benchtop Power Supply - Stock Photo [33]

If continued fluctuations are observed, the transducer signal circuit should be redesigned.

6.3.2 Gauge and Valve Board

The current test stand setup has the various subassemblies such as the inlet manifolds, control air manifold, and vent manifold resting independently on the deck of the table. A gauge and valve board could be created to mount these components off the wall, providing better access to the manual valves and viewing angle of the gauges. This would reduce the required deck space and thus shrinking the overall footprint for the test stand. Figure 111 shows an example of a gauge and valve board for a hydraulic test stand. The board for my pressure chamber would not need to be as complicated.

Figure 111: Staley Co. Hydraulic Test Stand Model D39110 – Stock Photo [34]

6.3.3 Thermocouple and Electrical Incorporation

In addition to pressure, temperature could be monitors during environmental testing within the chamber. Companies such as Conax Technologies offer several varieties of thermocouples high pressure testing. The pressure ratings vary depending on the type of thermocouple required; however, the MK with High Pressure Mount Thermocouple has a rating of up to 60,000 psi and uses the same port design as the pressure chamber currently uses. Incorporating this simply requires purchasing a thermocouple and reader and then incorporate monitoring into the DAQExpress Virtual Instrument. Figure 112 shows the MK with High Pressure Mount Thermocouple.

Figure 112: Conax Technologies MK with High Pressure Mount Thermocouple – Stock Photo [35]

Conax Technologies also makes electrical feedthroughs for passing circuitry into the pressure chamber if desired for future testing. Up to 10 wires 26 gage wires at 30,000 psi can be passed through one port using their High Pressure Sealing Insulated Wire Glands (HPPL) shown in Figure 113. This could be used for monitoring resistance of a material at pressure or monitor strain gauges attached to a structure inside.

Figure 113: Conax Technologies High Pressure Sealing Insulated Wire Glands (HPPL) – Stock Photo [35]

6.3.4 Drain Port Addition

Water was used during the proof pressure test. When testing was completed, I identified that there was no way to drain the fluid below the centerline of the pressure chamber. Though the volume of fluid is small, it still caused an unnecessary mess when I was forced to remove the plug from the chamber. The addition of drain ports would alleviate this from occurring if additional liquid fluids are used with the chamber. The addition of the port would require the chamber to be taken to a machine shop for machining however at the same time, additional ports could be added for additional chamber functionality.

6.3.5 Coupon Holder Redesign

During material testing it was difficult to achieve the proper polish for etching and material testing. This was due to the need to have the coupons not encased in resin while in the chamber. I required that each coupon be exposed to the hydrostatic pressure on each side. Encasing materials in resin ensured a stable assembly for mechanical polishing. The pucks that are created for this also ensure that the material is orientated ideally for microhardness testing and imagine.

My demonstration test encased the coupons in resin for initial polishing and microhardness, but I was required to break the coupons out of the resin pucks and could not re-encase them for post testing imaging because this would harm the surface of interest and may mask the small changes in surface topography that I was hoping to find, indicating changes caused by the pressurization cycle.

For future testing, I designed a new coupon holder that would enable the coupons to be permanently held in a puck-like shape but would also enable pressure to reach each side. This would enable proper orientation for microhardness and imaging before and after pressurization with minimal risk of damage to the surfaces of the coupons.

The holder, shown in Figure 114, was designed to be assembled by clamping the coupons between two aluminum or stainless-steel clamshells and then using pins and a nut and bolt to properly align and hold the coupons under the correct tension.

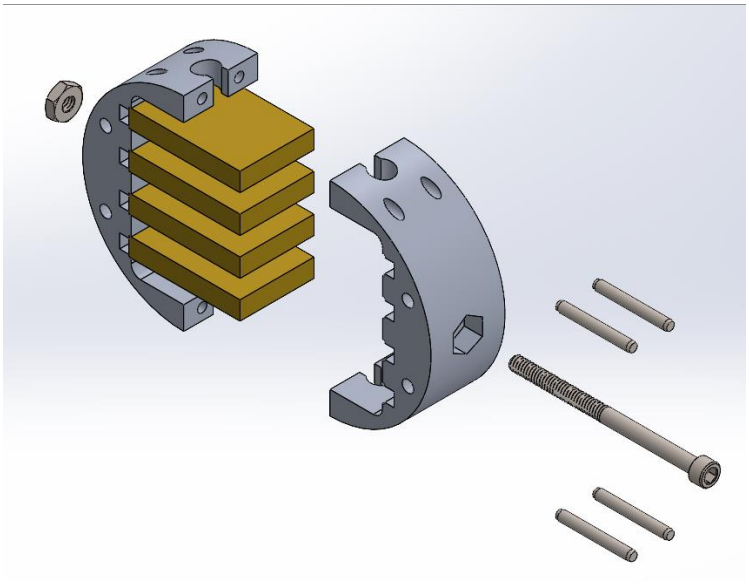

Figure 114: New Coupon Holder - Exploded View

Next, the design requires filling the voids around the coupons with a fluid mandrel material, such as Aquacore [36] or Aquapour [37]. These materials are used to fill voids and then when dried or compressed become rigid enough for machining and other manufacturing activities. The brown portion of Figure 115 represents these mandrel materials for use in my puck preparation.

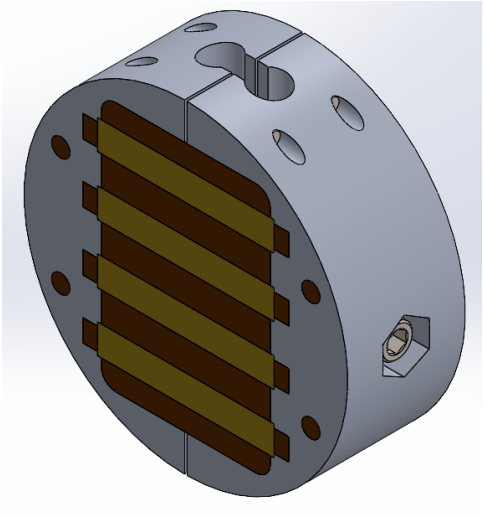

Figure 115: New Coupon Holder with Mandrel Material

Following the manufacturing activity, the material can be removed from the voids by washing it away with water. I would use the material to fill the void to keep resin from filling those

regions around the clamshell puck but allow the puck to be formed for use in mechanical polishers and provide a consist orientation before and after testing within my chamber, enabling a more consistent analysis. Figure 116 shows the encased holder with the mandrel material removed. One remaining question is related to the performance of the resin would perform in a high-pressure environment, but the metal clamshell should provide sufficient strength to ensure rigid orientation.

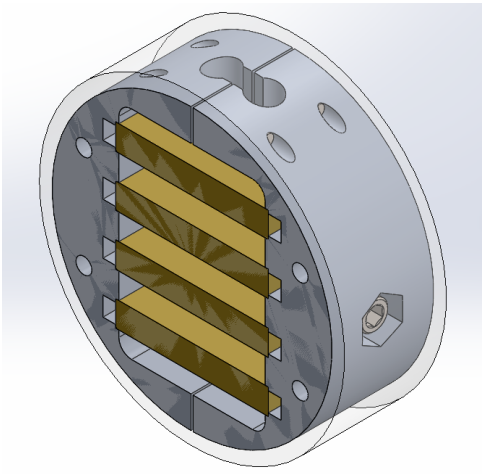

Figure 116: New Coupon Holder with Resin Encasement

A redesigned puck holder would be required to support the coupon holders inside of the pressure chamber. Figure 117 shows a possible design for a puck holder. The design would allow multiple pucks to be suspended in the chamber for testing.

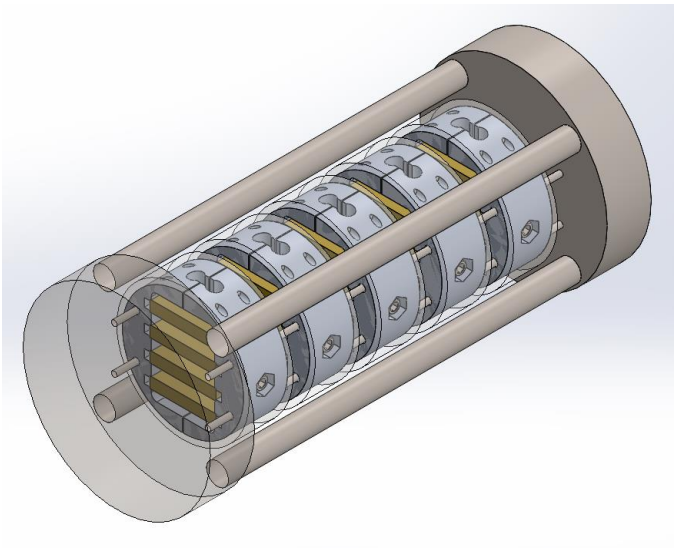

Figure 117: New Coupon Holder Testing Assembly

6.4 Other Areas of Research

During my investigation into demonstration tests of my chamber, I identified several areas for additional testing.

6.4.1 Reperformance of Deep Dive Simulation

Chapter 4 identifies several problems with the performance of my demonstration test. Additional research on the materials that were used, as well as additional material typess, may help to better understand the effects of pressure on material properties and may help to identify uses for this information. The following changes can be made to provide the best conditions for data collection and analysis and to address the shortcomings in data gathering in the experimental design.

1. Conduct a series of tests to identify the correct seal design and configuration to control the small leak rate observed while using Helium.
2. Using the proposed redesigned coupon holder described in Section 6.3.5, maintain the flatness of the samples for imaging and hardness from pretesting through post testing to provide the best possible conditions for direct comparison.

3. Take cleanliness precautions to protect the integrity of the polished surface throughout testing from corrosion, dust, and scratches. During the initial demonstration testing, the expected magnification range of interest was 500x. With the observation of smaller changes at 4000x and 6000x the range of interest has increased significantly requiring more care to be taken. Dust, corrosion, and scratches are more detrimental at higher magnification because they can completely erase a section of interest that may have shown signs of change.
4. Expand my property tests to include stiffness, tensile strength, conductivity, and take more detailed images across a wider range of the surface at the highest magnifications possible in both 2D and 3D to provide more opportunities for comparative analysis that may identify more instances of structural changes.
5. Use a Knoop microhardness test along with or in place of a Vickers microhardness test. The Knoop indenter is more sensitive to subtle changes in microhardness but less common in industry. It can also be orientated to follow a grain line to focus on this area, where structure changes most likely occur.

6.4.2 Copper and Aluminum Material Property Testing

During the analysis of the hardness data, I identified a possible method of affecting the hardness of copper and aluminum alloys. The copper alloys showed a reduction of the average hardness without affecting the distribution across the surface. The aluminum alloys both showed a consistent average hardness but a narrow distribution across the surface. These change in material properties could be investigated to alter hardness without introducing temperature to a component or altering the dimensions of the part. The applications of such controls could span from high

performance copper and brass component creation and post processing machined aluminum components to create a uniform hardness for better performance predictability.

6.4.3 Hydrogen Environment Material Testing

The University of Oklahoma Aerospace and Mechanical Engineering department is currently setting up a hydrogen research laboratory to research materials exposed to hydrogen. The purpose of this research is to better understand the failure mechanisms and aging that occurs from this kind of exposure. The research will begin with a focus on hydrostatic testing of polymer seals with hydrogen and then expand into possible heated and flowing hydrogen experiments. My chamber's size and mass could be used to perform these types of tests with modifications. The position of the ports would enable fluid to flow in and out of the chamber and the thickness and types of materials use can provide a safe environment.

Hydrogen testing could also be expanded to investigating coatings that may protect materials from monotonic hydrogen diffusion into the material crystal structure. Material selection is also an option in combatting this; therefore, my chamber can be used to test various materials and coatings to determine the effectiveness of these methods. The coupons could be treated and exposed, then following exposure, cut in half, and the coating-to-surface boundary area can be inspected and compared to unexposed material to identify and quantify any voids and damage.

6.5 Summary

I designed numerous improvements to the pressure chamber and test stand designed for my Master's research. My hope is that these improvements can be incorporated by myself or other researchers to continue the use of my chamber and validate my effort in creating a useful engineering product and contributes to the capabilities of the University of Oklahoma. By using the test stand for more purposes, the cost in time and material can be reduced.

Chapter 7: Conclusion

There were four key goals during the performance of my thesis research, and the first goal was to design, build, and prove the functionality of a high-ambient pressure chamber that can be used for high-pressure environment research. The volume needed to be sufficiently large so a meaningful apparatus could be placed inside for complete hydrostatic testing. I accomplished this by designing a chamber with a theoretical design limit of 60,000 psi and proved its functionality with a proof-pressure test up to 30,000 psi. The volume was proven large enough for meaningful experimentation by enabling the simultaneous testing of up to 32 material coupons in a custom designed coupon holder during a simulated dive experiment. The key design parameter of safety was ensured by the incorporation of remote operability components, safety devises, and sensors. The chamber's capabilities were expanded with the addition of extra pressure ports for sensor and component connections and the use or standard threads and components, which were captured in a full CAD model that other researchers can be use in the future.

The second goal of my research was to use the pressure chamber to simulate a real-world event that could benefit from high-pressure testing of materials and components. I accomplished this by recreating the dive of the DeepSea Challenger to Challenger Deep in the Marianas Trench. Though the simulation did not exactly match the dive track of the original craft, I am confident the dive successfully proved in proving the capabilities of the test stand. With minimal modification to the support systems and sealing methods of the chamber, the dive could be reperformed and the dive track would better match the exact dive.

The third goal of my research was to analyze the data collected as part of the demonstration testing to identify methods that could be used to investigate changes in mechanical properties and changes in microstructure. Using physical measurements, Vickers microhardness testing, and

optical imaging methods I identified statistically-significant changes in the material coupons. Any change in material properties at ambient pressure indicate that the material's properties changed while exposed to high-ambient pressure. Changes at pressure may need to be investigated and considered in a design for proper functionality and survivability.

The last goal of my research was to theorize additional features that can be used to increase the functionality of the pressure chamber test stand and suggest areas of additional research. In Chapter 6, I presented various seal improvement ideas as well as temperature sensors and electrical port passthroughs that can be used to monitor the pressurization sequence and utilize electronic devices at pressure. These could be used for the addition of strain gauges, motors, and other sensors that could benefit from being testing at pressure. I also suggested additional material testing including expanding the material coupons tested to include other alloys as well as more careful controls for better results. From my demonstration test results, I identified changes in the copper and aluminum alloys which could benefit from additional testing to benefit design efforts. Moving away from metallic material testing with inert fluids, I proposed using the chamber for hydrogen testing to better understand how pressurized hydrogen affects materials including polymers which will be crucial in the use and distribution of hydrogen as a clean fuel.

Bibliography

[1] National Geographic, "DeepSea Challenge 3D," Neo-Pangea, 2023. [Online]. Available: http://www.deepseachallenge.com/. [Accessed 12 March 2023].

[2] A. O. Salameh, "Trieste Vs. Deepsea Challenger 2012," [Online]. Available: https://www.sutori.com/en/story/trieste-vs-deepsea-challenger-2012--tt7UrDL3KT1kAHJ2NUfA3gP7. [Accessed 18 December 2020].

[3] A. Nugent, "Why Heron's Aeolipile Is One of History's Greatest Forgotten Machines," 29 November 2020. [Online]. Available: https://www.popularmechanics.com/science/energy/a34554479/heron-aeolipile/. [Accessed 16 March 2023].

[4] R. M. Hazen, "High-Pressure Phenomena," 03 March 2009. [Online]. Available: https://www.britannica.com/science/high-pressure-phenomena. [Accessed 14 March 2023].

[5] T. W. Hong and A. Toudehdehghan, "A Critical Review and Analysis of Pressure Vessel Structures," IOP Conference Series: Materials Science and Engineering, 2019.

[6] J. Kiusalaas and A. Pytel, Mechanics of Materials, Pacific Grove: Bill Stenquist, 2003.

[7] W. D. Callister Jr., Materials Science and Engineering - An Introduction, 6th ed., New York, New York: John Wiley & Sons Inc., 2003.

[8] ASTM International, ASTM E8/E8M, Standard Test Methods for Tension Testing of Metallic Materials, West Conshohocken, PA: ASTM International, 2013.

[9] K. Herrmann, Hardness Testing - Principles and Applications, K. Herrmann, Ed., Materials Park, OH: ASM International, 2011.

[10] H. E. Boyer, Ed., Hardness Testing, Metals Park, OH: ASM International, 1987.

[11] F. Campbell, Inspection of Metals - Understanding the Basics, Materials Park: ASM International, 2013.

[12] J. Darul, C. Lathe and P. Piszora, "Mn3O4 under High Pressure and Temperature: Thermal Stability, Polymorphism, and Elastic Properties," *The Journal of Physical Chemistry*, vol. 117, pp. 23487 - 23494, 2013.

[13] R. Gaddama, M. Hörnqvistb, M.-L. Anttia and R. Pedersona, "Influence of high-pressure gaseous hydrogen on the low-cycle fatigue and fatigue crack growth properties of a cast titanium alloy," *Materials Science and Engineering: A,* vol. 612, pp. 354-362, 2014.

[14] E. Fangnon, E. Malitckii, R. Latypova and P. Vilaca, "Prediction of hydrogen concentration responsible for hydrogen-induced mechanical failure," *International Journal of Hydrogen Energy,* 2022.

[15] V. Kathavatea, D. Pawarb, N. Bagalc and A. Adkined, "Mechanical Behavior of Metal under Hydrostatic Pressure and Low Temperature," in *Materials Today: Proceedings 5, no. 5,* 2018.

[16] S. A. B. Patinet, M. Lerbinger, D. Vandembroucq and A. Lemaître, "Origin of the Bauschinger effect in amorphous solids.," *Physical Review Letters,* vol. 124, no. 20, p. 205503, 2020.

[17] World Material, "SAE AISI 4340 Steel Properties, Heat Treatment, Equivalent, Hardness Chart, Density, Machinability," World Material, [Online]. Available: https://www.theworldmaterial.com/astm-sae-aisi-4340-alloy-steel/. [Accessed 25 April 2023].

[18] F. P. Ford and P. M. Scott, "Environmentally-Assisted Degradation of Carbon and Low-Alloy Steels in Water Cooled Nuclear Reactors," *Advanced Nuclear Technology International Europe AB,* pp. 2-I4 (2-I8), 2008.

[19] ASM International, "Austempered Steel," in *ASM Handbook, Volume 4A, Steel Heat Treating Fundamentals and Processes,* vol. 4A, G. T. J. Dossett, Ed., ASM International, 1991, pp. 152-163.

[20] High Pressure Equipment Co., "How Spreague Air Driven Hydraulic Pumps Work," [Online]. Available: https://www.highpressure.com/products/pump-products-and-systems/sprague-air-driven-pumps/related-sprague-content/how-sprague-air-driven-hydraulic-pumps-work/. [Accessed 03 March 2023].

[21] Cerakote, "MICRO SLICK DRY FILM LUBRICANT COATING (Oven Cure) P-109," Cerakote, [Online]. Available: https://www.cerakote.com/shop/cerakote-coating/P-109/micro-slick-dry-film-lubricant-coating-oven-cure. [Accessed 1 02 2023].

[22] National Instrument, DAQ X Series - X Series User Manual, Austin, Texas: National Instruments, 2019.

[23] Honeywell, Model TJE - Precision Gage/Absolute Pressure Transducer, Golden Valley, Minnesota: Honeywell International Inc., 2008.

[24] High Pressure Equipment Co., "Sprague Air Driven Pumps," [Online]. Available: https://www.highpressure.com/products/pump-products-and-systems/sprague-air-driven-pumps/. [Accessed 03 March 2023].

[25] SpectroGraphic Limited, "Struers Rotopol 31-Rotoforce 3," [Online]. Available: https://spectrographic.co.uk/products/struers-rotopol-31-rotoforce-4. [Accessed 3 March 2023].

[26] AFFRI Inc, "Wiki JS," AFFRI, [Online]. Available: https://affri.com/wiki-js/. [Accessed 3 March 2023].

[27] Keyence Corporation of America, "Digital Microscope - VHX-7000 Series," [Online]. Available: https://www.keyence.com/products/microscope/digital-microscope/vhx-7000/. [Accessed 3 March 2023].

[28] Zach, "How to Determine Equal or Unequal Variance in T-Tests," 11 April 2021. [Online]. Available: https://www.statology.org/determine-equal-or-unequal-variance/. [Accessed 20 February 2023].

[29] National Institute of Standards and Technology, "Anderson-Darling and Shapiro-Wilk Tests," [Online]. Available: https://www.itl.nist.gov/div898/handbook/prc/section2/prc213.htm. [Accessed 20 February 2023].

[30] National Institute of Standards and Technology, "Chi-Square Test for the Variance," [Online]. Available: https://www.itl.nist.gov/div898/handbook/eda/section3/eda358.htm. [Accessed 25 February 2023].

[31] ASTM International, ASTM E112-13, Standard Test Methods for Determining Average Grain Size, West Conshohocken, PA: ASTM International, 2021.

[32] Hercules Sealing Products, "800 Polyurethane U-Seals, U12-2.75-25B," [Online]. Available: https://herculesus.com/product.php?pd=Y&pid=1157&productcode=U12-2.75-25B. [Accessed 16 February 2023].

[33] Keysight, "E36150 Series Autoranging Benchtop Power Supply," [Online]. Available: https://www.keysight.com/us/en/products/dc-power-supplies/bench-power-supplies/e36150-series-autoranging-power-supply.html. [Accessed 15 February 2023].

[34] Staley Co., "Hydraulic Test Stand Model D39110," [Online]. Available: https://www.staleyco.com/product/hydraulic-test-stand-model-d39110/. [Accessed 16 February 2023].

[35] Conax Technologies, "High Pressure Thermocouples and RTDs," November 2020. [Online]. Available: https://www.conaxtechnologies.com/wp-content/themes/conax/pdf/6073.pdf. [Accessed 17 February 2023].

[36] Advanced Ceramics Manufacturing, "Aquacore," 2023. [Online]. Available: https://acmtucson.com/acm_products/aquacore/. [Accessed 17 February 2023].

[37] Advanced Ceramics Manufacturing, "Aquapour," 2023. [Online]. Available: https://acmtucson.com/acm_products/aquapour/. [Accessed 17 February 2023].

[38] High Pressure Equipment Compant, "Valves, Fittings & Tubing, Pressure Vessels & Reactors Catalog," 16 October 2020. [Online]. Available: https://www.highpressure.com/pdfs/FullLineCatalog1020.pdf. [Accessed 01 02 2023].

Appendix A – Chamber Drawings and Embedded CAD Files

Vertical Loading Chamber Technical Data Files


Original Pressure Chamber.zip


Original Pressure Chamber TDP.pdf

Horizontal Loading Chamber Technical Data Files


PMR-MS2-10R0.zip


PMR-MS2-10R0 Drawings.zip


Bauman Chamber Material Testing.pdf


PMR-MS2-10R0.pdf

Appendix B – Final Test Stand Schematics

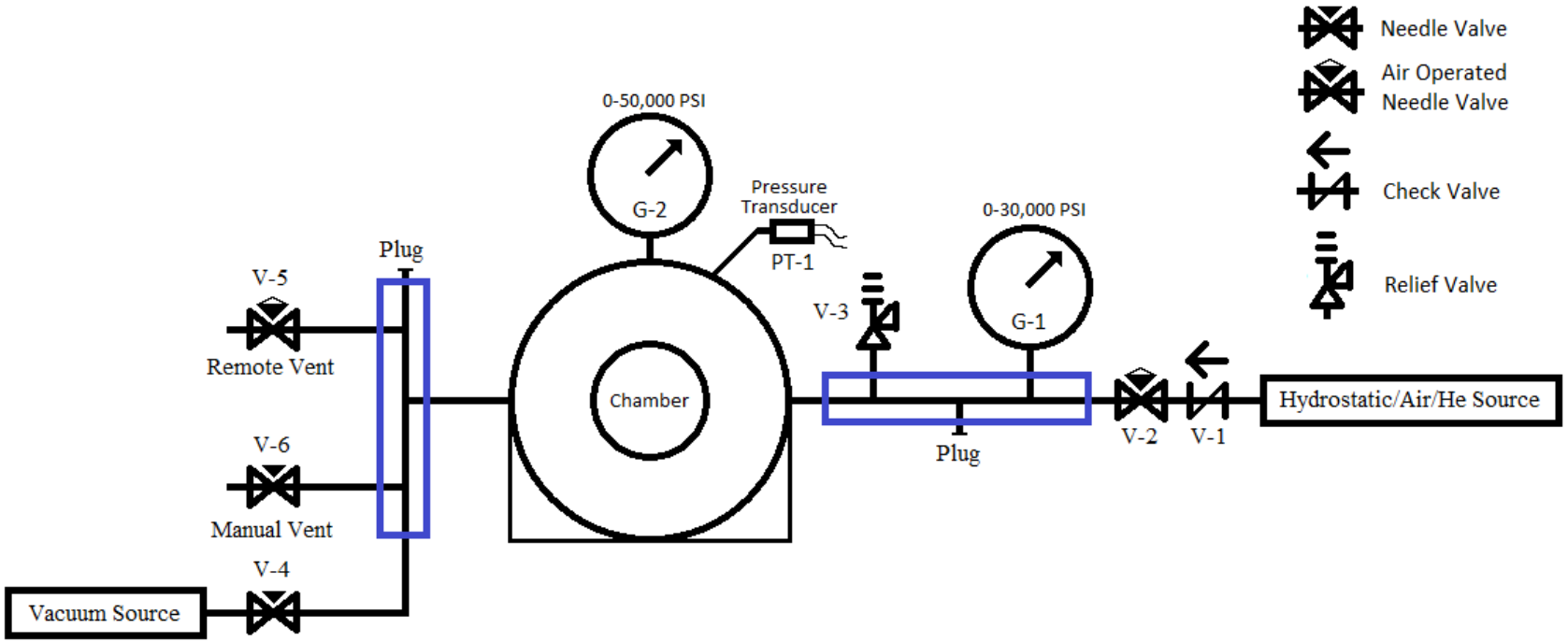

Appendix B.1 Test Stand Fluid Control Functional Schematic

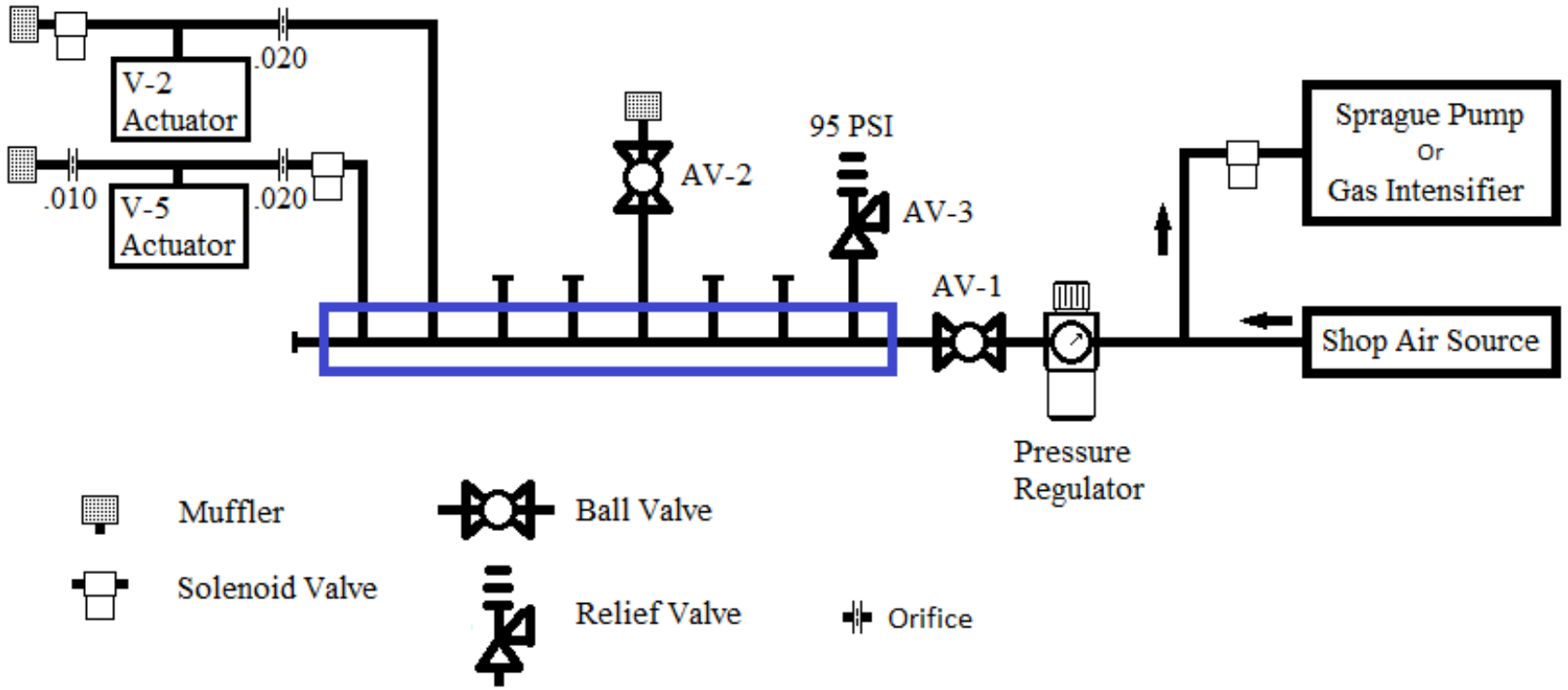

Appendix B.2 Air Control System Functional Schematic

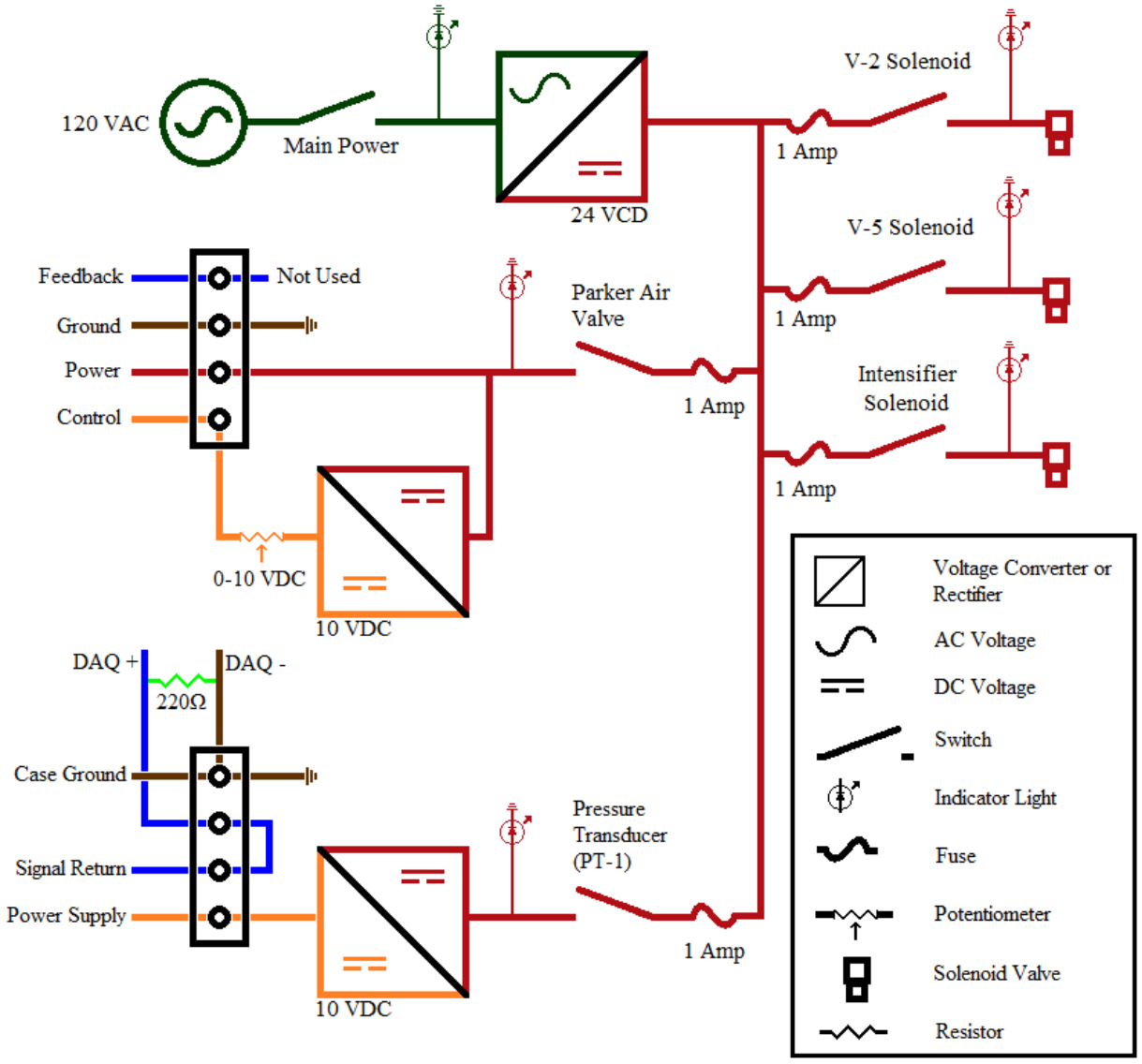

Appendix B.3 Electronic Control System Functional Schematic

Appendix C – Experimental Test Procedure and Data Table Embedded Word File

Resnick Thesis Final
Test Procedure.docx

Appendix D – Dive Pressure Transducer Embedded Excel Files

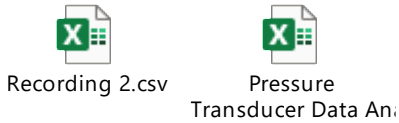

Appendix E – Statistic Testing Embedded Excel Files


Dimensional Repeated-Measures


Hardness Data Shapiro_Wilk for No


Hardness Data Frequency.xlsx


Hardness Repeated-Measures


Hardness Data Chi_Square.xlsx

Appendix F – Project BOM Embedded Excel File

Final BOM.xlsx